Dissertation

submitted to the
Combined Faculties for the Natural Sciences and for Mathematics
of the Ruperto-Carola University of Heidelberg, Germany
for the degree of
Doctor of Natural Sciences

presented by

Diplom-Chemiker Christian Graf
born in Saarbrücken

Oral examination: 19.06.2008

Analysis of the Conformational Dynamics of Hsp70 and Hsp90 Chaperones

Referees: PD Dr. Matthias P. Mayer

Prof. Dr. Irmgard Sinning

Meinen Eltern

Table of contents

Publications from this thesis

Rist, W.*, Graf, C*, Bukau, B. and Mayer, M.P. (2006): "Amide hydrogen exchange reveals conformational changes in Hsp70 chaperones important for allosteric regulation", *Journal of Biological Chemistry 281*, 16493-16501 **contributed equally*

Graf, C., Stankiewicz, M., Kramer, G., Mayer, M.P. "Kinetically and spatially resolved conformational changes in the dynamics of the Hsp90 chaperone machine" *submitted*

Graf, C., Stankiewicz, M., Mayer, M.P.: "Differences in conformational dynamics within the Hsp90 chaperone family" *manuscript in preparation*

Graf, C., Nikolay, R., Mayer, M.P.: "Conformational properties of the E3 ubiquitin ligase CHIP in complex with molecular chaperones and E2 ligases" *manuscript in preparation*

Wegrzyn, R.D., Hofmann, D., Merz, F., Nikolay, R., Rauch, T., Graf, C., Deuerling, E (2006): "A conserved motif is prerequisite for the interaction of NAC with ribosomal protein L23 and nascent chains", *Journal of Biological Chemistry 281* ,2847-2857

Summary

Molecular chaperones of the Hsp70 and Hsp90 family are central components in protein folding processes in the cell. In addition to their general chaperone function in protein quality control, Hsp70 and Hsp90 cooperate in the control of stability and activity of some 200 natively folded clients including receptors, protein kinases and transcription factors, many of which are key regulators in essential signal transduction pathways. Both chaperones are multi-domain proteins that use ATP-controlled cycles for substrate binding and release which are regulated by co-chaperones. The aim of this thesis was to elucidate the allosteric mechanism of Hsp70 and Hsp90 chaperones and their interactions with the co-chaperone CHIP by investigating their conformational changes and dynamics in solution. These conformational studies were performed primarily using amide hydrogen exchange (HX) combined with high-resolution mass spectrometry (MS) and fluorescence spectroscopy.

HX-MS experiments with the *E. coli* Hsp70 homologue DnaK revealed specific ATP-induced conformational changes. Upon ATP binding, the nucleotide-binding domain was more compact, while the substrate binding domain was more flexible. The exposed interdomain linker became completely protected from solvent upon ATP binding. Comparison of the dynamics of the full-length protein with the dynamics of the isolated domains demonstrated a mutual stabilization of both domains. Substrate binding to DnaK in the ATP-bound state reverses the ATP-induced conformational changes in the linker and selected parts of the NBD. The HX-MS data outline a pathway for allosteric interdomain communication which mediates ATP-induced opening of the substrate binding pocket and the substrate-induced stimulation of ATP hydrolysis.

Continuous-labeling and pulse-labeling HX-MS experiments with the dimeric *E. coli* Hsp90 homologue HtpG demonstrate drastic ATP-induced conformational changes throughout the protein that do not occur simultaneously but progress slowly like a wave from the nucleotide binding site towards the N-terminus and the middle domain. A conformation-sensitive fluorescent probe allowed the elucidation of the kinetics of the ATPase cycle of HtpG. Conversion into a compact conformational state was shown to be rate-limiting for ATP hydrolysis and the nucleotide-coordinating residue Glu^{34} was important for the rate of conversion.

Analysis of the conformational dynamics of the eukaryotic Hsp90 homologues from yeast and human, Hsc82 and Hsp90β, by HX-MS revealed a significant higher flexibility as compared to the prokaryotic HtpG. Segments with higher dynamics were located predominantly in the middle and the dimerization domains. Nucleotide binding had long-range effects on the conformation of all domains, but these were more subtle compared to HtpG. Consistent with the hypothesis that conformational dynamics of Hsp90 is linked to regulation by co-chaperones, it could be shown by fluorescence resonance energy transfer experiments with fluorescent Hsp90β that the binding of the co-chaperone p23 in presence of ATP leads to movement of the N-terminal Hsp90 domains towards each other. Two Hsp90 inhibitors competitive for nucleotide affected the conformational dynamics of Hsp90β differently from nucleotides and from each other.

The human E3-ubiquitin ligase CHIP exhibited an extraordinary flexibility with an almost completely unfolded N-terminal TPR domain as measured by HX-MS. Complex formation with intact Hsp70 and Hsp90 or their respective C-terminal octapeptides induced folding of the TPR domain to a defined, stabilized structure. Interaction of CHIP with two different E2 ubiquitin-conjugating enzymes, UbcH5a and Ubc13, resulted in distinct effects on the conformational dynamics of CHIP suggesting different roles of the CHIP-E2 interaction for the ubiquitination of substrates.

Zusammenfassung

Molekulare Chaperone der Hsp70 und Hsp90 Familie sind an einer Vielzahl von zellulären Proteinfaltungsprozessen beteiligt. Neben der allgemeinen Chaperon-Funktion in der Proteinqualitätskontrolle spielen Hsp70 und Hsp90 eine wichtige Rolle in der Kontrolle der Stabilität und Aktivität von über 200 nativ gefalteten Substraten, darunter Rezeptoren, Proteinkinasen und Transkriptionsfaktoren, von denen viele Schlüsselproteine wichtiger Signaltransduktionswege sind. Beide Chaperone sind Multi-Domänproteine, die ihre Substrate in ATP-kontrollierten Reaktionszyklen binden und wieder freisetzen, und dabei zusätzlich durch Co-Chaperone reguliert werden. Ziel dieser Arbeit war es, die allosterische Funktionsweise von Hsp70 und Hsp90 Chaperonen und deren Interaktion mit dem Co-Chaperon CHIP durch die Untersuchung ihrer Konformationsdynamik und ihrer Konformationsänderungen in Lösung aufzuklären. Diese strukturellen Untersuchungen wurden hauptsächlich mit Wasserstoff-H/D-Austausch (HX) in Verbindung mit hochauflösender Massenspektrometrie (MS) sowie Fluoreszenzspektroskopie durchgeführt.

Durch HX-MS Experimente mit Hsp70 aus *Escherichia coli*, DnaK, konnten spezifische ATP-abhängige Konformationsänderungen in beiden funktionellen Domänen des Proteins nachgewiesen werden: die Nukleotidbindedomäne wird durch ATP-Bindung kompakter, während es in der Substratbindedomäne zu einer Öffnung kommt. Der exponierte Linker zwischen beiden Domänen wird in Gegenwart von ATP stark von der austauschenden Umgebung geschützt. Durch den Vergleich der Konformationsdynamik des Volllängenproteins mit den isolierten Domänen konnte eine wechselseitige Stabilisierung der Domänen gezeigt werden. Die Bindung von Substratpeptid an ein DnaK im ATP gebundenen Zustand führt zu einer Umkehrung der ATP-induzierten Konformationsänderungen im Linker und in Segmenten der Nukleotid-bindedomäne. Die gewonnenen Ergebnisse zeigen somit die Signalwege der allosterischen Domänen-Kommunikation von Hsp70, durch die einerseits die ATP induzierte Öffnung der Substratbindetasche bewirkt wird und andererseits die ATP-Hydrolyse durch Substratbindung stimuliert wird.

Mithilfe kontinuierlicher und gepulster HX-MS Messungen mit dem dimeren Hsp90 Homolog aus *Escherichia coli*, HtpG, konnten starke ATP-induzierte Konformationsänderungen im gesamten Protein beobachtet werden, die allerdings nicht konzertiert ablaufen, sondern sich langsam und schrittweise wie eine Welle von der unmittelbaren Nukleotidbindestelle zum N-terminalen Ende und zur Mitteldomäne des Proteins ausbreiten. Ein konformationsempfindlicher Fluorophor gekoppelt an HtpG konnte zur Bestimmung der Kinetiken des gesamten ATP-Reaktionszyklus verwendet werden. Es konnte gezeigt werden, dass der Übergang zu einer stabilisierten Konformation geschwindigkeitsbestimmend für die ATP Hydrolyse ist und dass dabei die Aminosäure Glu^{34} wichtig für diesen Konformationsübergang ist.

Die Analyse der Konformationsdynamik der eukaryotischen Hsp90 Homologen, dem Hsp90β des Menschen und Hsc82 aus Hefe, zeigte eine signifikant höhere Flexibilität im Vergleich zum prokaryotischen HtpG. Die meisten Bereiche mit höherer Dynamik befanden sich in der Mitteldomäne und in der Dimerisierungsdomäne. Nukleotidbindung führte in allen Hsp90-Domänen zu Konformationseffekten, die allerdings erheblich schwächer waren als in HtpG. Mithilfe von Fluoreszenz-Resonanz-Energie-Transfer-Messungen konnte indes gezeigt werden, dass die Bindung des Co-Chaperons p23 an fluoreszenzmarkiertem Hsp90 in Gegenwart von ATP zu einer Bewegung der N-terminalen Domänen zueinander führt. Die

Bindung von zwei mit ATP kompetitiven Hsp90-Inhibitoren beeinflusste die Dynamik von Hsp90β in einer von Nukleotiden verschiedenen Weise.

HX-MS Experimente mit der E3-Ubiquitin-Ligase CHIP zeigten, dass das Protein eine außerordentlich hohe Dynamik mit stark entfalteten Bereichen in der N-terminalen TPR Domäne aufweist. Durch Komplexbildung mit intaktem Hsp70 und Hsp90 oder deren C-terminalen Oktapeptiden konnte die Faltung der TPR-Domäne zu einer stabilisierten Konformation induziert werden. Die Interaktion mit zwei E2-Ubiquitin-verknüpfenden Enzymen, UbcH5a und Ubc13, führte zu unterschiedlichen Effekten auf die Konformationsdynamik von CHIP und weist damit auf eine spezifische Rolle der E2-CHIP Interaktion für die Ubiquitinierung von Substraten hin.

1 Introduction

1.1 Protein Folding and Dynamics

Newly synthesized proteins must fold into a native three-dimensional structure to become functionally active. The complexity of the protein folding process can be illustrated as follows: given a protein of 100 amino acids and assuming only two different conformational states for each amino acid (e.g. *cis* and *trans* conformation of the peptide bond), the polypeptide can adopt $2^{100} = 1.3 \times 10^{30}$ conformational states. It would take longer than the age of the universe to find the native structure if protein folding proceeds via random search of all possible conformations even at the highest sampling rate possible. This conclusion is in contrast to the experimental finding that many proteins fold within milliseconds to seconds; this dilemma is known as "Levinthal's paradox" (Levinthal, 1968).

This folding paradox is elegantly solved within the framework of the energy landscape description of directed folding pathways (Dinner et al., 2000; Onuchic et al., 2000). In this description, the folding process is interpreted in terms of conformational ensembles that undergo a biased diffusion on a multi-dimensional free-energy surface. The native state of a protein corresponds the global free-energy minimum on the conformational energy landscape, thus resulting in a "folding funnel". The denatured state, on the other hand, is represented by a large ensemble of conformations with high internal energy and flexibility. On the way to its native state a protein can follow trajectories from the unfolded state over different partially folded states and intermediates. Many proteins form an intermediate during early folding termed "molten globule" which describes a fairly compact folding state with pronounced secondary structure but few ordered tertiary structure elements.

The protein structure under native conditions is with very few exceptions not a static crystalline state as analyzed in X-ray crystallography, but a rather dynamic ensemble involving local unfolding and refolding; proteins "breathe". For many proteins, dynamics are essential to function. Protein motions can be categorized in three classes, local, rigid, or large-scale motion. These identified motions cover a wide range of timescales (10^{-15} to 10^{3} s), amplitudes (0.01 to 100 Å) and energies (1 to 400 kJ/mol) (Brooks et al., 1990). Such conformational changes can include local fluctuations affecting only few atoms within the secondary structure as well as global fluctuations altering the whole protein structure. Many of these conformational alterations are induced by binding of ligands or other proteins by an

”induced fit” mechanism (Koshland, 1958; Koshland, 1998). A large variety of proteins use dynamics as a means of communication between different domains. This process of allostery is best shown for haemoglobin conformations changing upon oxygen binding (Perutz, 1972; Perutz et al., 1998). Another important protein class demonstrating the importance of conformational dynamics is the group of “intrinsically unstructured proteins” that contain large segments of disorder under native conditions, and seem to have a large variety of regulatory functions *in vivo* (Dyson and Wright, 2005).

Conformational properties of proteins can be monitored on the global level by conventional biophysical and analytical methods, including far-UV circular dichroism (CD) (Pelton and McLean, 2000), tryptophane fluorescence and infrared spectroscopy (Barth, 2000). In addition, small-angle X-ray scattering and cryo-electron microscopy can reveal changes in the conformational shape and assembly of proteins (Koch et al., 2003).

In terms of detailed amino acid resolution, few techniques can compete with X-ray crystallography which is capable of determining structure from a highly ordered crystallized protein with a resolution in the range of 1-2 Å (Moffat, 2001). Newly developed “time resolved” crystallographic methods have shown some promise in determining dynamic information, but need large amounts of pure protein and the formation of crystals (Moffat, 2001; Schlichting et al., 2000). Multi-dimensional nuclear magnetic resonance (NMR) spectroscopy has been used for many years to monitor protein dynamics in solution under steady-state conditions and on multiple time scales at the amino acid level (Dyson and Wright, 2004). NMR experiments have traditionally been limited to small, soluble proteins up to 35 kDa. However, new spectrometer technology (such as high magnetic fields and cryoprobes) and new NMR pulse sequences have pushed the size limit upward to 100 kDa and even the size of the ribosome, depending on the system and biological question (Henzler-Wildman and Kern, 2007).

Hydrogen exchange (HX) methods, which can be analysed by either mass spectrometry or NMR spectroscopy, provide a powerful tool to detect global or local unfolding on timescales of milliseconds and longer. Since this technique was extensively used in this work to investigate conformational changes in chaperone proteins, the details will be discussed in a later section.

1.2 Molecular Chaperones

Protein folding in the cell is a much more complex process than it is *in vitro*. The conditions in a living cell seem to be not beneficial for effective folding, mainly because of high temperature and high concentration of proteins in the cell (ca. 200 mg/ml). This molecular crowding effect leads to strong competition between productive folding processes and aggregation or misfolding. Protein aggregation is fatal for the cell as it can interfere in important cellular processes and is the cause of many neurodegenerative diseases like Alzheimer's disease, Parkinson's disease or prion diseases (Chiti and Dobson, 2006).

Cells harbour a set of proteins called molecular chaperones which assist folding and prevent the aggregation of misfolded proteins during *de novo* protein synthesis as well as under stress conditions such as high temperature (Young et al., 2004). The fact that the level of many chaperones is elevated under heat shock conditions led to the term "heat shock protein" (Hsp) (Ellis, 1987). Hsp proteins exist in several evolutionary conserved families, which are named according to the apparent molecular weight of a typical member, e.g. Hsp110, Hsp100, Hsp90, Hsp70, Hsp60 or Hsp40 and the small Hsps.

The characteristic feature of chaperone action is the transient and stoichiometric binding to their substrate proteins. The Hsps can be grouped into three functional categories: holder chaperones, folder chaperones and disaggregases. The "holders" prevent unfolded proteins from interacting with each other by binding to them and, hence, counteract protein aggregation. Typical examples for this functional group are the small heat shock proteins (e.g. *E. coli* IbpA and IbpB, human Hsp26), members of the Hsp40 family (e.g. *E. coli* DnaJ, human Hdj-2, *S. cerevisiae* Ydj1) and Trigger factor.

The folder chaperones have the unique feature to actively assist folding processes. Members of this group typically possess an ATPase domain because this function requires energy. Two well studied examples are the Hsp60 chaperones, also called chaperonins (e.g. *E. coli* GroEL, human TRiC), and the Hsp70 protein family (e.g. *E. coli* DnaK, human Hsp70) (Bukau and Horwich, 1998).

The proteins with disaggregating activity are able to dissolve already formed protein aggregates to release polypeptide chains for refolding or degradation. Examples for this protein group are the Hsp100 family members *E. coli* ClpB and *S. cerevisiae* Hsp104. They are able to resolubilize protein aggregates in cooperation with members from the Hsp70 family (Glover and Lindquist, 1998; Mogk et al., 1999).

1.2.1 The Hsp70 chaperone machinery

1.2.1.1 Cellular functions of Hsp70

The 70-kDa heat shock proteins (Hsp70) constitute the central part of a ubiquitous chaperone system that is present in most compartments of eukaryotic cells, in eubacteria and in many archaea. They assist an extraordinarily broad spectrum of folding processes within the entire life span of proteins (Fig. 1.1) (Mayer et al., 2001; Mayer and Bukau, 2005). These processes include the folding of newly synthesized and misfolded proteins and the prevention or reversion of protein aggregation (Deuerling et al., 1999; Goloubinoff et al., 1999; Mogk et al., 1999; Teter et al., 1999). Such quality control functions, mostly in cooperation with co-chaperones and chaperones of other families, play an essential role in stress situations like heat shock or harsh environmental conditions.

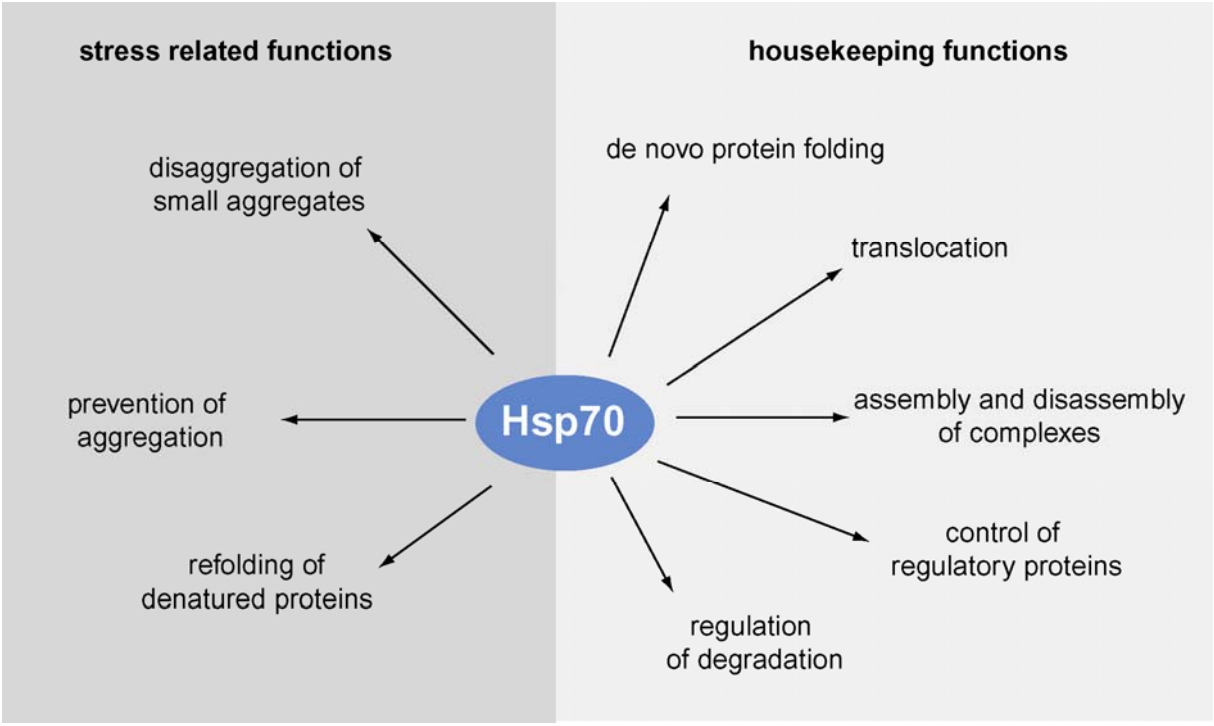

Fig. 1.1 Functions of Hsp70 chaperones in the cell

All of these activities appear to be driven by the basic property of Hsp70s to interact with short hydrophobic peptide segments of protein substrates in an ATP-dependent fashion. Hsp70 chaperones also have important housekeeping functions in the cell under normal conditions, e.g. the disassembly of protein complexes such as clathrin coats (Chappell et al., 1987; Ungewickell, 1985), the import of proteins into the endoplasmic reticulum (ER) lumen (Lyman and Schekman, 1997; Matlack et al., 1999) and the mitochondrial matrix (Voisine et al., 1999), the regulation of the heat-shock response and the control of regulatory proteins in

cooperation with the Hsp90 system. The main Hsp70 chaperone of *E. coli* is DnaK which is highly expressed under all conditions but even more expressed under heat shock conditions, being regulated by the heat-shock transcription factor σ^{32}. In higher eukaryotes there are Hsp70 isoforms that are either constitutively expressed (e.g. the human Hsc70) or stress-inducible (e.g. the human Hsp70) under the control of the heat-shock response.

1.2.1.2 Hsp70 structure

The structure of Hsp70 proteins is highly conserved and consists of an N-terminal 44-kDa nucleotide binding domain (NBD) and a C-terminal substrate-binding domain (SBD) of at about 25 kDa, which are connected by a conserved short hydrophobic linker (Bukau and Horwich, 1998). At the beginning of this work, no high resolution structure of a full-length Hsp70 molecule was available, but the individual domains were characterized extensively by X-ray crystallography and NMR spectroscopy.

The nucleotide-binding domain of Hsp70s is structurally homologous to actin, hexokinase and glycerokinase. It consists of two equal-sized lobes forming a V-like shaped domain with a deep cleft. Each lobe can be further divided into two subdomains IA, IB and IIA, IIB (Fig. 1.2b). The binding pocket for nucleotide and the required Mg^{2+} and K^{+} ions is formed at the bottom of the cleft by all four subdomains and the cross-connecting helices, contacting the adenosine nucleotide with two β- and γ-binding loops (Flaherty et al., 1990). The many available X-ray structures of the ATPase domain of bovine, human and bacterial Hsp70 indicate that there are only subtle conformational changes in response to nucleotide binding or hydrolysis (Flaherty et al., 1994; Harrison et al., 1997; Sondermann et al., 2001). NMR data revealed a high degree of flexibility in the NBD with a shearing and tilting motion of the different subdomains relative to each other, leading to an opening and closing of the nucleotide binding cleft (Zhang and Zuiderweg, 2004). The opening frequency seems to be highest in the order nucleotide-free>ADP>ATP (Gassler et al., 2001).

Most structural information on the substrate-binding domain of Hsp70 exist for *E. coli* DnaK. The X-ray structure of the SBD (residues 389-607) was solved in complex with a heptameric peptide NRLLLTG by Hendrickson and co-workers (Zhu et al., 1996) (Fig. 1.2b). Additional studies in solution were performed in presence or absence of substrate by NMR spectroscopy (Bertelsen et al., 1999; Morshauser et al., 1999; Pellecchia et al., 2000; Stevens et al., 2003). The peptide binding domain forms a sandwich of two fourstranded β-sheets with four upwards protruding loops (two inner and two outer loops) and two helices A and B which are

packed against the inner loops. The peptide binding site lies in between the loops $L_{1,2}$ and $L_{3,4}$ which form the direct hydrogen bond interactions with the peptide substrate backbone. Helix B constitutes a lid which closes the cavity through a salt bridge and two hydrogen bonds to the outer loops $L_{3,4}$ and $L_{5,6}$. The distal part of helix B together with 3 additional helices C, D and E forms a subdomain of unknown function. The very C-terminus of DnaK is highly flexible and could not be structurally resolved (Bertelsen et al., 1999), while a crystal structure for a C-terminal construct of *C. elegans* Hsp70 is reported showing a multimeric assembly of α-helices (Worrall and Walkinshaw, 2007).

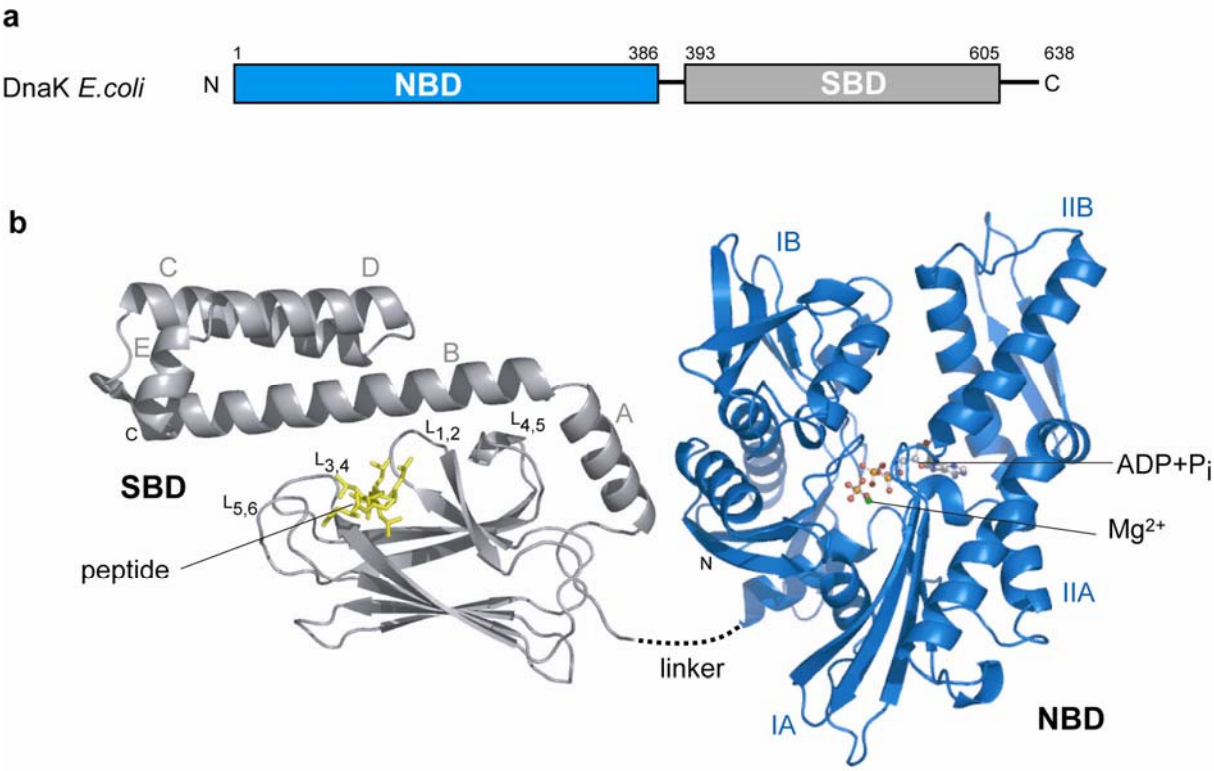

Fig. 1.2 Domain architecture and structure of Hsp70. (a) Domain organisation of DnaK with nucleotide-binding domain (NBD) and substrate binding domain (SBD) **(b)** Secondary structure representation of the SBD and the NBD of Hsp70. Left, secondary structure representation of the *E. coli* DnaK SBD (393-607, PDB code 1DKZ) with bound heptameric substrate peptide NRLLLTG (yellow) (Zhu et al., 1996). Right, standard representation of the NBD of bovine Hsc70 (PDB code 1HPM) in complex with ADP+P_i with lobes I and II, formed by subdomains A and B respectively.

Five central residues of the substrate peptide NRLLLTG show important interactions with the DnaK SBD: hydrogen bonding between the peptide backbone and the loops $L_{1,2}$ and $L_{3,4}$ and van-der-Waals interactions of the hydrophobic peptide side chains with the hydrophobic cavity of the SBD and the arch (formed by Met^{404} and Ala^{429}) bridging over the peptide backbone. The principal preference of DnaK for hydrophobic peptides was investigated by peptide library screening. The experimentally determined binding motif for DnaK consists of five consecutive residues enriched in hydrophobic amino acids and flanking regions enriched

in basic amino acids (Rudiger et al., 1997a; Rudiger et al., 1997b). Such binding sequences occur frequently within protein sequences, approximately one DnaK binding site every 36 residues and are typically buried within the hydrophobic core of the folded proteins.

Cytosolic eukaryotic Hsp70 proteins have an entirely conserved motif (EEVD) at the very C-terminus, which is unstructured and, therefore, flexible and accessible for interaction partners. The EEVD-motif facilitates binding of proteins with a tetratricopeptide binding motif (TPR) to Hsp70 proteins (Scheufler et al., 2000). Examples for interacting TPR-proteins are the Hsp70/Hsp90 organizing protein (Hop/Sti1) or the mammalian E3 ligase CHIP (Nikolay et al., 2004; Odunuga et al., 2003) which will be introduced later in this chapter.

It was unclear for long time, how both SBD and NBD are oriented to each other in the fully functional two-domain molecule. Residual dipolar coupling in NMR was used to align both domains in a DnaK two-domain construct of *Thermus thermophilus* (Revington et al., 2005). Recently, the first structure of an intact bovine Hsc70 two-domain construct in the high-affinity state was reported (Jiang et al., 2005). This structure and other new structural data will be discussed on the basis of the data of this thesis in the results section.

1.2.1.3 Hsp70 functional cycle

The basic principle of Hsp70-mediated folding processes relies on the transient interaction with unfolded polypeptide stretches within the SBD which is controlled by the nucleotide status of the NBD in an allosteric manner. ATP binding and hydrolysis is absolutely essential for the chaperone activity. Hsp70 chaperones seem to assist folding by repeated cycles of substrate binding and release between two nucleotide states (Bukau and Horwich, 1998; Hartl and Hayer-Hartl, 2002) (Fig. 1.3). In the ATP bound state, the affinity for substrates is low, but the association and dissociation rates of the substrate are high (low-affinity state). In contrast, the ADP bound state resembles the high-affinity state for substrates, but has low association and dissociation rates.

Hsp70 proteins have a higher affinity for ATP (~1 nM) than for ADP/P_i (~ 10 nM) implying that at most conditions in vivo (3 mM ATP), they are in the ATP bound state. However, the basal ATP hydrolysis rate for DnaK ($6 \cdot 10^{-4}$ s^{-1}, half-life τ = 19 min) is too low to be physiologically relevant (Flynn et al., 1989; Gao et al., 1993; Ha and McKay, 1994; Jordan and McMacken, 1995; Karzai and McMacken, 1996; McCarty et al., 1995; Theyssen et al., 1996). Therefore, Hsp70 proteins interact *in vivo* with members of the Hsp40 protein family (J-domain proteins JDP), which accelerate the ATP hydrolysis reaction (Gamer et al., 1996).

Substrate binding to the SBD in synergism with the J-protein triggers the ATP hydrolysis in the NBD of Hsp70. Substrate and the J-domain protein DnaJ can stimulate the ATPase activity of DnaK synergistically more than 1000-fold (Laufen et al., 1999). Since JDPs can bind itself substrates, they are proposed to be targeting factors for Hsp70 substrates which bind the substrates first and allow efficient transfer to Hsp70 by enhancing the coupling of ATP hydrolysis and substrate binding. Cells usually encode a broad spectrum of JDPs which differ in their domain composition and cellular functions (Kelley, 1998; Mayer and Bukau, 1998). The number of different J-proteins is much higher than the number of Hsp70 homologs in the cell (e.g. 6 JDP in *E. coli*, 20 in *S. cerevisiae*, 44 in human cells), some of which display a restricted substrate specificity.

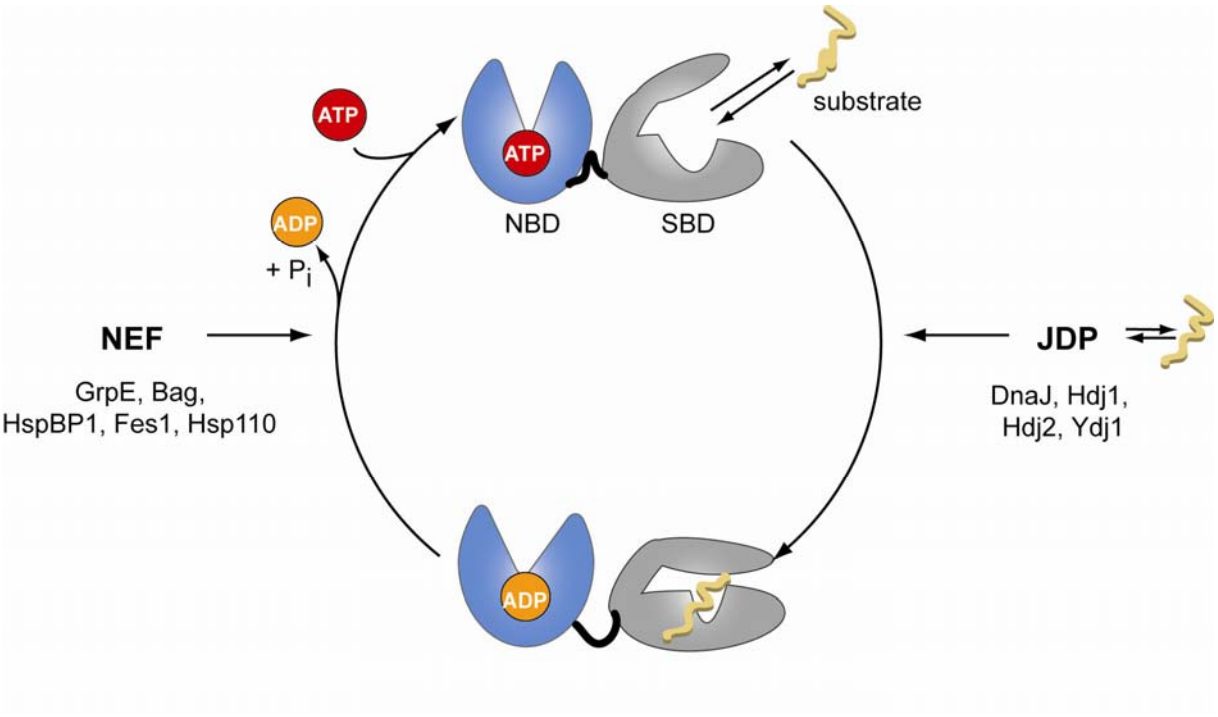

Fig. 1.3 Functional ATPase cycle of Hsp70. The cycle involves the high-substrate-affinity ADP state and the low-affinity ATP state. ATP hydrolysis is catalyzed by the synergistic action of J-domain-proteins (JDP) of the Hsp40 family and the substrate. Nucleotide-exchange factors (NEF) accelerate nucleotide release and the subsequent ATP binding leads to substrate release.

The next step in the Hsp70 functional cycle is the release of ADP and inorganic phosphate. Subsequent rapid association of a new ATP molecule triggers the release of the bound substrate and returns the Hsp70 machinery back to its low-affinity state. With stimulation of the Hsp70 ATPase rate by Hsp40 proteins, release of the product ADP becomes the rate-limiting step. A number of Hsp70 proteins interact *in vivo* with co-factors, which accelerate the nucleotide exchange.

Bacterial and eukaryotic organellar Hsp70 homologues are bound by the GrpE family members (Dekker and Pfanner, 1997; Liberek et al., 1991a; Miao et al., 1997), which lower the affinity for ADP and increase the nucleotide exchange rate by a factor 5000 (Brehmer et al., 2004; Packschies et al., 1997). The crystal structure of a GrpE dimer in complex with nucleotide-free ATPase domain of DnaK gave some insight into how GrpE decreases the affinity of DnaK for nucleotides (Harrison et al., 1997). In the functional model, GrpE inserts a helical bundle into the ATP binding cleft, actively widening the groove and accelerating the dissociation of bound ADP. Eukaryotic cytosolic and ER-resided Hsp70 homologues interact with members of the HspBP1/Fes1 or the Bag family, which bind in a completely different manner than GrpE to the ATPase domain (Bimston et al., 1998; Gassler et al., 2001; Kabani et al., 2002a; Kabani et al., 2002b; Sondermann et al., 2001). Recently, a member of the yeast Hsp70 family, the Hsp110 protein Sse1 was shown to bind itself to cytosolic Hsp70s and to act as nucleotide exchange factor (Raviol et al., 2006). The binding and exchange mechanism of Sse1 onto Hsp70 is still unclear but seems to be activated in a nucleotide-driven process (Andreasson et al., 2008).

Allosteric communication between both the NBD and SBD of Hsp70 is critical for the regulated interaction between chaperone and its substrate polypeptide. This process is strongly coupled in a nucleotide-/substrate controlled manner: ATP binding in the NBD induces conformational changes in the SBD leading to the transition from the high affinity to an open low affinity state. Conversely, substrate binding to the SBD in synergism with the JDP triggers ATP hydrolysis in the NBD, leading to a closing of SBD which traps the substrate. The mechanism by which this allosteric communication works on the structural level is still poorly understood. Biochemical studies including fluorescence, limited proteolysis, CD spectroscopy and small angle X-ray scattering (SAXS) of Hsp70 have given more insights into the coupling mechanism.

SAXS measurements determined that ATP binding induces a significant reduction in the radius of gyration of both a bovine Hsc70 fragment (1-554) (Wilbanks et al., 1995) and full-length DnaK (Shi et al., 1996). Further evidence is demonstrated by proteolysis studies, where ADP and ATP-bound states distinctly showed different cleavage patterns (Buchberger et al., 1995; Liberek et al., 1991b).

An important part of the interdomain communication mechanism is the hydrophobic linker between the ATPase domain and the β-sheets of the substrate-binding domain. Mutations of

the linker motif VLLL in DnaK abolish the substrate/Hsp40 induced stimulation of ATP hydrolysis and ATP-induced substrate release (Laufen et al., 1999).

It is still enigmatic, how Hsp70 proteins interact with substrates in order to assist protein folding. There are at least two alternative modes of action possible (Mayer and Bukau, 2005). In the first mechanism, Hsp70s play a rather passive role. Through repetitive substrate binding and release cycles they keep the free concentration of the substrate low to prevent aggregation, while allowing free molecules to fold to the native state (kinetic partitioning). In the second mechanism, binding and release cycles induce local unfolding in the substrate which helps the substrate polypeptide to overcome kinetic barriers for native folding.

1.2.2 The Hsp90 chaperone machinery

The homodimeric 90 kDa heat shock proteins (Hsp90) are essential chaperones in all eukaryotic cells. They belong to the most abundant proteins making up about 1 – 2% of all cellular proteins under normal growth conditions and even more under heat shock conditions. The Hsp90 family of proteins is also evolutionary highly conserved with 60% sequence identity between yeast and human and 40% between *E. coli* and human members. Eukaryotic Hsp90 chaperones are global players in the signal transduction networks of the cell, interacting with numerous client substrates in a complex system together with Hsp70 chaperones and a large number of co-chaperones. In yeast and human two cytosolic Hsp90 proteins with 99% sequence identity are found, one of which is constitutively at high levels present (yeast Hsc82, human Hsp90β) and the second is produced under heat shock conditions (yeast Hsp82, human Hsp90α) under the control of the heat-shock transcription factor HSF-1. Other compartmentalized Hsp90 chaperones include the ER-resident Grp94 in higher eukaryotes or the mitochondrial TRAP1 which is a descendent of the bacterial Hsp90 protein HtpG. Hsp90 is essential for the survival of all eukaryotes tested, whereas HtpG knockouts results in no detectable phenotype.

1.2.2.1 Cellular functions of Hsp90

Although Hsp90 chaperones can bind misfolded proteins (Jakob et al., 1995), their main and essential function is to interact with native or near native proteins, so-called clients, most of them are regulatory components of signal transduction pathways such as steroid hormone receptors, protein kinases and transcription factors, controlling stability and activity of these proteins. Hsp90 chaperones are therefore involved in the regulation of cell homeostasis, cell

cycle, proliferation, differentiation, and programmed cell death. Up to now, more than 200 of such Hsp90 client substrates have been identified (see Tab. 1 for selected substrates) in interaction studies. Since the activity of many of those client proteins is important in hallmarks of cancer growth and survival, Hsp90 has become a central target for anti-cancer drug development.

A recent genome-wide chemical-genetic screen in baker's yeast combined with bioinformatics identified unknown functions of Hsp90 in cellular transport and the secretory pathway under normal conditions (McClellan et al., 2007).

Tab. 1 Hsp90 substrate proteins

	Protein
Transcription factors	Steroid hormone receptors (AR, ER, GR, MR, PR)
	HSF-1
	p53
	v-erbA
Protein kinases	Cdk2, Cdk3, Cdk4,Cdk9
	ErbB2
	Raf family kinases (v-Raf, c-Raf, B-Raf)
	v-Src, c-Src
	Aurora B
	eIF-2α
	Wee1
	Hck, Lck
Others	Telomerase
	Apaf-1
	CFTR
	Histones H1, H2A, H2B, H3, H4
	Tubulin
	Myosin
	DNA-polymerase α
Viral proteins	SV40 large T antigen
	Hepatitis B virus reverse transcriptase
	AdV-CP
	λP
	HPV-E7

See www.picard.ch/downloads/hsp90interactors.pdf for full list and references

Apart from the function in various regulatory cellular processes, Hsp90s have been implicated as capacitors in morphogenic evolution allowing the phenotypically neutral accumulation of mutations by buffering their effects until stressful environmental conditions expose them to the forces of selection (Queitsch et al., 2002; Sangster et al., 2004).

In addition to these functions, the cellular Hsp90 chaperone system seems to play an important role in the assembly and maturation of viral proteins in the host cell. Hsp90 inhibitors have been shown to reduce the replication of several viruses *in vitro* (Geller et al., 2007; Okamoto et al., 2006).

The bacterial Hsp90 protein HtpG (High temperature protein G) is, though structurally highly homologous to its eukaryotic family members, poorly characterized in terms of function and interaction to substrates. HtpG is already an abundant protein under normal conditions (0.35% of total protein) and becomes highly induced under heat shock conditions, being under control of the heat shock transcription factor σ^{32} (Heitzer et al., 1990). Deletion of the HtpG gene causes no detectable phenotype. Solely HtpG knockouts in cyanobacteria resulted in slightly impaired thermotolerance and intolerance against oxidative stress (Hossain and Nakamoto, 2003; Tanaka and Nakamoto, 1999). In addition, no client substrates and co-factors of HtpG could be identified so far.

1.2.2.2 Hsp90 structure

The dimeric Hsp90 consists of three highly conserved domains: an N-terminal nucleotide binding domain (NBD), a middle domain (MD) and a C-terminal dimerization domain (DD) (Fig. 1.4a). In eukaryotes, a charged unstructured linker region of 50 to 60 residues inserts between the N- and M-domain, being poorly conserved and biologically dispensible (Pearl and Prodromou, 2006). In contrast to the prokaryotic HtpG, eukaryotic Hsp90 contain a C-terminal EEVD motif which serves as the binding site for cytosolic co-chaperones containing TPR domains. Structural information exists for the NBD of yeast and human Hsp90 in complex with different nucleotides and inhibitors, the MD of yeast Hsp90, the two domain construct of NBD plus MD of the *E. coli* homologue HtpG and the DD of HtpG (Harris et al., 2004; Huai et al., 2005; Prodromou et al., 1997a; Stebbins et al., 1997). Recently, an almost full-length construct of yeast Hsp90 in complex with the cochaperone Sba1/p23, a full-length structure of *E. coli* HtpG and a full-length structure of Grp94 were published (Ali et al., 2006; Dollins et al., 2007; Shiau et al., 2006).

The first crystal structure of the N-terminal ATPase domain (NBD) of yeast Hsp82 was solved in 1997 and revealed a new type of binding site for ATP and for the inhibitor geldanamycin (Stebbins et al., 1997). The NBD contains an unusual adenine nucleotide-binding pocket known as the “Bergerat” fold (Dutta and Inouye, 2000). The nucleotide is bound in a cleft formed by α-helices on top of an eight-stranded β-sheet (Fig. 1.4c). Binding induces a special kinked conformation of the nucleotide with the γ-phosphate being completely surface exposed. This fold and orientation shares homology with the superfamily of the GHKL-ATPases, including DNA-modifying proteins GyraseB, MutL and the histidine kinases CheA and EnvZ. All these related proteins contain a flexible structural element, the ATP ‘lid’, a loop consisting of two α-helices that claps over the nucleotide-binding pocket

when ATP is bound and forms a closed conformation. This lid seems to be one important conformational switch for the ATP hydrolysis function of Hsp90 and is also the binding site for co-chaperones like p23/Sba and Cdc37 (Ali et al., 2006; Roe et al., 2004; Zhang et al., 2004). The middle domain (MD) consists of a large and a small α-β-α-domain connected by a helical coil. The yeast Hsp82 MD could be crystallized in complex with the co-chaperone Aha1 (Meyer et al., 2004). In analogy to the GHKL-ATPases MutL and GyrB, the middle domain contains a catalytic loop with an arginine (Arg^{380} in yeast Hsp82) that interacts with the γ-phosphate of ATP bound in the N-terminal domain and promotes ATP hydrolysis. Two elements in the middle domain were further implicated in binding to client proteins, an exposed hydrophobic patch surrounding Trp^{300} and an amphipathic loop (residues 329–339). Mutations in this loop region showed severe effect in the maturation of v-Src kinase (Meyer et al., 2003).

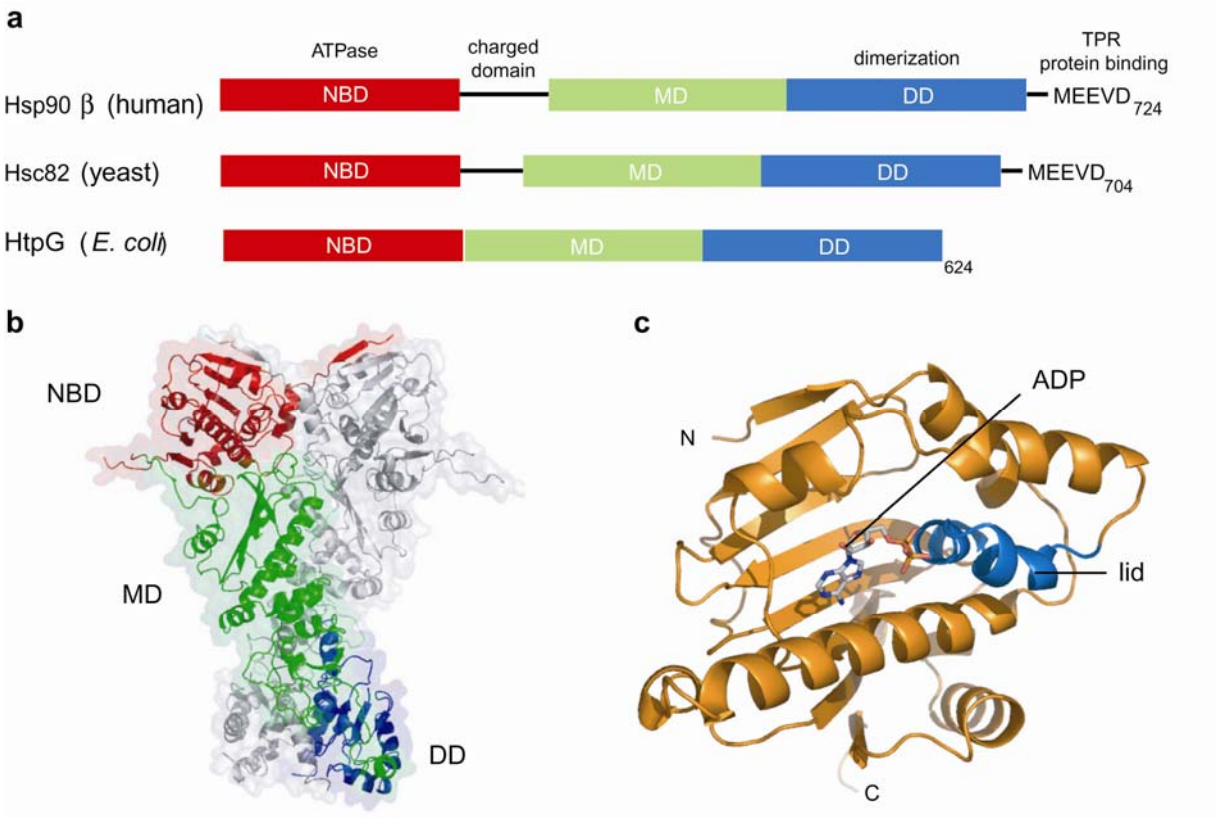

Fig. 1.4 (a) Domain structure representation of Hsp90 homologs. Eukaryotic Hsp90 proteins contain a charged flexible linker between the N-terminal nucleotide binding domain (NBD) and the middle domain (MD), and a dimerization domain (DD) which harbours the C-terminal MEEVD motif for binding TPR co-chaperones. The charged linker is absent in the prokaryotic HtpG **(b) Crystal structure of the yeast Hsp82 in complex with the non-hydrolysable ATP analogue AMPPNP and p23/Sba1** (PDB 2CG9)**.** One protomer of the dimer is shown in color reflecting the domains specified in (a), Sba1 was omitted for clarity. The N-terminal strand exchanges via hydrogen bonding with the other protomer, forming a N-terminal closed conformation **(c) Secondary structure representation of yeast Hsp82 nucleotide binding domain in complex with ADP** (PDB 1AM1). Shown in blue is the conformation of the lid that closes over the nucleotide binding pocket upon ATP binding.

The C-terminal domain is essential for the dimerization of a functional Hsp90 molecule (Minami et al., 1994). The crystallized HtpG C-terminal structure is a dimer of mixed α/β domain (Harris et al., 2004). The dimer interface is formed by a pair of helices at the C-terminal end of the domain packing together to create a four-helix bundle. An exposed and flexible amphipathic helix (HtpG residues 549-558) was suggested to play a role in client protein binding (Harris et al., 2004). Several reports provided evidence for a second putative ATP-binding site in the C-terminal domain of Hsp90 which is also the suggested binding site for the drugs novobiocin and *cis*-platin (Garnier et al., 2002; Marcu et al., 2000; Soti et al., 2002). All available structures cannot resolve the last 30 amino acids including the C-terminal MEEVD TPR domain-binding sequence in eukaryotic Hsp90s, because this region is largely disordered.

The chaperone function of Hsp90 is closely coupled to its ATPase activity. In the yeast Hsp90, the two N-terminal domains undergo conformational changes to become closely associated in the ATP bound state, but not in the apo or ADP-bound state. Together with the constitutive C-terminal dimerization, the Hsp90 dimer forms then a closed "molecular clamp" which is supposed to entrap client substrates (Prodromou et al., 2000).

The first view of the ATP-bound conformation of a full-length Hsp90 came from the co-crystal structure of yeast Hsp82 with the co-chaperone p23/Sba and the non-hydrolysable ATP analogue AMPPNP (Ali et al., 2006) (Fig. 1.4b). This closed structure could only be obtained when the charged flexible linker between N-and M-domain was deleted. The two molecules in the Hsp90 dimer twist around each other, interacting via a constitutive dimer interface at the C-terminus and a transient N-terminal dimerization via a strand-swap of the most N-terminal strand to the other protomer. This conformation is only possible by a large rearrangement of the ATP lid in the nucleotide binding pocket. As a second "switch", the catalytic loop of the MD remodels to form direct contacts between the catalytic Arg^{380} with the γ-phosphate of the bound nucleotide in the NBD to promote hydrolysis. Interestingly, the co-chaperone p23/Sba binds to both of these switches, the exposed surface of the lid and the catalytic residues of the middle domain, and thus stabilize the closed conformation and slows down the ATP hydrolysis.

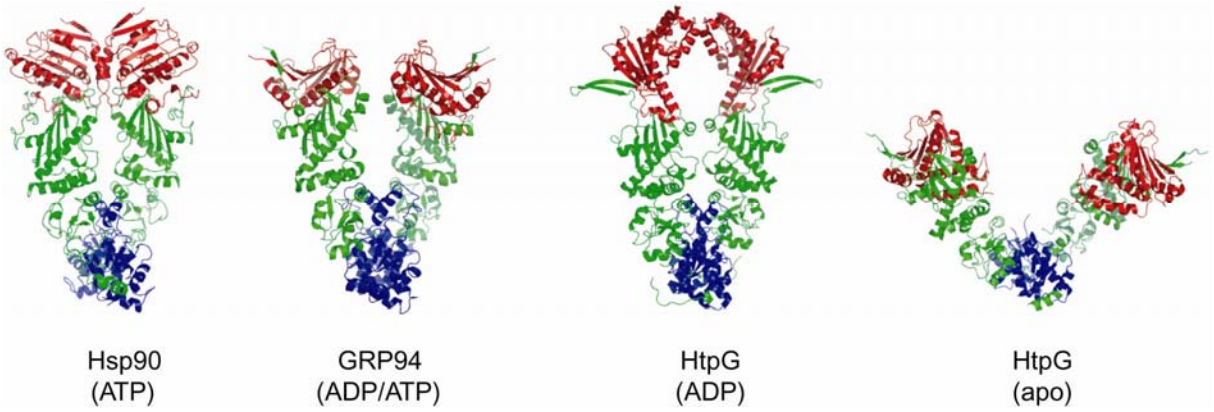

Fig. 1.5 Conformation of currently available full-length structures of Hsp90 and homologues. The closed N-terminally dimerized state is only observed in the ATP-bound conformation of yeast Hsp90 (PDB code 2CG9). GRP94 forms a open V-shaped dimer in either ADP or the ATP bound state (PDB code 2O1U). The prokaryotic Hsp90 homologue HtpG could be resolved in a flexible open *apo*-state (PDB code 2IOQ) and a compact ADP-state (PDB code 2IOP).

Crystal structures and negative stain electron micrographs of the intact *E. coli* HtpG reveal dramatic conformational changes upon nucleotide binding (Shiau et al., 2006). The *apo* HtpG structure has high conformational flexibility and forms an open V-shaped dimer (Fig. 1.5). In contrast, the ADP bound state appears to be more compact and is proposed to undergo large rigid body movements of the domains around two hinges to form a more twisted dimer with the N-terminal regions approached to each other. However, these conformations are strongly influenced by crystal lattice contacts (Fig. 1.5). The asymmetric unit of the ADP bound HtpG crystal contains a tetramer of two interlocked, inverted dimers and the biological relevance of this state is questionable. Recent full-length structures of the ER-resident Grp94 in complex with ADP or the ATP analogue AMPPNP revealed almost identical open twisted V-shaped conformations (Dollins et al., 2007) (Fig. 1.5). In contrast to the yeast Hsp90, the ATP-bound state seems to populate the more open N-terminal state which is reflected in a slower uncoupled ATP hydrolysis rate. The existence of the fixed closed conformation in the ATP-bound state may also be dependent on the presence of co-chaperones and the presence of the flexible charged linker which is deleted in all crystallized constructs.

1.2.2.3 Hsp90 chaperone cycle

Hsp90 function in client activation and maturation is highly dependent on binding and hydrolysis of ATP (Obermann et al., 1998; Panaretou et al., 1998) which drives a dynamic conformational cycle that involves interactions with the Hsp70 system and an increasing number of co-chaperones (Fig. 1.6).

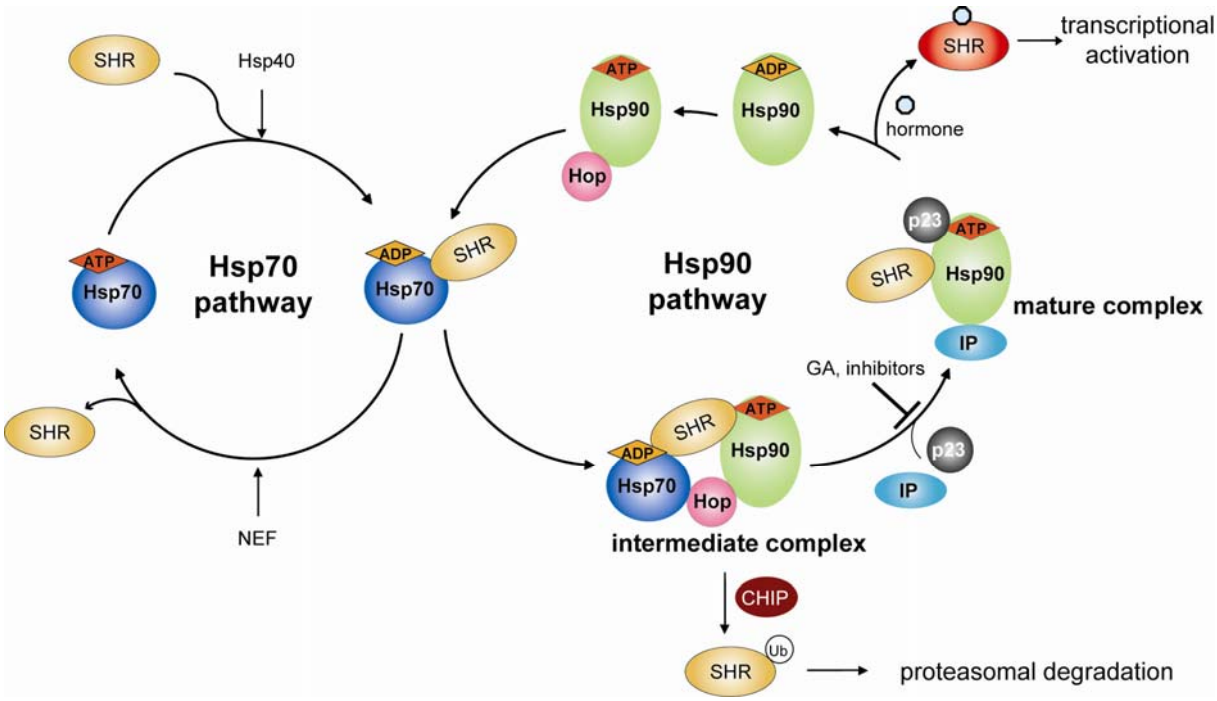

Fig. 1.6 Hsp70/Hsp90 chaperone cycle postulated for steroid hormone receptor (SHR) as a client. SHR first interacts with Hsp40 and Hsp70 in an early complex and is then transferred via the adaptor co-chaperone Hop to Hsp90 to form an intermediate complex. As a next step, the co-chaperones p23 and immunophilins lead to dissociation of Hop and Hsp70 and build the mature Hsp90 complex. Upon ATP hydrolysis of Hsp90, SHR becomes competent for hormone binding and is than able to activate gene transcription in the nucleus. Unproductive folding or maturation of the client leads to re-entering in the cycle or to substrate ubiquitination mediated by the E3 ligase CHIP and targeting to the ubiquitin-proteasome pathway. Competitive Hsp90 inhibitors like geldanamycin (GA) block the formation of the mature complex and cause degradation of the client controlled by CHIP.

Hsp90 cooperates in its chaperone cycle with co-chaperones including Cdc37, p23, Aha1, and the TPR containing proteins Hop (Hsp70-Hsp90-organizing protein), the phosphatase PP5, and the immunophilins FKBP51, FKBP52 and Cyp40. Some of these cochaperones like Cdc37 and Hop are important for client binding to Hsp90 respectively transfer from Hsp70 to Hsp90. Others like Aha1 and p23 regulate the ATPase cycle of Hsp90. The TPR containing proteins compete for binding to the C-terminal EEVD motif of Hsp90 thereby influencing progression through the chaperone cycle (Mayer et al., 2002; Pearl and Prodromou, 2001; Pratt and Toft, 2003).

Mostly through studies using steroid hormone receptors (SHR) as clients a progressive chaperone cycle for Hsp90 was established (Pratt and Toft, 1997; Smith, 2000). The unliganded hormone receptor first interacts with the Hsp70 chaperone and its J-domain cochaperone in an ATP hydrolysis dependent step (Hernandez et al., 2002). Coordinated by the TPR protein Hop, which binds to the C-termini of Hsp70 and Hsp90 at the same time, an intermediate Hsp90-Hsp70-client complex is formed. Hop and Hsp70 are replaced by p23 and immunophilins to form the mature complex. This step depends on ATP binding to Hsp90. The mature complex leads to an active SHR which is competent for hormone binding. Hormone binding results in the release of the SHR and transcriptional activation of target genes in the nucleus. In the absence of hormone, the mature complex decays with a half-life of about 5 min (Smith and Toft, 1993) in an ATP hydrolysis dependent step (Young and Hartl, 2000). The released client reenters the cycle by binding to Hsp70. Other clients of the Hsp90 system depend on additional cochaperones like Cdc37, which is important for protein kinases. If maturation of client substrates cannot proceed through the chaperone cycle due to misfolding or blockage of Hsp90 by inhibitors, the client accumulates in the intermediate complex and is targeted to degradation via the ubiquitin-proteasome pathway by the E3-ubiquitin ligase CHIP.

The kinetics of the ATPase cycle of yeast Hsp90, human Hsp90, Grp94 and TRAP1 has been analyzed in more detail in biochemical and structural studies (Frey et al., 2007; Leskovar et al., 2008; McLaughlin et al., 2002; Weikl et al., 2000). Based on the structurally related GHKL-ATPases DNA gyrase B and MutL the ATPase cycle of Hsp90 is proposed to involve several conformational changes including ATP-dependent docking of NBD and MD of the same monomer and a dimerization of the two NBDs in the Hsp90 dimer resulting in a ring-shaped “closed” structure (Fig. 1.5) (Ali et al., 2006; Pearl and Prodromou, 2001). Evidence for such conformational changes was also found in the kinetics of ATP hydrolysis of wild-type and mutant proteins in yeast Hsp90 but is still disputed for the human homologue (McLaughlin et al., 2004; Richter et al., 2001). NMR studies of wild-type and truncated NBDs in the absence and presence of different nucleotides and inhibitors suggested ligand-induced conformational changes in this domain and changes linked to the ATPase cycle (Dehner et al., 2003; Richter et al., 2006). The slow hydrolysis rate of Hsp90 (1 ATP/min for yeast Hsp90 and 0.05 ATP/min for human Hsp90) suggest the slow formation of the dimeric state of N-terminal domains prior to hydrolysis, presenting the rate-limiting step in the cycle. The Hsp90 ATPase activity is further regulated by the transient association with the various co-chaperones. The co-chaperone p23/Sba1 inhibits the ATPase activity, arresting the Hsp90

cycle to trap client proteins (McLaughlin et al., 2006; Richter et al., 2004; Siligardi et al., 2002), while the partner protein Aha1 strongly stimulates the ATPase activity (Panaretou et al., 2002).

How the coordinated ATPase cycle of Hsp90 is coupled to client activation or processing is poorly understood. Client binding seems to stimulate the Hsp90 ATPase activity significantly, as shown for the ligand binding domain of the glucocorticoid receptor (McLaughlin et al., 2002). However, the binding sites and the effects of the Hsp90 interaction to client proteins remain unknown. The first glimpse of Hsp90 in a complex with a client protein delivered an EM structure of Hsp90 bound to the protein kinase Cdk4 together with the kinase-specific cochaperone Cdc37 (Vaughan et al., 2006). An electron-micrographic reconstruction of this complex revealed an interaction of the Cdk4 lobes to the NBD and the MD of only one Hsp90 protomer.

1.2.2.4 Hsp90 inhibitors and cancer treatment

The importance of ATP hydrolysis in Hsp90 became evident by the discovery of the ansamycin antibiotic geldanamycin (Whitesell et al., 1994) and the macrolide radicicol (Schulte et al., 1998) (Fig. 1.7). Challenging cells with these natural product inhibitors resulted in a variety of phenotypes caused by the impaired cellular maturation of various Hsp90 clients. Crystal structures demonstrated clearly that geldanamycin (GA) and radicicol are competitive inhibitors that act by selectively docking in the N-terminal nucleotide binding site (Roe et al., 1999; Stebbins et al., 1997) of Hsp90, thereby inhibiting the intrinsic ATPase activity and thus blocking the formation of the mature client complex. These client proteins are then targeted for ubiqitination and proteasomal degradation. The finding of Hsp90 inhibitors led to an explosion of discoveries in the Hsp90 pathway which identified many client proteins and co-chaperones. Many of these client proteins are involved in oncogenic processes including all hallmarks of cancer (Neckers, 2007), making Hsp90 a potential drug target for anti-cancer treatment (Whitesell and Lindquist, 2005). Clinical trials with derivatives of GA and newly developed small-molecule inhibitors are ongoing.

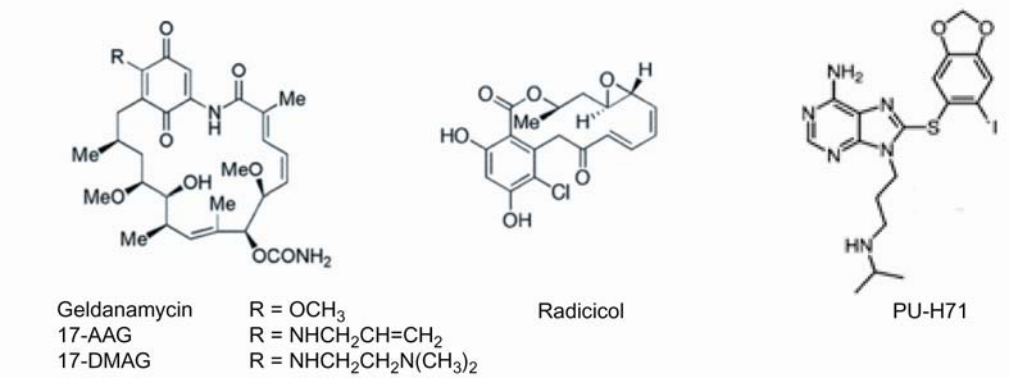

Fig. 1.7 Examples of the three main classes of Hsp90 inhibitors. Geldanamycin derivatives 17-AAG and 17-DMAG have entered clinical trials. GA and the water-soluble purine-scaffold inhibitor PU-H71 were used in this study.

Geldanamycin (GA) as a benzoquinone ansamycin binds to the human Hsp90 nucleotide binding pocket in an unusual C-shaped conformation via strong hydrophobic van-der-Waals interactions and via a direct hydrogen bond between the Asp^{93} (in yeast Asp^{79}) and the carbamate group of geldanamycin (Stebbins et al., 1997) and indirect hydrogen bonding to water molecules. Although GA has an affinity *in vitro* in the low micromolar range, it was found that GA preferentially accumulates in cancer cells (Chiosis et al., 2003a; Kamal et al., 2003), exhibiting low nanomolar anti-proliferative activity *in vivo*. The explanation for these differences is still under debate. One explanation for the preferential binding of GA to Hsp90 in cancer cells is that more Hsp90 is engaged in active multi-chaperone complexes which might have a higher affinity for GA than un-complexed Hsp90 in normal cells (Kamal et al., 2003). Recent data suggest two alternative mechanisms for the *in vivo* efficiency of geldanamycin. The first suggests a reducing event of the quinone moiety in vivo which increases the binding affinity of GA (Maroney et al., 2006). In the second mechanism, Hsp90 was suggested to undergo a slow conformational change upon binding to GA, leading to an increased affinity for tumour-specific Hsp90 (Gooljarsingh et al., 2006). While geldanamycin has limitations for clinical development including limited oral bioavailability, low solubility and liver toxicity, the semisynthetic analogue 17-allylaminogeldanamycin (17-AAG) and the more soluble 17-dimethylaminoethylamino-demethoxygeldanamycin (17-DMAG) have displayed promising activity in clinical trials (Pearl et al., 2008).

Structure-function based design led to development of a series of synthetic small-molecule Hsp90 inhibitors with markedly improved drug-like properties. The first of these were the purin-scaffold inhibitors designed by Chiosis and co-workers (Chiosis et al., 2003b; Solit and Chiosis, 2008) which combine the structure of the adenine moiety of ADP and the C-shaped conformation of the natural inhibitors geldanamycin. Co-crystal structures with the first

generation purin-scaffold inhibitor PU3 showed binding like ADP, but the compounds induced a conformational change in the ATP binding site, opening a lipophilic pocket in a unpredicted way (Wright et al., 2004). Subsequent studies led to the design of a range of potent and soluble purine-scaffold inhibitors (e.g. PU-H71) with good activities in animal models (He et al., 2006; Zhang et al., 2006)(Fig. 1.7).

Workman and colleagues used a high-throughput screen based on inhibition of Hsp90 ATPase activity to identify 3,4-diarylpyrazoles as a novel class of Hsp90 inhibitors (Cheung et al., 2005; Dymock et al., 2005). The bacterial gyrase antibiotic novobiocin, a member of the coumeromycin family, and *cis*-platin have been shown to be potent Hsp90 inhibitors, however differently acting by binding to the C-terminus of Hsp90 (Marcu et al., 2000). The biochemical basis for the inhibitory effect of novobiocin is unclear.

1.2.3 TPR Co-chaperones

The majority of Hsp90 co-chaperones interact with the Hsp90 C-terminus through tetratricopeptide (TPR) repeat motifs (Smith, 2004). TPR repeats are degenerated sequence motifs of 34 amino acids that often occur repetitively and mediate protein-protein interactions found in all kingdoms of life (D'Andrea and Regan, 2003). Most of the investigated TPR domains contain 3.5 tetratricopeptide repeats each forming a conserved helix-turn-helix motif (Das et al., 1998). The best characterized TPR co-chaperones are the Hsp70/Hsp90 adaptor protein Hop, the proline isomerases FKBP51 and FKBP52, protein phosphatase 5 (PP5) and the E3 ubiquitin ligase CHIP. The structure and function of two TPR containing chaperones, Hop and CHIP, will be described below.

1.2.3.1 Hsp70/Hsp90 organizing protein (Hop)

The dimeric co-chaperone Hop (Sti1p in yeast) has been identified by specific interaction with Hsp90-containing steroid hormone receptor complexes (Smith and Toft, 1993). The 60 kDa protein consists of three TPR domains with three tandem repeats each, and two domains which are enriched in aspartate-proline repeats (DP1 and DP2) (Fig. 1.8a). Based on structural and genetic data it is known that the N-terminal TPR1 domain binds specifically the Hsp70 C-terminus, and TPR2a binds to Hsp90 but needs the cooperation with TPR2b (Brinker et al., 2002; Scheufler et al., 2000) (Fig. 1.8b). The function of the DP regions is not clear yet. The ability to bind both the chaperones simultaneously enables Hop to function as an adaptor connecting Hsp70-client complexes with Hsp90 and mediate the transfer of substrates on Hsp90 to form an intermediate complex (Pratt and Toft, 2003; Wegele et al.,

2006). In addition to binding to their C-termini, Hop/Sti1 can influence the ATPase activity of the chaperones, by inhibiting the ATPase activity of yeast Hsp90 (Prodromou et al., 1999; Richter et al., 2003) but stimulating the ATPase of yeast Hsp70 protein Ssa1 (Wegele et al., 2003). None of these effects are observed for the human Hsp90 system indicating that the regulation of the Hsp90 system underwent evolutionary changes. The cellular localization of the mainly cytosolic Hop is posttranslationally controlled by phoshorylation in vivo. Phosphorylation promotes nuclear localization whereas dephosphorylation mediates cytoplasmic retention (Daniel et al., 2008; Longshaw et al., 2004).

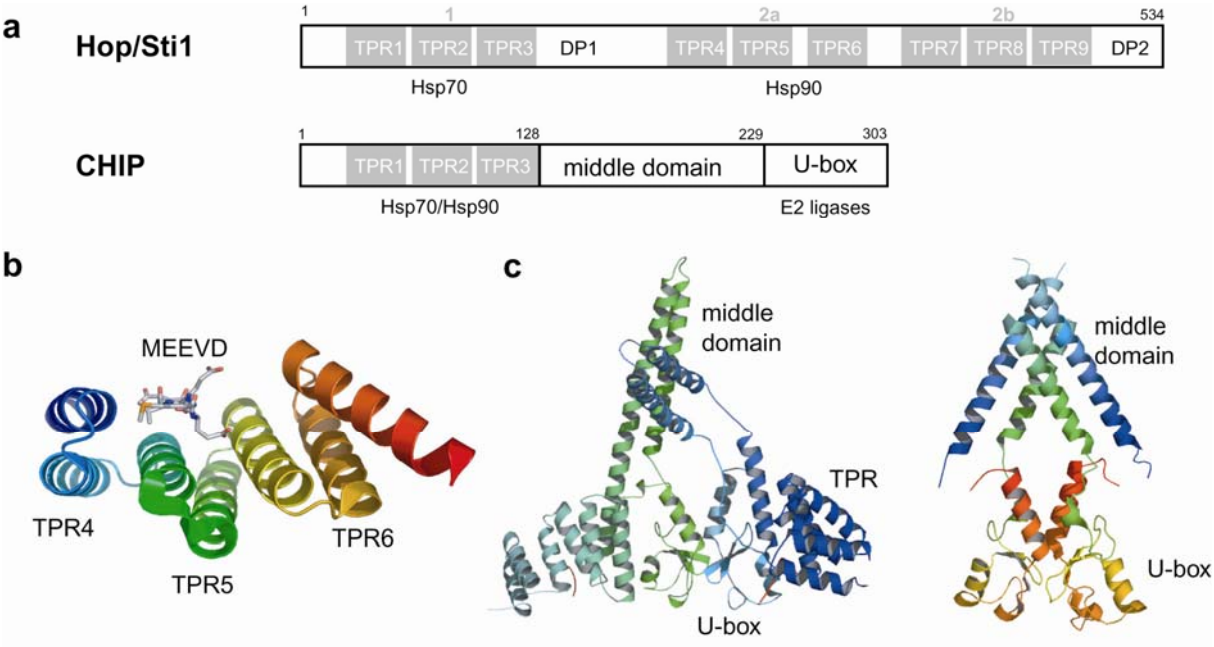

Fig. 1.8 Domain organization and cystal structures of the TPR-containing co-chaperones Hop/Sti1 and CHIP. (**a**) 60 kDa adaptor protein Hop contains three TPR domains with three TPR repeats each, TPR1 binds exclusively Hsp70, while TPR2a/b bind Hsp90. 35 kDa protein CHIP has an N-terminal TPR domain that binds both Hsp70 and Hsp90, and a C-terminal U-box domain that cooperates with E2 ligases in substrate ubiquitylation. (**b**) Crystal structure of the middle TPR domain 2a of Hop in complex with the Hsp90-pentapeptide MEEVD shown in stick representation (PDB code 1ELR). One TPR repeat consists of a helix-turn-helix motif. (**c**) Crystal structures of CHIP showing different homodimeric assemblies. Mouse CHIP dimer (PDB code 2C2L, left) complexed to MEEVD-peptide was found to form an asymmetric dimer, zebrafish CHIP lacking the TPR domain (PDB code 2F42, right) crystallized as a symmetric dimer.

1.2.3.2 The E3 ubiquitin-ligase CHIP

The C-terminus of Hsc70-interacting protein (CHIP) is a co-chaperone that links Hsc/Hsp70 and Hsp90 to protein degradation as a complementary function to protein stabilization and refolding in protein quality control (Arndt et al., 2007). CHIP is a multidomain protein composed of an N-terminal TPR domain, a middle domain and a U-box domain which is

typical for a RING-finger type E3 ligase involved in the ubiquitination cascade (Pickart, 2001) (Fig. 1.8a). Unlike the HECT domain E3 ligases which play an active role in ubiquitination, E3's containing RING domains (zinc-finger really new interesting gene) enable the direct transfer of ubiquitin chains from the E2 ubiquitin-conjugating enzyme to the substrate lysine side chain, serving as a scaffold. The U-box of CHIP selectively cooperates with members of the UbcH4 and UbcH5 family that are stress-activated (Demand et al., 2001; Jentsch et al., 1990; Jiang et al., 2001; Murata et al., 2001) and possess a conserved Ser-Pro-Ala sequence that is required for interaction with CHIP. These canonical ubiquitin-conjugating enzymes link polyubiquitin chains via the Lys^{48} to the mono-ubiquitinated substrate to form a typical proteasomal degradation signal. Recently, the heterodimeric E2 complex Ubc13-Uev1a was found to interact to CHIP and could be crystallized as a complex (Zhang et al., 2005). Ubc13-Uev1a forms an E2-conjugating enzyme that facilitates non-canonical Lys^{63} polyubiquitination which seems not to play a role as protein degradation signal but rather modifies the activity of substrates.

Full-length mouse CHIP (23-303) could be crystallized in complex with a C-terminal Hsp90 peptide and revealed a dimeric assembly with an asymmetric arrangement, showing one protomer with an elongated helix and the other protomer with a partially unfolded helical hairpin within the middle domain (Zhang et al., 2005) (Fig. 1.8c). The middle domain harbours the most critical interfaces for dimerization which was shown to be important for CHIP's function in ubiquitination (Nikolay et al., 2004). In contrast to Hop/Sti1, CHIP binds both C-termini of the chaperones unselectively to the same TPR. The crystal structure of the CHIP-peptide complex revealed that the peptide is bound in a curled conformation in which only the common (M/I)EEVD sequence is in contact with the TPR domain, allowing to bind different types of chaperones. A recent crystal structure of zebrafish CHIP lacking the TPR domain differs substantially from the mouse CHIP structure, showing a symmetric dimer assembly with elongated helices in the middle domains (Xu et al., 2006).

Overproduction of CHIP *in vivo* targets a diverse group of different chaperone clients for degradation (Arndt et al., 2007). These include members of the steroid hormone receptor family, protein kinases (e.g. the oncogenic receptor tyrosine kinase ErbB2) and members of the Smad family of TGF-β signal transducers and the tumour suppressor protein p53. Another important class of substrates are aggregation-prone proteins implicated in various neurodegenerative diseases and pathologies that are recognized by chaperones during protein quality control. Among these substrates are the cystic fibrosis transmembrane-conductance regulator (CFTR), hyperphosphorylated tau protein (Alzheimer's disease), α-synuclein

(Parkinson's disease) and the polyglutamine-repeat protein huntingtin. Overexpression of CHIP has a significant protective effect on the formation of aggregates and promotes the clearance of aggregates.

Nevertheless, how CHIP's decision making process between chaperone folding and targeting to proteasomal degradation is regulated is still unclear.

1.3 Biomolecular Mass Spectrometry

Mass spectrometry (MS) has become an indispensable analytical tool in many areas of science and technology. In mass spectrometric analyses, the mass-to-charge ratios (m/z) of gas-phase ions are determined. The technique was first introduced in the pioneering work of Thomson (Thomson, 1913), and has since then been an important tool for the discovery of elements and isotopes, the exact determination of atomic and molecular weights and the investigation of chemical reaction mechanisms. By definition, a mass spectrometer consists of three main parts: (1) an ion source which volatizes and ionizes the analyte into the gas-phase, (2) a mass analyzer and (3) an ion detector that registers the number of ions at each m/z value.

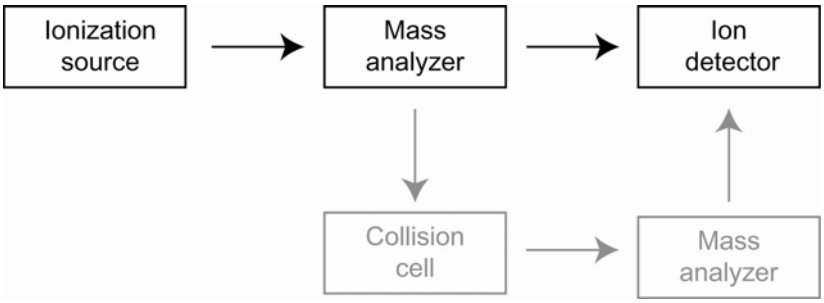

Fig. 1.9 Principal components of a mass spectrometer. Elements shown in gray are used in tandem MS measurements to generate fragment ion spectra.

With the introduction of "soft ionization" techniques of matrix-assisted laser desorption/ ionization (MALDI) and electrospray ionization (ESI), mass spectrometry has become a powerful tool for the study of intact biomolecules, especially in protein and peptide analysis, but also in lipid, sugar and oligonucleotide analytics.

For MALDI-MS analysis, the analyte is co-crystallized with an UV-absorbing compound, referred to as the 'matrix' (e.g. 4-hydroxy-α-cyanocinnamic acid, HCCA), and applied to a

target plate (Kussmann and Roepstorff, 2000). Ionization and vaporization of the embedded analyte is achieved by a pulse of a UV laser under vacuum. This results in the formation of predominantely singly charged protonated molecular ions (MH^+) by mechanisms which are still poorly understood (Karas and Kruger, 2003; Zenobi and Knochenmuss, 1999). Laser desorption is an efficient process for producing gaseous ions and tolerates varying levels of contaminants, e.g. salts. MALDI-MS has the advantage of easy and fast sample preparation, which allows automation and a high sensitivity, but can have the problem of non-reproducibility of matrix conditions and the limited possibility of separating different analytes.

In the electrospray ionization (ESI) process, the polar analyte in a volatile solvent is delivered through a small capillary which is held under a high electric potential. The voltage applied to the tip generates an aerosol of charged analyte-containing droplets. Solvent evaporation leads to formation of smaller droplets driven by repulsive Coulombic forces between charged molecules until free ions are present and extracted to the high-vaccum of the mass analyzer. The exact mechanism of ion formation, whether it be by ion evaporation (ion-evaporation model) (Iribarne and Thomson, 1976; Thomson and Iribarne, 1979) or by complete solvent removal (charge-residue model) (Dole et al., 1968; Schmelzeisen-Redeker et al., 1989) from the charged droplet is under debate.

In contrast to MALDI, electrospray generates ions at atmospheric pressure and results in the formation of multiple charged analyte ions and thus can produce more complicated spectra. Since ESI is a continuous process, it can be coupled easily to high-performance liquid-chromatography (HPLC) systems. ESI is a concentration- rather than a mass-dependent process and improved sensitivity can be obtained for high-concentration samples with low-volume. This led to the development of Micro- (100-1 µl/min) and Nano-flow (100-1 nl/min) systems with excellent sensitivity which are often used for biomolecular MS (Wilm and Mann, 1996).

Mass analyzers are the central part of the MS technology. Four basic types of mass analyzers are common in biological MS: ion trap, time-of-flight (TOF), quadrupole and Fourier transform ion cyclotron (FT-MS) analyzers. All these analyzers are different in design and performance in terms of the key parameters sensitivity, resolution, mass accuracy and the ability to generate fragment spectra (tandem MS or MS/MS) (Aebersold and Mann, 2003).

The mass spectrometer mainly used in this work was an ESI-quadrupole-TOF instrument (Fig. 1.10). In this setup, the ions are first selected in a quadrupole mass filter by applying a

particular sinusoidal potential (a combination of DC voltages and radiofrequency RF voltages) on four diagonally connected electrodes. The ions which are transmitted on a stable trajectory pass into a second quadrupole, the collision cell, and can herein be fragmented into smaller ions by collision-induced dissociation (CID) with an inert collision gas (argon or nitrogen). The mass of the ions generated in such an MS/MS experiment is then measured by the combined orthogonal time-of-flight (TOF) analyser. In the TOF instrument, the ions of different m/z are dispersed in time during their flight along a field-free drift path of known length. An electrostatic reflector acts as an ion mirror that focuses ions of different kinetic energies in time and improves the mass resolution (Mamyrin et al., 1973).

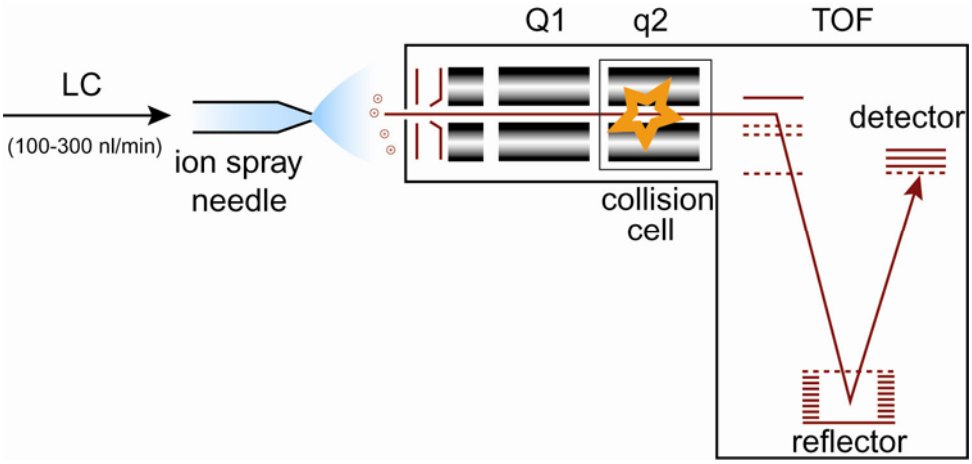

Fig. 1.10 Setup of a ESI-quadrupol-TOF (Q-TOF) hybrid mass spectrometer coupled to LC-electrospray source. Ions generated in the electrospray process are transmitted and filtered through are quadrupole (Q1) into a collision cell (q2) which can fragment the parent ion by CID (MS/MS). The parent and fragment ions are then analyzed in an orthogonal time-of-flight (TOF) analyzer and detected by a electron multiplier.

The ion detector is usually a secondary electron multiplier (SEM) consisting of metal dynodes. In TOF type instruments the ion beam is not as focused and several miniaturized electron multipliers, so-called microchannel plates, are used to improve the detection.

A key application of ESI and MALDI mass spectrometry is the protein identification and quantification for proteome research. Mass spectrometric protein identification usually involves the analysis of peptides produced by digesting the protein mixture of interest or a gel band with a proteolytic enzyme, e.g. trypsin (Steen and Mann, 2004). These peptides are introduced into a one-dimensonal (LC) or multi-dimensional (LC/LC) liquid-chromatography system and eluted into an ESI tandem mass spectrometer. After generating a mass spectrum of the eluting peptides, parent peptide ions are isolated and then fragmented by CID in the collision cell. The mass-to-charge ratios of the resultant fragments produce a MS/MS spectrum of the parent peptide ion which can reveal the amino acid sequence of the precursor ion. Low-energy CID usually leads to the fragmentation of peptides on the amide backbone,

resulting mainly in ions called b-ions when the charge is retained by the N-terminus or y-ions when the charge is retained by the carboxy-terminus (Biemann, 1992; Roepstorff and Fohlman, 1984).

The final step of a proteomic MS experiment is the data analysis of the obtained mass spectra. One approach for identifying the protein is the peptide mass fingerprint (PMF) which compares specifically proteolytic cleaved peptides masses with in silico calculated masses of the theoretical digests of protein sequences in databases (Henzel et al., 2003). Two different methods using MS/MS data from peptides are currently applied for protein identification. One approach uses experimental tandem mass spectra and compares the data obtained by MS/MS with in silico generated product ion spectra of theoretical proteolytic peptides of all the proteins contained in a database. In these cases, the significance of the protein identification is either based on autocorrelation (SEQUEST algorithm, (Eng et al., 1994)) or on probability-based matching (MASCOT, (Perkins et al., 1999)). The other approach is the peptide sequence tag algorithm which makes use of a short partial sequence information, the total mass of the peptide and the protease specificity (Mann and Wilm, 1994).

Mass spectrometry has become the dominant method for proteomics research including the study of protein function, protein-protein interactions, posttranslational modifications and the quantification of proteins and peptides in complex samples (Aebersold and Mann, 2003; Cravatt et al., 2007; Domon and Aebersold, 2006). In addition, MS has developed to an important technique to investigate protein structure and conformation. It can be used to determine the stoichiometry, the assembly and the dynamics of macromolecular complexes (Hernandez and Robinson, 2007; Sharon and Robinson, 2007) or to identify protein-protein interaction sites after chemical crosslinking and proteolytic digestion (Vasilescu and Figeys, 2006). In this study, mass spectrometry was used to probe protein conformation and dynamics in combination with amide hydrogen exchange experiments.

1.4 Amide Hydrogen Exchange

1.4.1 Hydrogen exchange mechanism

Amide hydrogen exchange (HX) has become a valuable tool for understanding protein dynamics and structure. Although conventionally used with NMR spectroscopy, mass spectrometry has developed as an important technique to monitor hydrogen exchange in proteins. Hydrogen atoms in proteins in NH-, OH- and SH- groups are "labile" and in continuous exchange with the solvent. These protons can be exchanged with deuterium (^{2}H) under suitable conditions (Fig. 1.11a). Amide hydrogens of the polypeptide linkages are of particular importance because they exchange in a measureable kinetics (100 ms-10 s) at pD 7.0 while the hydrogens attached to functional groups in side chains and on the ends of the protein exchange too rapidly to be measured. An amide proton can only undergo exchange if it is (1) accessible to the solvent and (2) if it is not involved in hydrogen bonding. Thus, the rate at which backbone amide hydrogens exchange with solvent deuterons is highly dependent on the protein conformation and secondary structure.

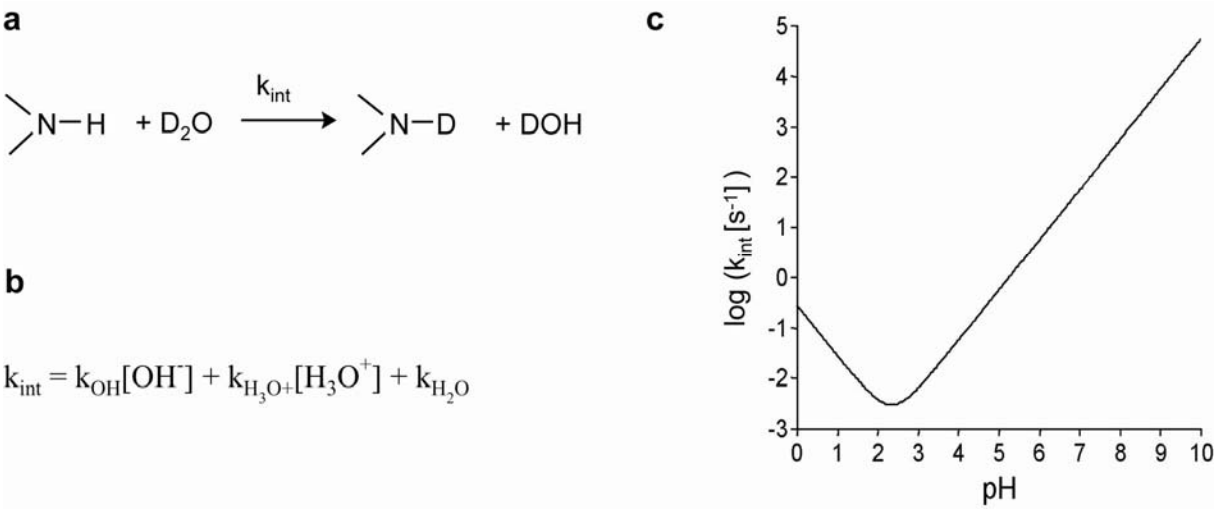

Fig. 1.11 Mechanism of intrinsic hydrogen exchange. (a) Principal reaction of deuterium transfer from D_2O to an amide with the intrinsical chemical exchange rate (k_{int}) **(b)** term that describes the pH dependence of the intrinsical exchange rate constant k_{int} **(c)** rate constants for amide hydrogen exchange in an unstructured peptide as a function of pH. Results were calculated for polyalanine at 25°C using equation in (b) and values of k_{OH^-}, $k_{H_3O^+}$, k_{H_2O} taken from (Bai et al., 1993)

The intrinsical exchange rate constant k_{int} describes the exchange rate for an amide proton in an unfolded, freely exposed peptide (Fig. 1.11b). Since the deuterium exchange is a base- and acid-catalyzed process, k_{int} is dependent on the pH. Fig. 1.11c illustrates the relationship between the exchange rate constants and the pH for a given peptide. For each change in pH

unit k_{int} changes one order of magnitude. The minimum exchange rate is at pH 2.5 to 3. At physiological pH, the exchange is predominantely base-catalyzed. The hydrogen exchange rate is also a temperature-dependent process following the Arrhenius equation. As a consequence, the rate of base-catalyzed hydrogen exchange can be further decreased by one order of magnitude when the temperature is lowered from 25°C to 0°C. In addition to their pH and temperature sensitivity, amide proton exchange rates are also affected by steric and inductive effects of the amino acid neighbours. Using model peptides, Bai et al. could quantitatively assess the neighbouring side-chain effects on the exchange rate. This NMR study enabled the calculation of intrinsic exchange rates in peptides based on the amino acid sequence.

In folded proteins, amide protons are protected due to hydrogen bonding or burial in the native structure and thus have much slower exchange rates than unfolded polypeptides. In a fully folded, native protein, amide hydrogen exchange rates (k_{ex}) may be eight orders of magnitudes smaller than the rates in the unfolded, random structure (Englander and Kallenbach, 1983). Hydrogens may exchange directly from solvent at unprotected amides or by reversible protein unfolding (Kaltashov and Eyles, 2002). As a result, the observed exchange rate k_{ex} is determined by both reactions. In a commonly accepted model, Linderstrøm-Lang proposed a two-state situation in which protected amide hydrogens can only exchange after a closed-to-open transition (Hvidt and Nielsen, 1966; Linderstrøm-Lang, 1956).

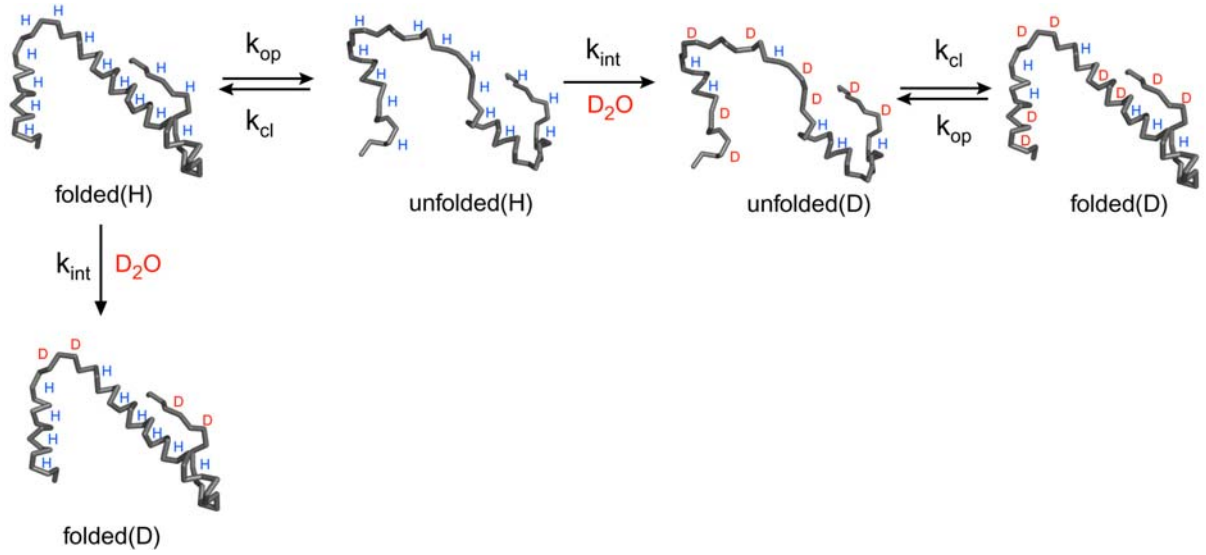

Fig. 1.12 Model of hydrogen exchange in proteins according to Linderstrøm-Lang.

Here, k_{op} and k_{cl} are the kinetic rate constants for the unfolding (opening) and refolding (closing) reactions, respectively. Exchange takes place only after opening, which breaks intramolecular hydrogen bonds, thereby exposing amide hydrogens to D_2O in the medium. This step is irreversible due to a high excess of solvent D_2O and its rate is identical with the intrinsical chemical exchange rate k_{int} from unstructured peptides which can be calculated (Bai et al., 1993).

Under steady-state conditions, the experimentally measured exchange rate constant k_{ex} can be defined as:

$$k_{ex} = \frac{k_{op}k_{\text{int}}}{k_{op} + k_{cl} + k_{\text{int}}} \approx \frac{k_{op}k_{\text{int}}}{k_{cl} + k_{\text{int}}}$$

The simplication is based on the assumption that the refolding for native proteins is much faster than the opening (k_{cl}>>k_{op}).

There are two limiting cases for this equation. Under EX2 (bimolecular exchange) conditions, the closing reaction is much faster than the intrinsic chemical exchange (k_{cl} >> k_{int}) and most sites must visit many times the open conformation before they undergo exchange. The overall exchange rate is given by

(EX2) $$k_{ex} = \frac{k_{op}k_{\text{int}}}{k_{cl}} = K_{op}k_{\text{int}} \quad , \; K_{op} = \frac{k_{op}}{k_{cl}}$$

where K_{op} is the equilibrium constant for the unfolding (opening) reaction. The free energy of stabilization of the unfolding process can then be calculated as

$$\Delta G_{HX} = -RT \ln K_{op} = -RT \ln\left(\frac{k_{ex}}{k_{\text{int}}}\right)$$

Under EX1 conditions (monomolecular exchange), the closing rate is much slower than the intrinsical chemical exchange rate (k_{cl} << k_{int}) and the experimental exchange rate correlates with the opening rate as follows

(EX1) $$k_{ex} = k_{op}$$

As a result, the EX1 exchange rate is a direct measure of the rate of protein unfolding and is often referred as correlated exchange (Hvidt and Nielsen, 1966). While most protein amides exchange under physiological conditions via the EX2 mechanism, EX1 is usually observed under destabilizing conditions like in the presence of chemical denaturants or extreme pH. Some proteins may contain regions that undergo EX1 and EX2 kinetics simultaneously.

1.4.2 Amide hydrogen exchange and mass spectrometry (HX-MS)

Traditionally, HX has been measured with multidimensional NMR spectroscopy to study protein dynamics (Bougault et al., 2004; Dempsey, 2001). In NMR experiments, the exchange rates of individual amides can be studied, but the method requires high concentrations of sample protein and is usually limited to proteins smaller than approximately 30 kDa. HX coupled to MS has become a powerful new tool to monitor protein dynamics and conformational changes (Hoofnagle et al., 2003; Kaltashov and Eyles, 2002; Konermann and Simmons, 2003; Wales and Engen, 2006). Since the mass difference between the isotopes hydrogen (^{1}H) and deuterium (^{2}H) is 1 Da, changes in deuteron incorporation in a protein can be detected by mass differences in MS. In contrast to NMR, MS data are not averaged over all molecules in the sample and allows the monitoring of the HX behaviour of co-existing species. Further advantages of the HX-MS technique over NMR are the low limits of detection, small sample requirement, the limitless mass range for larger proteins and the ability to monitor individual peptides and proteins in a mixture. ESI-MS has become the most commonly used ionization method in HX studies because of its coupling to HPLC, but there is also an increasing number of reports using MALDI for amide hydrogen exchange experiments (Nazabal et al., 2003).

In a typical HX experiment, undeuterated proteins can be labelled with deuterium by dilution in a D_2O buffer, or vice versa. There are two ways of HX labelling methods: continuous labelling and pulse-labelling (Deng et al., 1999).

In continuous labelling experiments, the protein is incubated for different time intervals in D_2O and the isotope exchange is monitored as a function of exchange time providing information on the conformational dynamics of a protein under equilibrium conditions. In a native continuous labelling protocols established by Smith and coworkers (Zhang and Smith, 1993), the exchange reaction is performed at physiological conditions for certain amount of time and subsequently quenched by lowering the pH to 2.5 and the temperature to 0 °C, which decreases HX rates at the peptide amide linkages by up to five orders of magnitude. Under these quench conditions, the half-life for amide hydrogen exchange is 30-120 min, giving enough time to analyze the sample by a reversed-phase HPLC coupled to ESI-MS without substantial loss of deuterons on the amides. The exchange behaviour of a protein can thus be measured on a global level by determining deuteron incorporation to the full-length mass. Information on the slow or fast exchanging regions in the protein can be obtained by proteolytic digestion of the deuterated protein and MS analysis of the resulting peptides.

Pepsin is the most commonly used acidic protease providing peptides with a spatial resolution of 4-15 amino acids. One weakness of the procedure is a continuous loss of deuterium during HPLC analysis in aqueous buffers, known as “back-exchange” which can be reduced by fast sample processing and low temperatures (Feng et al., 2006).

In isotopic pulse-labelling experiments, a population of protein molecules is induced to undergo a conformational change by addition of a pertubing agent or a ligand and is then exposed to deuterium for a very short time (pulse). The resulting deuterium levels indicate the population of folded and unfolded molecules and thus can reveal protein folding mechanisms.

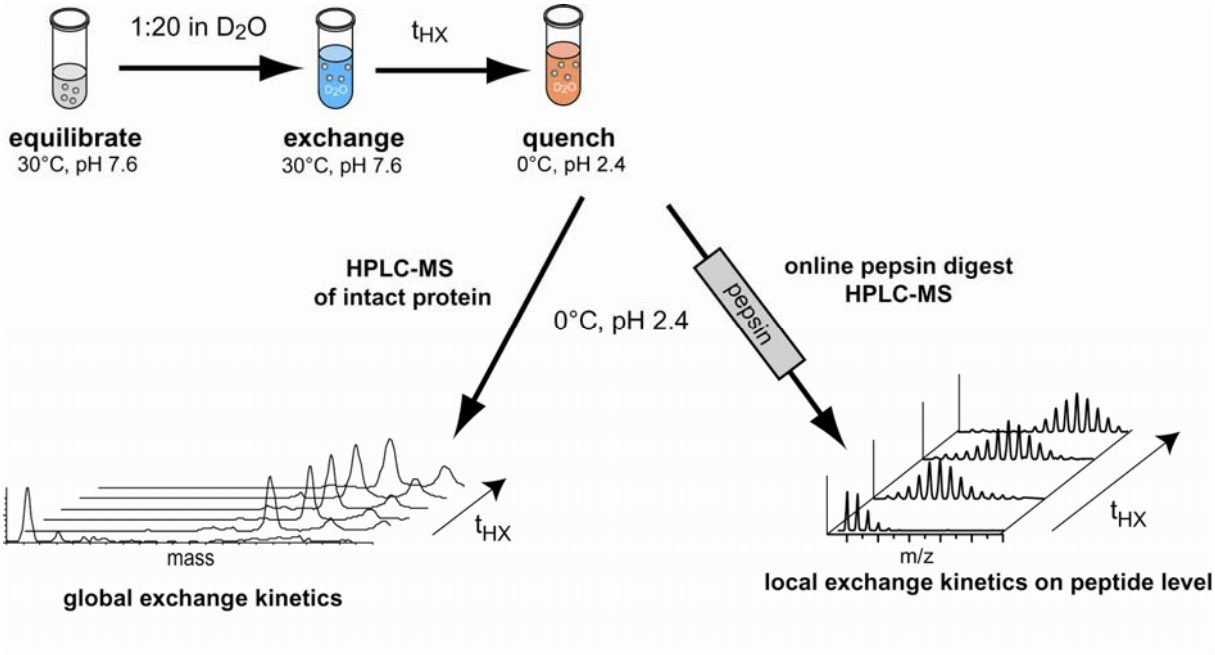

Fig. 1.13 Experimental setup of an amide hydrogen exchange experiment combined with mass spectrometry. The protein is equilibrated under physiological conditions and then diluted into D_2O buffer for certain time intervals (t_{HX}). After a quench at low pH and low temperature, the deuterated protein is injected to an HPLC for desalting and subjected to ESI-MS. Measurement of the deuteron incorporation in full-length protein mass spectra results in information about global exchange kinetics. In addition, the deuterated protein can be digested during the HPLC step by pepsin and the deuteration kinetics of the peptic peptides (i.e. shifts of the isotopic cluster to higher m/z by deuteration time) provides information about slow and fast exchanging regions in the protein.

HX-MS has been successfully used for numerous studies of protein dynamics, protein assemblies and conformational changes in proteins (Bai, 2006; Wales and Engen, 2006). It can also be used for monitoring complex formation and binding sites of ligands; and even to analyze interfaces of protein-protein interactions.

1.5 Aims of this thesis

The aim of the thesis was to elucidate the molecular mechanism of the Hsp70-Hsp90 chaperone machinery by studying their conformational dynamics and conformational changes. In order to study conformational properties of the chaperones, this work employed mainly the technique of amide hydrogen exchange combined with mass spectrometry (HX-MS) and fluorescence spectroscopy.

The conformational dynamics within three central proteins of the cellular chaperone machinery should be investigated: **Hsp70**, **Hsp90** and the co-chaperone **CHIP** that can bind both Hsp70 and Hsp90 and links chaperone substrates to ubiquitination and proteasomal degradation.

Hsp70: The structural dynamics of Hsp70 chaperones should be analyzed by HX-MS for the *E. coli* Hsp70 DnaK to understand conformational changes transmitting allostery within the chaperone upon nucleotide binding. At the beginning of this work, no full-length two domain structure of an Hsp70 was known. The aim was to identify regions in the protein that transmit the ATP binding signal in interdomain communication to the substrate binding domain. In addition, the orientation and influence of the two functional domains on each other should be analyzed. The interaction of DnaK with high affinity substrate peptides should also be studied.

Hsp90: The conformational dynamics of Hsp90 should be investigated by HX-MS and fluorescence spectroscopy to elucidate the effects of nucleotides and inhibitors on the mechanism of the Hsp90 ATPase cycle. Moreover, this study should compare the conformational properties of different Hsp90 family members (human Hsp90, yeast Hsp90 and the bacterial HtpG) that were proposed to have mechanistic differences. The results should than be transferred to interaction studies of Hsp90 in complex with co-chaperones and client proteins.

CHIP: HX-MS should be used to investigate conformational properties of human E3 ligase CHIP and its interaction with Hsp70 and Hsp90 chaperones or E2 ligases. The dynamics of CHIP might provide insights into its function in the decision making process between chaperone folding and ubiquitination.

2 Results and Discussion

2.1 Conformational studies of the Hsp70 chaperone allostery

To analyze the conformational dynamics in Hsp70 proteins that allow substrate binding in the high-affinity state and the nucleotide-dependent conformational changes we used native state amide hydrogen exchange (HX) technology in combination with mass spectrometry (MS) and mapped the solvent accessibility of the backbone amides in *Escherichia coli* DnaK in dependence of bound nucleotide.

2.1.1 Conformational flexibility of the *E. coli* Hsp70 DnaK

We initially measured deuteron incorporation into wild-type DnaK in the absence of nucleotides or substrates to analyze the overall kinetics of the HX reaction. We therefore incubated DnaK for different time intervals in D_2O, quenched the reaction by lowering the pH to 2.2 and the temperature to 0°C, and subsequently analyzed the reaction on an HPLC-electrospray ionization tandem mass spectrometry setup (Rist et al., 2003; Rist et al., 2005b). Deuterons incorporated into full-length DnaK with apparent triple exponential kinetics leaving approximately 40% of amide protons unexchanged after one hour (Fig. 2.2). A protected core of 40 to 50% of all amide protons under such conditions is typical for a well-folded native protein.

To localize fast and slow exchanging regions in DnaK and to elucidate the flexible parts in the SBD, which allow substrate binding in the high-affinity state, we performed the analysis of the HX reaction on our HPLC-MS setup including two columns with immobilized pepsin and *Aspergillus saitoi* protease XIII, both of which are active under quench conditions at 0°C, to generate on-the-fly peptide fragments of DnaK. The average peptide size was around 17 residues and the overall sequence coverage with peptides that could be detected in every run was about 80% (Fig. 2.1a). Sample spectra are shown in Fig. 2.1b and in Fig. 2.1c secondary structure representations of the NBD and SBD of DnaK are shown color-coded according to the relative deuteron incorporation after 10 s, 60 s, 10 min and 60 min.

Overall there is good agreement between crystallographic data and the protection against HX. Well-folded secondary structure elements incorporate deuterons to a lower degree than coil regions or less well defined helices and sheets. After 10 s incubation in D_2O only the C-terminal region of the SBD exchanged its amide protons almost completely for deuterons.

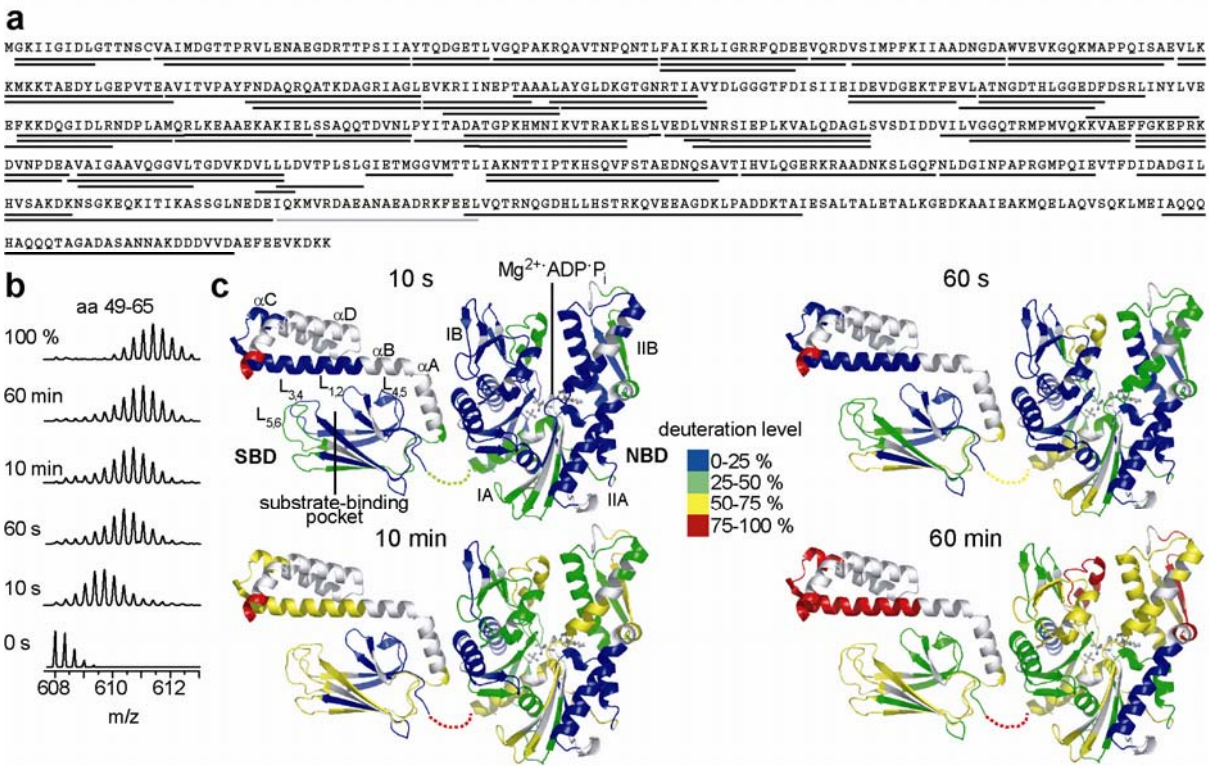

Fig. 2.1 Conformational flexibility of *E. coli* DnaK. (a), Amino acid sequence of DnaK and peptic peptides used for the analysis (underlined). Sequence coverage was ca. 80%. The gray line indicates the peptide that was only visible using specific elution conditions for the reversed-phase HPLC column. **(b),(c)** Time-dependent deuteron incorporation into DnaK. **(b)** Example spectra of the peptic peptide amino acids 49 to 65 in H_2O and after 10 s, 60 s, 10 min and 60 min in D_2O as indicated. Control spectrum of the same peptide of a fully deuterated DnaK sample (top).**(c)**, Secondary structure representation of DnaK NBD (residues 4-386 modelled on bovine Hsc70 NBD 1HKM using Swiss-Model (Guex and Peitsch, 1997; Peitsch, 1996)) and SBD (residues 393 to 607, 1DKX; (Zhu et al., 1996)) colored according to deuteron incorporation as indicated in the middle after 10 s, 60 s, 10 min and 60 min. The missing 6 residues between NBD and SBD are symbolized as dotted line colored accordingly. The images were created in PyMOL (http://www.pymol.org).

This is not surprising since the corresponding peptide includes most of the 30 C-terminal residues not contained in the crystal structure and therefore not visible in Fig. 2.1c, which were shown by NMR to be unstructured (Bertelsen et al., 1999). The outer loops ($L_{3,4}$ and $L_{5,4}$) of the β-sheet subdomain of the SBD exchange amide protons faster than the inner loops ($L_{1,2}$ and $L_{4,5}$), which are packed against helices αA and αB. Interestingly, helix αB incorporates deuterons surprisingly fast with 20 of the 32 amide protons (62%) exchanged after 10 min and 26 (81%) after 60 min leaving only 12 and 6 amide protons protected corresponding to three and one and a half helix turns, respectively. These data indicate significant flexibility of this helix with transient opening of hydrogen bonds.

The NBD subdomain IA appears to incorporate deuterons more rapidly than other parts of the NBD. However, since the resolution of our method is limited by the size of the peptides analyzed, close inspection of the data showed that most of the deuteron incorporation into

subdomain IA can be accounted for by the unstructured coil regions. For example, the peptide, which includes the C-terminal helix of the NBD and the N-terminal part of the SBD, residues 371-391 (yellow in the 60 s time point in Fig. 2.1c), incorporates 11 deuterons within 60 s leaving 9 amide protons unexchanged. Even after one hour 7 amide protons remain protected from exchange, corresponding to two helix turns, which is exactly the number of turns of the C-terminal helix of the NBD that is included in the peptide. It is therefore likely that this helix is very stable and that the part, which links the NBD to the SBD (indicated as dotted line in Fig. 2.1c), is almost completely solvent accessible consistent with the recent crystal structure of the two-domain construct of Hsc70 (Jiang et al., 2005) (Fig. 2.7a)

2.1.2 Nucleotide-dependent solvent accessibility changes in full-length DnaK

To assess the effects of nucleotides on the solvent accessibility of amide protons of DnaK we first determined the overall kinetics of nucleotide-induced changes in HX. To analyze HX in DnaK in the presence of ATP over longer incubation times without interference with ATP hydrolysis, we used the DnaK-T199A mutant protein that is deficient in ATP hydrolysis but still proficient in ATP binding and undergoes ATP-induced conformational changes in the SBD like the wild-type protein (Barthel et al., 2001). This protein was incubated in D_2O in the nucleotide-free or ATP-bound state and analyzed after different time intervals by our HPLC-MS setup excluding the columns with immobilized proteases. As for wild-type DnaK deuteron incorporation into DnaK-T199A occurred with apparent triple exponential kinetics (half lives τ_1 = 2.5 s; τ_2 = 110 s; τ_3 = 1430 s) leading to the exchange of 354 (58%) of a total of 613 amide protons after 60 min (Fig. 2.2a). HX in the ATP-bound state occurred with similar kinetics (τ_1 = 2.0 s; τ_2 = 73 s; τ_3 = 1670 s), but, surprisingly, leveled of at a significantly lower number of total incorporated deuterons (327) as compared to the nucleotide-free state (Fig. 2.2a). Since biochemical evidence, including substrate association and dissociation measurements and partial tryptic digestion, clearly demonstrated that ATP binding induces an opening of the SBD, we hypothesized that ATP-induced increase in solvent accessibility in the SBD may be counteracted by a decrease in solvent accessibility in other parts of the protein. We therefore repeated the experiment adding ATP at a later time point (20 min, > 10 τ_2) when most of the rapidly exchanging amids in nucleotide-free DnaK were already deuterated. Under these conditions addition of ATP led to the incorporation of 7 additional deuterons as compared to the control without addition of ATP (Fig. 2.2b). These

data show that ATP binding to the NBD leads to an increased solvent accessibility in some parts of the proteins that is counterbalanced by a decreased solvent accessibility in other parts.

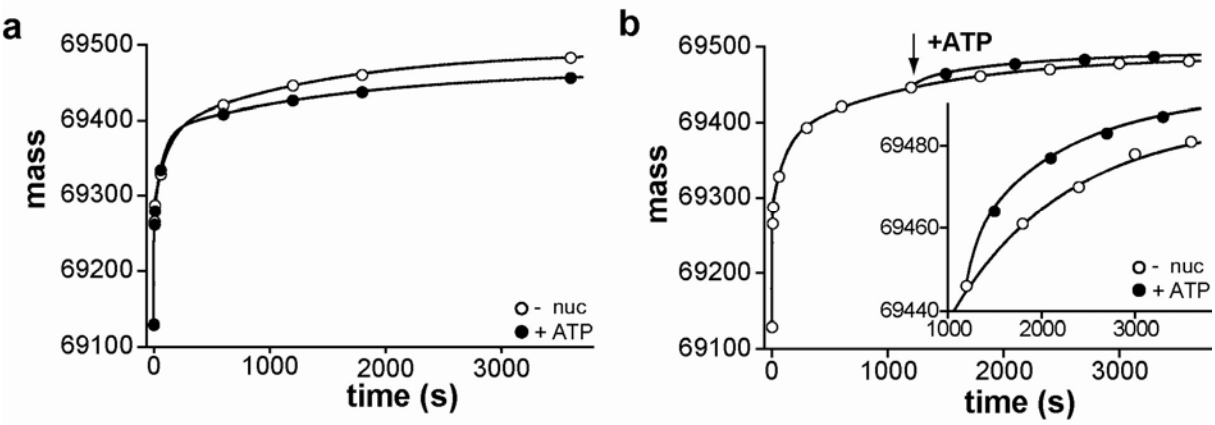

Fig. 2.2 Nucleotide-dependent incorporation of deuterons into full-length DnaK-T199A. (a) Time-dependent mass increase of full-length DnaK-T199A in the absence of nucleotide (open circles) and in the presence of ATP (filled circles). **(b)** Time-dependent incorporation of deuterons into DnaK-T199A in the absence of nucleotide. After 20 min the reaction was split into two aliquots and ATP was added to one aliquot. The inset shows an enlargement of the time between 20 min and 60 min.

Calculation of the observed protection factors of the DnaK in absence and presence of ATP resulted in a global stabilization energy of $\Delta G = 160$ kJ/mol upon ATP binding.

2.1.3 Localization of nucleotide-induced conformational alterations

To localize the regions within DnaK with increased and decreased solvent accessibility we repeated the analysis using the HPLC-MS setup with included protease columns (Fig. 2.3). 24 of 29 analyzed segments of DnaK incorporated less deuterons in the presence of ATP as compared to the nucleotide-free state coherent with our data on the full-length protein. The β-sheet subdomain of the SBD (fragments 413-437 to 486-511) exchanged amide protons more rapidly in the ATP-bound state as compared to the nucleotide-free state. In contrast, helix αB and the C-terminal part of the SBD exchanged amide protons more slowly (Fig. 2.3a, b). Most segments of the NBD incorporated deuterons more slowly in the ATP-bound state as compared to the nucleotide-free state indicating a tightening of the NBD conformation (Fig. 2.3a, b). Although the differences are small they are highly reproducible and well reflected in the kinetics of deuteron incorporation as shown for selected segments in Fig. 2.3c. Most prominent is the difference between nucleotide-free and ATP-bound states in the linker region (segments 372-391 and 389-392 Fig. 2.3a and b). In the nucleotide-free state segment 389-392 exchanges all exchangeable amide hydrogens within 10 s indicating complete exposure to

solvent consistent with the recent crystal structure (Jiang et al., 2005) (Fig. 2.3b). In contrast, in the ATP bound state this segment does not exchange its amide hydrogens indicating complete protection. The overlapping segment 372-391 shows a similar behavior, high solvent accessibility in the nucleotide-free state and almost complete protection in the ATP bound state (Fig. 2.3a and b).

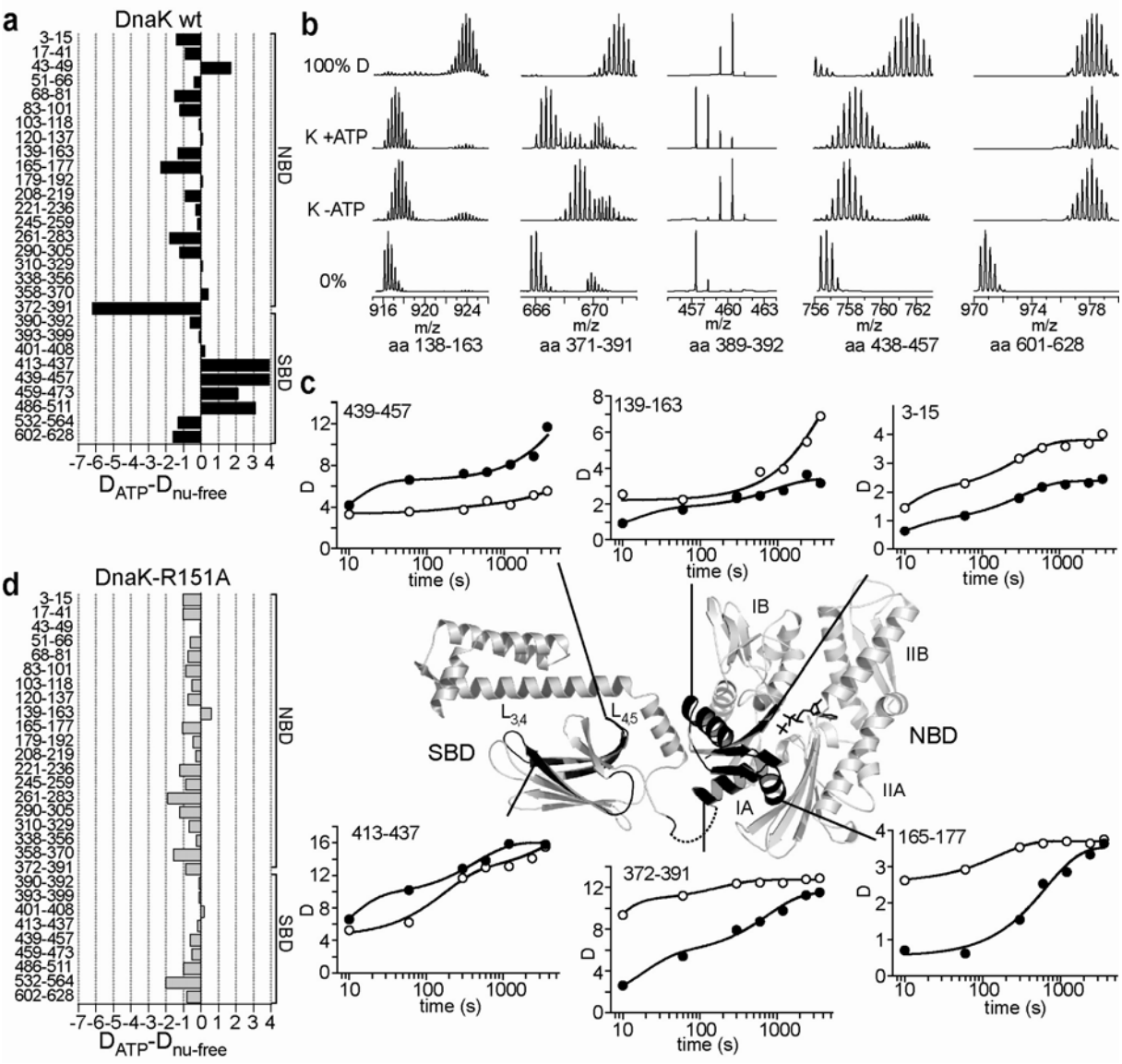

Fig. 2.3 Localization and kinetics of nucleotide-dependent deuteron incorporation into DnaK. Difference of deuteron incorporation into **(a)** wild-type DnaK and **(d)** DnaK-R151A in the presence of ATP minus deuteron incorporation in the absence of nucleotide after 1 min incubation in D_2O. Numbers at the right indicate the corresponding protein segments (= amino acids of the peptic peptide minus the N-terminal residue). **(b)** Mass spectra of representative peptic peptides (residues 138-163, 371-391, 389-392, 438-457, 601-628) of DnaK-T199A incubated in H_2O (0%) or for 10 s in D_2O in the nucleotide-free state (K – ATP) and in the presence of ATP (K + ATP). The spectra of the same peptides from a 100% deuterated control (100% D) are shown at the top. (**c**), Kinetics of deuteron incorporation into selected segments of DnaK-T199A in the absence (open circles) and presence of ATP (black circles). The segments are indicated in black in the secondary structure representation of NBD and SBD in the middle.

As comparison we analyzed the DnaK-R151A variant, which we recently identified as completely devoid in interdomain communication (Vogel et al., 2006a) (Fig. 2.3d). ATP-induced changes in deuteron incorporation into the NBD during a 1-min incubation in D_2O were similar in this variant protein as compared to the wild-type protein (compare Fig. 2.3a and d segments 3-15 to 358-370). However, ATP-induced changes in deuteron incorporation into the SBD were strongly reduced (compare Fig. 2.3a and d segments 401-408, 413-437, 486-511, 602-628). Most notable was the difference in segment 372-391. Upon ATP binding, 6 amide protons were protected from exchange in the wild-type protein but only 1 was protected in the DnaK-R151A variant.

Together these data demonstrate that ATP binding leads to pronounced changes in solvent accessibility in the NBD and in the substrate enclosing loops in the SBD. If communication between the two domains of DnaK is compromised by a mutational replacement in subdomain IA of the NBD the changes in the SBD are not anymore observed. HX analysis thus allows to monitor the conformational changes occurring in DnaK during ATP-dependent interdomain communication.

In the presence of ATP four additional segments (segments 139-163, 164-177, 338-356, 372-382) exhibit slower deuteron incorporation in the full-length protein as compared to the isolated NBD (Fig. 2.4a, c). These four segments represent two regions of the NBD, the subdomain IA and parts of subdomains IIA and IIB that are located on the opposite face of the NBD as compared to the region in subdomain IA.

The comparison of the deuteron incorporation into the isolated SBD (DnaK(389-638)), with the incorporation into full-length DnaK also revealed surprising results (Fig. 2.4b). Overall, the isolated SBD exchanged in five of the eight segments investigated more amide protons than the full-length protein in the nucleotide-free state (Fig. 2.4b white bars). This is most pronounced in segment 486-511, comprising half of β-strand 7, β-strand 8 and the first turn of helix αA, which exchanges on average 6.6 of the 26 amide protons in the full-length protein but 13.9 amide protons in the isolated SBD.

Since helix αA of the SBD contains the major contact sites with the NBD in the recent crystal structure of the two-domain construct of Hsc70 we were eager to see whether these contacts would be measurable in solvent accessibility of this helix. Using an altered solvent gradient of the reversed-phase column we were able to analyze a peptic peptide that contained the C-terminal part of helix αA and the N-terminal half of helix αB (512-532; Fig. 2.4d). This

peptide showed one deuteron difference when incubating the isolated SBD as compared to full-length DnaK in the nucleotide-free state suggesting only a slight stabilizing influence of the NBD on this region.

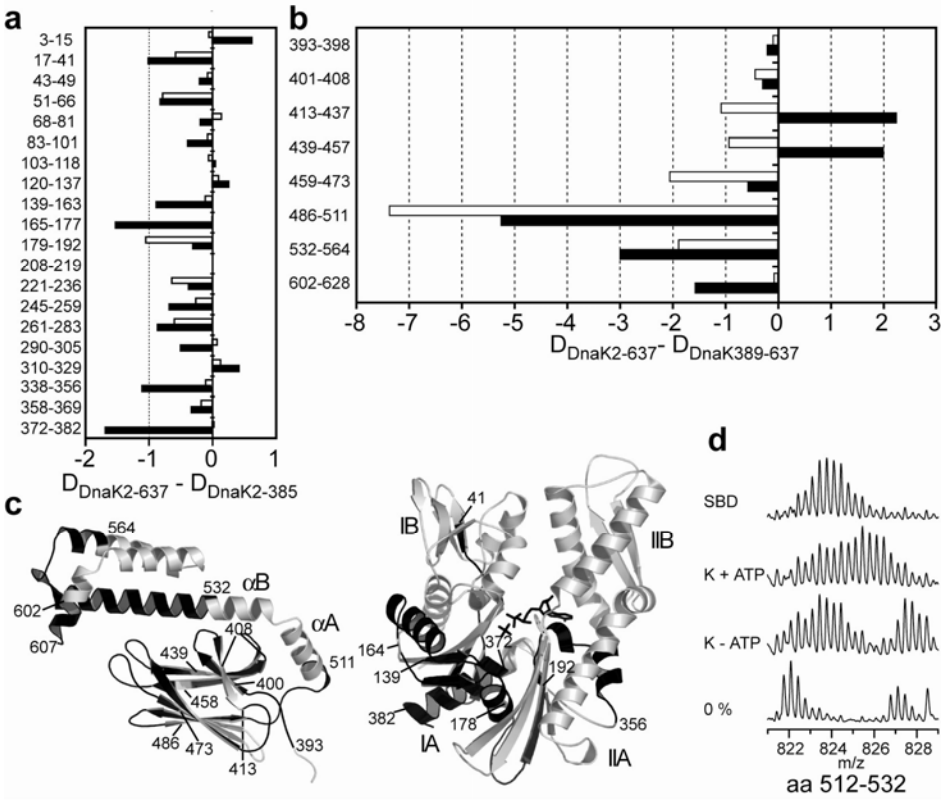

Fig. 2.4 Comparison of deuteron incorporation into wild-type DnaK and isolated NBD and SBD (a) Difference of deuteron incorporation into DnaK(2-638) minus deuteron incorporation into the NBD (DnaK(2-385)) in the nucleotide-free state (white bars) or the presence of ATP (black bars) after 1 min of incubation in D_2O. **(b)**, Difference of deuteron incorporation into DnaK(2-638) minus deuteron incorporation into the SBD (DnaK(389-638)) in the nucleotide-free state (white bars) or the presence of ATP (black bars) after 1 min of incubation in D_2O. **(c)**, Secondary structure representation of the SBD (left) and the NBD (right) with specific segments in black and residue positions indicated. **(d)**, mass spectra of the peptic peptide residues 512-532 (representing the C-terminal part of helix αA and the N-terminal part of αB; m/z = 821.74, z = 3) of wild-type DnaK in the nucleotide-free state (K-ATP) or the presence of ATP (K+ATP) and of the same peptide from the SBD after 1 min incubation in D_2O. The undeuterated peptide is shown for comparison at the bottom. The spectra were obtained using specific conditions for eluting the peptides from the reversed-phase column. Spectra for the fully deuterated peptide could not be obtained.

When the isolated SBD is compared to full-length DnaK in the ATP-bound state significant differences are still observed (Fig. 2.4b black bars). The four C-terminal segments of the SBD still incorporate less deuterons in the full-length protein as compared to the isolated SBD and only two segments (413-437 and 439-457) exchanged more in the full-length protein demonstrating the ATP-induced opening of the substrate-binding pocket. Similarly, the region 512-532 incorporates at least 4 deuterons more in the full-length protein in the presence of

ATP than in the isolated domain, indicating that ATP-induced conformational changes also lead to an increased solvent accessibility of the amides of helices αA and αB (Fig. 2.4d).

Taken together our comparison of HX into the isolated domains of DnaK with HX of full-length DnaK indicate that the two domains stabilize each other, an effect that is much more pronounced in the SBD than in the NBD.

2.1.4 Substrate-induced conformational alterations in DnaK

To analyze possible substrate-induced conformational changes in the SBD and the NBD we compared the HX of full-length DnaK in the absence and presence of the peptide σ^{32}-M195-N207, which was identified earlier to be a high-affinity substrate for DnaK (McCarty et al., 1996), and in the absence and presence of ATP. In the absence of ATP overall little changes in deuteron incorporation were observed except for the segments that form the substrate-enclosing loops $L_{1,2}$ and $L_{3,4}$. The HX kinetics of these two segments is shown in Fig. 2.5. The segment representing the inner loop $L_{1,2}$ (residues 401-408) incorporates one to two deuterons very rapidly and a third over a period of about 1 h in the absence of the substrate peptide, while in the presence one of the three amide protons is completely protected from exchange (Fig. 2.5a). This result is consistent with the crystal structure which shows one amide proton completely free, one in a loose internal hydrogen bond (distance between amide N and carbonyl O 3.4 Å), and one forming a hydrogen bond to the backbone of the substrate peptide (Zhu et al., 1996). The HX kinetics of the segment representing the outer substrate enclosing loop $L_{3,4}$ (residues 413-437) changed in a more surprising way upon substrate binding. In the absence of the substrate peptide about 6 deuterons were incorporated within the shortest time interval measured (10 s). Consistent with the X-ray structure which shows 6 of the 23 amide protons directly coordinated to water (PDB entry code 1DKX). Deuteron incorporation continued more slowly to arrive at 15 after 1 h, leaving 8 amide protons protected consistent with the number of strong hydrogen bonds (O-N distance below 3Å) within this segment in the x-ray structure. In the presence of a substrate deuteron incorporation was much slower. Only three amide protons exchanged within the first 10 s, and after 1 h deuteron incorporation approached 10 leaving 13 amide protons completely protected within this time frame. Since only two hydrogen bonds are formed with the substrate in the crystal structure it must be concluded that parts of the segment represented by the analyzed peptide are stabilized upon substrate binding.

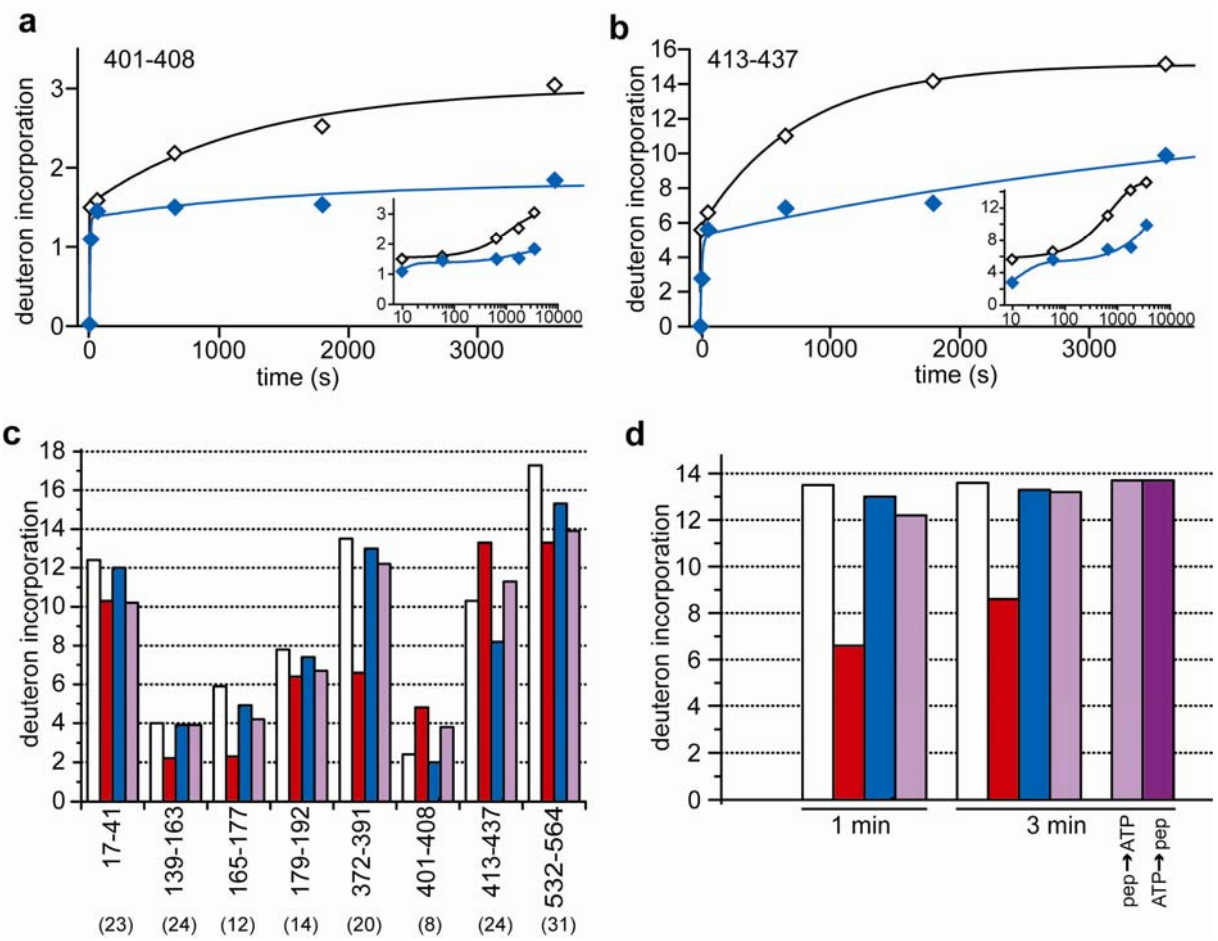

Fig. 2.5 Substrate dependence of deuteron incorporation into DnaK. Kinetics of deuteron incorporation into two segments of the SBD (residues 401-408 **(a)** and 413-437 **(b)**) in the absence (white diamonds) or presence (blue diamonds) of the substrate peptide σ^{32}-M195-N207 (MAPVLYLQDKSSN;(McCarty et al., 1996)). Insets show same data with a logarithmic time scale. **(c)** ATP and substrate induced conformational changes. Nucleotide-free DnaK-T199A was incubated in the absence (white) and presence of ATP (red), in presence of peptide σ^{32}-M195-N207 (blue) and presence of both peptide and ATP (purple) for 1 min in D_2O. Shown is the deuteron incorporation into selected segments as indicated. Numbers in parenthesis give the number of exchangeable amide hydrogens in the segments. **(d)**, deuteron incorporation into the linker segment 372-391 after 1 min and 3 min in D_2O in the absence or presence of ATP or peptide. pep→ATP (bright purple), incubation of nucleotide-free DnaK-T199A in the presence of peptide for 1 min in D_2O, then addition of ATP and incubation for additional 2 min. ATP→pep (dark purple), incubation of ATP-bound DnaK-T199A for 1 min in D_2O, then addition of peptide and incubation for additional 2 min.

To analyze the allosteric mechanism by which substrates induce ATP hydrolysis we wanted to measure HX in the presence of peptide and ATP. To circumvent the problem of ATP hydrolysis during the incubation in D_2O we made use of the DnaK-T199A variant. None of the resulting mass spectra showed indications for a bimodal distribution of the isotopic peaks indicating that all DnaK molecules were in the same conformation. Fig. 2.5c shows the comparison of deuteron incorporation after 1 min in D_2O into selected segments of nucleotide-free DnaK-T199A in the absence or presence of the peptide σ^{32}-M195-N207 and in the absence or presence of ATP. Three different situations can be distinguished. First, the

effects of ATP are dominant over the effects of peptide (segments 17-41, 401-408) indicating that ATP was not hydrolyzed during the incubation time. Second, the effects of peptide are dominant over the effects of ATP (segments 139-163, 165-177, 372-391) suggesting conformational changes that could be linked to allosteric control (discussed in detail below). Third, the effects of ATP and peptide seem independent and additive (segment 413-437) suggesting that this segment consists of parts that react independently one according to the first and one according to the second situation. To analyze the ATP and peptide effects more closely we performed order-of-addition experiments. We incubated nucleotide-free DnaK-T199A in the presence or absence of ATP or peptide for 1 min in D_2O and than added peptide to the ATP-containing sample or ATP to the peptide-containing sample and continued incubation for an additional 2 min and compared the deuteron incubation with samples to which nothing was added. The outcome was principally the same as in the previous experiment, shown exemplarily for the linker segment in Fig. 2.5d. Peptide overrides the effect of ATP on this segment of DnaK and leads to an exposure of the linker to solvent. Taken together these data clearly indicate that ATP-induced conformational changes in some parts of the NBD and the linker are reversed by peptide binding suggesting a mechanism for the mutual allosteric control of the two domains.

2.1.5 Discussion of the conformational changes within Hsp70

This study revealed several new insights into the structural dynamics of Hsp70 proteins and the ATP-dependent communication between the nucleotide and substrate-binding domains, which mediates the allosteric regulation of this class of chaperones. Nucleotide-dependent changes in deuteron incorporation demonstrate an overall tighter folding of the NBD and an increased solvent exposure of several regions in the SBD visualizing the conformational changes accompanying the opening of the substrate-binding pocket. Comparison of the isolated domains with the full-length protein indicates a stabilizing effect of the domains onto each other, which is specifically pronounced in the lower β-sheet of the substrate-binding domain. The observation that the linker is completely accessible to solvent in the absence of nucleotides and solvent protected in the presence of ATP reveals nucleotide-dependent conformational changes of the linker, which may be part of the mechanics by which the two domains communicate with each other.

The time-dependent incorporation of deuterons into DnaK in the nucleotide-free state allows three conclusions. First, the NBD shows significant flexibility consistent with a shearing

movement of the four subdomains relative to each other that was recently proposed based on dipolar coupling NMR data (Zhang and Zuiderweg, 2004). Second, the lid forming helix αB in the SBD exchanges much more rapidly than expected for a well-folded helix, leaving the hydrogen bonds of only 3 and 1.5 helix turns intact over a period of 10 and 60 min, respectively. This is consistent with local unfolding that accompanies the opening movement, which allows substrate binding and release even in the absence of ATP. Such a movement was proposed by Hendrickson and coworkers on the basis of a second crystal form in which helix αB was bent upward by 11° (Zhu et al., 1996). This flexibility of helix αB would not be necessary in other models, which propose that the opening of the lid occurs either by a pivoting movement of the entire lid around helix αA or by an upward movement of the entire helix αB without helix melting and with a hinge between helix αA and αB (Mayer et al., 2000; Wang et al., 1998). Our data are also consistent with the NMR and x-ray structures of truncated versions of the SBD of DnaK and Hsc70, which show a helical secondary structure only up to residue 535 (Jiang et al., 2005; Morshauser et al., 1999; Wang et al., 1998). The estimated half-life of the HX in this helix (ca. 10 min) is similar to the half-life of the DnaK-peptide complex (ca. 15 min). Consistently, the substrate enclosing outer loops $L_{3,4}$ and $L_{5,6}$ and β-strand 3 incorporate deuterons with similar kinetics. Third, the C-terminal part of the NBD and the linker that connects NBD and SBD are highly solvent exposed in the nucleotide-free state, in agreement with data from partial tryptic digestion, which shows an exposed cleavage site N-terminal of the linker, and the recent crystal structure of a two-domain construct of bovine Hsc70 (Buchberger et al., 1995; Jiang et al., 2005) (Fig. 2.7a). Taken together, Hsp70 proteins show a high degree of flexibility in both, NBD and SBD.

The comparison of deuteron incorporation into full-length DnaK with the incorporation into DnaK(2-385) in the absence of nucleotide revealed small changes throughout the NBD. These data are consistent with a recent NMR study, which compared chemical shifts of the residues in the NBD in a *Thermus thermophilus* DnaK two-domain construct with the isolated NBD (Revington et al., 2005). It was found that chemical shift perturbations caused by the presence of the SBD are scattered throughout the NBD. The absence of a defined area, which is protected by the presence of the SBD, is surprising. It should be noted, however, that mere side chain interactions, which do not affect the backbone amide hydrogen accessibility, would not be detected by this method. The differences in HX observed in the presence of ATP as compared to the nucleotide-free state revealed three regions of the NBD, the major part of subdomain IA and small parts of subdomains IB and IIA, both of which are located on the

opposite face of the NBD as compared to the region in subdomain IA. The slight stabilizing effect exerted by the SBD on the NBD is therefore enhanced by ATP binding to the NBD indicating a more tightly coupled state. These data provide a structural basis for earlier observations with small X-ray scattering and partial tryptic proteolysis (Buchberger et al., 1995; Wilbanks et al., 1995). Both investigations show that the NBD and SBD are more tightly coupled with each other in the ATP-bound state as compared to the nucleotide-free state with a smaller radius of gyration of the full-length protein and the linker connecting both domains not accessible for proteolytic cleavage.

The comparison of amide hydrogen exchange of full-length DnaK in the presence and absence of ATP as well as with the isolated NBD at the peptide level provides insights into the allosteric regulatory mechanism by which ATP binding induces the opening of the substrate-binding pocket and by which substrate binding stimulates the ATPase activity. In the NBD the segments with the largest nucleotide-dependent changes in HX kinetics of full-length DnaK cluster in subdomain IA (Fig. 2.3b, c), as do the changes between full-length DnaK and DnaK(2-385) in the presence of ATP (Fig. 2.4a, c). The nucleotide-dependent alterations of HX are explained easily for the segments 3-15 and 165-177. The former contains residues Asp^{8}, Thr^{11}, Thr^{12}, Tyr^{13} and Cys^{15} corresponding to Asp^{10}, Thr^{13}, Thr^{14}, Tyr^{15} and Cys^{17} of bovine Hsc70, which contact the β- and γ-phosphate of the bound ATP in the crystal structure, and nucleotide binding may therefore stabilize this loop (Flaherty et al., 1990; O'Brien et al., 1996). The latter segment (165-177) contains Glu^{171} corresponding to Glu^{175} in Hsc70 that is involved in the coordination of Mg^{2+} and may therefore also be stabilized by ATP binding (Flaherty et al., 1994). The segments 139-163 and 372-391 do not have such an obvious connection to nucleotide binding. The first region, however, contains Pro^{143} that was recently shown to constitute the molecular switch, which stabilizes the two alternating conformations of Hsp70 proteins, and Arg^{151}, which relays the proline switch position and therefore ATP binding to the SBD and substrate and DnaJ binding to the NBD (Vogel et al., 2006a). The second region contains the linker that connects NBD and SBD. Alterations in the HX behaviour in this region are particularly interesting because it also has implications on the allosteric interdomain control mechanism. Since the residues in this region are highly conserved we propose that these conformational changes are intimately linked to allosteric interdomain control. Consistent with this hypothesis are the earlier observations that replacement of the hydrophobic residues 389 to 392 with alanine (Laufen et al., 1999) blocks completely ATP-induced stimulation of substrate release and substrate and DnaJ-mediated triggering of ATP hydrolysis. The linker which is exposed in the nucleotide-free state and

becomes protected upon ATP binding, therefore seems responsible for triggering the conformational change in the NBD that is necessary for the induction of ATP hydrolysis. Consistent with this hypothesis is the fact that a NBD construct including the linker (DnaK(2-393)) has a strongly increased ATPase activity similar to full-length DnaK in the presence of DnaJ and a substrate protein (Swain et al., 2007; Vogel et al., 2006b).

When the mutual allosteric control between the NBD and the SBD is abolished by the Arg^{151} to Ala replacement (Vogel et al., 2006a) most nucleotide-dependent changes in the HX kinetics in the NBD are still observed but not the changes in the linker or the SBD (Fig. 2.3d). Together these data clearly demonstrate that the HX kinetics reveal segments in Hsp70 proteins that are involved in nucleotide-dependent allosteric control. In particular the linker region seems to play a pivotal role in this mechanism.

Our comparison of HX into the isolated SBD with the HX of full-length DnaK indicated a strong stabilizing effect of the NBD on the SBD, which may be part of the linker-mediated allosteric control. The largest difference in deuteron incorporation between full-length DnaK and the SBD was observed in segment 486-511 (Fig. 2.4b and d). In the isolated SBD we observed an exchange of around 14 of the 26 amide protons within a time span of 1 min demonstrating an unexpectedly high degree of flexibility in this region. The protection of more than 6 amide protons observed by us for the full-length protein indicates that the NBD stabilizes this region significantly. The recent crystal structure of an Hsp70 protein in the nucleotide-free state that contains the NBD and parts of the SBD shows the helix αA of the SBD docked onto subdomain IA of the NBD (Jiang et al., 2005) (Fig. 2.7a). Since in this structure no additional hydrogen bonds are observed between the NBD and the region 486-511 the stabilizing effect must be transduced through helix αA and the entire β-sheet.

The ATP-induced changes in deuteron incorporation into the SBD lead to increased HX in four segments (residues 413-437, 439-457, 459-473, 486-511) representing the β-sheet subdomain and a decreased HX in helix αB and the C-terminus (Fig. 2.3a and c and Fig. 2.4). This demonstrates that the ATP-induced opening of the SBD involves mainly the β-sheet subdomain and not helix αB consistent with earlier biochemical data (Mayer et al., 2000) but incompatible with a mechanism that proposes melting of helix αB as the first step for SBD opening (Zhu et al., 1996).

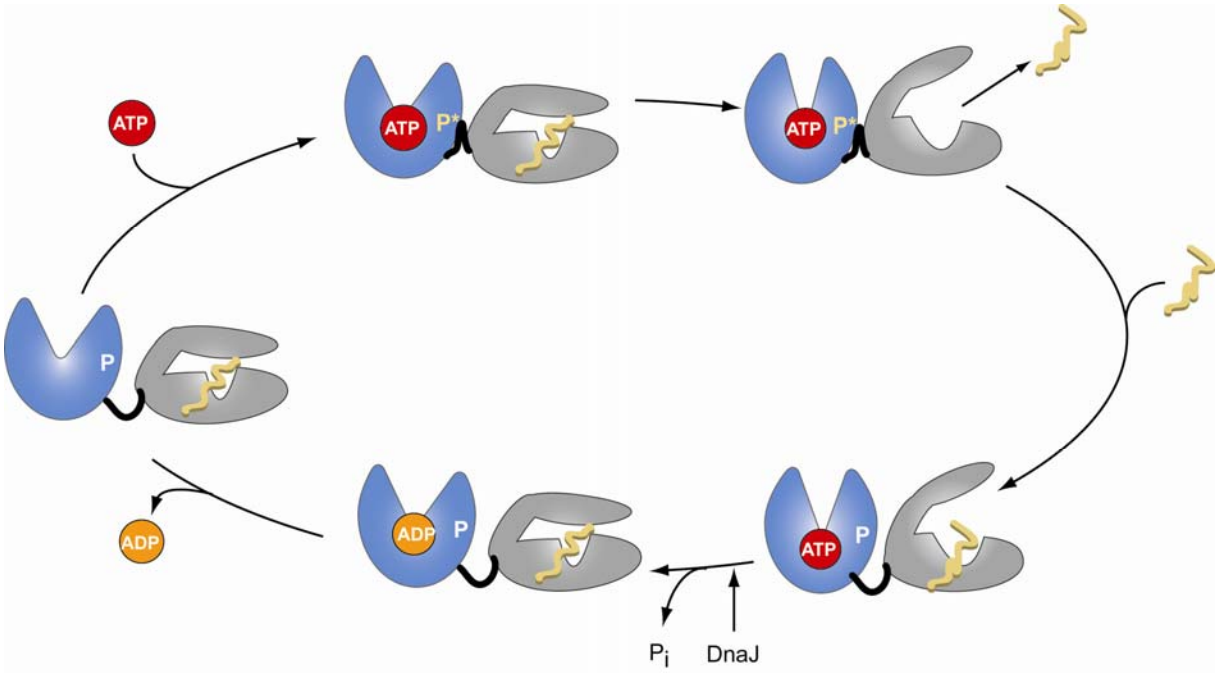

Fig. 2.6 Proposed model of the Hsp70 chaperone cycle based on HX-MS data and biochemical analysis. ATP binding to DnaK leads to conformational changes in the hydrogen bonding network around Pro^{143} (P) and the linker (shown in black), as measured by the protection of hydrogens in these segments. P^{143} undergoes *trans-cis* isomerization (P*) and this signal is transmitted through the linker to the SBD. This conformational change leads to an opening of the SBD and to substrate release (low-affinity state). Substrate binding reverts these conformational changes and stimulates in cooperation with DnaJ ATP hydrolysis which converts the chaperone into the high-affinity state. The cycle restarts after nucleotide release.

Increase in deuteron incorporation into β-sheet 3 and the outer substrate inclosing loops $L_{3,4}$ (residues 413-437) and $L_{5,6}$ (residues 458-473) are obvious requirements for the opening of the substrate-binding pocket. The increase in HX kinetics of the inner loop $L_{4,5}$ (residues 439-457) is surprising since the inner loops together with the framing helices αA and αB appear to constitute a stable entity in the crystal structure. However, Hendrickson and coworkers pointed out the unexpected high number of charged residues in this region (Zhu et al., 1996). The increased deuteron incorporation may be linked to the interdomain communication and the mechanism through which ATP effects the opening of the SBD. Interestingly, residue Lys^{414}, which is essential for interdomain communication, is close to the base of this loop (Montgomery et al., 1999). In addition, segment 512-532, comprising the C-terminal part of helix αA and proximal half of helix αB, incorporates at least 4 deuterons more in the ATP bound state as compared to the nucleotide-free state. There are two alternative explanations for this observation. Either the proximal part of helix αB or the C-terminal part of helix αA becomes more flexible. In the first case this would indicate a local unfolding that accompanies the opening of the lid, which together with the absence of large changes in solvent accessibility of the distal half of helix αB suggests the proximal part of the helix as hinge

region for the ATP-induced lid opening: this scenario is consistent with the increased solvent accessibility of the inner loop $L_{4,5}$. In the second case this could indicate a detachment of the upper part of helix αA from the NBD as part of the ATP-induced movement of both domains relative to each other, which would lead to a burial of the linker region consistent with the loss of solvent accessibility of the linker. In consideration of all available data it seems that a combination of both models is most likely.

Substrate binding to nucleotide-free DnaK reduced solvent accessibility in two segments of the SBD by one and six amide hydrogens, respectively. While the protection observed in segment 401-408 comprising parts of β-sheets 1 and 2 and loop $L_{1,2}$ corresponds exactly to the hydrogen bond between this part of the SBD and the substrate peptide suggested by the x-ray structure, the protection in segment 413-437 comprising the loop between β-sheets 2 and 3, β-sheet 3, and loop $L_{3,4}$ exceeds the expected reduction of solvent accessibility through hydrogen bonds with the substrate peptide by 4 amide hydrogens. Although an exact localization of the stabilized position is not possible due to the low spatial resolution of our MS analysis in this part of the SBD, it is likely that conformational changes in the loop between β-sheets 2 and 3 contributes at least in part to this loss of solvent accessibility, since this part contains Lys^{414} implicated in interdomain communication (Montgomery et al., 1999). This hypothesis is supported by the results in the presence of ATP (Fig. 2.5c) showing the protection of exactly two amide hydrogens after 1 min in D_2O presumably corresponding to the two hydrogen bonds formed with the peptide substrate, while the overall deuteron incorporation increased.

The ATP-induced changes in solvent accessibility was affected or even totally reversed by the peptide substrate in four segments (139-163, 165-177, 372-391, 413-437). These results have two important implications: first, they show the protein segments involved in transmitting the substrate-binding signal to the catalytic center; second, they suggest that substrate triggers ATP hydrolysis by reverting certain ATP-induced conformational changes and converting certain parts of the protein into an ADP-like state. These results are consistent but go well beyond earlier observations that peptide binding leads to an increase of intrinsic tryptophane fluorescence that precedes ATP hydrolysis (Slepenkov and Witt, 1998). Especially interesting is the substrate-triggered reversion of the ATP-induced conformational change in segment 139-163, which is fully consistent with the recently proposed proline switch (Vogel et al., 2006a). We showed in this publication that Pro^{143} in the NBD undergoes a conformational change, possibly a *trans* to *cis* isomerization upon ATP binding. This conformational change

is relayed to the SBD through Arg^{151}. Substrate was proposed to trigger ATP hydrolysis by inducing the reversion, *cis* to *trans*, of this conformational change. The changes observed in segment 165-177 most likely also contribute to the stimulation of ATP hydrolysis since the Mg^{2+}-coordinating Glu^{171} is in this segment. The two other segments with significant effects of peptide on the ATP-induced conformational change seem to mark the pathway by which peptide triggers ATP hydrolysis.

Taken together, our data suggest the following mechanism of allosteric interdomain control (Fig. 2.6): ATP binding to the NBD induces a conformational change in segment 139-163 and 165-177 most likely in Pro^{143} (*trans-cis* isomerization), Arg^{151} and Glu^{171}. This leads to a conformational change in the linker region (segment 372-391), which becomes protected from solvent and is transduced from there to segment 413-437 most likely onto the loop between β-sheet 2 and 3 of the SBD around Lys^{414}, resulting in an opening of the substrate binding pocket with increased solvent accessibility of segment 439-457. Substrate binding reverts all of these conformational changes in particular in Pro^{143} (*cis-trans* isomerization) and Glu^{171} thereby bringing the catalytic Lys^{70} with its coordinated water molecule into the ideal position for γ-phosphate cleavage.

This work provided for the first time local structural information of the ATP coupling mechanism of Hsp70 in peptide resolution. However, there is still a need for high-resolution structures of the chaperone showing the interdomain docking sites that transmit the ATP signal. Two recent papers have described a docked conformation of the two Hsp70 domains, but surprisingly the interdomain docking site and the relative orientation of the domains differ between the two. Zuiderweg and co-workers used NMR chemical shift mapping and residual dipolar couplings to orient the two domains of a truncated version of a bacterial Hsp70, DnaK from *Thermus thermophilus*, in the ADP-bound state (Revington et al., 2005). In this model, the region of the β subdomain near the entry point of the interdomain linker interacts with a cleft in the ATPase domain on the outside of the hinge between the two lobes. The new crystal structure of a truncated version of the bovine Hsp70 family member Hsc70 in the absence of nucleotide shows a different packing arrangement, in which a portion of the helical lid of the SBD (which is missing in the *T. thermophilus* DnaK construct) interacts with the same ATPase domain cleft, but at an adjacent site (Jiang et al., 2005). However, both studies reveal some inconsistency with previously published data. On the one hand, the *T. thermophilus* DnaK construct used contained mutations that might impair allosteric function. On the other hand, the central involvement of a portion of the SBD helical lid at the

interdomain interface in the Hsc70 crystal structure is inconsistent with the fact that a truncated *E. coli* DnaK lacking the entire helical lid is allosterically functional (Pellecchia et al., 2000). In particular, the exact positioning of the hydrophobic linker in the ATP bound state in the context of allosteric coupling remains enigmatic.

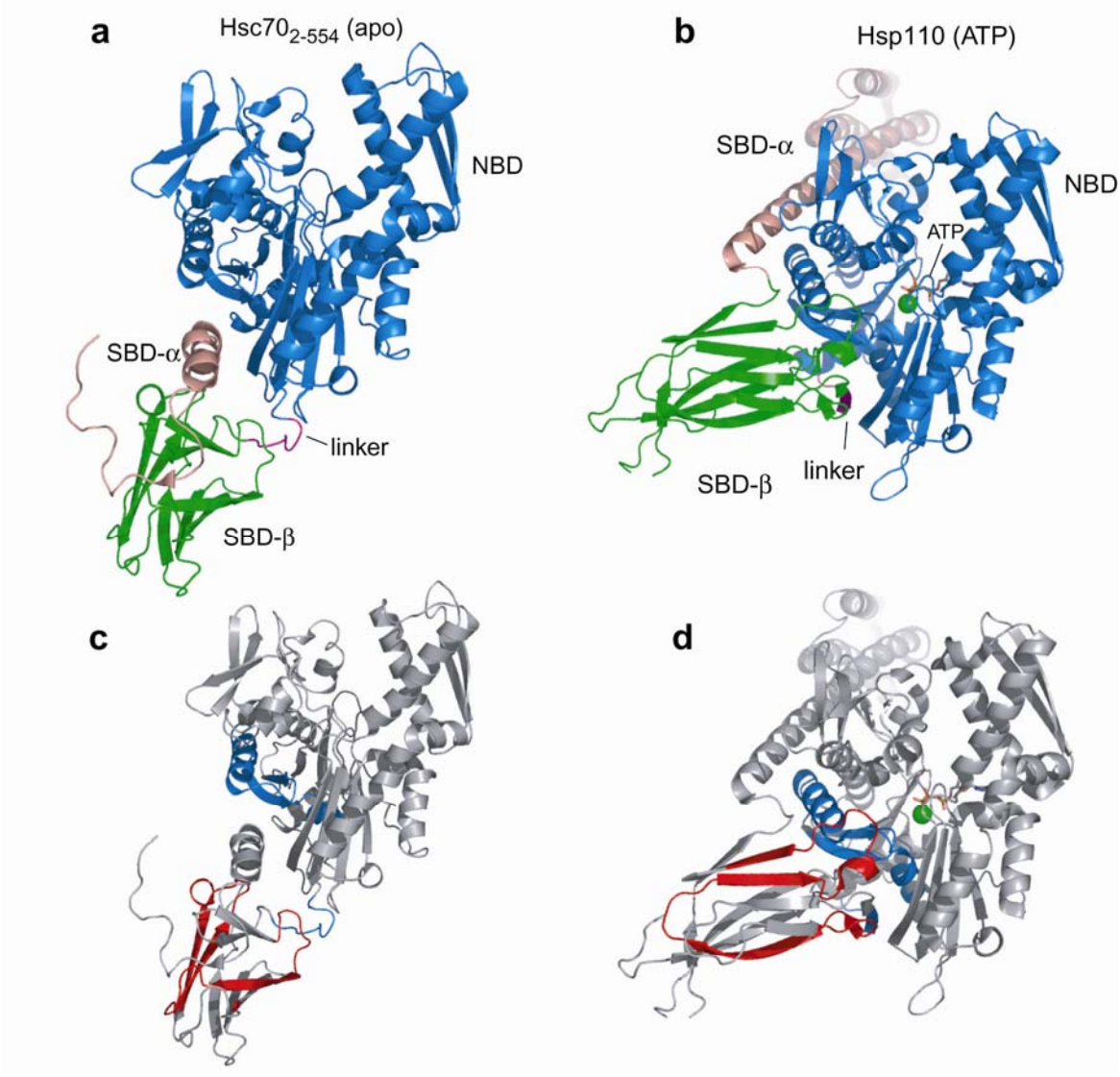

Fig. 2.7 Recent crystal structures of Hsp70 homologs and comparison with DnaK HX-MS data. (a) Secondary structure representation of bovine Hsc70 two-domain construct (2-554) in nucleotide-free state (PDB code 1YUW). NBD is shown in blue, the SBD is colored green (β-sheet part) and red (helical part). The linker (magenta) is solvent-exposed. **(b)** Yeast Hsp110 (Sse1) in ATP bound state (PDB 2QXL). **(c)** and **(d)** Same representations are colored with homologous segments from DnaK that were shown by HX-MS to be important in interdomain communication. Blue segments were protected, red segments became more flexible upon ATP binding. Only in the Hsp110·ATP structure, these segments are in close proximity to each other, suggesting that this model represents the correct conformation of the coupled ATP bound state of Hsp70.

New insights into the conformation of the low-substrate-affinity ATP state of Hsp70s were reported by NMR studies of DnaK and Hsc70 constructs. By performing NMR of the NBD construct of DnaK including the linker (1-392), Gierasch and coworkers could localize docking sites of the linker to residues Leu^{177} and Ile^{373}, which are located between the "crossing helices" of subdomains IA and IIA of the NBD (Swain et al., 2007) and may activate the ATPase. Using a fully functional truncated *E. coli* DnaK, they also demonstrate that docking of the two domains occurs only when ATP is bound (Swain et al., 2007). This is in contrast to recent NMR data from the mammalian Hsc70, which also revealed interdomain interactions in the ADP state (Jiang et al., 2007).

New structural information about the low-affinity conformation of a full-length Hsp70 homologue revealed a recent crystal structure of the Hsp110 Sse1 dimer in complex with ATP (Liu and Hendrickson, 2007) (Fig. 2.7b). This crystal structure identified interdomain contacts between the SBD β-sheet region and the backside of NBD at the IA/IIA interface with the linker residues (Asp^{396}) bound to the NBD via hydrogen bonds to Thr^{176}, Asn^{173} and Arg^{154} and hydrophobic contacts. Interestingly, the proximal helix αB of the SBD packs between NBD subdomains IA/IIA, too. The hydrogen network of the NBD-linker-SBD shown in this structure is consistent with the regions identified by our HX-MS data that are important for allosteric coupling (Fig. 2.7d)

Though Hsp110 itself lacks interdomain communication, all current biochemical and genetical data (Liu and Hendrickson, 2007) and our HX data on DnaK demonstrate indeed that the Sse1 structure represents the correct model for an ATP bound conformation of Hsp70.

2.2 Conformational dynamics of the bacterial Hsp90 HtpG

To analyze the conformational dynamics of Hsp90 during progression through the ATPase cycle we employed HX-MS and fluorescence spectroscopy. The study focused first on the bacterial Hsp90 homologue HtpG because it is the most simple representative of the Hsp90 family and is not regulated by co-chaperones. In this study we resolved the changes in conformational dynamics in space and time. We demonstrate that ATP binding induces a series of conformational changes in order to attain a compact pre-hydrolysis state.

2.2.1 Deuteron incorporation into full-length HtpG

In order to analyze the conformational flexibility of HtpG we performed HX-MS experiments as described previously (Rist et al., 2006; Rist et al., 2003). *Apo*-HtpG exchanged about 38% of its exchangeable amide hydrogens within 10 s and around 60% within one hour. These exchange kinetics are consistent with a well-folded native protein with globular domains (Fig. 2.8a). Addition of ADP induced a small protection (ca. 7 amide hydrogens). A much larger protection was observed in the presence of ATP. During the first 60 s almost 50 amide hydrogens were protected. This protection decreased to the level of the ADP state by 1200 s (Fig. 2.8a). These data indicate that the most compact state of HtpG can only be reached through addition of ATP and not ADP, which seems to be at odds with a structural study on HtpG (Shiau et al., 2006). However, our experiments do not exclude that the compact ATP-induced state is a post-hydrolysis conformation. We considered this possibility because the generation of the ATP-induced protection required a pre-incubation of HtpG with ATP that was much longer than we had expected for a protein with high nucleotide association rates (see below).

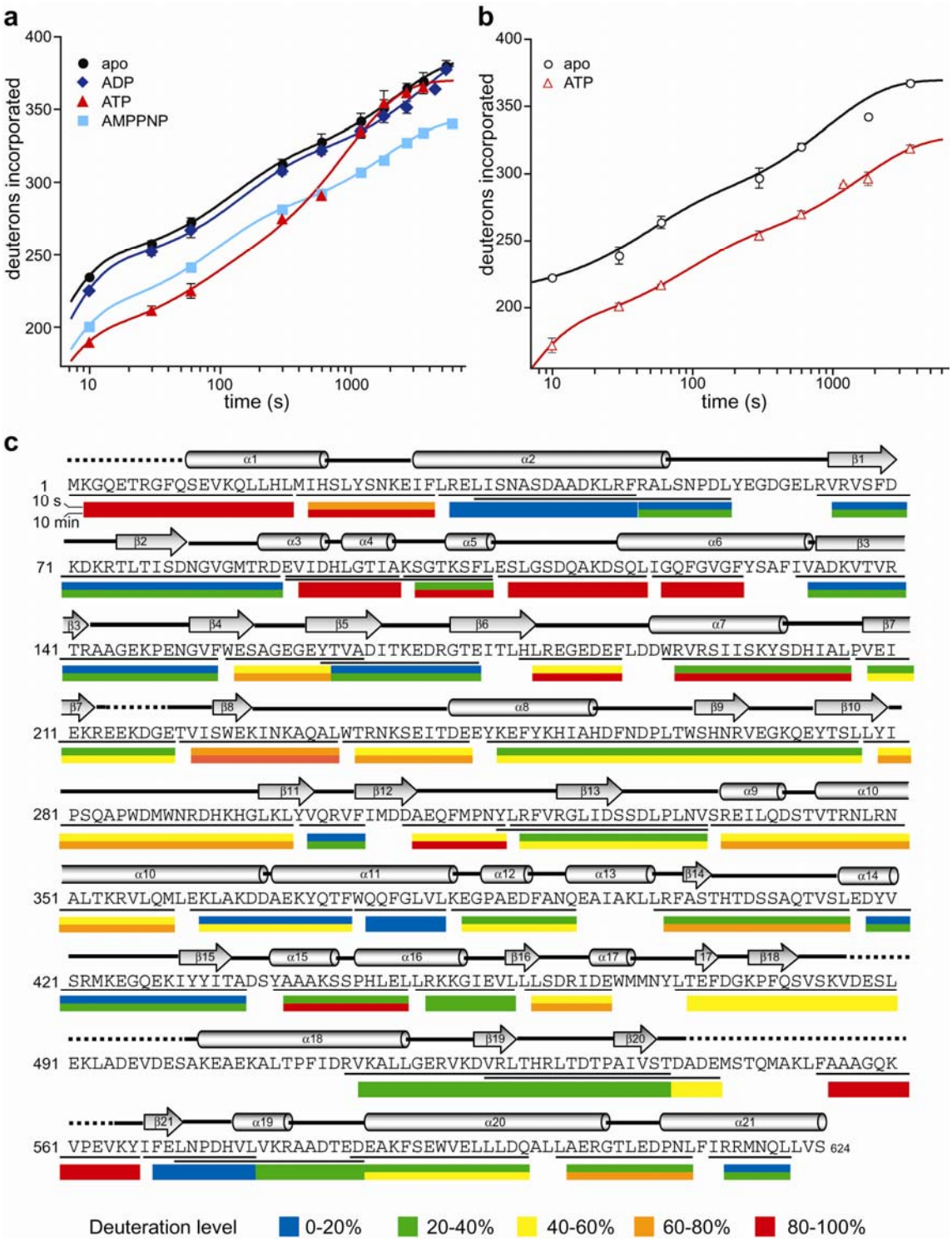

Fig. 2.8 HX kinetics of the full-length HtpG and localization of fast and slow exchanging regions. (a) Deuteron incorporation into full-length *E. coli* HtpG in the absence of nucleotides (black circles) and in the presence of ADP (blue diamonds), ATP (red triangles), and AMPPNP (cyan squares). The solid lines are fits of a tri-exponential equation to the data. **(b)** Deuteron incorporation into full-length HtpG-E34A variant in the absence of nucleotides (open black circles) and in the presence of ATP (open red triangles). **(c)** Sequence coverage of peptic peptides of HtpG. The amino acid sequence of *E. coli* HtpG is shown with the secondary structure elements as found in the crystal structure of nucleotide-free HtpG (PDB entry code 2IOQ) above the sequence (dashed lines are not resolved in the crystal structure). The black lines below the sequence indicate the peptic peptides that were found consistently in our HX-MS experiments. The colored bars show deuteron incorporation of the respective segment (i.e. the peptic peptide minus the N-terminal amino acid, which lost any incorporated deuteron during peptic cleavage) after 10 s and 10 min in D_2O as specified at the bottom of the figure.

2.2.2 The ATPase cycle of HtpG

The issue, whether the highly protected state was an ATP-bound state or a post-hydrolysis state, could be resolved by determining the rate-limiting step of the ATPase cycle. To this end we measured the ATPase rate of HtpG under steady state and single turnover conditions. The ATPase rate of HtpG increased with increasing ATP concentrations according to normal Michaelis-Menten kinetics with a k_{cat} of 0.011 ± 0.001 s^{-1} (τ = 90 s) and a K_M of 250 ± 82 µM at 30°C (Fig. 2.9). Under single turnover conditions the amount of ATP decreased with single exponential kinetics resulting in a hydrolysis rate k_{hyd} of 0.0077 ± 0.0003 s^{-1}, which is smaller but close to the steady state ATPase rate. These results demonstrate that product release is not rate-liming in the ATPase cycle of HtpG. Therefore, in the presence of high concentrations of ATP the majority of HtpG molecules is in the ATP-bound state.

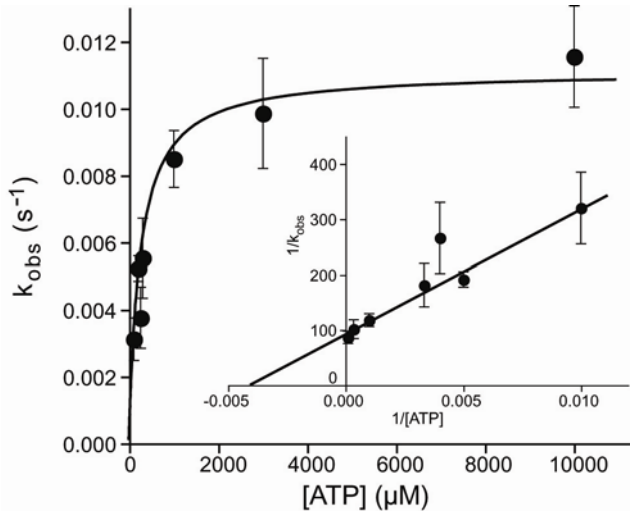

Fig. 2.9 Michaelis-Menten kinetics of the ATPase activity of HtpG. The observed steady-state ATPase rate is plotted against the ATP concentration. Error bars represent the standard error of means of at least 3 independent determinations. The solid line shows a non-linear regression fit of the Michaelis-Menten equation to the data. The inset shows a Lineweaver-Burk representation of the data and the fit.

As an independent confirmation of these results, we repeated the HX experiments in the presence of the non-hydrolysable ATP analogue AMPPNP, which was devoid of any detectable amounts of ATP (Fig. 2.8a). Here we also observed a strong protection of about 35 amide hydrogens as compared to 7 in the presence of ADP and 47 in the presence of ATP. Strikingly, in the presence of AMPPNP we observed the same protection throughout the entire kinetics up to 3600 s incubation time, which contrasts the loss of protection observed after 1200 s in the presence of ATP. We made the same observation when using an HtpG variant with Glu^{34} replaced by Ala (HtpG-E34A; constructed in analogy to the hydrolysis-deficient yeast Hsp82-E33A (Obermann et al., 1998; Panaretou et al., 1998), which in our

hands hydrolyses ATP about 10-times more slowly (τ = 1071 s) at 30°C (Fig. 2.8b). These data indicate that the loss of protection in the presence of ATP is linked to ATP hydrolysis. Taken together, our results demonstrate that (1) ATP hydrolysis is the rate-limiting step in the ATPase cycle of HtpG, (2) the ATP-bound state is the most compact state with least solvent accessible amide hydrogens, and (3) the ADP state shows only little protection as compared to the nucleotide-free state suggesting similar conformations. The most compact ATP-bound state we will call henceforth the tensed (T) state and the nucleotide-free the relaxed (R) state.

2.2.3 Localization of fast and slow exchanging regions in nucleotide-free HtpG

In order to localize the regions within HtpG that contain slow and fast exchanging amide hydrogens we digested the protein after the HX reaction under quench conditions using a column with immobilized pepsin in our HPLC setup as described previously (Rist et al., 2003). The regularly observed peptic peptides of HtpG had an average length of 14.5 residues and covered 88% of HtpG's sequence. Fig. 2.8c shows the deuteration level of the analyzed peptic fragments when the protein was incubated for 10 s or 10 min in D_2O. Our HX data of HtpG free in solution are in good agreement with the published crystal structure of HtpG in the apo state (PDB entry code 2IOQ). Two regions of the NBD, the very N-terminus (residues 1-31) and the so-called ATP-lid (residues 90-127), exhibited a high degree of solvent accessibility with almost complete deuteration within 10 s despite the fact that the crystal structure indicates secondary structure with a significant number of hydrogen bonds. However, these regions have a relatively high b-factor denoting high degrees of positional variation consistent with our data.

2.2.4 Localization of nucleotide-induced changes in HtpG

Recently, it was proposed that HtpG undergoes conformational changes as rigid body movements (Shiau et al., 2006). If this is the case, nucleotide-induced changes in solvent accessibility should be located primarily at hinge regions. To localize nucleotide-induced conformational changes, we compared deuteron incorporation into different segments of HtpG in the absence of nucleotide and presence of ADP, ATP, and AMPPNP (Fig. 2.10). Addition of ADP only had small effects on the incorporation of deuterons. For example, amide hydrogens were protected in the nucleotide-binding site (residues 90-98) and in the N-

terminal segment (residues 2-19). In addition, a small but significant deprotection was detected in specific segments in the NBD (residues 108-119), the MD (residues 279-299, 401-416 and 437-449) and almost the entire C-terminal DD.

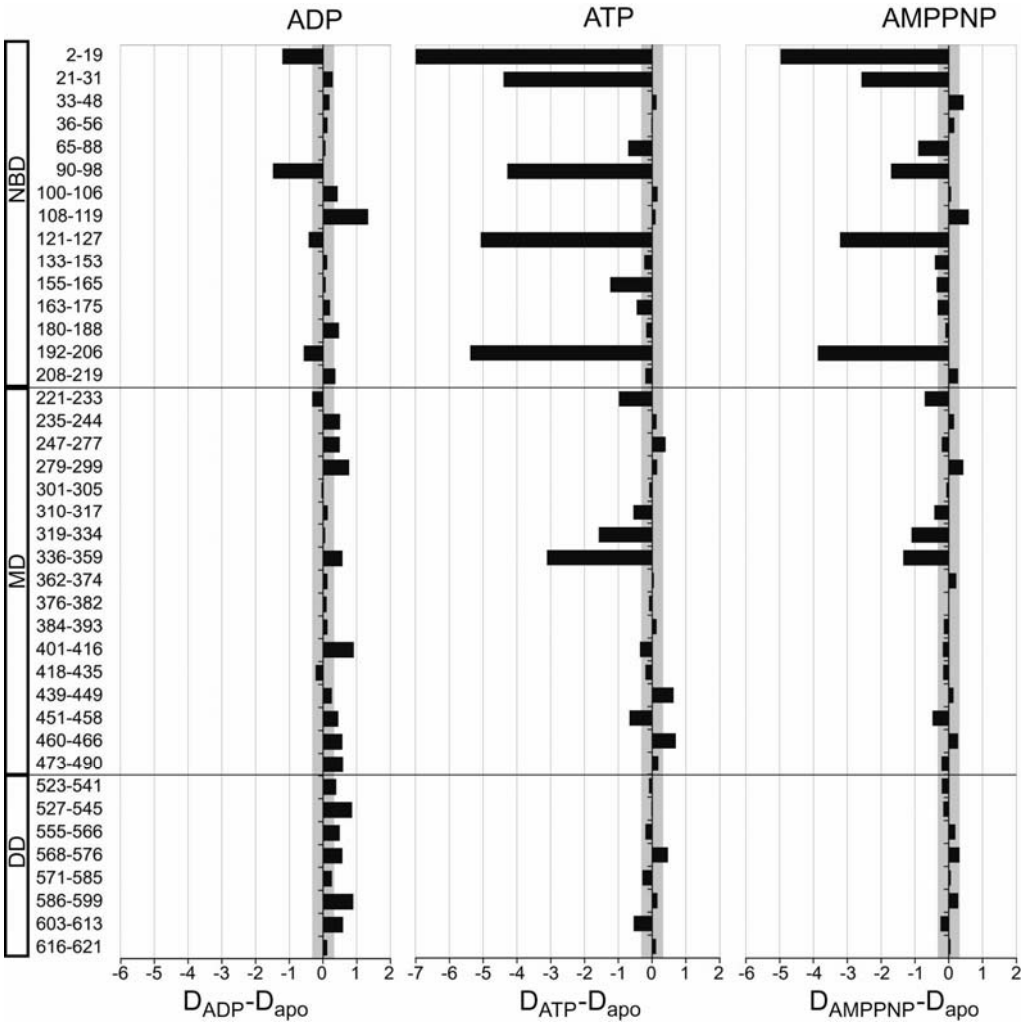

Fig. 2.10 Nucleotide-dependent changes in HtpG. Difference plots of deuterons incorporated in the presence of ADP (left panel), ATP (middle panel) and AMPPNP (right panel) minus deuterons incorporated in the absence of nucleotides into HtpG after 30 s in D_2O. The domain structure of HtpG and numbers of the corresponding segments are given at the left of the panels. The data are the average of three independent experiments. The gray area indicates the average standard error and bars within the gray area are not significantly different from zero.

In the presence of ATP, we observed in seven segments a large protection (up to 7 amide hydrogens) compared to the nucleotide-free state (Fig. 2.10 middle panel and Fig. 2.11 dark blue segments): the N-terminal segments 2-19 and 21-31, the ATP-lid segments 90-98 and 121-127, the last helix of the NBD (residues 192-206), and the loop in the MD that contains the catalytic arginine (residues 319-334 and 336-359). We detected a small but significant protection in additional segments scattered throughout the entire protein (Fig. 3 cyan segments). A few segments in the C-terminal region exhibited slightly more exchange in the

presence of ATP than in the nucleotide-free state (Fig. 2.11, orange segments). Thus, our data demonstrate that ATP induces large conformational changes not only in the NBD but throughout the HtpG protein leading to a significant loss of conformational dynamics.

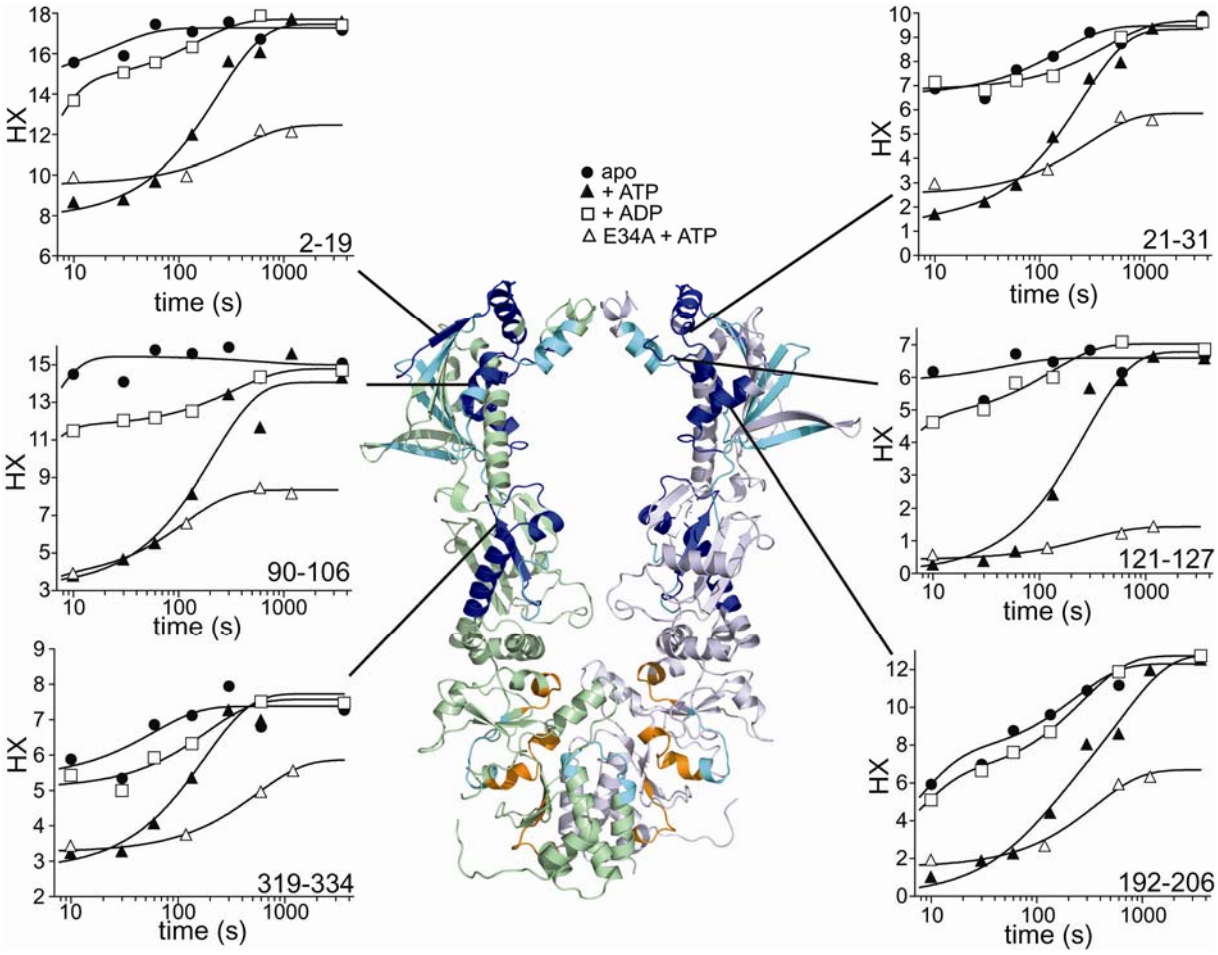

Fig. 2.11 Nucleotide-dependent HX kinetics of selected segments of HtpG. Secondary structure representation of the crystal structure of full-length *E. coli* HtpG in complex with ADP (PDB ID code 2IOP; only one dimer shown with one monomer in gray and the other in pale green). Segments with more than 1.5 amide hydrogens protected in the presence of ATP at time point 30 s are colored in dark blue and the HX kinetics for these segments in the absence of nucleotides (black circles) and the presence of ADP (open squares) and ATP (black triangles) and for HtpG-E34A in the presence of ATP (open triangles) are shown. The solid lines are fits of a bi-exponential equation to the data to guide the eye. Segments with one to two amide hydrogens protected at 30 s are colored in cyan. Segments deprotected upon ATP binding are colored in orange.

The kinetics of deuteron incorporation in all of the highly protected segments in the presence of ATP was nearly identical with an average rate of 0.0038±0.0005 s^{-1} (Fig. 2.11). This is very unusual, since different segments of a protein usually exchange with different kinetics (see Fig. 2.11). These findings could be explained by the hypothesis that a process different from protein unfolding and folding, explicitly ATP hydrolysis, is rate-limiting for HX in the ATP-bound state. Indeed, the mutant protein HtpG-E34A exhibited a similar protection in the presence of ATP and this protection was observed over a much longer time interval, which

demonstrates that the HX reaction follows different kinetics in HtpG-E34A. These data suggest that ATP hydrolysis is rate-limiting for HX. Consistent with this hypothesis is the observation of a bimodal distribution of the isotope peaks in several peptides (Fig. 2.12). Bimodal isotopic peak distributions are indicative of the coexistance of two different conformational states. These two conformational states are the ATP-bound T state, in which the segments are largely protected from HX, and the ADP-bound and nucleotide-free R state with higher HX rates.

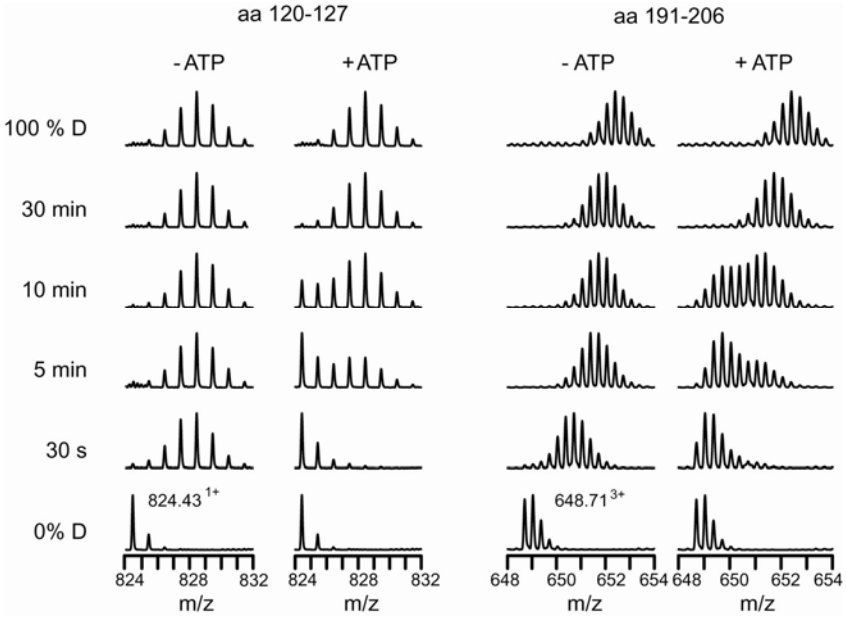

Fig. 2.12 Effects of ATP on deuteron incorporation into selected segments of HtpG. Mass spectra of two peptic peptides (120-127, 191-206) of HtpG in the absence of nucleotides and the presence of ATP after 30 s, 5 min, 10 min, and 30 min incubation in D_2O as indicated at the left. The spectra of the peptic peptides in the undeuterated (0% D; bottom) and the fully deuterated (100% D; top) state are shown for comparison. The spectra of the samples in the presence of ATP exhibit a bimodal distribution of the isotope peaks indicative of coexisting conformations.

In the presence of AMPPNP, the same changes in deuteron incorporation occurred as in the ATP-bound state, which confirms that the T state is the pre-hydrolysis state (Fig. 2.10). The magnitude of the observed protection was slightly reduced compared to the ATP-bound state consistent with our HX data for full-length HtpG.

Taken together, significant nucleotide-dependent changes of the conformational dynamics of HtpG were observed which were not localized to hinge regions but to all three globular domains of the protein. Our data not only demonstrate the existence of an R and a T state but show which structural elements of the protein are more tightly folded in the T state.

2.2.5 Kinetics of R to T transition

In order to investigate whether γ-phosphate cleavage or preceding conformational changes are rate-limiting for the ATPase cycle of HtpG we determined the rate of R to T transition using pulse-labeling HX experiments. HtpG and HtpG-E34A were incubated for different time intervals with ATP and then pulse-labeled for 10 s with D_2O. Since the HX reaction times were always identical, changes in the numbers of incorporated deuterons are due to the ATP-induced transition from the R to the T state. In the absence of ATP or at the shortest time-point after addition of ATP only one mass peak is observed Fig. 2.13a and b).

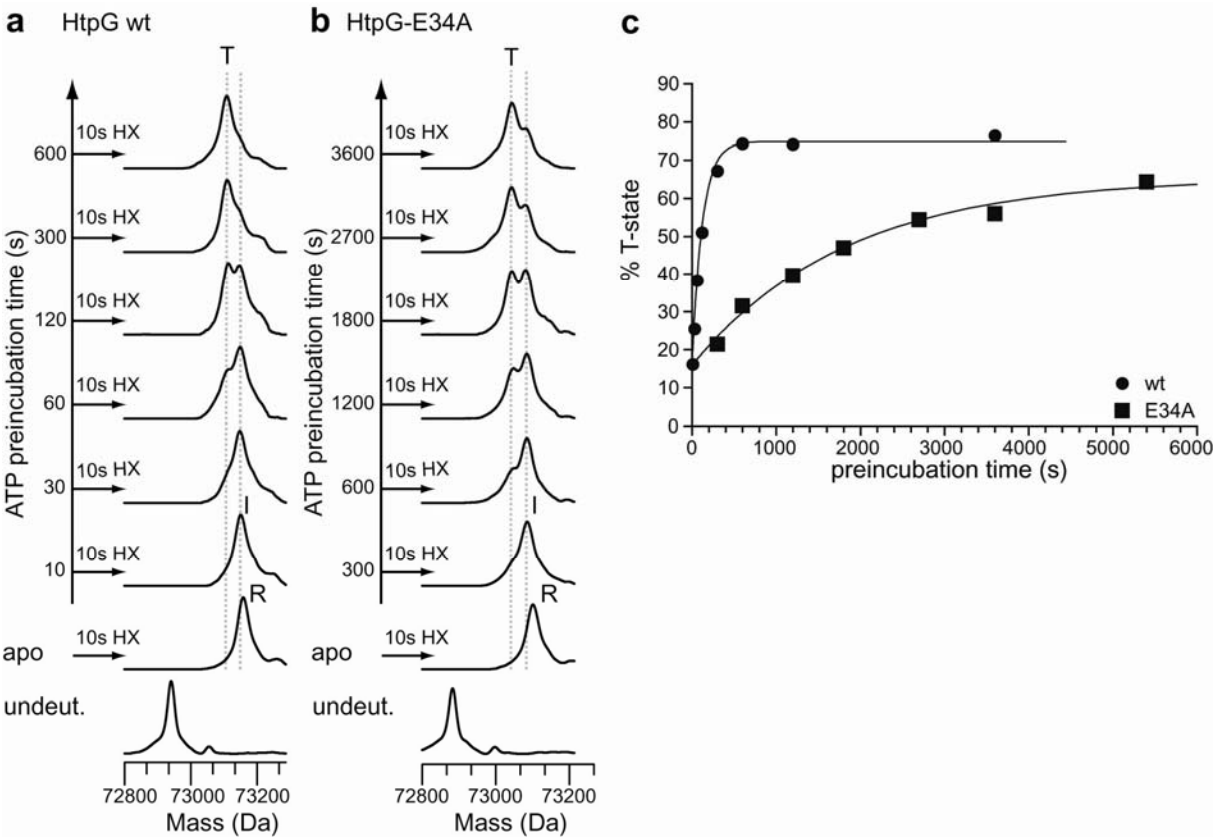

Fig. 2.13 Kinetics of the ATP-induced R to T transition of HtpG. Deconvoluted mass spectra of wild type HtpG **(a)** and HtpG-E34A **(b)** before incubation in D_2O (bottom curve), after 10 s in D_2O in the absence of nucleotides (apo; R state) or after different pre-incubation times in the presence of ATP (as indicated to the left) followed by pulse-labeling for 10 s in D_2O. Dashed gray lines indicate the maximum of the mass peaks after 10 s preincubation in the presence of ATP (I state) and after 600 and 3600 s preincubation in ATP (T state) as designated. **(c)** Relative amount of T state versus the pre-incubation time in ATP. A first order rate equation was fitted to the data (solid line) to give the I to T conversion rates of 0.01 s^{-1} and 0.0006 s^{-1} for wild type HtpG and HtpG-E34A, respectively.

However, the mass of pulse-labeled HtpG after the shortest incubation with ATP was already smaller than the mass of pulse-labeled *apo*-HtpG indicating a conformational transition that happens within 10 s. At later time points a second species with a still lower mass appeared

and became dominant. These data strongly suggest a two-phase transition: a rapid transition between the fast exchanging R state to a slightly protected intermediate (I) state and a subsequent slow transition to the fully protected T state. The second transition is much slower in HtpG-E34A. We fitted an equation for two Gaussian peaks with different means and areas but similar width to the data and determined the percentage of I and T states. The average I to T conversion rates for wild type HtpG and mutant HtpG-E34A were 0.01 s^{-1} and 0.0006 s^{-1}, which are within the error of the experiment identical to the ATP hydrolysis rates demonstrating that the conformational changes are rate-limiting for ATP hydrolysis.

2.2.6 Spatial resolution of the R to T transition

Our peptide data revealed ATP-dependent conformational changes in regions close to the nucleotide-binding site but also in regions far distant in space. This raises the question of whether all ATP-induced conformational changes occur simultaneously in a concerted fashion or whether they occur in an ordered succession of events. In the first scenario, the protein would oscillate continuously between an open and a closed state with ATP-binding trapping the closed state. In the second scenario ATP would bind to the open state and trigger local conformational changes that are subsequently propagated throughout the protein. To distinguish between these two scenarios, we performed spatially resolved pulse-labeling HX experiments by including peptic digestion under quench conditions after pulse-labeling.

The comparison of the mass spectra of selected peptic peptides of HtpG in the nucleotide-free state with 10 s of incubation with ATP already revealed a significant shift of the center of the isotopic peak distribution towards lower m/z values most notably in peptides 89-98 and 120-127 but also in peptides 1-19 and 335-359 (Fig. 2.14a). These data locate the conformational changes that lead to the I state. At subsequent time points the isotope peaks in most spectra formed a clear bimodal distribution, which demonstrates the simultaneous presence of two HtpG states with different solvent accessibility. The more accessible state slowly converts into a more protected state. From the intensities of the highest peaks in the two states we determined the rates for the I to T transition for each of the peptides analyzed. Interestingly, the rate of I to T conversion was different in the analyzed segments (Fig. 2.14b). The transition rate was highest in the ATP-lid (segments 90-98 and 121-127) and decreased towards the N-terminal segment 2-19 and the MD segments 320-334 and 336-359, which contains the catalytic Arg^{336} (homologous to Arg^{380} in yeast Hsp82). For the HtpG-E34A variant protein, we observed the same phenomenon, albeit with overall much lower rates (Fig. 2.14c). These data confirm that the R to T transition occurs in two phases: a fast

phase, which cannot be resolved by HX, and a slow phase. Since the first phase not only affects the ATP-lid region but also the N-terminus and segments in the MD, it is a global transition to an intermediate state (I) that may happen in a concerted fashion. The major second phase, the transition from the I state to the T state, does not occur in all segments simultaneously but in sequential steps. The I to T conversion in the MD segments has the same rate as the single turnover ATPase rate indicating that this conformational change is rate-limiting for γ-phosphate cleavage.

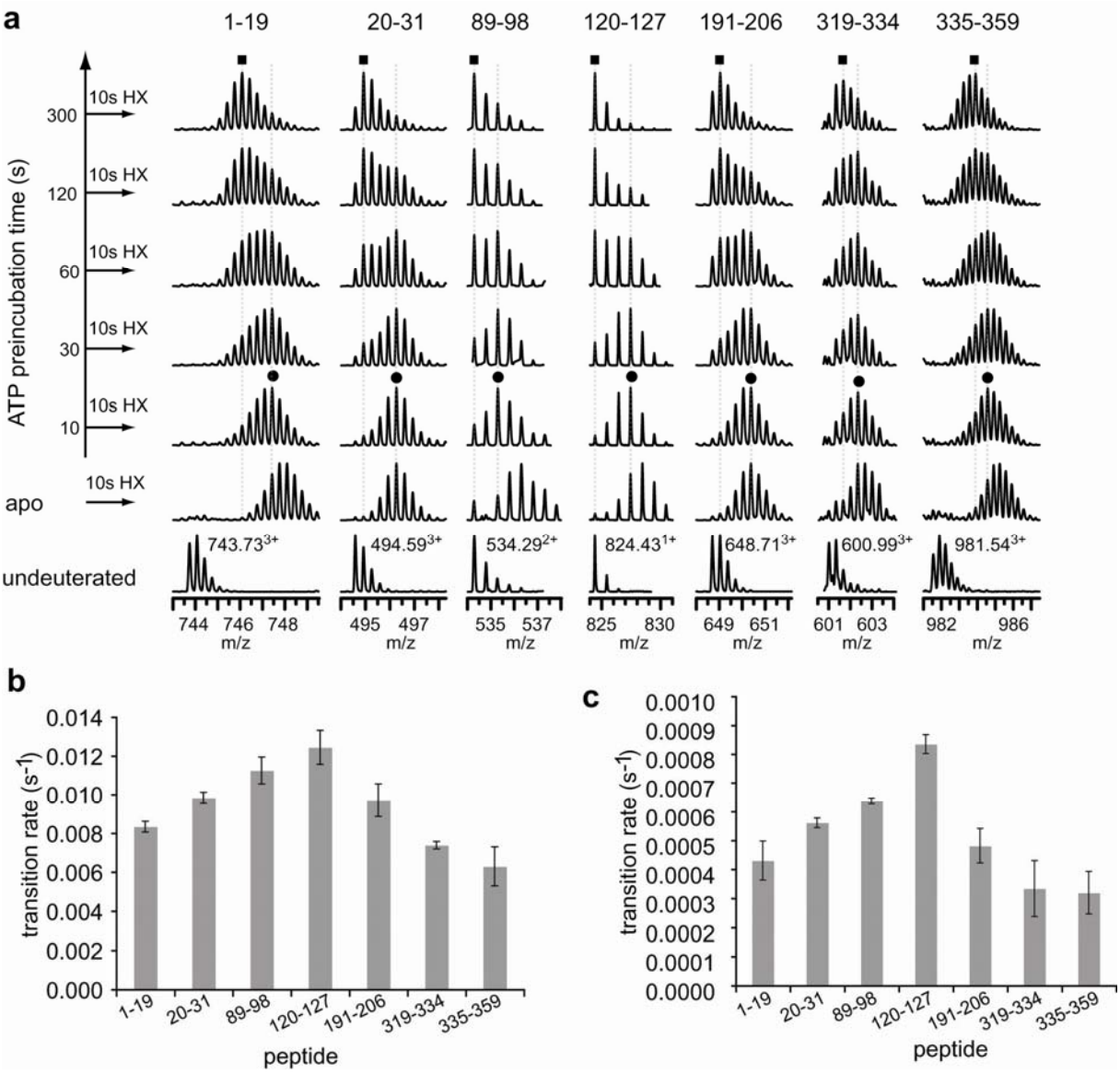

Fig. 2.14 Spatially resolved kinetics of R to T transition. **(a)** Representative mass spectra (m/z scale) of selected peptic peptides of wild type HtpG before incubation in D_2O (bottom curve; monoisotopic mass and charge state are given), after 10 s in D_2O in the absence of nucleotides (apo) or after pre-incubation for 10 to 300 s in the presence of ATP (as indicated to the left) followed by pulse-labeling for 10 s in D_2O. The residue numbers of the peptides are given above the spectra. Dotted gray lines indicate the highest peak after 10 s pre-incubation in ATP followed by 10 s HX (I state, black circle) and the highest peak after 300 s pre-incubation in ATP followed by 10 s HX (T state, black square). **(b)** I to T transition rates for selected peptides of wildtype HtpG calculated as described in Materials and Methods. The bars represent the mean of 3 independent determinations and standard error of mean. **(c)** I to T transition rates for selected peptides of HtpG-E34A.

2.2.7 Conformational changes in HtpG followed by fluorescence

We wished to extend our study to the analysis of global domain movements. To this end, we introduced fluorescent labels at position 12 in HtpG in order to perform fluorescence resonance energy transfer (FRET) experiments. Prodromou and coworkers previously used the homologous position in yeast Hsp82 for pyrene excimer fluorescence (Prodromou et al., 2000). HtpG-E12C was labeled with Hilyte Fluor™ 488 ($HtpG_{FL}$) as donor and the quantum dot QXL520 as fluorescence quencher ($HtpG_Q$). Upon mixing of $HtpG_{FL}$ and $HtpG_Q$, donor fluorescence decreased significantly, which indicates that heterodimers formed and that the two fluorescent dyes were within the Förster distance of each other. Addition of ATP but not ADP induced a time-dependent decrease in fluorescence. However, a similar ATP-dependent decrease in fluorescence was also observed in the absence of $HtpG_Q$ (Fig. 2.15a) demonstrating that the decrease in donor fluorescence was caused by a change in the environment of the donor fluorophor. The same fluorescence decrease was observed for the HtpG-E34A variant albeit with slower kinetics (Fig. 2.15b). Addition of a large excess of ADP to reactions of $HtpG_{FL}$ already equilibrated with ATP led to an increase in fluorescence (Fig. 6c). Close inspection of the fluorescence traces after addition of ATP revealed that the fluorescence emission first increased rapidly before it decreased again (Fig. 2.15a and c). We determined the kinetics of the first phase in dependence of the ATP concentration using stopped-flow measurements (Fig. 2.15d and e). The observed rate increased with increasing ATP concentrations according to a hyperbolic relationship, which indicates a two-step process with a fast equilibrium as first step and a subsequent isomerization. The equilibrium constant for the first step was determined to 3.6 ± 0.6 mM and the forward and back reaction rates for the isomerization step to 227 ± 12 s^{-1} and 30 ± 5 s^{-1}. The isomerization step was followed by a much slower conformational change, which caused a decrease in fluorescence. The rate for this step was determined to 0.0089 ± 0.0003 s^{-1}, which is very close to the conversion rate of segment 2-19 as determined by HX-MS (Fig. 2.14b). The reversion of the fluorescence decrease upon addition of a large excess of ADP to the equilibrated reaction of $HtpG_{FL}$ with ATP occurs with a rate of 0.0062 ± 0.0003 s^{-1}, which is similar to the ATP hydrolysis rate at the HtpG and ATP concentrations used. This argues that ATP hydrolysis is rate-limiting for the fluorescence change and that ATP dissociation from this stage occurs at a rate of $\leq 0.0062\ s^{-1}$. These data suggest that once the ATPase cycle has reached this point ATP is committed to catalysis.

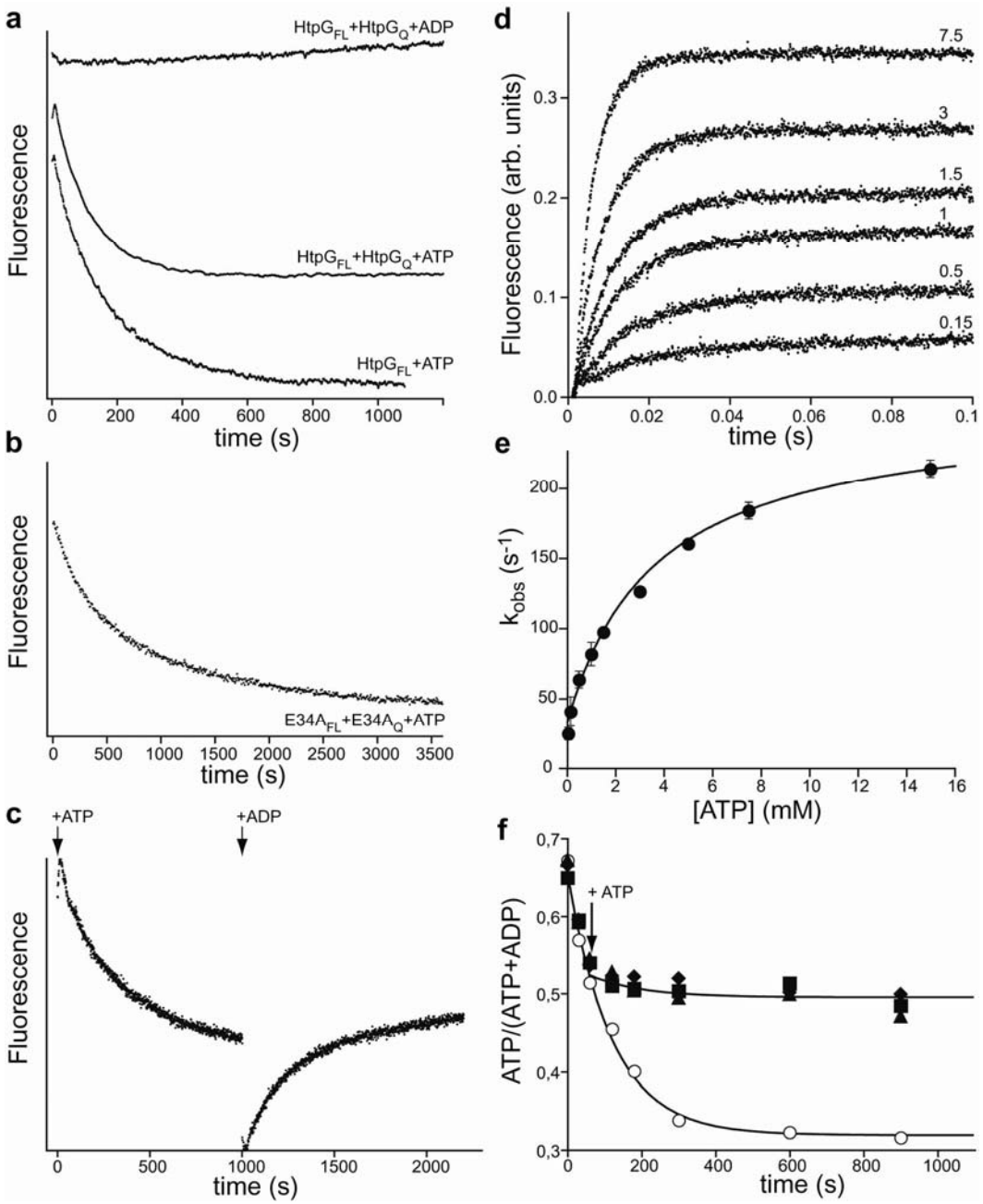

Fig. 2.15 Kinetics of nucleotide-induced conformational changes followed by fluorescence. (a) Fluorescence trace of HtpG-E12C-Hilyte Fluor™ 488 (HtpG$_{FL}$; 300 nM) in the absence or presence of HtpG-E12C-QXL-520 (HtpG$_{Q}$; 600 nM) after addition of ADP (20 mM) or ATP (20 mM) as indicated (excitation 475 nm; emission 525 nm). For better visibility the curves were shifted in y-axis direction. **(b)** Fluorescence trace of HtpG-E12C,E34A-Hilyte Fluor™ 488 (HtpG-E34A$_{FL}$; 300 nM) in the presence of HtpG-E12C,E34A-QXL-520 (HtpG-E34A$_{Q}$; 600 nM) after addition of ATP. **(c)** Fluorescence trace of HtpG$_{FL}$ (300 nM) after addition of ATP (20 mM) and subsequent addition of ADP (60 mM) as indicated by the arrows. **(d)** Fluorescence traces of HtpG$_{FL}$ (150 nM final concentration) after mixing 1:1 with 0.15 to 7.5 mM ATP (final concentrations) (excitation 488 nm; cut-off filter 530 nm). **(e)** Plot of the observed rates of fluorescence increase versus the ATP concentration. The solid line represents the non-linear regression fit of a hyperbolic equation giving a K_{D1} of 3.6 ± 0.6 mM, k_2 of 227 ± 12 s^{-1} and k_{-2} of 30 ± 5 s^{-1} (means of two independent determinations). **(f)** Single-turnover ATPase assay to determine the degree of commitment to catalysis of bound ATP. HtpG (50 µM) was mixed with [α-^{32}P]ATP (40 µM; 3.7 kBq) and ATP hydrolysis followed by thin layer chromatography and phosphoimaging. The ratio of ATP divided by ATP plus ADP is potted versus incubation time. At the indicated time point 5 mM unlabeled ATP was added to the samples with filled symbols (3 independent experiments shown); open circle, control sample. The solid lines are non-linear regression fits of a single exponential decay function to the data.

In order to test this hypothesis, we performed single turnover ATPase assays using [α-^{32}P]ATP and adding an excess of unlabeled ATP 60 s after the start of the reaction (Fig. 2.15f). After addition of unlabeled ATP conversion of [α-^{32}P]ATP into ADP did not stop immediately but continued with essentially the same rate but the total amount of ATP that was converted decreased to 13 % of the control sample. These data indicate that 13% of the ATP could not be replaced by cold ATP and was therefore committed to catalysis. Approximately the same fraction of HtpG molecules is converted into the T state under these conditions.

Upon addition of ADP to $HtpG_{FL}$ we also observed a rapid increase in fluorescence but no subsequent slow decrease. (Fig. 2.16, Fig. 2.15a). These data are consistent with our HX-MS experiments, which revealed a small protection in segment 2-19 in the presence of ADP but not the large conformational change observed in the presence of ATP.

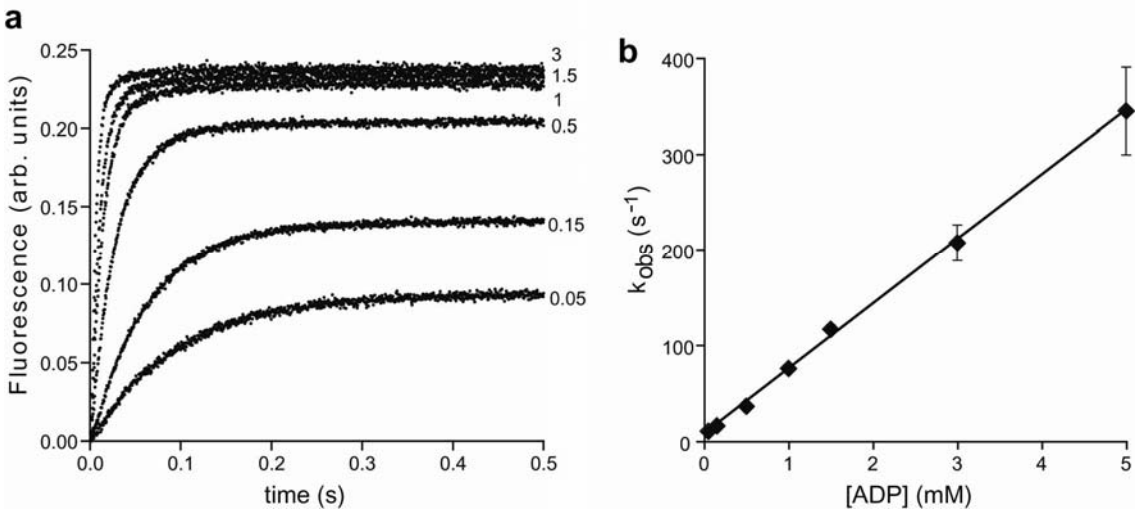

Fig. 2.16 Association of ADP to HtpG followed by fluorescence spectroscopy. (a) Fluorescence traces of $HtpG_{FL}$ (150 nM final concentration) after mixing 1:1 with 0.15 to 3 mM ADP (final concentrations) (excitation 488 nm; cut-off filter 530 nm). **(b)** Plot of the observed rates of fluorescence increase versus the ADP concentration. Linear regression analysis resulted in association and dissociation rate constants of 70,000 ± 2,000 M^{-1} s^{-1} and 5.4 ± 1.6 s^{-1}, respectively, from which a K_D of 78 ± 23 µM could be calculated.

Taken together, our fluorescence experiments allowed us to dissect the ATPase cycle of HtpG Fig. 2.18a). The fluorescent probe monitored a series of nucleotide-dependent conformational changes in the segment 2-19, which are fully consistent with our HX-MS experiments. These data also demonstrate that the last slow conformational change after addition of ATP leads to the trapping of ATP and commitment to catalysis.

2.2.8 Distances between the two NBDs in the HtpG dimer

Our FRET experiments could not detect nucleotide-dependent changes in the distance between the two NBDs of the HtpG dimer. We therefore used site-specific crosslinking to detect domain movements. First, we tried to form disulfide bonds between the two NBDs of the HtpG-E12C dimer. To this end, nucleotide-free HtpG was completely reduced and then treated with diamide in the absence or presence of ADP or ATP. Subsequently, iodoacetamide was added to block any free thiols and the samples were analyzed by non-reducing SDS-polyacrylamide gelelectrophoresis (Fig. 2.17a). Disulfides formed only in the absence of nucleotides and the presence of ADP but not in the presence of ATP indicating that the cysteines in position 12 come within 4 Å in the nucleotide-free and the ADP-bound state.

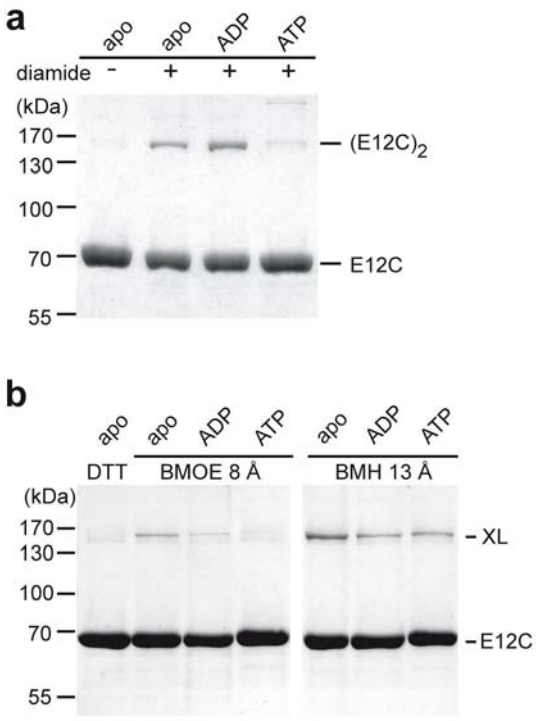

Fig. 2.17 Determination of the proximity of position 12 in the two NBD of the HtpG dimer. (a) Disulfide bond formation. SDS-polyacrylamide gel of reduced HtpG-E12C pre-incubated with the indicated nucleotide for at least 10 min, treated with diamide for 10 min (where indicated) and subsequently with iodoacetamide. Gel was run under non-reducing conditions and stained with Coomassie Brillant Blue. Molecular weights are given at the left, the disulfide linked HtpG-dimer is indidated at the right.
(b) Crosslinking of HtpG-E12C with bis(maleimido)ethane (BMOE) and bis(maleimido)hexane (BMH) in the absence of nucleotide or the presence of ADP or ATP as indicated. SDS-polyacrylamide gels were run under reducing conditions and stained with Coomassie Billant Blue. The HtpG and crosslink (XL) bands are designated.

To obtain information on the distance of the thiol groups of Cys^{12} in the HtpG dimer in the presence of ATP we added the homobifunctional thiol-specific crosslinker bismaleimidoethane (BMOE) and bismaleimidohexane (BMH) with a length of 8 and 13 Å, respectively (Fig. 2.17b). As expected, both crosslinker were able to crosslink the HtpG dimer in the absence of nucleotides and in the presence of ADP. In the presence of ATP a crosslinking product only formed when BMH was used but not with BMOE suggesting that the thiol groups of Cys^{12} have a distance of more than 8 Å and less than 13 Å in the presence of ATP. These data are consistent with the formation of a strand exchange between the two

NBDs of the HtpG dimer since the distance of the Cβ and Cγ atoms of the two Glu^{12} in the dimeric homology model of HtpG on the Hsp82 dimer structure is 12.2 and 11.3 Å, respectively.

2.2.9 Discussion

Our analysis of the conformational dynamics of the *E. coli* Hsp90 homologue HtpG yielded the following novel insights into the ATPase cycle of HtpG: (1) Nucleotide binding induces conformational changes in NBD, MD and C-terminal DD; (2) The ATP-bound state is the most compact state of HtpG with least backbone amide hydrogens solvent accessible; (3) The majority of the ATP-induced conformational changes happen surprisingly slow in a sequential fashion, starting with the nucleotide binding pocket and progressing like a wave to the very N-terminus and to the MD; (4) Glu^{34} is important for the rate of R to T conversion; (5) The slow conformational change leads to trapping of the ATP and to commitment to catalysis; this step is rate-limiting for ATP hydrolysis and therefore acts like a timer for the chaperone cycle of HtpG; (6) In the ATP-bound state the two NBDs of the HtpG dimer are within 13 Å of each other consistent with the strand exchange mechanism of yeast Hsp82. In addition our fluorescent probe allowed us to determine the kinetics of ATP-binding, which occurs in a multi-step process.

Our data differ significantly from a recent HX-MS study on human Hsp90 (Phillips et al., 2007). Jackson and coworkers analyzed in this study the influence of two inhibitors, which bind into the nucleotide-binding pocket, and of the cochaperone Cdc37 on the conformational flexibility of Hsp90. Although some of the inhibitor-induced changes in human Hsp90 occurred in similar regions as the ATP-induced changes in HtpG, the magnitude was much smaller and it remains an open question whether inhibitors in general cause smaller changes than nucleotides or whether the human Hsp90 protein is less affected by ligand binding to the nucleotide binding pocket.

A recent crystallographic and electronmicroscopic study provided evidence that HtpG performs dramatic conformational changes when progressing through the ATPase cycle (Shiau et al., 2006). In this study the ADP-bound state was proposed to be the most compact conformation within the ATPase cycle of HtpG. Our data demonstrate that the ATP-bound state and not the post-hydrolysis or the ADP-bound state is the least solvent accessible and most rigid state of HtpG.

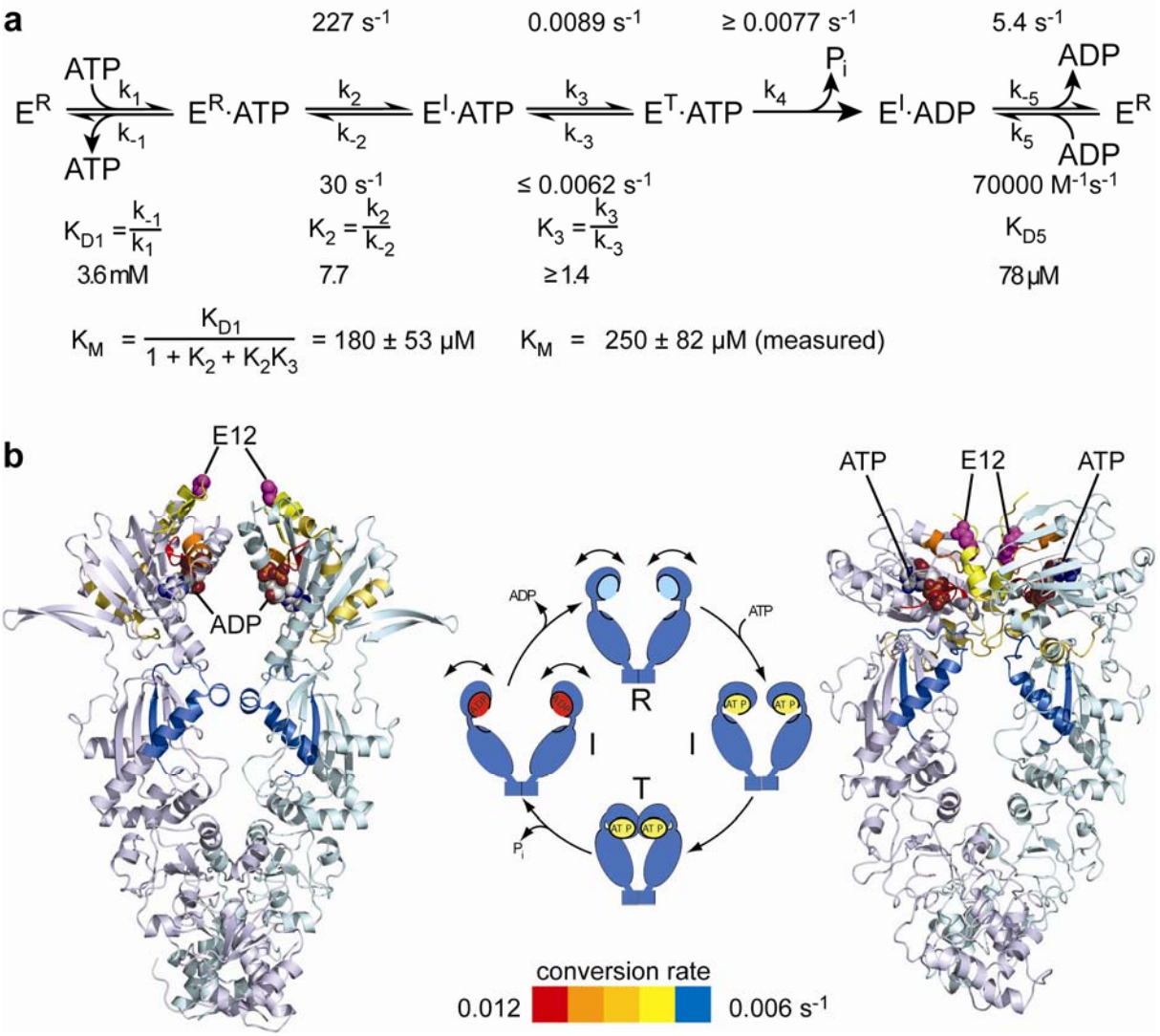

Fig. 2.18 ATPase cycle of HtpG and model of conformational changes. (a) Steps of the ATPase cycle of HtpG with rate and equilibrium constants as determined by fluorescence spectroscopy and biochemical assays. E^R, E^I, and E^T, HtpG in the relaxed, intermediate and tensed states. **(b)** Model of conformational changes of HtpG during the ATPase cycle. Secondary structure representations of the crystal structure of ADP-bound HtpG (PDB entry code 2IOP (Shiau et al., 2006); left panel) and of an homology model of HtpG on the crystal structure of yeast Hsp82 in complex with AMPPNP and Sba1 (PDB entry code 2CG9 (Ali et al., 2006; Guex and Peitsch, 1997; Peitsch, 1996)) as model for the ATP-bound structure of HtpG (right panel) colored according to the I to T transition rates with red (high rates) to blue (low rates). Residue Glu^{12} (E12), where the fluorescent dye was attached in the HtpG-E12C variant, is shown in magenta. Between the structural representations a model of the ATPase cycle is shown which includes the nucleotide-free R state, the first intermediate (I state) after ATP binding, the T state and the ADP-bound state, which is similar to the I state. The nucleotide-free and ADP-bound states can assume several conformations as indicated by the double arrows since the distance of E^{12} in the crystal structure is 38 Å but could be crosslinked with an 8 Å crosslinker or form disulfide bridges requiring a 4 Å proximity.

While the ADP-bound state may have a more compact shape as proposed by Agard and coworkers (Shiau et al., 2006), it is nonetheless almost as flexible as the nucleotide-free state, whereas the ATP-bound state has a much lower degree of conformational dynamics.

Such flexibility of the nucleotide-free and ADP-bound states cannot be restricted to secondary structure but must also accompany domain movement. In neither the dimer structure of ADP-bound HtpG (PDB entry code 2IOP) nor the dimeric model of the nucleotide-free structure of HtpG (PDB entry code 2IOQ) are the Glu^{12}s of the two protomers within 30 Å of each other. These conformations would not allow crosslinking with BMH or BMOE nor disulfide bond formation. We conclude that the NBDs sample conformations that bring the two Glu^{12} within 4 Å of each other.

The reduced flexibility in the ATP-bound state could be important for high-affinity client binding. ATP hydrolysis might release the strain and therefore lower the affinity for clients. Such a model would be consistent with data for yeast Hsp90 demonstrating that ATP hydrolysis leads to client dissociation (Young and Hartl, 2000). Our results provide a thermodynamic explanation for this phenomenon: In the nucleotide-free state the conformational flexibility, and therefore the conformational entropy, is much higher than in the ATP-bound state. It is conceivable that client binding reduces the conformational entropy in the interacting parts of HtpG. Client release in the ADP-bound or nucleotide-free state would therefore be accompanied by an increase in conformational entropy, which would favor the dissociation reaction. In the ATP-bound state this increase in conformational entropy upon client dissociation would be much smaller due to the more rigid structure of HtpG. This would result in shifting the equilibrium to the bound form. The chaperone cycle of HtpG may start with client binding to the nucleotide-free state with relatively high conformational entropy. ATP binding leads to a tight binding of the client due to the conformational rigidity. Subsequent ATP hydrolysis relaxes HtpG, which favors client dissociation. The slow ATP-induced conformational change in HtpG might impose a strain on the client protein performing mechanical work on their conformation.

Our HX-MS and fluorescence data demonstrate that ATP binding induces a series of consecutive conformational states that are in equilibrium with each other (Fig. 2.18a). ATP associates with the R-state of HtpG to form an initial encounter complex that has a dissociation equilibrium constant of 3.6 mM. The encounter complex is converted rapidly with a rate of 227 s^{-1} into an intermediate state. This I state is characterized by reduced solvent accessibility of backbone amide hydrogens in several regions of the protein including the N-terminal segment 2-19 and segments in the middle domain and an increase in

fluorescence of a fluorophor at position 12. The transition to the I state occurs most likely in a concerted conformational change. ADP binding also induces a small protection in segment 2-19 (Fig. 2.10) and a fluorescence increase of $HtpG_{FL}$ (data not shown). Thus, the ADP-bound state might be similar to the ATP-induced I state. However, the subsequent slow step to the T state only occurs upon binding of ATP and not ADP. This conversion involves a succession of conformational changes starting in the nucleotide-binding pocket, for which we measured the highest conversion rate, and progressing like a wave towards the N-terminus and the catalytic loop of the MD, which reach the T state conformation with lower rates. This is the first time that such stepwise changes in the conformation in an Hsp90 protein could be spatially and temporally resolved.

Our data are consistent with the proposed ATPase cycle of yeast Hsp82 (Richter et al., 2001; Weikl et al., 2000). ATP associates rapidly with Hsp82 to form an encounter complex. Based on the observed cooperativity of ATP hydrolysis in the dimeric protein, it has been proposed that the encounter complex undergoes two sequential conformational changes: First, docking of the NBD with the MD; second, N-terminal dimerization with strand exchange, which is proposed to be very slow. In the present study, we provide direct evidence for these conformational changes. Our data suggest that N-terminal dimerization of HtpG occurs at the same time as or even precedes docking with the MD. Similar conformational changes were proposed based on crystal structure data and the structural similarity of Hsp90 with DNA gyrase B (Meyer et al., 2003; Prodromou et al., 2000). Evidence for a multi-step ATPase cycle with conformational changes was reported recently for the mitochondrial Hsp90 homologue Trap1 (Leskovar et al., 2008). The ATPase cycle of human Hsp90 and the Hsp90 homologue in the endoplasmic reticulum, Grp94, seem to be less complex and do not involve a slow isomerization step (Frey et al., 2007; McLaughlin et al., 2004). In all investigated Hsp90 proteins ATP hydrolysis was rate-limiting. Based on the correlation of the conversion rates with hydrolysis rate, we propose that the slow conformational change which leads to the docking of NBD and MD is rate-limiting rather than γ-phosphate cleavage itself. Our experiments with the HtpG-E34A variant, which has an ATPase activity of less than 10% of wild type HtpG and also a much lower conversion rate from the I to the T state (Fig. 2.14c) also support this mechanism. It is very unexpected that a single amino acid change would affect the conformational transition rates in distant parts of the protein. However, in the Hsp82 crystal structure, the homologous Glu^{33} is in a central position in the ATPase pocket. One of its carboxyl oxygens forms a hydrogen bond with the γ-phosphate of the AMPPNP,

and the other carboxyl oxygen is 3.6 Å away from one of the terminal nitrogens of Arg^{380} of the middle domain, which is essential for γ-phosphate cleavage. It is conceivable that Glu^{33} guides Arg^{380} to the γ-phosphate, and therefore its replacement with alanine could slow down the formation of a hydrogen bond between Arg^{380} and the γ-phosphate, which would explain the reduced conversion rate of the middle domain segments from the I to the T state and the reduced ATPase activity. In addition, the interaction of this Glu with the ATP could stabilize helix 2 which may favor the formation of the strand exchange complex.

Glu^{33} in Hsp82 was originally linked to catalysis of γ-phosphate cleavage due to the structural similarity to DNA gyrase B, in which the homologous Glu^{42} was shown to act as general base (Jackson and Maxwell, 1993; Obermann et al., 1998; Panaretou et al., 1998). Based on our data, we propose that Glu^{34} in HtpG has an additional role in coordinating the docking of the NBD with the MD and the NBD of the second protomer in the HtpG dimer by guiding Arg^{336} to the γ-phosphate and by stabilizing helix 2, which favors strand exchange.

2.3 Comparative study on the dynamics of eukaryotic Hsp90 chaperones

The HX-MS study on the bacterial HtpG revealed dramatic compaction and stabilization of the protein upon ATP binding and provided insights in the sequential steps of conformational changes during the ATPase cycle. Based on this data we wondered if the dynamics of HtpG is similar to the eukaryotic Hsp90 homologues, the constitutively expressed yeast Hsc82 and human Hsp90β. In contrast to HtpG, eukaryotic Hsp90 chaperones are essential and co-operate with various co-chaperones in order to function in client maturation and activation. However, the nucleotide-dependent dynamics and the binding sites of clients and co-chaperones in eukaryotic Hsp90s are still poorly understood. A recent study performed amide hydrogen exchange and MS on human Hsp90 in complex with inhibitors or the co-chaperone Cdc37, but could only detect minor conformational changes which affected all domains throughout the protein (Phillips et al., 2007). We performed HX-MS experiments with yHsc82 and hHsp90β in absence or presence of nucleotides and inhibitors in order to elucidiate the effect of real ligands on the Hsp90 conformation.

2.3.1 Global deuteron incorporation into human Hsp90β and yeast Hsc82

Both hHsp90β and yHsc82 were purified from *E. coli* with the SUMO-strategy resulting in pure nucleotide-free proteins without any additional tag. The activity of the proteins was tested by measuring the steady-state ATPase activity at 30°C using an enzyme-coupled assay. Human Hsp90 was determined to have a low ATPase activity of 0.0915±0.004 min^{-1}, while yeast Hsc82 displayed a higher activity of 0.73 ±0.054 min^{-1} at 5 mM ATP. The activities were slightly higher but close to published turnover numbers (McLaughlin et al., 2002; Panaretou et al., 1998; Weikl et al., 2000).

To analyze the conformational flexibility of the full-length Hsp90 proteins we performed HX-MS at 30°C and compared the results with the data acquired for *E. coli* HtpG. We found that the yeast and human Hsp90 proteins are extremely flexible at the secondary structure level exchanging in the nucleotide-free state close to 50% of their amide hydrogens within 10 s and more than 70% within one hour (Fig. 2.19a). Well folded proteins are expected to retain 40 to 50% of their amide hydrogens during a 60 min time period. In contrast to the eukaryotic Hsp90 proteins, HtpG is more stable exchanging only 38% within 10 s and around 60%

within one hour. This difference in mobility is not due to the different length of the charged linker connecting nucleotide binding domain (NBD) and middle domain (MD) (see Fig. 2.20a) and also apparent when the numbers of linker amide hydrogens are subtracted from the data (Fig. 2b).

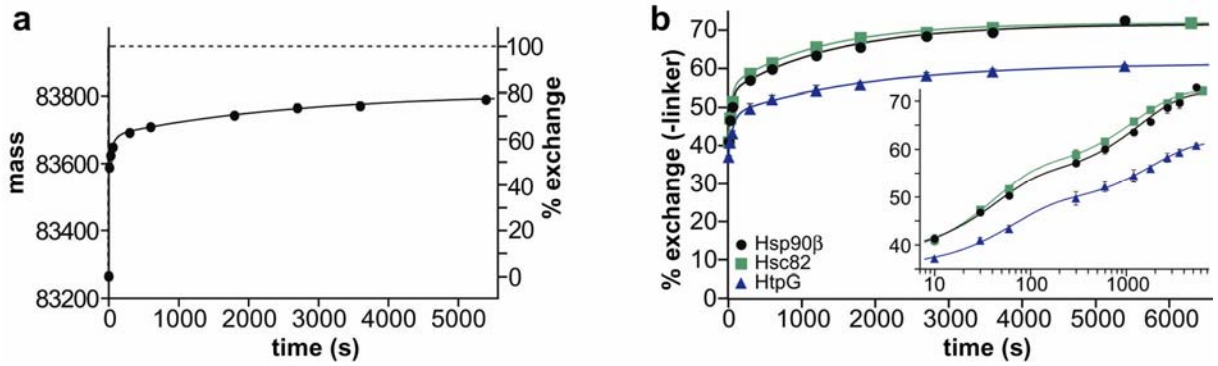

Fig. 2.19 Deuteration kinetics of the Hsp90 homologs. (a) HX kinetics in hHsp90β. The mass of hHsp90β and the percentage of hydrogen exchange, respectively, is plotted versus the incubation time in D_2O. The data points are averages of up to four independent experiments and the error bars represent the standard error of mean. The solid line is a fit of a tri-exponential equation to the datapoints. The dashed line represents the theoretical exchange curve including the backexchange during the desalting process calculated for the completely unfolded Hsp90 protein using the HXPep program (courtesy of Z. Zhang). **(b)** Comparison of the HX kinetics of full-length hHsp90β (black circles), yHsc82 (green squares), and *E.coli* HtpG (blue triangles). Relative percentage of exchange (amide hydrogens of the charged linker substracted, see Fig. 2.20a) is plotted versus the time in D_2O. The inset shows the same data with a logarithmic time scale.

2.3.2 Localization of slow and fast exchanging regions in the eukaryotic Hsp90s

Online peptic digestion under quench conditions at 0°C allowed us to map fast and slow exchanging regions with a sequence coverage of 82% and 65% for the human and the yeast protein, respectively, including parts of the charged linker, which is absent in any crystal structure.

High secondary structure stability was observed in the NBD except for the ATP-lid (residues 99 to 133 in hHsp90β) which exchanged 60 to 78% of all amide hydrogens within 10 s and more than 90% after 10 min.

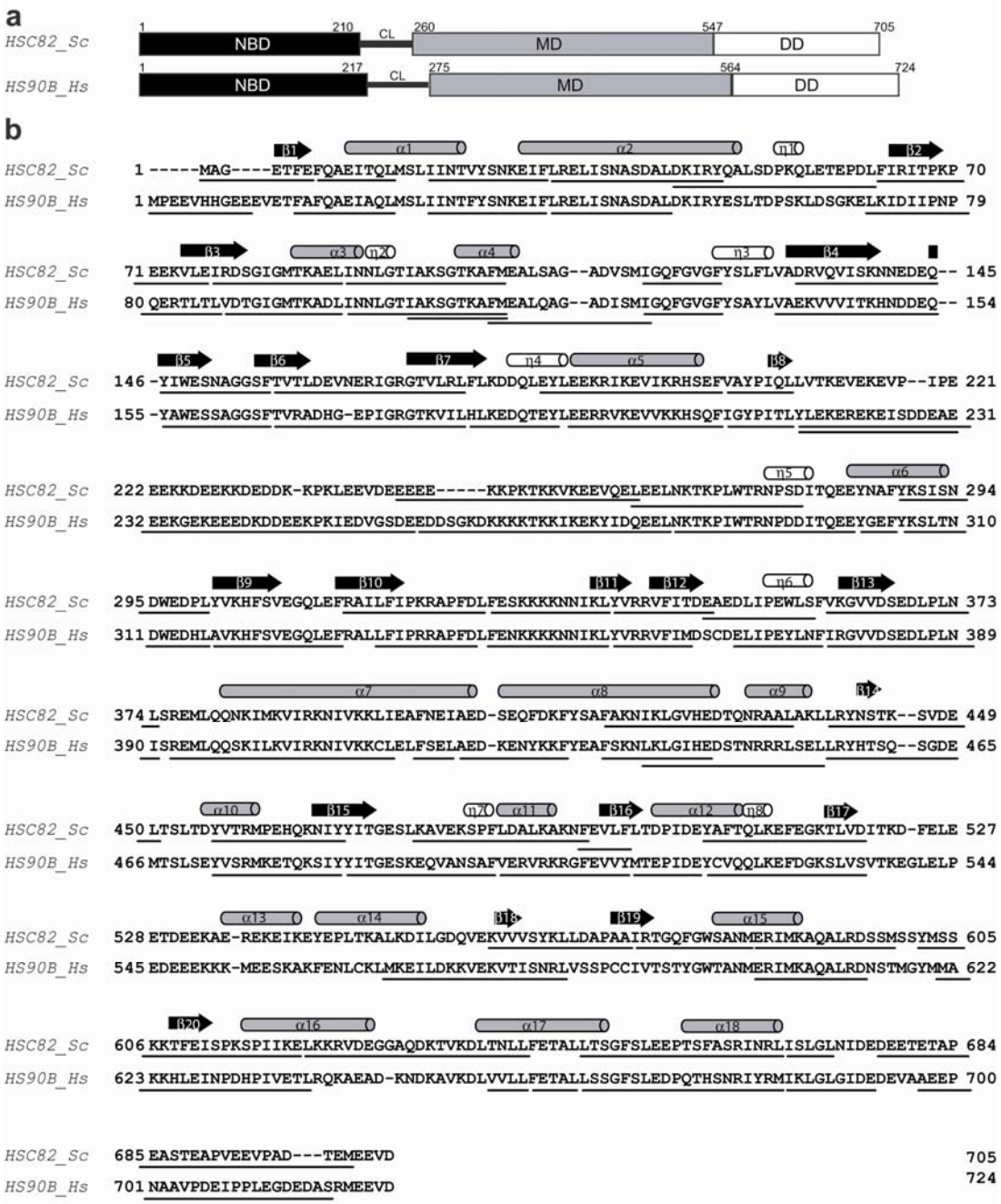

Fig. 2.20 Comparison of yHsc82 and hHsp90. (a) Domain organization **(b)** Clustal W alignment of the amino acid sequence of yeast Hsc82 and human Hsp90β. Secondary structure elements, α helices (α1-18), 3_{10} helices (η 1-8), and β strands (β1-20) are derived from the crystal structure of yHsp82 (PDB ID code 2CG9). The lines under each sequence indicate the peptic fragments covering the Hsp90 sequences that were analyzed in this HX-MS study.

The MD and the C-terminal dimerization domain (DD) are much more flexible than the NBD (Fig. 2.21c). Not surprisingly, the charged linker (residues 216-275 in hHsp90β), which connects NBD and MD and which is symbolized as dashed line in Fig. 2.21c, exchanged almost all of its amide hydrogen within 10 s. The catalytic loop in the MD (residues 382-402 in hHsp90β) was observed in two peptides which exchanged 39 and 52% within 10 s,

respectively. Since the peptic fragments also covered adjacent secondary structure elements, which can account entirely with their hydrogen bonds for the degree of protection observed in the fragments, it is very likely that the catalytic loop exchanged all amide hydrogens within this time frame.

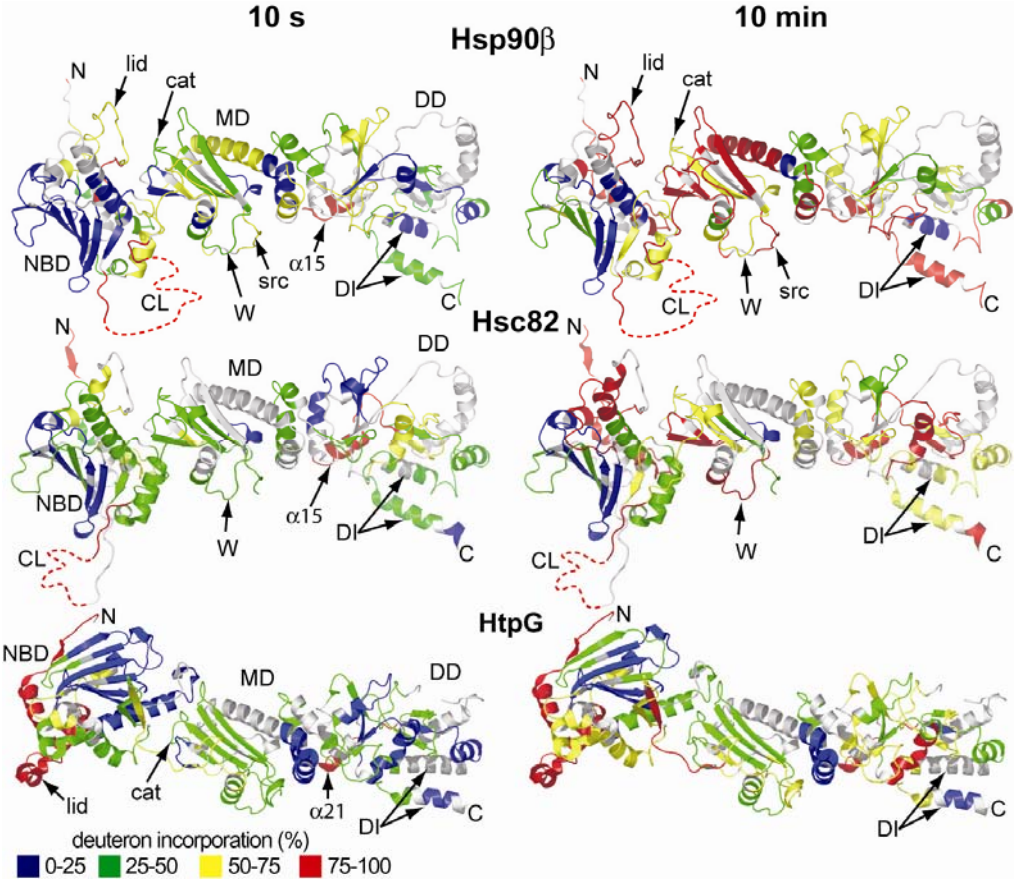

Fig. 2.21 Comparision of deuteration levels within segments of all three Hsp90 homologues. Secondary structure representation of a homology model of human Hsp90 onto the structure of yeast Hsp82 (PDB ID code 1CG9; 42; 43; 44; upper panels), the crystal structure of yeast Hsp82 (PDB ID code 1CG9; middle panels), and the crystal structure of *E. coli* HtpG (PDB code 2IOP; lower panels) colored according to the degree of deuteron incorporation after 10 s (left panels) and 10 min (right panels) as indicated. N, N terminus; C, C terminus; NBD, nucleotide binding domain; MD, middle domain; DD, dimerization domain; CL, charged linker; lid, ATP-lid; cat, loop containing the catalytic arginine; DI, dimerization interface. Elements implicated in substrate binding: W, loop containing Trp^{312} (human Hsp90; position 300 in yeast Hsp82; (Sato et al., 2000)); src, src-loop (Meyer et al., 2003); α15 , helix 15 (numbering according to Fig. 2.20b).

A similar degree of flexibility exhibited three structural elements implicated in substrate binding: the loop, which contains Trp^{312} in hHsp90β (position 300 in yeast Hsp82; (Sato et al., 2000)), the so-called Src-loop (residues 324-340 in yeast Hsp82 and not resolved in the structure; (Meyer et al., 2003)), and the α-helix 15. Even one or both of the helices involved in the dimer interface incorporated deuterons to a high degree within 10 min consistent with a fast dimer-monomer equilibrium (Fig. 2.21c right panels) (Richter et al., 2001). The

difference in stability between HtpG and the eukaryotic Hsp90 proteins resides clearly in the MD and DD. The NBD exhibited a similar degree of stability in the central β-sheet region but a higher degree of conformational dynamics within the very N-terminal part (residues 1-19) and the ATP-lid (residues 97-127). In the MD it is especially the first β-sheet and the α-helical coil that exchanges with slower kinetics in HtpG than in the eukaryotic proteins (compare right panels in Fig. 2.21c). The helices in the DD of HtpG also incorporate deuterons to a lower degree at 10 s and 10 min as compared to the yeast protein. In particular, the one of the helices involved in the dimer interface in HtpG is more stable than its counterpart in yeast or human Hsp90 suggesting a less dynamic dimer-monomer equilibrium. Taken together, the high degree of flexibility of the nucleotide-free eukaryotic Hsp90 proteins resides mainly in the MD and the DD and in the ATP-lid of the NBD.

2.3.3 Nucleotide-dependent conformational changes in yHsc82 and hHsp90β

To analyze the influence of nucleotides on the conformational dynamics we preincubated the Hsp90 proteins with a large excess of ADP and ATP for at least 10 min before the start of the exchange reaction as done with HtpG in the previous chapter. Deuteron incorporation into the proteins was significantly reduced in the presence of nucleotides (Fig. 2.22a, b). For human Hsp90β we found at the 10 s time-point an overall protection of around 16 and 19 amide hydrogens in the presence ATP and ADP, respectively. The degree of nucleotide-induced protection was observed throughout the exchange kinetics. For yeast Hsc82 the degree of protection observed in the presence of ADP and ATP was slightly lower (ca. 10 amide hydrogens). Interestingly, a large protection in presence of ATP as observed in the prokaryotic HtpG could not be found in both proteins. To localize the regions in the chaperones affected upon nucleotide-binding, we included peptic digestion in the HPLC-MS set-up.

Mapping the nucleotide-induced differences onto the primary sequence of hHsp90β revealed that a stabilizing effect of ATP was observed in the ATP-lid (residues 100-114 and 127-133; Fig. 2.22c left panel, Fig. 2.23).

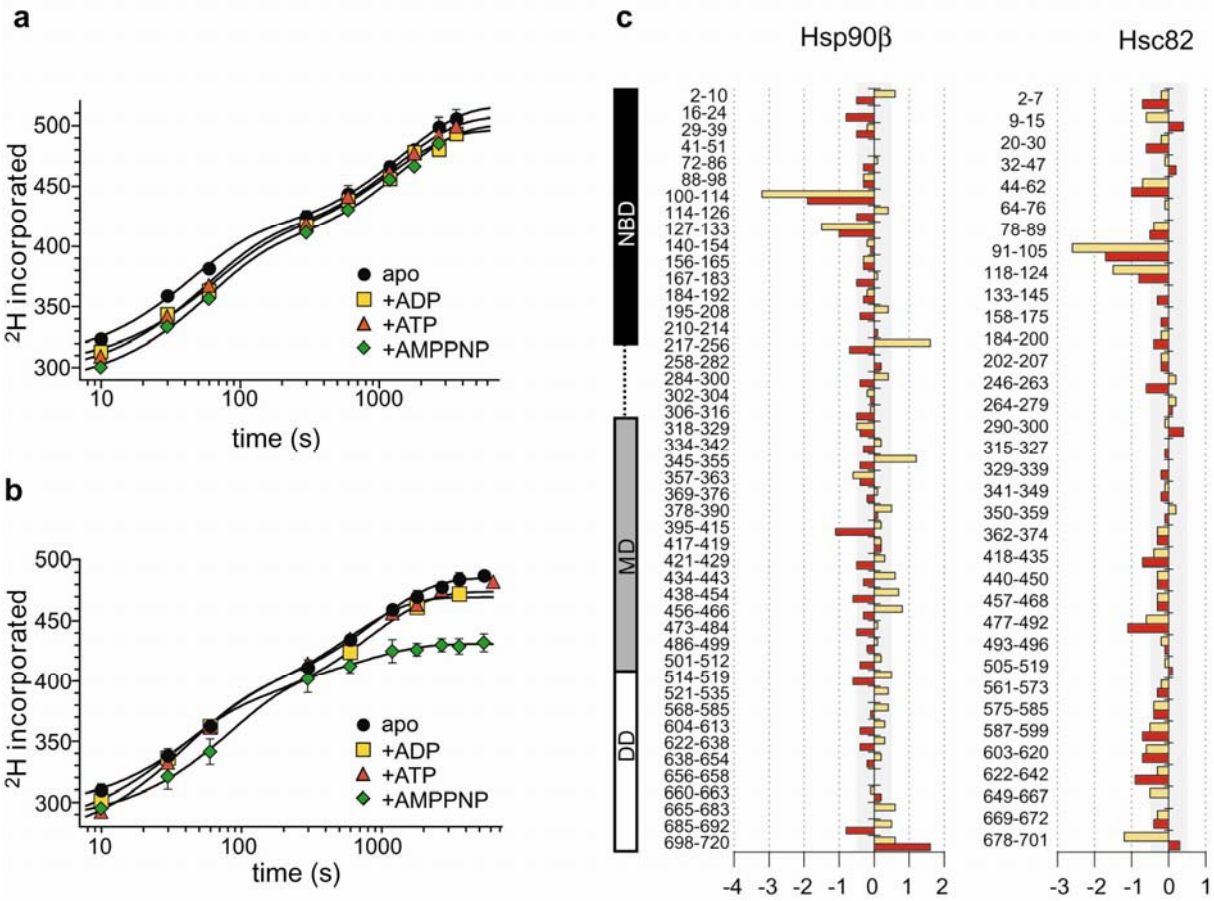

Fig. 2.22 Nucleotide-dependent conformational changes in hHsp90β and yHsc82.
Global HX kinetics of **(a)** Hsp90 and **(b)** Hsc82 in absence or presence of ADP, ATP and AMPNP (colours as indicated). The data points are averages of at least two independent experiments. The solid lines are fits of a biexponential equation to the data. **(c)** Difference plots of deuterons incorporated in the presence of ATP (red bars) and ADP (orange bars) minus deuterons incorporated in the absence of nucleotides into human Hsp90β (left panel) and yeast Hsc82 (right panel) segments after 30 s in D_2O. The numbers to the left of each panel indicate the corresponding segments in the proteins. The gray bar indicates the standard error of mean, defining the detection level of significant changes.

A small stabilization was also observed throughout the entire protein down to the very C-terminus. In particular the segment following the catalytic Arg-392 exhibited a significant stabilization in the presence of ATP suggesting a contact between the NBD and the MD upon ATP binding consistent with the currently favoured ATPase mechanism for Hsp90 proteins. The situation was similar but not as prominent in yeast Hsc82. Only parts of the ATP-lid (residues 91-105) were significantly protected in the presence of ATP (Fig. 2.22c right panel, Fig. 2.23). But the overall small protection of the MD and DD was also observed in the yeast protein. Unfortunately, we did not detect the peptic fragment, which contained the catalytic arginine for the yeast protein. One segment near the N-terminus (residues 9-15) and one segment of the MD of Hsc82 (residues 264-279) adjacent to the charged linker (residues 210-260 in yHsc82) showed a small deprotection (Fig. 2.22c right panel).

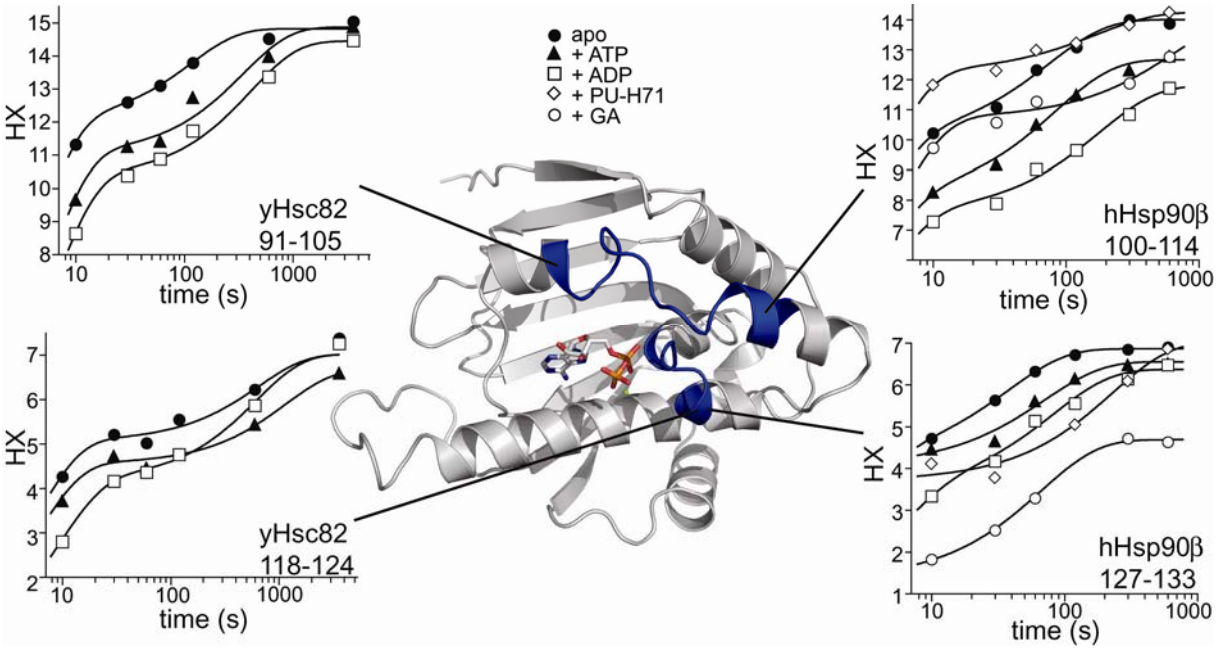

Fig. 2.23 Kinetics of deuteron incorporation in selected segments of yHsc82 and hHsp90β. Secondary structure representations of the human Hsp90α NBD crystal structure in complex with ADP (PDB ID code 1BYQ). Segments, residues 100-114 and 127-133, for which HX kinetics are shown in the left (for yeast Hsc82) and right panels (for human Hsp90β) are colored in blue (1BYQ). Symbols as indicated in the figure.

In the presence of ADP the situation is quite different for the human and bacterial Hsp90 proteins. Though a protection of the ATP-lid was also observed in the two proteins in the presence of ADP, several segments of significant deprotection occurred throughout the proteins contrasting the protection in the presence of ATP (Fig. 2.22c, orange bars). In the human protein part of the charged linker (residues 217-256), the src-loop (residues 345-355), and the helical coiled-coil of the MD (residues 434-466) exhibited this deprotection. In contrast, yeast Hsc82 showed overall very similar changes in the presence of ADP as compared to the presence of ATP.

We also analyzed the effect of the ATP analogue AMPPNP on the conformational dynamics of both proteins. Interestingly, the deuteration kinetics of full-length Hsc82 in presence of AMPPNP was similar to ATP after 30 s in D_2O, but showed a much higher protection of amide protons after long deuteration intervals indicating reduced flexibility (Fig. 2.22b). HX-MS on peptide level revealed that almost all regions in Hsc82 were significantly stabilized after 30 min in D_2O in presence of AMPNP Fig. 2.24).

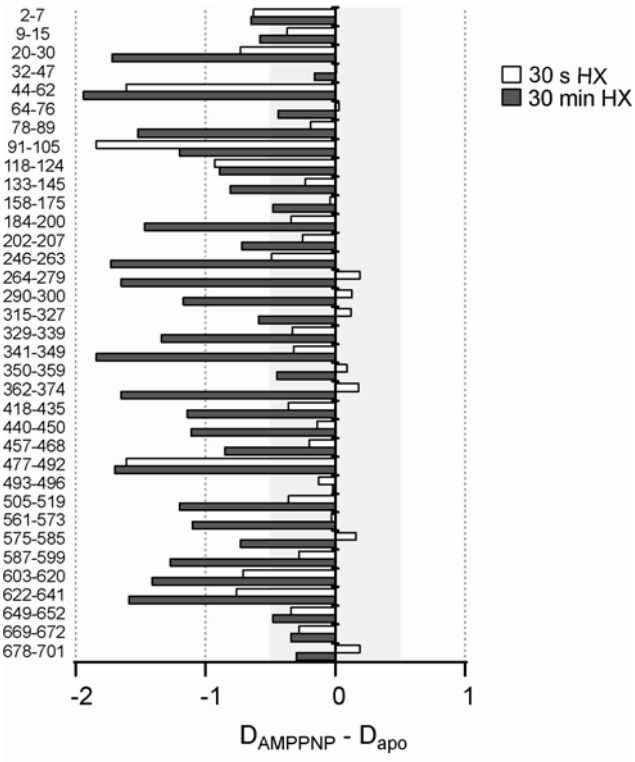

Fig. 2.24 Deuteron incorporation of Hsc82 segments in the *apo* state versus the AMPPNP bound state. Plots show the difference in numbers of deuterons incorporated in presence of AMPNP minus the number of deuterons incorporated in the absence of nucleotide for two different deuteration times, 30 s (white bars) and 30 min (black bars) in D_2O.

Taken together, significant nucleotide-dependent changes of the conformational dynamics were observed in both eukaryotic Hsp90s ranging from the NBD to the MD and even the DD. The stabilization effects upon ligand binding, however, are minor compared to the dramatic effects in the bacterial HtpG.

2.3.4 Differential effects of inhibitor binding on hHsp90β conformation

Since human Hsp90 became a prime target for anti-cancer therapy in recent years we wondered how inhibitors change the conformational dynamics of Hsp90 while arresting the chaperone cycle. We tested two different inhibitors, the ansamycin inhibitor geldanamycin (GA) and the watersoluble purin-scaffold inhibitor PU-H71 (courtesy of G. Chiosis; (He et al., 2006)), both of which bind to the nucleotide binding pocket. We first analyzed the deuteron incorporation into full-length hHsp90β in the presence of the two inhibitors and compared the HX kinetics with the apo and the ATP bound Hsp90 (Fig. 2.25a). Surprisingly, the two inhibitors had different effects on the overall HX kinetics of Hsp90. While GA induced an overall protection that is similar to the effect of ATP, PU-H71 did not induce a

significant protection and the kinetics of deuteron incorporation were similar to the HX kinetics of the *apo* protein.

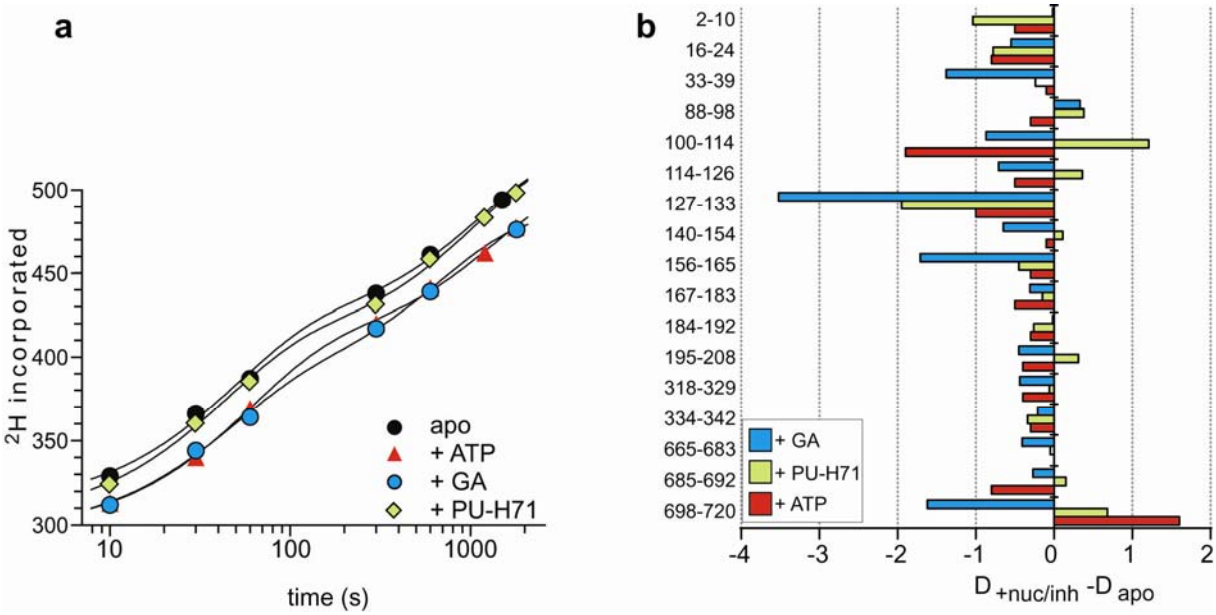

Fig. 2.25 Effects of inhibitor binding on conformational dynamics of Hsp90 (a) Global deuteron incorporation kinetics of hHsp90β in absence or presence of ATP, geldanamycin (GA) and purin-scaffold inhibitor PU-H71. **(b)** Difference plot of deuteron incorporation in presence of inhibitors or ATP as indicated minus the deuteron incorporation in unliganded hHsp90β after 30s in D_2O. Shown are selected segments throughout the entire protein.

When comparing the HX behaviour of Hsp90 on the peptide level in presence of GA with the HX in presence of ATP, significant differences were observed. One part of the ATP lid (segment 127-133) was much stronger protected in the presence of GA than in the ATP bound state while the other lid part was less protected (Fig. 2.25b, Fig. 2.23). GA also induced a significant protection in segments 33-39 and 156-165, which were barely affected by ATP, and in the very C-terminal segment 698-720, which was even deprotected in the presence of ATP. While the purin-scaffold inhibitor PU-H71 also induced a protection in the segment 127-133, it induced a deprotection in segment 100-114 contrasting the effects of ATP and GA (Fig. 2.25b). Interestingly, the exchange behavior of this segment was very similar in the presence of PU-H71 as compared to GA except for the number of amide hydrogens that exchanged in the dead-time of the experiment, which was higher in the case of PU-H71 (Fig. 2.23). Some segments adjacent to residues 100-114 and the very last segment, residues 698-720, also showed a slight deprotection. Our data show that both inhibitors deviated in their effect on the conformational dynamics of Hsp90 from nucleotides and from each other.

2.3.5 Co-chaperone p23 binding stabilizes the N-terminal dimer conformation of hHsp90β

HX data could not detect nucleotide-dependent effects in the N-terminal strand of hHsp90β that would implicate strand-exchange and hydrogen-bond formation during N-terminal dimerization as shown for yeast Hsp82. In order to investigate N-terminal dimerization and monitor nucleotide-dependent movements of the two NBD, we performed fluorescence resonance energy transfer (FRET) experiments. We designed and purified an hHsp90β mutant that was devoid of all other cysteines but contained an E20C mutation in analogy to the previously investigated HtpG-E12C mutant (2.2.7). The cysteine mutant was labelled with the fluorescent FRET probes Cy3 and Cy5 to completeness and mixed to form hetero-dimers. No increase in the acceptor fluorescence of Cy5 could be monitored by fluorescence spectroscopy in the mixed dimer solution, showing that the FRET-probes in the *apo*-hHsp90β dimer are not within the Förster distance. There was also no FRET observed upon addition of either ADP, ATP or AMPPNP to the solution.

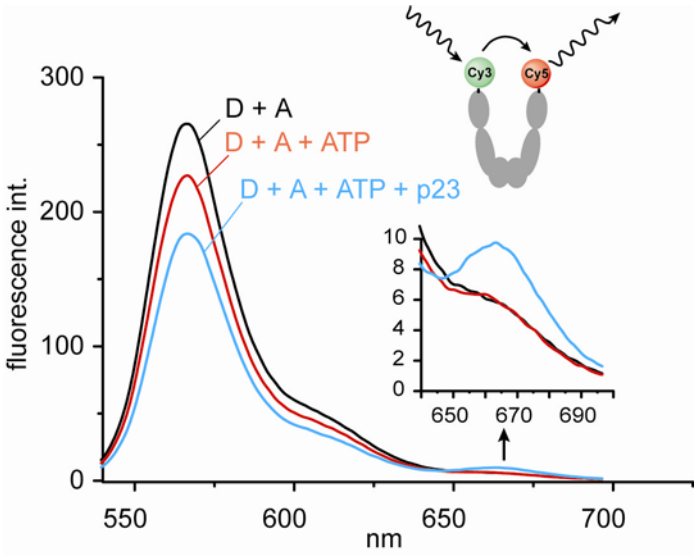

Fig. 2.26 Fluorescence resonance energy transfer (FRET) experiments with mixed fluorescently labelled hHsp90β dimers. hHsp90β-E12C was labelled with Cy3 as donor (D) or with Cy5 as acceptor (A). Shown are the emission spectra of the mixed heterodimers upon excitation at 520 nm. The inset shows a magnification of the Cy5 acceptor fluorescence spectrum. Only in presence of both ATP and the co-chaperone p23, there is an increase in acceptor fluorescence observed indicating FRET.

Next, we asked whether the co-chaperone p23 could influence N-terminal dimerization since the closed Hsp82 crystal structure could only obtained in complex with the protein p23/Sba1 (Ali et al., 2006). Indeed, the Hsp90-Cy3/Cy5 FRET pair showed a small, but significant time-dependent increase in acceptor fluorescence when purified p23 was added in presence of

ATP, while the presence of ADP had no effect (Fig. 2.26). Thus, these data show that co-chaperone p23 in presence of ATP modulates the dynamics within the NBD of the hHsp90β dimer and might be necessary for correct N-terminal dimerization.

2.3.6 Discussion of the conformational dynamics of prokaryotic and eukaryotic Hsp90s

Our analysis of the conformational dynamics of eukaryotic Hsp90 proteins and the comparison to the evolutionarily distant bacterial protein HtpG yielded the following novel insights into structure and function of Hsp90 proteins. (1) The conformational dynamics of the eukaryotic Hsp90s is much higher than the dynamics of prokaryotic HtpG. (2) Nucleotides induced small conformational changes that are not restricted to the NBD but observed throughout the Hsp90 proteins,. (3) The two nucleotide competitive inhibitors, GA and PU-H71, alter the conformational dynamics of Hsp90 in a way that is different from nucleotides and different from each other.

The dramatic increase in conformational flexibility in the eukaryotic Hsp90 proteins as compared to the prokaryotic HtpG could have several different reasons. The eukaryotic proteins evolved to bind to a large number of natively folded proteins, many of which are unrelated in sequence or structure. Such a large spectrum of clients may rely on a highly flexible structure to allow Hsp90 to quasi mold into different shapes to provide an optimal interface for client binding. Although it is currently unknown how many and what kind of clients are bound by *E. coli* HtpG, it is assumed that these are much lower in number and either not essential themselves or not stringently dependent on HtpG, since HtpG is not essential under any conditions tested so far and *htpG* deletion has no phenotype. Alternatively or in addition, the flexibility of the eukaryotic proteins could be linked to the interaction with the plethora of cochaperones (Picard, 2006). No cochaperones were identified for HtpG so far. While HtpG appears to work as a stand-alone machine, the eukaryotic Hsp90s may require the cochaperones not only to regulate progression through the ATPase cycle but also to stabilize certain parts of the eukaryotic Hsp90 proteins as required for the binding of specific clients. Mapping of the fast exchanging regions revealed that the differences in solvent accessibility between HtpG and the eukaryotic Hsp90 mainly reside in the MD and the DD, both of which are implicated in client binding (Meyer et al., 2003; Sato et al., 2000; Shiau et al., 2006). In addition, the ATPase stimulating cochaperone Aha1 contacts with its N-terminal domain the MD of Hsp90 over the entire length with interactions involving all

three subdomain of the MD (Meyer et al., 2004). It is conceivable that these interactions stabilize major parts of this domain. The C-terminus of all eukaryotic cytosolic Hsp90 proteins ends in the MEEVD motif, which is bound by a large number of TPR-domain cochaperones, many of which are dimeric proteins like Hsp90 itself. Flexibility in the DD, especially influenced by binding of clients and cochaperones in other regions of the protein, could influence association and dissociation of the TPR-domain cochaperones and thereby coordinate progression through the chaperone cycle. Another important issue that might regulate the dynamics and stability of eukaryotic Hsp90 is posttranslational modification. Human Hsp90β was found in proteomics screens to be phosphorylated at various positions in the intrinsically unfolded linker (Ser^{226}, Ser^{255}, Ser^{261}) and in the middle domain (Thr^{297}) (Beausoleil et al., 2006; Matsuoka et al., 2007). Moreover, several acetylation sites (Lys^{294}, Lys^{624}) were reported in Hsp90 which play an important function in regulating the chaperone cycle (Kim et al., 2006; Scroggins et al., 2007). Certainly, the presence of these modifications can influence the conformational changes in the Hsp90 significantly. Flexibility in Hsp90 could also facilitate the access of kinases/phosphatases and acetylases/deacetylases to those sites.

ATP binding induced an overall protection in all three proteins. This protection was particularly prominent in the segments, which constitute the hinges of the ATP-lid (residues 100-114 and 127-133 in hHsp90β, 91-105 and 118-124 in yHsc82), similar to the more drastic protection effects in these segments in HtpG.

These nucleotide-dependent changes are in agreement with structural studies since these segments are found in different conformations in crystal structures of the *apo* NBD of Hsp90s (PDB ID code 1AH6, 1AH8, 1YES; (Prodromou et al., 1997b; Stebbins et al., 1997)) as compared to the full-length structures of yeast Hsp82 and *E. coli* HtpG in complex with AMPPNP and Sba1/p23 or ADP (PDB ID codes 2CG9 and 2IOP; (Ali et al., 2006; Shiau et al., 2006)). They are also consistent with an NMR study on the isolated NBD (Dehner et al., 2003). In addition to the stabilization in the ATP-lid we found an ATP-induced stabilization in segment 395-415 in hHsp90β. The changes in solvent accessibility in this segment supports the currently favored mechanism of ATP hydrolysis, which assigns a crucial role to arginine 380 in yeast Hsp82 (392 in hHsp90β) (Ali et al., 2006; Meyer et al., 2003; Meyer et al., 2004). A contact between nucleotide and Arg^{380} was recently shown in the crystal structure of full-length Hsp82 in complex with AMPPNP and Sba1/p23 (Ali et al., 2006). Our data now demonstrate that a communication between nucleotide and this arginine-containing loop also

occurs in human Hsp90β and in *E. coli* HtpG in the presence of ATP and the absence of the Sba1/p23 cochaperone.

The full-length crystal structure of yeast Hsp82 also shows an N-terminal dimerization with an exchange of the first β-strand. In the structure this strand exchange is stabilized by 4 hydrogen bonds. The stabilization observed in HX-MS in the first segments of hHsp90β and yHsc82 was only very small presumably because any N-terminal dimerization is very transient in the presence of ATP and the absence of stabilizing cochaperones like Sba1/p23 like in the crystal structure. Indeed, our FRET experiments with mixed fluorescently labelled Hsp90 dimer revealed that only in presence of p23 and ATP, the N-termini of both NBD moved towards each other. In contrast, in HtpG we observed a very prominent protection of almost 8 amide hydrogens in this segment which together with crosslinking data is consistent with a stable N-terminal dimerization with strand exchange. The larger number of hydrogen bonds formed in HtpG as compared to yeast Hsp82 could be necessary for lack of stabilizing cochaperones.

ADP binding also induced an overall protection in all three Hsp90 proteins. However, aside from the ATP-lid, ADP had quite different effects on the exchange behaviour of hHsp90β and HtpG as compared to ATP. While ATP induced a slight stabilization throughout the MD and DD of hHsp90β, ADP rather destabilized these parts of the protein. In HtpG a deprotection was also observed in many segments in the presence of ADP. In yHsc82, however, there was no such destabilization effect by ADP observed. It is tempting to speculate that progression through the ATPase cycle from ATP to ADP influence also the stability of the C-terminal dimerization and regulates subunit exchange of protomers differently in the species. Interestingly, a recent biochemical study showed that subunit exchange in human Hsp90β is much slower than in yeast Hsp90 and seems to be different in the human isoforms (Richter et al., 2008), thus pointing at an additional level of functional regulation in the dimeric Hsp90.

Our data indicate that ATP and ADP induce different conformational states in all three Hsp90 homologues and that these conformational changes are not restricted to the NBD but propagated throughout the entire proteins. In this context it was important to investigate how inhibitors of Hsp90 would affect the conformational flexibility. The two inhibitors affected the conformational dynamics of hHsp90β quite differently. While the overall conformational stability of Hsp90 in the presence of GA was similar to the state in the presence of ATP or ADP, the conformational flexibility of Hsp90 in the presence of PU-H71, which binds to the same site as nucleotides and GA, resembled rather the nucleotide-free state. However, the

overall changes in solvent accessibility in the presence of PU-H71 are misleading since in some segments of the NBD a protection was observed that is similar to a protection induced by ATP or GA, while in other parts a deprotection counterbalanced these effects. Our data clearly show that the two inhibitors cause changes in the conformational flexibility that are different from nucleotides and from each other. We believe that the conformation flexibility is important for client and cochaperone binding and consequently divergent effects on these dynamics should affect client and cochaperone binding differentially. Different inhibitors therefore might bias Hsp90 for binding of different subsets of clients or cochaperones and prevent binding of other clients and cochaperones. These data could explain the different *in vivo* effects of various types of drugs (Kasibhatla et al., 2007).

2.4 Conformational properties of the E3-ubiquitin ligase CHIP

The dimeric U-box E3 ligase CHIP binds the C-terminus of Hsp90 and Hsp70 via its TPR-domain. By ubiquitylating chaperone bound clients, CHIP links the chaperone machinery to the proteasomal degradation pathway. Two recently published crystal structures of mouse and zebrafish CHIP differ substantially, showing either asymmetric or symmetric homodimeric assemblies.

In order to analyze the conformational properties of CHIP in solution, HX-MS with human CHIP was performed to monitor conformational changes upon binding of Hsp70 and Hsp90 chaperones or their respective C-terminal EEVD peptides, and in complex with the E2 ubiquitin-conjugating enzymes UbcH5a and Ubc13.

2.4.1 Unliganded CHIP is a symmetric dimer in solution with highly flexible regions

To analyze the conformational flexibility of human CHIP, we performed HX-MS experiments as described earlier (Rist et al., 2006). The purified protein was diluted into D_2O buffer at physiological pH and incubated for different time intervals at 30°C. Subsequently, the exchange reaction was quenched by lowering the pH to 2.5 through the addition of ice-cold phosphate buffer. The sample was digested online by a pepsin column in the HPLC setup, desalted on a reversed phase trap column and eluted over an analytical reversed-phase column into an electrospray ionization hybrid quadrupol-time-of-flight mass spectrometer. The sequence coverage of identified CHIP peptic peptides was 95 %, allowing detection of deuteron incorporation in nearly all regions of the entire 35 kDa protein (Fig. 2.27 a).

HX experiments with unliganded human CHIP revealed highly flexible and dynamic regions within in the protein (Fig. 2.27 b). Particularly, the very N-terminal peptides of the TPR domain, including residues 1-48 and 49-60 (forming the first TPR repeat in the crystal structure), seem to be largely unfolded, exchanging 99% and 73% of the accessible amide protons within 10 s, respectively.

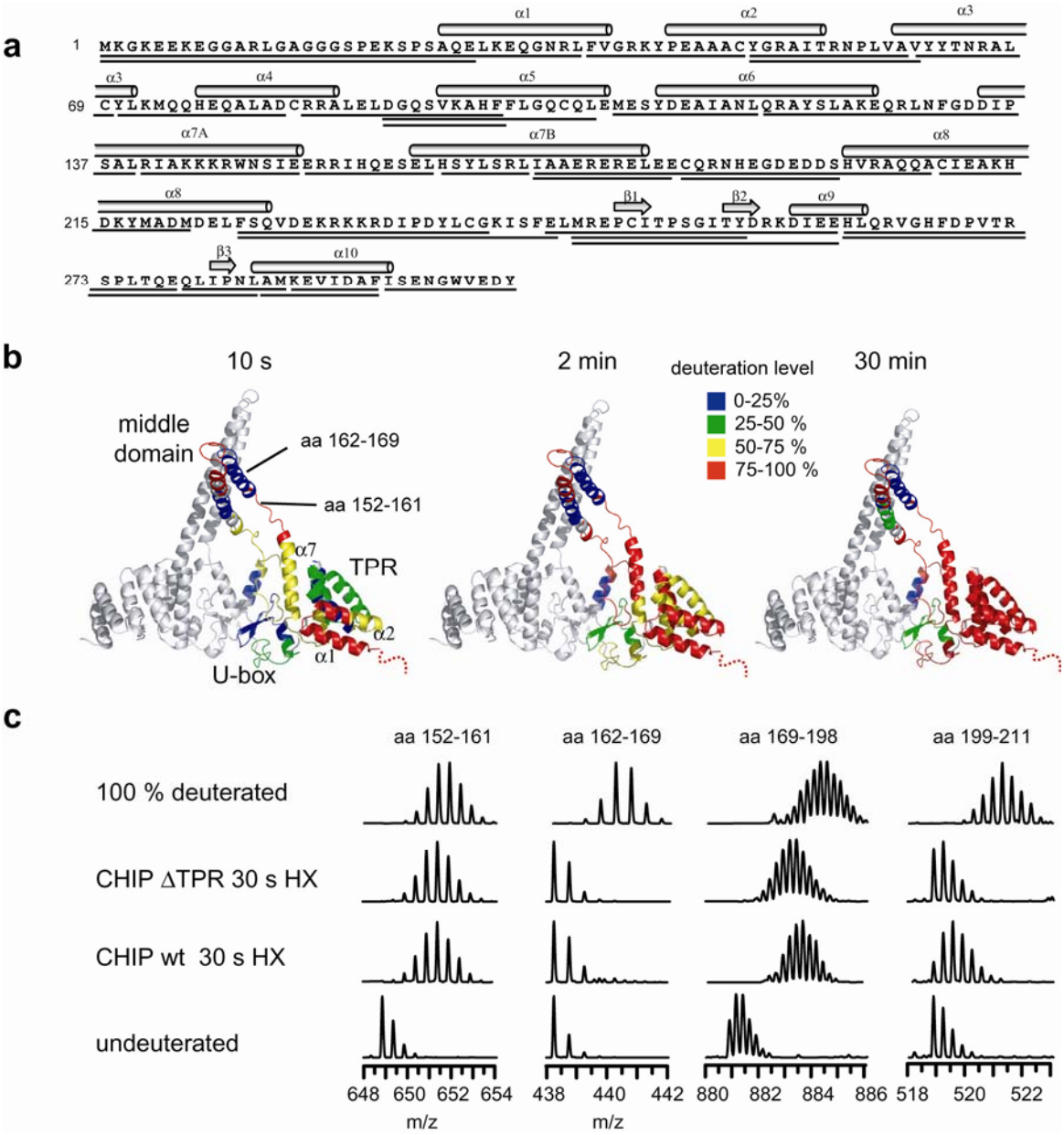

Fig. 2.27 Conformational flexibility of human CHIP. (a) Amino acid sequence and peptic peptides of CHIP used for the HX analysis. Sequence coverage is 95 %. Secondary structure elements on top are derived from the crystal structure of mouse CHIP (PDB code 2C2L) **(b)** time-dependent deuteron incorporation shown on cartoon representation of the asymmetric mouse CHIP dimer structure in complex with MEEVD-peptide (residues 25-304, PDB code 2C2L). The deuteration level of analyzed peptides after 10 s, 2 min and 30 min in D_2O is shown in the color code as indicated for only one protomer in the dimeric structure. **(c)** original spectra of CHIP peptic peptides amino acids 152-161 and 162-169 in undeuterated, 30 s deuterated and fully deuterated state. The experiment was performed for comparison with hCHIP wildtype and hCHIP(128-303) lacking the TPR domain.

The highly flexible character of unliganded hCHIP could also be monitored in additional HX experiments with longer deuteration intervals. After 2 min and 30 min incubation in D_2O, almost all TPR domain peptides completely exchanged their amide protons (Fig. 2.27 b), suggesting a highly dynamic conformation in the helical repeat domain. Solvent accessibility of other regions is in good agreement with crystallographic data, as can be seen in the amide proton protection of helical parts within the hCHIP middle domain (peptide 162-169) and the

C-terminal U-box domain (Fig. 2.27 b, c) and rapidly exchanging loop regions. The data also monitors the dimeric contacts in CHIP. Both segments in the helical middle domain, peptide 160-169 and peptide 201-211 show a stable protection even after long exchange time intervals (Fig 1. b) which is consistent with the reported dimer interface of the CHIP crystal structure (Zhang et al., 2005). Also the second important hydrophobic dimerization interface in the U-box domain, which is oriented around Asn^{284} (peptide 287-293) is highly protected from deuteron incorporation.

Interestingly, the region including residues 153-161, which is the base of the helical hairpin of the charged middle domain, was found to be almost fully exchanged within 10 s. This indicates that this part is in solution either unfolded or alternating in the seconds time scale between the two conformations, helical and unfolded, as shown in the asymmetric crystal structure of mouse CHIP. No bimodal distribution could be observed in the deuterated peptide spectrum, suggesting CHIP being a symmetric dimer in solution with flexible regions in the helical coiled-coil domain. Since the crystal structure of *Danio rerio* CHIP lacking the TPR domains shows the protein as a symmetric dimer with the helical hairpin of the middle domain completely folded, we asked whether deletion of the TPR domain in hCHIP would also result in stabilization of this unfolded part into an elongated helix. Deuteron incorporation after 30 s HX into segment 153-161 of ΔTPR construct (hCHIP 128-303) was the same as in the full-length hCHIP (Fig. 2.27c), showing unchanged high flexibility in this part. However, deletion of the TPR domain led to a slightly increased protection of amide hydrogens in segments of the distal part of the middle domain and the U-box region (170-198, 200-211, Fig. 2.27c), demonstrating a destabilizing effect of the unliganded TPR domain on other regions of the full-length protein.

2.4.2 Chaperone binding results in large stabilization of the CHIP TPR domain

CHIP has been shown to bind to the C-terminus of Hsp70 and Hsp90 chaperones with high affinity via its single TPR domain (Zhang et al., 2005). To analyze possible conformational changes induced by individual chaperone binding, we performed HX in the absence and presence of purified Hsp70 and Hsp90 chaperones and their respective octameric C-terminal peptides. CHIP was preincubated for 30 min with an excess of full-length chaperone or peptide to allow stable complex formation. After 30 s incubation in D_2O, the samples were

analyzed in our HPLC-MS system including columns with immobilized pepsin. With the HPLC gradient used in this study, it was possible to separate almost all deuterated CHIP peptides from the majority of chaperone peptides for a detailed analysis of solvent accessibility. Overall, Hsp70/90 chaperone and peptide binding led to a significant decrease in deuteron incorporation in the TPR domain of CHIP.

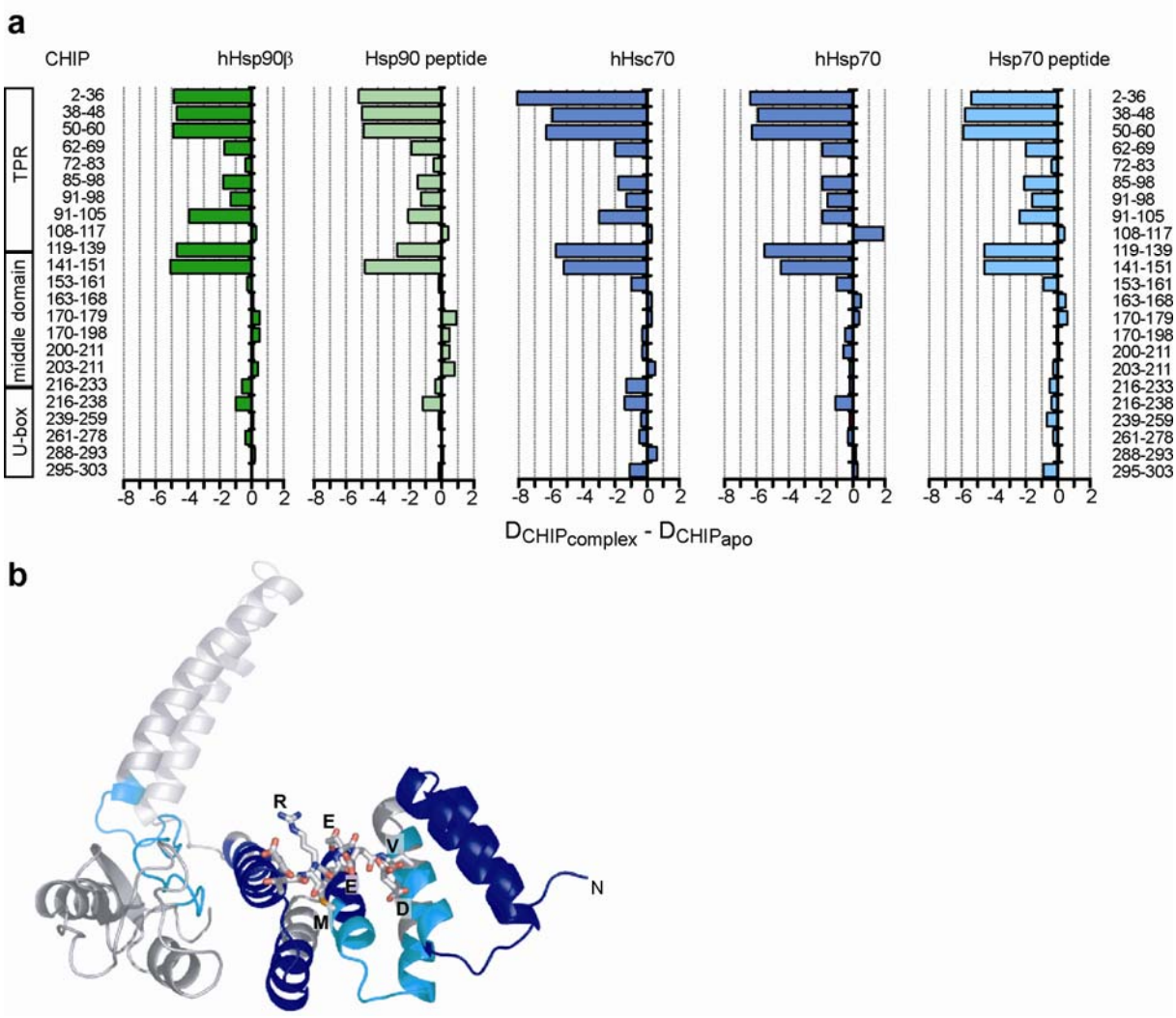

Fig. 2.28 Effects in deuteron incorporation of CHIP segments upon TPR-ligand binding
(a) Difference in number of deuterons incorporated of CHIP peptides in complex with Hsp90, Hsp70, Hsc70 or the octapeptides ASRMEEVD (Hsp90 C-terminus) and GPTIEEVD (Hsp70 C-terminus) minus the deuteron incorporation in absence of ligands after 30 s deuteration . **(b)** Secondary structure representation of mouse CHIP monomer visualizing the segments which show large (dark blue) and small (light blue) protection effects upon ligand binding. Unaffected regions are shown in grey.

Especially the flexible N-terminus with the first helix-turn-helix repeat (segments 2-36, 38-48, 50-60) and the third distal repeat (segment 119-139) in the TPR domain show a large stabilization in presence of peptides and full-length chaperones, having a total of almost 30

amide hydrogens protected in the complex compared to the *apo* form in a 30 s HX experiment. Another flexible region stabilized upon ligand binding is the proximal helix of the charged middle domain, segment 141-151, which shows a protection of 5 of 10 possible amide hydrogens in the formed complex. The adjacent flexible segment, 153-161, exchanged in presence of chaperones to the same high extent suggesting no influence on the symmetry of CHIP in this region upon ligand binding. No obvious difference in the deuteron incorporation was measured between CHIP-chaperone or CHIP-peptide complexes of both Hsp90 and Hsp70 type. This indicates that there is no additional contribution of the full-length chaperone binding to the conformation of CHIP, which is also reflected in similar binding affinities of CHIP to peptide and intact chaperones as measured by isothermal calorimetry or surface plasmon resonance spectroscopy (Zhang et al., 2005) (R. Nikolay, M. Stankiewicz, unpublished work). Binding of the human Hsc70 and Hsp90 had a slight protective effect on flexible U-box segments, but no significant differences between Hsp70 and Hsp90 were found that could point at differential ways of chaperone action on CHIP E3 ligase activity in terms of conformational changes.

2.4.3 Effects of E2 ligase binding on the conformation of CHIP

As an E3-ubiquitin ligase, CHIP cooperates with E2-ubiquitin-conjugating enzymes to transfer ubiquitin to target proteins. Recently, two different E2 ligases have been shown to interact with the U-box of CHIP, the canonical Lys^{48}-ubiquitin chain linking enzyme UbcH5 and the non-canonical Lys^{63}-specific ubiquitin-conjugating enzyme Ubc13-Uev1a (Murata et al., 2001; Zhang et al., 2005). Structural information of this interaction, however, is only available for hCHIP U-box constructs in complex with Ubc13-Uev1 and the CHIP-U-box-UbcH5 complex from *Danio rerio* (PDB code 2OXQ), showing a conserved binding interface for all E2 ligases. To analyze possible specific long-range effects of E2 binding on the CHIP conformation in solution, we performed HX experiments with CHIP-UbcH5a and CHIP-Ubc13 complexes with large excess of E2s and measured the deuteron incorporation into CHIP peptides in comparison to unbound CHIP.

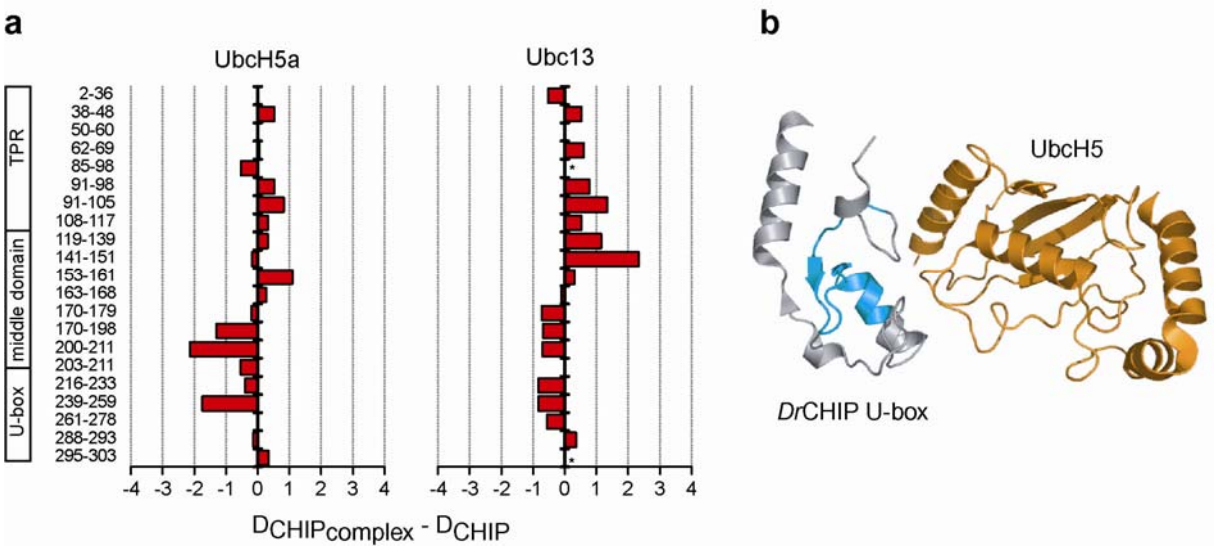

Fig. 2.29 Effects of E2 ligase binding on the deuteron incorporation of CHIP segments (a) Difference in deuteron incorporation into CHIP segments in presence of the E2 ligases UbcH5a and Ubc13 minus the deuteron incorporation into unbound CHIP after 30s deuteration. Peptides that could not be analyzed are marked with an asterisk **(b)** Secondary structure representation of the zebrafish CHIP-U-box-UbcH5 co-crystal structure (PDB code 2OXQ) visualizing segments stabilized in HX-MS data upon UbcH5a binding (blue).

In the CHIP-UbcH5a complex, subtle effects can be monitored on CHIP solvent accessibility caused by the E2 binding. One segment in the U-box domain, peptide 239-259, and two segments at the distal end of the helical middle domain, including residues 170-211, show a small but significant protection of 1-2 amide protons upon complex formation. The stabilized regions in the U-box resemble the reported interaction site of UbcH5 in the co-crystal structure and from NMR data (Xu et al., 2006), (PDB code 2OXQ). Interestingly, some segments in the TPR domain exhibit increased deuteron incorporation, though to a very low extent. In the CHIP-Ubc13 complex, there is also less exchange detected in the segments of the U-box, indicating the hydrophobic contacts of Ubc13 to this region as shown in the crystal structure (Zhang et al., 2005). Strikingly, there is a deprotection of amide protons detected in many segments of the TPR domain and the first part of the middle domain which is very dominant in peptide 141-151, a region that is highly stabilized in presence of Hsp70 and Hsp90 chaperones (Fig. 2.28).

2.4.4 Discussion

This study shows different novel aspects in understanding conformational properties of CHIP in solution. Unliganded CHIP is a highly dynamic protein that forms a symmetric dimer in solution. HX data can resolve the solvent accessibility of the dimeric 35 kDa protein with

complete sequence coverage including the very N-terminus which could not be crystallized due to high dynamics. Indeed, the N-terminus and the adjacent peptides up to residue 60, forming the first TPR helix-turn-helix, seem to be completely unfolded in unliganded CHIP, exchanging almost all accessible amide protons in 10 s. But all other segments in the TPR domain of unliganded CHIP exhibit high dynamics and exchange almost all their amide protons after 30 min exchange time, as well as distinct parts of the middle domain and the U-box.

We show here with HX-MS that human CHIP adopts a symmetrical dimer in solution with a highly flexible part at the beginning helical hairpin in the middle domain. This is in contrast to two recently published crystal structures of CHIP. The crystallization of a zebrafish CHIP construct that was missing the TPR domains but contained the helical linker and the U-box revealed a symmetric dimer with a folded helix at the N-terminus of the middle domain (helix α7 in the full-length protein) (Xu et al., 2006). When mouse CHIP was co-crystallized with a C-terminal Hsp90 peptide that contained an EEVD motif, CHIP was found to exist as an asymmetric homodimer, forming one protomer with an elongated helix α7 in the middle domain and the other protomer forming a "broken" helix α7. If this were the case for the human CHIP in solution, a bimodal distribution of the deuterated peptide indicating two different conformational states should be observed in this region. Our HX-MS data revealed that peptide 152-161 is highly flexible without bimodal conformational states and thus demonstrate a model of a symmetric homodimer that contains a "broken" helix 7 in each protomer. Due to the flexibility of this segment, it is still possible that this region in the middle domain is rapidly alternating between the helical and the unfolded which is trapped in the asymmetric conformation of mouse CHIP crystals. Under physiological conditions in solution though, the symmetric flexible dimer seems to be highly populated even in presence of ligands. This puts into question the speculated role of CHIP's asymmetric assembly in connecting the "dimeric" chaperone binding function to the monomeric E2-ubiquitin-conjugating function (Zhang et al., 2005).

The highly dynamic character of CHIP TPR domain might also contribute to the recently discovered chaperone activity of CHIP. CHIP was shown to possess intrinsic chaperone activity that enables refolding of denatured luciferase and is enhanced under heat stress (Rosser et al., 2007). This study suggests that the chaperone activity resides in the TPR domain because deletion of the TPR domain is unable to refold luciferase. It is tempting to speculate that the flexible and unfolded regions in the TPR of ligand-free CHIP expose

hydrophobic patches that interact with nonnative polypeptides for disaggregation. Moreover, this would explain the heat-induced aggregation of wild-type CHIP which is absent in TPR deletion constructs (Rosser et al., 2007). In addition, the highly solvent-exposed N-terminal region of CHIPs TPR domain seems to be an important recognition site for posttranslational modifications. Several proteomic studies report two phosphorylation sites at Ser^{19} and Ser^{23} (Beausoleil et al., 2006; Imami et al., 2008; Olsen et al., 2006) and an ubiquitination site at Lys^{22} that was identified upon auto-ubiquitination by the E2 ligase UbcH5a (Wang et al., 2005). The flexibility and accessibility of this region might therefore have an important function for regulation and specificity of CHIP action.

Data presented demonstrate that CHIP dynamics is extremely stabilized in the presence of Hsp70 and Hsp90 chaperones. Ligand binding induced a significant protection of amide hydrogens in the TPR domain which was strongest in both TPR repeats flanking the ligand binding site. The most conserved residues in the crystal structures of mouse CHIP and Hop-TPR in complex with Hsp90 peptides were found to form a positively charged "clamp" that holds the two carboxylate groups of the final aspartate. In contrast to HOP-TPRs which show selective binding for the individual chaperones EEVD motifs (Scheufler et al., 2000), there is no specifity for Hsp70 or Hsp90 binding in view of the fact that the stabilization occurs to the same extend for both chaperones and the octameric C-terminal peptides. This demonstrates the promiscuity of the CHIP-TPR domain for all EEVD-containing ligands which is also reflected in similar binding affinities of full-length chaperones and peptides to CHIP (Zhang et al., 2005) (Marta Stankiewicz, Rainer Nikolay, unpublished results).

The stabilization of the helical fold in the TPR domain by ligand binding was also observed in NMR and CD spectroscopic study of protein phosphatase 5 (PP5) that is targeted to Hsp90 via its N-terminal TPR domain (Cliff et al., 2006; Cliff et al., 2005). The isolated *apo*-TPR of PP5 was found to be not fully folded and could be stabilized significantly by addition of a pentapeptide MEEVD, increasing the helical content from 64% to 98 % as measured by CD spectroscopy (Cliff et al., 2005). The authors proposed that folding coupled to binding might be a common mechanism of ligand recognition by TPR domains although this idea has been debated (Cortajarena and Regan, 2006). Recently published data on the interaction of the TPR protein Ssn6 with Tup1 emphasize however the coupled folding-binding mechanism as a common principle in TPR mediated interactions (Palaiomylitou et al., 2008).

Our data HX-MS clearly demonstrate that CHIP follows such a folding-binding mechanism as shown in PP5. However, the regions stabilized include mainly the outer TPR repeats 1 and 3

of the concave binding surface of CHIP TPR domain and the helix 7 which is part of the middle domain, an effect which is different in PP5 (Cliff et al., 2006). Interestingly, there is no significant effect upon complex formation on the conformational flexibility of other neighbouring regions of CHIP which might explain specifity differences of CHIP on the ubiquitylation of Hsp70 or Hsp90 substrates. Additional factors or modifications might thus be necessary for CHIP's triage decision process in the protein quality control of chaperone-bound client.

Using HX-MS, we characterized the effect of E2 ligase binding on the CHIP dynamics. Complex formation with both E2 ligases, the canonical UbcH5a and the non-canonical Ubc13 which bind both with micromolar affinity, led to a small stabilization in U-box peptides 216-233 and 239-259 which resembles the interaction interface in the co-crystal structures of mouse CHIP-U-box-Ubc13 and zebrafish CHIP-U-box-UbcH5 (Xu et al., 2006; Zhang et al., 2005). As a common E2-E3 interface, the hydrophobic ridge of the E2 is bound in a hydrophobic groove of the CHIP U-box between the short helix α9 (residues 255-266) and the tips of two hairpin turns (235-240 and 270-274). The interaction is mainly based on hydrophobic interactions and polar contacts of side-chains where no amide hydrogens of CHIP are involved, explaining the small protection in hydrogen exchange in the complex. Furthermore, it was shown that also transient U-box E2 interactions are sufficient for substrate ubiquitination (Demand et al., 2001). In the CHIP-UbcH5a complex but not in the CHIP-Ubc13 complex, however, a second stabilization was observed localizing to the intrinsically unfolded loop region and the adjacent helix α8 of CHIP. Interestingly, binding of a different E2 ligase resulted in differential effects on the dynamics CHIP's TPR domain. While binding of the canonical UbcH5a had no significant effect on the HX kinetics in the TPR, complex formation with Ubc13 led to a measurable deprotection of numerous segments at the C-terminal end of TPR and the helix α7 of the middle domain. This finding could give insights into the different E2 specificity of the E3 ligase CHIP. UbcH5a was shown to be highly active in unspecific mono- and poly-ubiquitination of various substrates while Ubc13 seems to play a more specific role in Lys^{63}-linked poly-ubiquitination. Interestingly, truncated forms a CHIP lacking the TPR domain are as active in polyubiquitination as full-length CHIP when paired with Ubc13-Uev1a, but far less active with UbcH5a (Windheim et al., 2008). Unlike Ubc13, UbcH5a required the TPR domain of CHIP not only for ubiquitination activity but also for auto-ubiquitination on Lys^{22} of CHIP. Based on our HX data, it is intriguing to speculate that Ubc13 is a chaperone-independent E2 ligase. The Ubc13-CHIP complex shows significant destabilization in segments which are on the other hand highly stabilized by

chaperone binding, which argues for an displacement of TPR bound ligands when Ubc13 is bound. Indeed, the chaperone Hsp90 was not affecting CHIP-Ubc13 dependent polyubiquitination (Windheim et al., 2008) and no Hsp90/Hsp70 linked substrate is known so far that is ubiquitinated specifically via the Ubc13/Uev1a pathway. Furthermore, the helix α7 which is affected upon Ubc13 binding seems to be critical for the stability of the whole TPR domain (Main et al., 2003).

Altogether, this work set the basis for further interaction studies between TPR co-chaperones and Hsp70/Hsp90 chaperones by HX-MS.

3 Conclusions and Outlook

This work provided important insights into the allosteric mechanism of the Hsp70 chaperones on the structural level. Up to now, this is the only study that provides local structural information on the conformation of the low-affinity ATP-state of a full-length Hsp70 and on the pathway of ATP signal communication through the protein.

Certainly, more information on structure and dynamics is needed to fully understand the molecular mechanism of Hsp70 action. An open question of fundamental interest is the molecular mechanism of the synergistic stimulation of Hsp70 ATPase activity by J-domain proteins. New details on the rather transient interaction between a JDP and Hsc70 were shown in a co-crystal structure of a disulfide-crosslinked auxilin J-domain to the NBD of bovine Hsc70 (Jiang et al., 2007). The presented data implicate a role of the J-domain in directing the interdomain linker to a hydrophobic patch including Ile^{181} and Tyr^{371} in the NBD. How the J signal is finally transmitted to stimulate the ATPase activity remains unclear yet, as well as the function of J-protein as targeting factors for substrates.

Another important question is how the ATP-driven conformational changes of Hsp70 affect the folding and refolding of substrates. In order to find Hsp70 binding sites within natively folded substrates, HX-MS of Hsp70-client complexes could be performed. Interaction sites between DnaK and the heat-shock transcription factor σ^{32} and the replication initiation factor RepE were already monitored using HX-MS methods and protease footprinting (Fernanda Rodriguez, unpublished results). Additionally, site-specific chemical crosslinking of modified Hsp70 to substrates and subsequent MS analysis of crosslinked peptides could be performed. Using heterotrifunctional crosslinkers containing a third biotin group, enrichment on affinity columns can be used to purify crosslinked peptides and to facilitate the mass spectrometric analysis.

Furthermore, this work made significant contributions to the understanding of the dynamics of the Hsp90 chaperone machine. For the first time, the sequential order of ATP-dependent conformational changes within a Hsp90 could be kinetically and spatially resolved, thus leading to the full description of the HtpG ATPase cycle. While the bacterial HtpG showed drastic conformational stabilization upon ATP binding, eukaryotic Hsp90 chaperones seem to require highly dynamic conformational states to allow productive binding and activation of client proteins, regulated by a plethora of co-chaperones. By characterizing the ATP-driven

conformational changes within the Hsp90 chaperone family by HX-MS, this work set the basis for studying the interplay of Hsp90 with its co-factors and substrates.

Hence, it would be now of keen interest to investigate the effect of co-chaperone binding on the Hsp90 dynamics by HX-MS. While this work has investigated the chaperone interaction to the TPR co-chaperone CHIP in detail, it would be interesting to compare the effects on the Hsp90 site. This should also include other TPR proteins like the co-chaperone Hop/Sti1 that interacts with the C-terminus of Hsp70/Hsp90 chaperones, but exhibits also long-range effects on their ATPase activities, resulting in stimulation of the Hsp70 and inhibition of the Hsp90 ATP turnover. Further interaction studies should focus on the regulatory effects of other TPR co-chaperones on Hsp90 including FKBP51, FKBP52 and other immunophilins whose functions in the chaperone cycle are poorly understood yet. One major problem when investigating large protein-protein complexes by HX-MS is, however, the complexity of peptides resulting after peptic digestion in the HPLC setup. This problem can be tackled by developing new separation strategies (e.g. immobilization one protein partner on a column), establishing sophisticated HPLC gradients or using new mass spectrometers with higher mass accuracy and resolution. One important task is the automation and acceleration of the HX-MS data analysis which still is very time-consuming and rate-limiting for the studies.

The main issue in the Hsp90 chaperone field remains the identification of Hsp90 binding sites within client proteins and the characteristics of substrate turnover in substrate-co-chaperone-Hsp90 complexes. *In vitro* studies of Hsp90-client complexes are difficult because client proteins are usually unstable and hard to purify, and it is hard to form stable Hsp90-substrate complexes *in vitro*. A minimal system of five proteins (Hsp70, Hsp90, p23, Hop, Hsp40) was shown to assemble an active chaperone complex that drives activation of antibody-bound glucocortoid receptor upon hormone binding (Morishima et al., 2003), however there are no reports for the stable reconstitution of other native Hsp90-client complexes *in vitro*. One strategy would be to purify native Hsp90-client complexes after overexpression in insect cells (as described for a Cdk4-Cdc37-Hsp90 complex (Vaughan et al., 2006)) and to analyze the binding interface by HX-MS. Another approach would be the investigation of stable client subdomains that interact with Hsp90, e.g. the DNA-binding domain of p53 or the ligand-binding domain of estrogen receptor. These proteins could be stably expressed in *E. coli* and purified during this work and their interaction to Hsp90 can be analyzed in future.

4 Materials and Methods

4.1 Materials

4.1.1 Software and Equipment

Computer Software:

Office 2003	Microsoft Corp.
EndNote 8.0	ISI ResearchSoft
Photoshop CS2	Adobe
Illustrator CS2	Adobe
Acrobat Professional	Adobe
Analyst QS 1.1 with BioAnalyst extensions	Applied Biosystems/MDS Sciex
GPMAW	Lighthouse Data
MagTran	Z. Zhang
HXPep	Z. Zhang
VB script “isotope-centroid.dll”	developed in-house
Origin 6.1	OriginLab Corp.
PyMOL	DeLano Scientific LLC
Clone Manager 5.0	Sci Ed Central

Mass spectrometers:

QSTAR Pulsar i Hybrid MS/MS System	Applied Biosystems/MDS SCIEX
UltraFlex MALDI-TOF/TOF	Bruker Daltonics

HPLC pumps:

1100 Series Capillary Pump	Agilent
1100 Series Binary HPLC Pump	Agilent
LC-10 AD*VP* HPLC	Shimadzu
Rheos 2000 Micro HPLV	Flux Instruments
Ultimate HPLC with Switchos and Famos	LC Packings

Other equipment:

Speed-Vac	Bachofer
UV lamp B-100AP	Ultraviolet Products
French Press	SLM-Amin.co
Microfluidizer EmulsiFlex-C5	Avestin
ÄKTA FPLC and columns	GE Healthcare (Amersham)
Spektrometer UV-1601	Shimadzu
Sonifier 450	Branson
PCR cycler T-Gradient	Biometra
Fluorescence Spectrometer LS50B	Perkin Elmer / Applied Biosystems
UV/VIS spectrophotometer NanoDrop ND-1000	Thermo Scientific
Centrifuges	Sorvall, Eppendorf, Heraeus

4.1.2 Chemicals

If not otherwise stated, all chemicals were analytical grade and obtained from Roth, Sigma or Merck. Only high purity solvents (HPLC grade) were used.

4.1.3 Bacterial Strains

Name	Genotype	Source
BB1553	*F⁻ araDΔ139Δ (argF-lac)U169 rpsL150 relA1 deoC1 pts F25 rpsR flbB5301*	Lab collection
BB1994	BB1553, pDMI.1	Lab collection
DH5α	*SupE44 ΔlacU169 deoR (f80lacZAM15)hsdR17 recA1 endA1 gyrA96 thi-1 relA1*	Lab collection
DH5αZ1	DH5α *lacI^q Tet^r Spec^r* ((Lutz and Bujard, 1997))	Lab collection
CJ236	*dut1, ung1, thi-1, relA1/*pCJ105(F'*cam^r*) (Kunkel et al., 1987)	Lab collection
BL21 (DE3) pLys	E. coli B, F-, *dcm, ompT, hsdS($r_{B-}m_{B-}$), gal(DE3)* [pLysS (Cam^r)]	Invitrogen
BL21(DE3)star pCodonPlus	F⁻ *ompT hsdS$_B$ (r_{B-} m_{B-}) gal dcm rne131 (DE3)* [pCodonPlus (Cam^r)]	Invitrogen
Fi8202 pCodonPlus	*ΔntrBC fadAB101::TN10 lacI^q lacL8/D202* [pCodonPlus (Cam^r)]	Lab collection

4.1.4 Plasmids

Name	Description	Source
pCA528 (= pSUMO)	pET24 based with N-terminal His_6-Smt3-Ulp1 site(SUMO)-tag, T7 promotor, Kan^R	Dr. C. Andreasson
pSUMO-hHsp90beta	His_6-SUMO-hHsp90β, Kan^R	This work
pSUMO-hHsp90beta-Cys⁻-E20C	His_6-SUMO-hHsp90β-Cys⁻-E20C, Kan^R	M. Stankiewicz
pSUMO-Hsc70-human	His_6-SUMO-hHsc70, Kan^R	This work
pSUMO-Hsc82-yeast	His_6-SUMO-Hsc82-Sc, Kan^R	This work
pSUMO-Hsp70-human	His_6-SUMO-hHsp70, Kan^R	This work
pET15b-p23	His_6-p23, Amp^R	M. Stankiewicz
pSUMO-Ubc13-human	His_6-SUMO-Ubc13 human, Kan^R	This work
pSUMO-Uev1a-human	His_6-SUMO-Uev1a human, Kan^R	This work
pET15b	bacterial expression vector, T7 promotor, N-terminal His_6-thrombin site fusion, Amp^R	Novagen
pMPM201-Rn-Hsc70	Hsc70-R.norvegicus, arabinose-inducible, Amp^R	Dr. C. Gässler
pET15b-hHsp90beta-MC	His_6-hHsp90β-285-723, Amp^R	This work
pET15b-hHsp90beta-N	His_6-hHsp90β-1-222, Amp^R	This work
pET15b-hHsp90beta-NM	His_6-hHsp90β-1-545, Amp^R	This work

pSUMO-hHsp90beta-E42A	His_6-SUMO-hHsp90β-E42A, Kan^R	This work
pSUMO-p53core(94-312)	His_6-SUMO-p53 human core domain (94-312), Kan^R	This work
pET15b-ER-LBD(302-552)	His_6-human ER-LBD-302-552, Amp^R	This work
pSUMO-Hsc82-yeast-E11C	His_6-SUMO-Hsc82-Sc-E11C, Kan^R	This work

4.1.5 Oligonucleotides

All primers were obtained from Thermo Electron or Operon. Mutagenesis primer were phosphorylated at the 5'end (p).

Name	Sequence (5'→ 3')
5-Ubc13-*BsaI*	CCAGTGGGTCTCAGGTGGTATGGCCGGGCTGCC
5-Uev1a-*BsaI*	CCAGTGGGTCTCAGGTGGTATGCCAGGAGAGGTTCAAGC
hHsp70-*BsaI*-5'	CCAGTGGGTCTCAGGTGGTATGGCCAAAGCCGCGGCGAT
hHsc70-*BsaI*-5'	CCAGTGGGTCTCAGGTGGTATGTCCAAGGGACCTGCAGTTG
5'-*BsaI*-hHsp90beta	CCAGTGGGTCTCAGGTGGTATGCCTGAGGAAGTGCACCATG
3'-*EcoRI*-*SalI*-hHsp90b	GAATTCGTCGACCTAATCGACTTCTTCCATGCGA
5'-*BsmBI*-Hsc82	CCAGTGCGTCTCAGGTGGTATGGCTGGTGAAACTTTTGAATT
3'-Hsc82-*XhoI*	GGGGTACCTCGAGCACTAGTTAATCAACTTCTTCCATCTCGGT
Hsp90b-*XbaI*-*NdeI*-5'	GCTCTAGACATATGCCTGAGGAAGTGCACC
Hsp90b-285-*XbaI*-*NdeI*-5'	GCTCTAGACATATGACCAAGCCTATTTGGACCAG
Hsp90b-220-*BamH1*-3'	CGCGGATCCTTATTCCTTCTCCAAATAAAGGGTG
Hsp90b-545-*BamH1*-3'	CGCGGATCCTTACTCAGGCAGCTCCAGACCCTC
Hsp90b-723-*BglII*-3'	TTTGGAAGATCTTAATCGACTTCTTCCATGCGAG
90B_E42A	pCATTAGAGATCAACGCGCGCAGGAAAATCTCC
hsc82-E11C	pCAACTGAGTGATGCATGCTTGAAATTC
3'-p53core312-*XhoI*	GGGGTACCTCGAGCACTAGTTAGGTGTTGTTGGGCAGTGCTC
5'-*BsmBI*-p53core-94	CCAGTGCGTCTCAGGTGGTTCATCTTCTGTCCCTTCCCAGAAA
5'-ER-302-*EcoRI*-*NdeI*	CGGAATTCATATGAAGAAGAACAGCCTGGCCTTG
3'-ER-552-*BamHI*	CGGGATCCTTAGGGCGCATGTAGGCGGTGGG

4.1.6 Standards and kits

QIAprep Spin Miniprep Kit	Qiagen (Hilden)
QIAGEN Plasmid Midi Kit	Qiagen (Hilden)
QIAquick PCR Purification Kit	Qiagen (Hilden)
QIAquick Gel Extraction Kit	Qiagen (Hilden)
apo-Myoglobin	Sigma
GeneRuler™ 1kb DNA Ladder	Fermentas
Prestained Protein Ladder (SM0441)	Fermentas
Protein Ladder (SM0431)	Fermentas
Prestained Protein Ladder (SM0671)	Fermentas
Gel filtration standard	BioRad

4.1.7 Proteins

DnaK (2-637) wildtype	Bukau lab collection
DnaK R151A	Bukau lab collection (Dr. Vogel)
DnaK T199A	Bukau lab collection (Klaus Paal)
DnaK(2-385)	Bukau lab collection (Klaus Paal)
DnaK(393-637)	Bukau lab collection (Klaus Paal)
HtpG-His_{10}	Dr. Kramer
HtpG-E34A-His_{10}	Dr. Kramer
HtpG-E12C-His_{10}	Dr. Kramer
HptG-E12C-E34C-His_{10}	Dr. Kramer
CHIP wildtype	Bukau lab collection (Dr. Nikolay)
CHIP delta TPR (128-203)	Bukau lab collection (Dr. Nikolay)
UbcH5a	Bukau lab collection (Dr. Nikolay)
Ulp1 (SUMO protease)	Bukau lab collection
Restriction enzymes, other enzymes	New England Biolabs, Fermentas, Roche
Poroszyme Immobilized Pepsin	Applied Biosystems

4.1.8 Peptides

Pep65 (σ^{32}-M195-N207)	MAPVLYLQDKSSN	Peptide Technology Laboratories
Hsp70-C terminus	GPTIEEVD	Thermo Hybaid
Hsp90β-C terminus	ASRMEEVD	Thermo Hybaid
NR-peptide	NRLLLTGC	lab collection

4.1.9 Media

LB (Luria-Bertani) medium	10 g/l tryptone 5 g/L yeast extract 5 g/l NaCl
2 x YT medium	16 g/l tryptone 10 g/l yeast extract 5 g/l NaCl

(for plates, medium was supplemented with 15 g/l agar and antibiotics)

4.1.10 Buffers

HKM	25 mM HEPES/KOH pH 7.6 50 mM KCl 5 mM $MgCl_2$
PBS	137 mM NaCl 2.7 mM KCl 10 mM Na_2HPO_4 2 mM NaH_2PO_4 adjust to pH 7.4 with HCl

4.1.11 Antibiotics

All concentration are final concentrations, stock solutions are filter-sterilized

Ampicillin (Na-salt)	100 µg/ml
Kanamycin	50 µg/ml
Chloramphenicol	25 µg/ml (in ethanol)

4.2 Methods

4.2.1 Molecular Biology Techniques

If not stated otherwise, standard method protocols were performed according to "Molecular Cloning" (Maniatis et al., 1989).

4.2.1.1 Agarose gel electrophoresis

Agarose flat-bed gels in various concentrations (0.6 – 2% agarose in 1x TAE buffer) and sizes were run to separate DNA-fragments in an electrical field (10 – 20 V/cm) for analytical or preperative use. The desired amount of agarose was boiled in 1x TAE buffer until completely molten. After it cooled down to ca. 60°C, ethidium bromide solution (5 µl per 100ml agarose) was mixed into the liquid agarose, and then poured in a flat-bed tray with combs. As soon as the agarose solidified, the DNA in DNA-loading buffer was loaded into the slots and separated electrophoretically. The DNA was detected on a UV-light tray (265 nm). For preparative gels, a less strong UV-light source was used (365 nm) to avoid irradiation damage to the DNA.

10x TAE buffer
400 mM Tris/acetate, pH 8.0
10 mM EDTA

6x DNA loading buffer
30% glycerol
0.25% bromophenol blue
0.25% xylene cyanol FF

4.2.1.2 Purification of DNA fragments

Fragments of DNA generated by restriction digest were separated using standard agarose gel electrophoresis (Maniatis et al., 1989). DNA bands corresponding to desired products were identified using a UV transilluminator and bands were excised from ethidium bromide stained gels using a scalpel. Separation of DNA from the gel was achieved using the QIAquick Gel Extraction Kit (Qiagen).

4.2.1.3 Restriction digest of DNA

Restriction enzymes (type II exonucleases) cut double strand DNA site-specifically. Restriction digests were used for analysis as well as cloning. The enzymes (NEB, Roche, Fermentas) were used in a concentration of 0.2 – 1 U with the recommended buffer in a total volume of 20 – 50 µl. The digests were incubated at the enzyme-specific temperature for at least two hours to a maximum of overnight. For partial digests, a serial dilution of the restriction enzyme was prepared and the DNA was cut for 30 min at optimum temperature and buffer conditions.

4.2.1.4 Ligation of DNA fragments

Ligases link DNA ends by catalyzing the phosphodiester-bonding. DNA fragments with matching digested ends were incubated in no more than 10 µl total volume with 40 U T4-DNA-ligase and the recommended ligation buffer. The optimal ratio of vector to insert DNA was 1:3 for "sticky end" ligations. Different conditions for incubation were used: over night at 16°C, 2 h at room temperature or 30 min at 30°C.

4.2.1.5 Production of chemical competent cells

Protocol according to (Nishimura et al., 1990): A 50 ml culture was inoculated with 0.5 ml of an overnight culture and grown in medium A (LB broth with 10 mM $MgSO_4 \cdot 7H_2O$ and 0.2% glucose) to mid-logarithmic phase. The cells were kept 10 minutes on ice, pelleted at 1500g for 10 minutes at 4°C and resuspended gently on ice in 0.5 ml medium A. 2.5 ml ice cold storage solution (LB broth with 36% glycerol, 12% PEG-7500 and 12 mM $MgSO_4 \cdot 7H_2O$)

were added and the suspension was mixed without vortexing. The cells were aliquoted in 100 µl portions, frozen in liquid nitrogen and stored at -80°C.

4.2.1.6 Transformation

For transformation, 1-5 µl DNA were incubated with 50 µl competent cells for 30 min on ice, then heat-shocked for 90 seconds at 42°C (40°C for ΔdnaK strains) and 2 minutes on ice. 500 µl of LB medium was added and the mixture was shaken for 45 min at 37°C (30°C) to allow bacterial recovery and expression of the antibiotic resistance gene. 100 µl of transformed cells were streaked onto LB agar plates containing the appropriate antibiotics.

4.2.1.7 Purification of plasmid DNA

Plasmid DNA isolation was performed using either the small-scale QIAGEN® Quick Spin method or the large-scale QIAGEN® Plasmid Midi Kit according to the protocol provided by the manufacturer.

4.2.1.8 Polymerase chain reaction (PCR)

The Polymerase Chain Reaction (PCR) was used to clone genes from plasmid or genomic DNA as well as to probe DNA samples for the presence or absence of a specific sequence. Generally, the reaction was performed in 50 µl total volume with 50 pmol of each primer and with a final concentration of 250 µM of a dNTP mix. Various polymerases with the recommended buffer systems were used, depending on the purpose: OptiTaq ™ (Roboklon) was used for cloning because of its productivity and proof-reading capability, and the Taq polymerase for analytical PCRs. The PCR reaction was performed in a cycler, using the following basic protocol: 3 min at 94°C, then 30 – 35 cycles of 1 min at 94°C, 30 sec – 1 min at optimum annealing temperature (between 52° and 62°C) 1 – 5 min at 72°C (depending on the length of the amplified fragment) and a final 10 min incubation at 72°C to allow the polymerase to fill up incomplete fragments. Conditions varied, and were optimized for every amplification. The PCR products were analyzed on an agarose gel and, if necessary purified with the Qiagen MiniElute PCR purification kit.

4.2.1.9 PCR cloning into pSUMO vector

The respective gene (*hsp70*, *hsc70*, *hsp90, hsc82, Ubc13, Uev1a*) was amplified by PCR from plasmid DNA or genomic yeast DNA that was provided by the lab collection. The 5'- and 3'-primers were designed such that they were complementary to the beginning and end of the gene and contained extended restriction sites for *Bsa*I (or alternatively *BsmB*I) and *Xho*I (*Sal*I), respectively. The obtained PCR product was cut with *Bsa*I (*BsmB*I) and *Xho*I and inserted by ligation into linearized pCA528 which was also cut with *Bsa*I and *Xho*I. The resulting plasmid was transformed into the *E. coli* strain DH5αZ1 and after DNA isolation confirmed by sequencing at GATC Biotech AG (Konstanz).

4.2.1.10 Site-directed mutagenesis (Kunkel Method)

The mutant genes were created by *in vitro* mutagenesis according to Kunkel (Kunkel et al., 1987). Single-stranded DNA (ssDNA) of the desired vector construct was prepared using the *E. coli* host strain CJ236 and helper phage M13KO7. CJ236 is dut$^-$ and ung$^-$ and therefore deficient for the enzymes dUTPase (Dut) and uracil-N glycosylase (Ung). A deficiency of dUTPase leads to the production of elevated levels of dUTP which in turn leads to the misincorporation of deoxyuridine into DNA in place of thymidine. A deficiency of uracil-N glycosylase makes the bacteria unable to remove the uracil residues from the DNA. The infection of these cells with M13 helper phages lead to formation of phages which contained ssDNA of the vector. Phages were harvested and ssDNA was extracted by phenol-chloroform extraction and ethanol precipitation.

The mutagenic 5'-phosphorylated oligonucleotide was annealed to the deoxyuridine-containing ssDNA, and was extended and ligated using T7 DNA polymerase and T4 DNA ligase, respectively. The DNA was transformed into *E. coli* DH5αZ1, which is ung$^+$, thereby degrading the original uridine-containing strand. The newly synthesized strand which contained the mutated bases was replicated to produce intact mutated plasmid which was confirmed by sequencing at GATC Biotech AG.

10x Annealing buffer
200 mM Tris/HCl pH 7.5
20 mM $MgCl_2$
500 mM NaCl

10x Polymerase buffer (Polmix)
200 mM Tris/HCl pH 7.5
20 mM DTT
100 mM $MgCl_2$
4 mM ATP
5 mM dNTP
0.5 mg/ml BSA

Annealing

1 µL phosphorylated primer , 1 µl ssDNA, 1 µl 10x annealing buffer, and 7 µl H_2O were heated to 70°C for 2 min in a thermomixer, slowly cooled to 30°C, and then placed on ice.

Elongation reaction (extension and ligation)

To the annealed template-primer 10 µl 10x Polmix buffer, 0.125 µl T7 DNA polymerase (5 units), 0.5 µl T4 DNA ligase (200 units), and 80 µl H_2O were added, incubated on ice for 5 min, at room temperature for 5 min, and at 37°C for 2 h. Then, 5 µl were used for transformation into DH5αZ1.

4.2.2 Biochemical Methods

4.2.2.1 SDS polyacrylamide gel electrophoresis (SDS-PAGE)

4x SDS stacking gel buffer
0.5 M Tris/HCl, pH 6.8
0.4% SDS

4x SDS separation gel buffer
1.5 M Tris/HCl, pH 8.8
0.4% SDS

1x SDS gel running buffer
25 mM Tris, pH 8.0
200 mM glycine
0.1% (w/v) SDS

4x SDS gel loading buffer
500 mM Tris/HCl, pH 6.8
8% (w/v) SDS
40% (v/v) glycerol
20% (v/v) β-mercaptoethanol
0.6% (w/v) bromophenol blue

Proteins of different sizes can be separated by discontinuous SDS-Polyacrylamide gel electrophoresis (SDS-PAGE) under denaturing conditions (Laemmli, 1970). The gels used for this are bipartite: A lower separation gel, with polyacrylamide concentrations from 8 to 15% depending on the size of the proteins to be separated, and a stacking gel with 4% polyacrylamide to focus all proteins before they enter the lower part.

Typically, the following concentrations were used for the separating part of one midi or maxi gel or four mini gels:

	8%	**10%**	**12%**	**14%**	**15%**
Acrylamide (30%) in ml	8	10	12	14	15
4x SDS separation buffer in ml	7.5	7.5	7.5	7.5	7.5
Water in ml	14.5	12.5	10.5	8.5	7.5
10% APS in µl	240	240	240	240	240
TEMED in µl	40	40	40	40	40

For the stacking gel, a fixed concentration of 4% polyacrylamide was used:

Acrylamide (30%) in ml	3
4x SDS stacking buffer in ml	5
Water in ml	12
10% APS in µl	90
TEMED in µl	40

The samples were prepared by mixing with protein loading buffer and boiling for 5 minutes at 95°C. Then, the samples were loaded into the rinsed slots of the gel with a Hamilton syringe. All gels were run with 120 V in 1x SDS gel running buffer until the samples entered the separating gels, and then the current was raised to 200 or 300 V, depending on the gel size. The gel was run till the bromphenol blue marker reached the bottom to guarantee optimal partitioning of the proteins.

4.2.2.2 Coomassie blue staining

Proteins can be visualized in SDS gels by coomassie blue staining. The dye complexes with basic and aromatic side chains, resulting in a blue colour of the protein bands.

Coomassie staining solution
0.2% (w/v) Coom. Brilliant Blue R250
50% (v/v) methanol
5% (v/v) acetic acid
-> filter before use

Coomassie destaining solution
50% (v/v) methanol
5% (v/v) acetic acid

Before staining, the gel was fixed with destaining solution for 15 to 30 minutes to wash out the SDS, which results in less background staining. Then, the gel was incubated on a shaker in staining solution for at least one hour or overnight. Finally, the coomassie solution was removed and the stained gel was again incubated in destaining solution until the background was clear and the protein bands were clearly visible.

4.2.2.3 Silver staining

The silver stain method is a sensitive staining method to visualize protein bands that cannot be detected with Coomassie staining. All steps are carried out at room temperature on a shaker.

Fixing solution
50% (v/v) ethanol
40% ddH_2O
10% acetic acid
0.05% formaldehyde (37%)

Washing solution
50% ethanol
50% ddH_2O

Prestaining solution
0.02% (w/v) $Na_2S_2O_3 \cdot 5H_2O$
in ddH_2O

Staining solution
0.2% (w/v) $AgNO_3$
0.075% (v/v) formaldehyde (37%)
in ddH_2O

Developing solution
6% (w/v) Na_2CO_3
0.0004% (w/v) $Na_2S_2O_3/5H_2O$
0.05% (v/v) formaldehyde (37%)
in ddH_2O

Stop solutiom
44% (v/v) ethanol
44% ddH_2O
12% acetic acid

SDS was washed out of the gel by incubation in an excess of fixing solution for at least 2 hours, or optimally, overnight. The gel should always be covered by the solutions added. After a wash step of 2 times 25 minutes in washing solution, the prestaining solution was applied for 1 minute, followed by 20 minutes incubation in the silver nitrate staining solution. To wash away the remains of the staining solution, the gel was rinsed with deionised water three times. Immediately afterwards, the gel was incubated in developing solution until the bands became clearly visible. Depending on the amount of the protein, this step took from 10 to 30 minutes. The complete reaction was stopped with stop solution.

4.2.2.4 Determination of protein concentration

Protein concentrations were determined spectrophotometrically at λ=595 nm using Bradford reagent (BioRad) and BSA calibration curves (Bradford, 1976).

Additionally, protein concentrations were determined by measuring absorption at a wavelength of λ=280 nm using a ND-1000 spectrophotometer (Nanodrop, Thermo Scientific). Buffer without protein was used as reference. Protein concentrations were calculated on the basis of the Lambert-Beer law and their theoretical extinction coefficients at λ=280 nm (Gill and von Hippel, 1989), as calculated by the ProtParam tool at the ExPASy proteomics server (http://www.expasy.ch).

4.2.2.5 Purification of Hsc70

Hsc70 was purified according to a DnaK purification protocol (Buchberger et al., 1994). Each step was analyzed by SDS-PAGE and Coomassie blue staining.

Buffer A	**Buffer B**	**Buffer C**
25 mM HEPES/KOH pH 7.6	Buffer A	50 mM Tris/HCl pH 7.6
10 mM KCl	+ 1 M KCl	10% Sucrose
5 mM $MgCl_2$		
10 mM β-Mercaptoethanol		
1 mM EDTA		
5% Glycerol		

Buffer D	**ATP buffer**
1 mg DNaseI	Buffer A
1 M $(NH_4)_2SO_4$	+ 10 mM ATP
50 mM EDTA	+ 10 mM MgCl2
50 mM DTT (freshly added)	(check pH = 7.6 !)

Cell growth and overproduction

Usually 9 l of 2x YT complemented with 100 µg/ml ampicillin were inoculated with an overnight culture of the ΔdnaK52 strain BB1994 carrying the plasmid pMPM201-Hsc70-Rn. The culture was grown under vigorous shaking at 30°C to an OD_{600} of ~0.6. For induction *L*-arabinose was added to a final concentration of 0.01% and the culture was incubated for at least 5 h or overnight at 30°C.

Cell lysis and ammonium sulfate precipitation

Cells were harvested by centrifugation at 4500 rpm for 20 min (Sorvall F7 rotor), and cell pellets (for every ~16 g of pellet) were resuspended in 60 ml Buffer C, 7 ml Buffer D and 1.4 ml PMSF (50 mM). All steps were carried out at 4°C or on ice. Cells were lysed by French press at a pressure of 1000 psi. Cell debris was separated from lysates by centrifugation for 30 min at 10000 rpm and additional 1 h at 40000 rpm. The cleared supernatant was precipitated with 0.33 g/ml $(NH_4)_2SO_4$ by stepwise addition on ice and then centrifuged for 20 min at 10 000 rpm in a Sorvall F14 rotor. Supernatant was discarded and the protein pellet was resuspended in 40 ml Buffer A and dialyzed against 3 l Buffer A overnight in the cold room.

Anion exchange chromatography (DEAE-Sepharose)

The dialyzed protein solution was cleared from particles by centrifugation for 15 min at 10000 rpm. After filtration through a 0.45 µm filter, the solution was loaded onto a 250 ml

DEAE-Sepharose column which was equilibrated with Buffer A. The column was washed with 300 ml Buffer A and eluted with a 700 ml gradient of 0 to 50% Buffer B into 10 ml fractions. Afterwards, the column was washed with 300 ml 100% Buffer B. The Hsc70 containing fractions were pooled .

ATP-agarose affinity chromatography

2.5 ml bed volume of ATP-agarose (Jena Bioscience, kept in 20% ethanol) for every 100 mL protein solution was first equilibrated with 10 ml Buffer A, then washed with 10 ml Buffer B and re-equilibrated with 10 ml Buffer A. The pooled fractions from DEAE-chromatography were added to the equilibrated ATP-agarose and incubated at 4°C in a 50 ml falcon tube shaking end-over-end for at least 30 min. The agarose was packed into a disposable column (BioRad) and washed with 20 ml Buffer A and 20 ml Buffer B. The washed ATP-agarose was resuspended in the column with ATP-Buffer (20 ml) and incubated for 45 min at 4°C. After incubation, agarose was repacked into the column and the eluate was collected.

Anion exchange chromatography (Resource Q)

The Hsc70-containing eluate of the ATP-agarose was loaded onto a 6 ml ResourceQ (GE Healthcare) strong anion exchange column. The column was washed with 40 ml Buffer A and Hsc70 was eluted with a linear gradient of 0 to 50 % Buffer B. Fractions of 1.3 ml size were collected. Hsc70 containing fractions were pooled, aliquots frozen in liquid nitrogen and stored at -80°C.

4.2.2.6 Purification of proteins with His_6-SUMO-tag strategy

All proteins overexpressed from the vector pCA528 (pSUMO) (Andreasson et al., 2008) were purified and processed according to the following protocol. The proteins are expressed with an N-terminal His_6-SUMO fusion tag which increases solubility of the proteins and can be removed by the specific SUMO protease Ulp1 without any remaining amino acids (Malakhov et al., 2004).

The purification protocol is described exemplary for the purification of human Hsp90β and was used likewise for purification of Hsc82, hHsp90β-E20C, hHsp70, hHsc70, Ubc13, Uev1a. The co-chaperone p23 was purified accordingly, but without His_6-tag removal step with Ulp1.

Lysis buffer	**Buffer A**	**Buffer B**
20 mM HEPES/KOH pH 7.6	20 mM HEPES/KOH pH 7.6	20 mM HEPES/KOH pH 7.6
100 mM KCl	100 mM KCl	10 mM KCl
5 mM $MgCl_2$	5 mM $MgCl_2$	5 mM $MgCl_2$
5% glycerol	5% glycerol	5% glycerol
1 mM β-mercaptoethanol	1 mM β-mercaptoethanol	1 mM β-mercaptoethanol
1 mM PMSF		
1 mg DNaseI/100ml		
10 µg/ml Aprotinin ,		
5 µg/ml Leupeptin		
8 µg/ml Pepstatin A		

Buffer C	**Gel filtration buffer**	**Storage buffer**
20 mM HEPES/KOH pH 7.6	20 mM HEPES/KOH pH 7.6	20 mM HEPES, pH 7.6
1 M KCl	300 mM KCl	20 mM KCl
5 mM $MgCl_2$	5%glycerol	5 mM $MgCl_2$
5% glycerol	1mM DTT	5% glycerol
1 mM β-mercaptoethanol		1 mM DTT

Cell growth and lysis

Human Hsp90 was overexpressed from the vector pSUMO-hHsp90beta in the *E. coli* strain BL21(DE3)Star/pCodonPlus. The culture was grown in 5 l 2xYT medium supplemented with kanamycin to OD_{600} = 0.8 and expression was induced with 0.5 mM IPTG for 5 h at 30°C. After harvesting by centrifugation at 4500 rpm using a Sorvall F7 rotor for 20 min at 4°C, cells were resupended in 100 ml lysis buffer and lysed by a microfluidizer .

Nickel-affinity chromatography

The lysate was clarified by ultracentrifugation (40,000 rpm for 30 min) and incubated with 5 g Ni-IDA-matrix (Protino, Macherey-Nagel) for 30 min. After incubation, the matrix was transferred to a disposable column and washed with 5 x 10 ml buffer A and bound protein eluted with buffer A containing 250 mM imidazole. The used Ni-IDA matrix was cleaned and regenerated with cleaning solution (6 M guadinium hydrochloride, 0.4 M acetic acid), washed with water and equilibrated with buffer B.

SUMO-tag cleavage and removal

The eluted fusion protein was supplemented with Ulp1 protease (10µl/10mg eluted protein), which cleaved the His_6-Smt3 tag and the mixture was dialyzed overnight at 4°C against buffer B. Cleaved Hsp90 was recovered in the flow-through fractions after a second

incubation with the regenerated Ni-IDA matrix whereas the N-terminal His_6-Smt3 tag and Ulp1 remained on the column.

Anion-exchange chromatography

The dialyzed and tag-depleted Hsp90 solution was then loaded on an anion exchange chromatography column (ReSourceQ 6 ml, GE Healthcare). The column was washed with 30 ml buffer B and the Hsp90 was eluted with a linear gradient of 0-100% buffer C over 120 ml.

Size exclusion chromatography

Pooled Hsp90 fractions were further purified by Superdex 200 (GE Healthcare) size exclusion chromatography in gel filtration buffer and finally dialyzed against storage buffer. After concentration of the protein fraction with VIVASPIN ultracentrifugation spin columns, aliquots were frozen in liquid nitrogen and stored at -80°C.

4.2.2.7 Determination of nucleotide content

100 µl of a 10 µM protein solution were incubated for 10 minutes at 99°C and denaturated protein was then centrifuged for 10 minutes at 13000 rpm in a table top centrifuge. The nucleotide content of the supernatant was analyzed by analytical anion exchange chromatography (ResourceQ 1ml) with a linear gradient in 25 mM HEPES/KOH pH 6.5, 0 to 1.5 M KCl.

4.2.2.8 ATPase activity assays

Single turnover assays were performed with 50 µM HtpG, 40 µM ATP and 0.1 µCi [α-^{32}P]ATP. At different time points the reaction was quenched in 10% acetic acid 400 mM LiCl, ATP was separated from ADP by thin layer chromatography and quantified by phosphoimaging as described (Laufen et al., 1999).

Steady state ATPase activity was measured in an enzyme-coupled colorimetric assay using pyruvate kinase/lactate dehydrogenase (PK/LDH) as described (Ali et al., 1993). The assay mixture contained HKM buffer (25 mM HEPES pH 7.4, 50 mM KCl, 5 mM $MgCl_2$), DTT (5 mM), PK/LDH mix (Sigma; 100-fold diluted), NADH (250 µM), phosphoenolpyruvate (1 mM), ATP (2 mM or as indicated), and HtpG or mutant HtpG proteins (3 µM). All assays were performed at 30°C. All reported ATPase values are the differences between the values measured in the absence and presence of 150 µM Geldanamycin.

Steady-state ATPase assays for hHsp90β and Hsc82 were performed in same way with 5 mM ATP.

4.2.3 Chemical crosslinking and modification of proteins

4.2.3.1 Disulfide crosslinking

100 pmol HtpG-E12C were reduced with 5 mM TECEP for 30 min at 30°C and then incubated with large excess of nucleotides ATP (120 mM), ADP (60 mM), AMPPNP (60 mM) for at least 10 min. Oxidation of the cysteines was performed with 10 mM aqueous diamide solution for 10 min at 30°C, free sulfhydryl groups were then blocked with 10 mM iodoacetamide. Crosslink products were analyzed on a non-reducing 12% SDS polyacrylamide gel.

4.2.3.2 Bis-maleimide crosslinking

5 µM HtpG-E12C were reduced with 10 mM TECEP for 30 min at 30°C and then incubated with an excess of nucleotides (ATP, ADP, AMPPNP, same concentrations as in 4.2.3.1) or HKM buffer as control for at least 10 min at 30°C. Dimer-crosslinking was then performed by incubation of the protein with 5 µM of the crosslinker bis(maleimido)ethane (BMOE) or bis(maleimido)hexane (BMH) (Thermo Scientific) dissolved in HKM buffer for one hour at 30°C. The reaction mixture was quenched by adding 20 mM DTT and analyzed on a 12% SDS polyacrylamide gel.

4.2.3.3 Fluorescent labelling of proteins

Protein solutions of HtpG-E12C and HtpG-E12C-E34A were reduced with 10 mM TECEP and then incubated with either Hilyte Fluor™ 488-C2-maleimide (AnaSpec. Inc.), QXL-520-C2-maleimide (AnaSpec Inc.) (dissolved in 100% dimethylformamide) at room temperature for 1 hour. Unreacted label was then blocked by addition of 10 mM β-mercaptoethanol and removed by desalting with a self-packed Sephadex-G-75 column (GE Healthcare) equilibrated in HKM buffer. The labeling efficiency was checked to be 100 % by MS and final concentration of labelled protein was determined by measuring UV/VIS absorption with a NanoDrop Spectrophotometer (Thermo Scientific).

Same procedure was used for labelling hHsp90β-E20C with either Cy3-maleimide or Cy5-maleimide (CyDye™, GE Healthcare).

Extinction coefficients:

ε(HiLyte Fluor™ 488)$_{503nm}$ = 80000 $M^{-1}cm^{-1}$; ε(QXL™ 520)$_{514nm}$ = 26300 $M^{-1}cm^{-1}$;
ε(Cy3)$_{550nm}$ = 150000 $M^{-1}cm^{-1}$; ε(Cy5)$_{670nm}$ = 250000 $M^{-1}cm^{-1}$

4.2.4 Fluorescence spectroscopy

4.2.4.1 Fluorescence resonance energy transfer (FRET)

FRET, also named Förster resonance energy transfer, is based on the dipolar coupling between the emission dipole of a fluorescent donor (D) and the absorption dipole of a fluorescent acceptor (A). FRET occurs as a non-radiative transfer of energy from the excited donor to the acceptor, resulting in a quenching of the donor emission and sensitized emission from the acceptor. The donor molecules typically emit at shorter wavelengths that overlap with the absorption of acceptors. The FRET efficiency (E_{FRET}) is highly dependent on the distance between the two fluorophores and varies with the sixth power of distance r_0 between donor and acceptor:

$$E_{FRET} = \frac{R_0^6}{R_0^6 + r_0^6}$$

The Förster radius R_0 is the characteristic distance between fluorophores where the FRET efficiency is 50%, which can be calculated for any pair of fluorescent molecules. FRET can thus be used as a spectroscopic ruler for distance measurements in proteins (Stryer, 1978) and for the detection of conformational changes (Jares-Erijman and Jovin, 2003). FRET is detected either by the appearance of sensitized fluorescence of the acceptor or by the intensity ratio change of donor/acceptor (if the acceptor is fluorescent), or the fluorescence decrease of the donor.

The Förster radius for the classical used FRET pair Cy3/ Cy5 is 53 Å. The second FRET pair HiLyte Fluor™ 488 /QXL-520 uses a quantum dot as a non-fluorescent acceptor (dark quencher).

For FRET experiments with hHsp90β, 100 nM fluorescent hHsp90β-E20C-Cy3 and 200 nM hHsp90β-E20C-Cy5 were mixed in HKM buffer and incubated for 30 min at 30 °C to ensure formation of mixed dimers. Fluorescence emission spectra were recorded in absence or presence of ATP (3 mM final concentration) or p23 (6 µM final concentration) or in presence

of both from 540-700 nm at an excitation wavelength of 520 nm on a Perkin Elmer LS-55 Luminescence Spectrometer at 30°C.

For fluorescence measurements of HtpG, labeled proteins HtpG-E12C-Hilyte Fluor™ 488 ($HtpG_{FL}$) and HtpG-E12C-QXL-520 ($HtpG_{Q}$) were mixed in a ratio 300 nM:600 nM in HKM buffer and incubated for 30 min at 30°C to ensure formation of mixed dimers. As a control $HtpG_{FL}$ was incubated with unlabeled HtpG in the same ratio of concentrations. Donor fluorescence emission spectra were recorded in absence or presence of nucleotides (20 mM final concentration) from 500-700 nm at an excitation wavelength of 475 nm on a Perkin Elmer LS-55 Luminescence Spectrometer at 30°C. The donor fluorescence at 525 nm was measured after addition of nucleotides in a time-course experiment over 20 min and 60 min for $HtpG_{FL}$ or the HtpG-E34A$_{FL}$, respectively. The data were fitted using GraphPad Prism software.

4.2.4.2 Stopped-flow analysis

Using a stopped-flow device (SX-18M Applied Photophysics, Surrey, UK) $HtpG_{FL}$ (300 nM) in HKM buffer was rapidly mixed 1:1 with a solution of 0.003 to 30 mM ATP or ADP. Fluorescence (excitation 488 nm; cut-off filter at 530 nm) was measured for 0.1 to 10 s at 30 °C. An exponential function was fitted to the time-dependent fluorescence increase using GraphPad Prism software.

4.2.5 Mass spectrometry

4.2.5.1 Molecular Weight Determination of Proteins by On-line LC/MS

In order to analyze the exact molecular mass of proteins by ESI-MS, the samples must be desalted from buffer before they can be eluted into the mass spectrometer. Protein molecular weights were determined by online LC/MS using a QSTAR Pulsar equipped with the electrospray ion source (Applied Biosystems/MDS SCIEX), two HPLC pumps (Agilent 1100 Series), a Rheodyne injection valve (Model 7725) with a 200 µl stainless steel sample loop, and a 2-position/10-port valve with microelectric actuator (Valco C2-1000EP6) as described in (Rist et al., 2005a). The protein samples (50-100 pmol) were injected and pushed onto a reversed-phase trap column with a high flow rate of 0.05 % TFA (400 µl/min) provided by pump A. As a trap column, either a micro-trap column (0.8 x 3 mm) (Rist et al., 2005a) or a micro-guard column (1 x 20 mm, Upchurch) packed with POROS 10 R1 or R2 material (PerSeptive Biosystems) was used. After 90 s, the 10-port valve was switched to elute the desalted protein with 80% buffer B (90% acetonitrile, 0.05% TFA) at 20 µl/min directly into the electrospray source of the Q-TOF-mass spectrometer. The timing and sequence of operation of the valves was controlled by the Agilent 1100 Series Capillary Pump, while each run was started by the electrical switch injection valve.

Mass spectra were acquired in positive ion mode with an ionspray voltage of 5000 V. Average molecular weights of proteins were deconvoluted from the ESI spectra using the Bayesian Reconstruct tool of the BioAnalyst software. All spectra were re-calibrated using myoglobin as standard.

4.2.5.2 Protein Identification by static nanoESI-MS or nanoLC ESI-MS

Peptides prepared from peptic or tryptic digestion were desalted using self-packed microcolumns. These were GELloader tips (Eppendorf) filled with a piece of fused silica (20 µm ID, 280 µm OD, LC Packings) and a small bedvolume of POROS 20 R2 bulk material (PerSeptive Biosystems). The column was first activated with 60% MeOH, followed by 10 µl 1% formic acid (FA). The acidified peptide mixture sample was loaded on the tip, washed twice with 10 µl 1% FA and then directly eluted in 2 µl of 60% MeOH, 1% FA into a gold/palladium coated boro-silicate nano-electrospray needle (Proxeon Biosystems).

Peptide sequencing by static nano ESI-MS was performed by tandem mass spectrometry using a QSTAR Pulsar instrument (Applied Biosystems/MDS SCIEX) equipped with a nanoelectrospray ion source (Proxeon Biosystems). Mass spectra were acquired in positive ion mode. The ionspray voltage IS (700-1000 V) applied to the nanoelectrospray needle was adjusted to produce a stable spray with a flow rate of ~20 nl/min, thereby allowing a long analysis time (~50 min on a sample of 1 µl). For MS/MS-spectra the precursor ion was selected in the first quadrupole (Q1) and fragmented in the collision cell. Nitrogen was used as the collision gas. The collision energy setting was increased until fragment ion signals were as abundant as the parent ion signal. Before the end of the measurement, the collision energy was further increased by 5-10 V to generate more small immonium ions which might be useful for data interpretation. The quadrupole time-of-flight mass spectrometer provided a resolution of >7000 FWHM and a mass accuracy of <50 ppm in both MS and MS/MS mode. For fast MS/MS data acquisition, information dependent data aquisition (IDA) experiments were performed with 1 s MS survey scan and 10 s product ion scan of the most abundant peptide signals.

For MS/MS analysis of samples by nanoLC-MS, peptides were concentrated nearly to dryness in a speedVac vacuum centrifuge, and diluted to a total volume of 30 µL with 0.1% TFA. Of each sample, 25 µL was analyzed using a nanoHPLC system (UltiMate: Dionex, Amsterdam, The Netherlands), equipped with a FAMOS auto-sampler (Dionex), coupled to an ESI Q-TOF hybrid mass spectrometer (Applied Biosystems, Foster City, CA). Samples were loaded on an Inertsil C18-trapping column (LC Packings, Amsterdam, The Netherlands) using 0.1% TFA and a flow rate of 20 µL/min. Peptides were eluted and separated on an analytical column (75 µm x 150mm) packed with Inertsil 3-µm C18 material (LC Packings) using a flow rate of 200 nL/min and applying a gradient of buffer A (0.1% formic acid/5% ACN) and buffer B (0.1% formic acid/80% ACN). The elution profile was as follows: 0–2 min, 5% B; 2–50 min, 5–40% B; 50–60 min, 40–60% B; and 60–63 min, 60–90% B. The column was connected to a nano-ESI emitter (New Objectives, Woburn, MA) and 2000 V were applied via liquid junction. The Q-TOF operated in positive ion mode. One MS survey scan (0.7 s) was followed by one information dependent (IDA experiment) product ion scan (3 s). Only double and triple charged ions were selected for fragmentation (MS/MS).

Proteins and peptides were identified by sending the MS/MS data to the MASCOT search engine or by peptide sequence tags, derived from fragment ion spectra of selected peptides, against the nonredundant protein database maintained and updated regularly by the European

Bioinformatics Institute (EBI) or the Swiss-Prot database using the program PepSea (MDS Proteomics) (Boeckmann et al., 2003). Every protein hit was confirmed by comparing the expected fragment ions with all the ions observed in the product ion spectrum.

4.2.6 Amide hydrogen exchange (HX-MS) experiments and data analysis

4.2.6.1 Materials and Buffers

D_2O buffer: 25 mM HEPES, pD 7.6, 50 mM KCl, 5 mM $MgCl_2$ (deuterated HKM buffer) was prepared using 99.85% D_2O (Euriso-top, Gif-sur-Yvette, France), lyophilized, and re-dissolved five times in fresh D_2O volumes. Usually 10x stock solutions were prepared and were diluted 1:10 in D_2O before use.

Quench buffer: 400 mM KH_2PO_4/H_3PO_4, pH 2.2.

For HX experiments with DnaK, 2 M guadinium hydrochloride was added to the quench buffer to facilitate proteolytic digest.

Immobilization of pepsin /protease XIII on POROS 20-AL beads (Wang et al., 2002):

160 mg protease powder (pepsin from Roche or protease XIII *Aspergillus saitoi* from Sigma) was dissolved in 4 ml 50 mM sodium-citrate buffer (pH 4.4). 0.5 g of POROS-20AL (Applied Biosystems) and 30.2 mg sodium-cyanoborohydride ($NaBH_3CN$) was added to the solution and mixed by gentle over top shaking. Immediately, 4 ml of 2 M Na_2SO_4 solution was added dropwise to increase surface concentration by salting out procedure. The suspension was then incubated overnight at 4°C by over top shaking and then quenched by addition of 10 µl 16.7 M ethanolamine for 2 hours. The mixture was then washed several times with 0.05% TFA solution.. Finally, the slurry was stored in 0.05% TFA solution with addition of 0.05% sodium azide. The immoblized protease was then packed into 2 x 20 mm microguard columns (Upchurch).

Fully deuterated protein controls

The protein solution of interest was unfolded in 6 M guanidinium hydrochloride, lyophilized and at least 3 times diluted in D_2O and lyophilized again.

4.2.6.2 Amide hydrogen exchange experiments

Continuous or pulse HX-MS experiments were carried out off-line and analyzed by a special HPLC-MS setup described below (Rist et al., 2003; Rist et al., 2005b) .

For the individual experiments with different chaperones, usually 100-200 pmol of the proteins of interest were preincubated in HKM buffer in absence or presence of excess ligands (nucleotides, inhibitors, peptides) or proteins at 30°C in a final volume of 5 µl.

DnaK/DnaK mutants: 40 µM DnaK was incubated with 60 mM ATP for 1 min and then subjected to HX. For the study of peptide binding to DnaK, 40 µM DnaK was incubated with 60 mM peptide Pep65 for 1 h before deuteration.

Hsp90/HtpG/HtpG mutants: Nucleotide-free Hsp90 proteins (40 µM) were pre-incubated with a large excess of buffered ATP (120 mM), ADP (60 mM), AMPPNP (60 mM), or PU-H71 (60 µM) for 10 min at 30°C to ensure complete binding. Geldanamycin was dissolved in DMSO, freshly diluted 1:100 in HKM buffer and then incubated with Hsp90β (40 µM) at a final concentration of 600 µM overnight on ice under light-protection. In all cases the ligand occupancy of Hsp90 as calculated from the published dissociation equilibrium constants using the quadratic solution of the binding equilibrium was more than 99% during pre-incubation and more than 95% during incubation in D_2O. For pulsed HX experiments, HtpG was pre-incubated with ATP for certain time intervals between 10 s-90min before 10s deuteration.

CHIP: 20 µM of ligand free human CHIP was incubated with 100 µM hHsp70, hHsc70 or hHsp90β, respectively for 30 min at 30°C. For complex formation with octapeptides, 40 µM CHIP was pre-incubated with 600 µM Hsp90 peptide (ASRMEEVD) or Hsp70 peptide (GPTIEEVD) for 30 min at 30°C. For complex formation with E2 ligases, 20 µM CHIP was pre-incubated with 100 µM of either Ubc13 or UbcH5a for 60 min at 30°C.

The amide hydrogen exchange reactions were initiated by a 20-fold dilution of the protein into D_2O buffer and incubated at 30°C. After various time intervals (10 s-90 min), the exchange reaction was quenched by decreasing the temperature to 0°C and the pH to 2.2 with 100 µl ice-cold quench buffer. Quenched samples were loaded with a prechilled Hamilton-syringe into the injection valve of the rapid desalting HPLC setup connected to the electrospray ion source of the quadrupole-TOF instrument. The deuterated mass of the full-length proteins was then measured as in the experimental setup in 4.2.5.1 with a desalting time of 90 s; however the whole system was immersed in an ice bath to minimize back-exchange.

For the on-line generation and analysis of peptic peptides, the setup contained an additional column (2 x 20 mm, Upchurch) packed with immobilized pepsin or protease XIII (or a combination of both) which was mounted after the injection valve (Fig 4.1). The resulting

peptides from online-digestion were than trapped on the reversed-phase column (POROS 50 R2 material) and desalted. After 3 min, the desalted peptides were eluted from the trap column over a 0.75 mm ID x 6 cm analytical reversed-phase colum packed with ZORBAX 300-SB-C8 (3.5 µm particles) directly into the electrospray source. The solvent for elution was delivered by Pump B with a flow rate of 17.5 µl/min using the following short gradient: buffer A (0.05 % TFA) to buffer B (90% acetonitrile, 0.05% TFA), having the profile: %B: 15-55 (0-10 min), %B: 55-100 (10-11 min), %B: 100-15% (11-12 min). The last eluted peptides were detected 13 minutes after sample injection. The whole system was immersed in an ice bath to minimize back-exchange. In all experiments, control samples with undeuterated and fully deuterated proteins were measured.

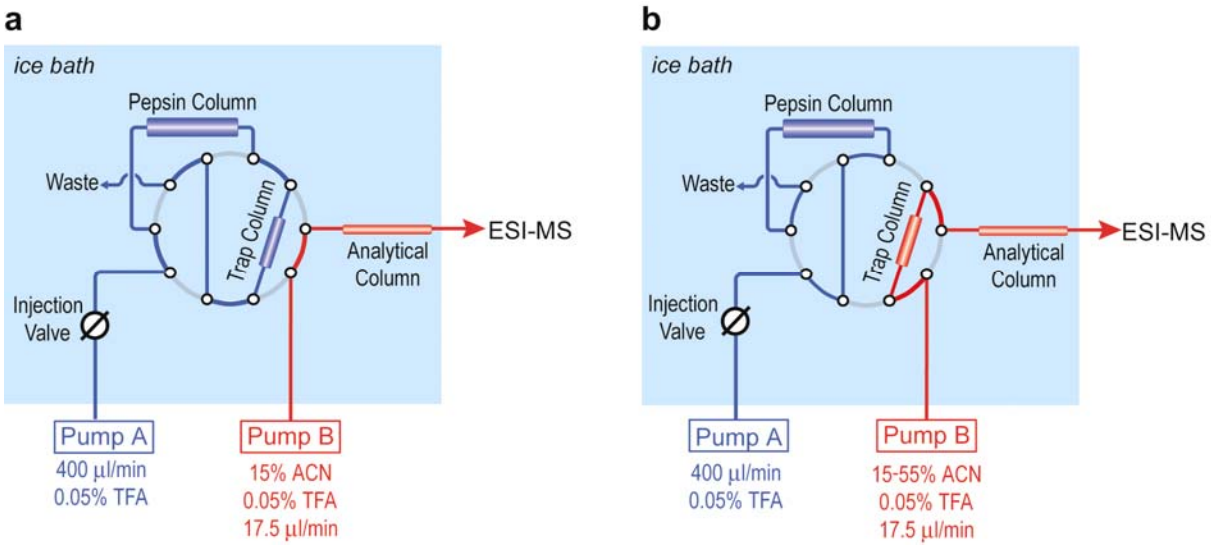

Fig. 4.1 Schematic drawing of the in-line peptic digestion/rapid-desalting HPLC setup used for HX-MS experiments. (a) Injected samples were pushed trough the pepsin column, trapped on a reversed phase column and desalted via Pump A **(b)** after a certain time, the 10-port valve was switched to elute the desalted peptides into the ESI-source of the MS via Pump B. All parts are immersed in an ice-bath to minimize back-exchange. For analysis of full-length proteins, the pepsin column was removed. (Figure modified from (Rist et al., 2005b))

4.2.6.3 HX-MS data analysis

Peptic peptides were identified either by static nanoESI-MS/MS or by on-line nanoLC/MS/MS as described in 4.2.5.2 on the basis of their fragment spectra. After internal calibration, the mass error was below 10 ppm and hence more peptides could be identified on the basis of their exact mass. Peptide identification lists are found in the appendix.

Data analysis of continuous HX labelling experiments

In order to analyze deuteron incorporation into full-length proteins, mass spectra of deuterated proteins were analyzed by the Protein Reconstruct tool of the BioAnalyst software. The

number of deuterons incorporated was determined by substracting the determined mass of the undeuterated protein.

The deuterium content of the peptides was calculated by using the average mass difference between the isotopic envelopes (centroids) of the deuterated and the undeuterated peptides.

The centroid <m> is calculated is by the following equation:

$$\langle m \rangle = \frac{\sum I_i m_i}{\sum I_i}$$

where I_i is the intensity of the peak at m/z = m_i

This data analysis was usually done with the MagTran software (Zhang and Marshall, 1998), which needed time-consuming steps of data export and import between different programs. During this work, a Visual Basic script was developed which could be implemented into the Analyst QS 1.1 software for fast isotopic centroid determination of an exchanged peptide. In this script, named "isotope-centroid.dll", an isotopic peak cluster can be selected and the resulting centroid m/z value is displayed and stored directly in an Excel data sheet for easy data processing. The script enabled extensive data analysis of large peptide data sets and even the distinguished analysis of overlapping species.

For the calculation of the deuteron incorporation into peptides, adjustments were made for deuterium losses due to back-exchange during analysis based on appropriate controls, a 0% deuterium control (undeuterated protein) and a 100% totally deuterated control according to following formula (Zhang and Smith, 1993):

$$D = \frac{\langle m \rangle - \langle m_{0\%} \rangle}{\langle m_{100\%} \rangle - \langle m_{0\%} \rangle} \cdot N$$

where D is the number of deuterons incorporated present in a particular peptic peptide after incubation of the protein in D_2O, N is the total number of exchangeable amide hydrogens in the peptide sequence (substracted by proline residues), and <m> is the experimentally observed average mass. $<m_{0\%}>$ is the undeuterated control and $<m_{100\%}>$ the fully deuterated control.

Experimental data were fit by nonlinear least squares to a sum of three exponential terms resulting in three exchange rates with the amplitudes corresponding to the number of exchanging amide hydrogens according to

$$D = N - \sum_{i=1}^{N} \exp(-k_i t)$$

where D is the deuterium content of a peptide with N peptide amide hydrogens and k_i is the rate constant for exchange for the peptide hydrogens.

The average chemical exchange rate was determined by simulating deuteron incorporation for different time intervals and back-exchange during the desalting step using the exchange rates for pD 7.6 and pH 2.4 calculated with the HXPep program (courtesy Z. Zhang) and fitting a single exponential equation to the values. Protection factors were calculated according to the equation for the EX2 exchange regime, $p = 1/K_{unf} = k_{ch}/k_{obs}$ (where K_{unf} indicates the unfolding equilibrium constant; k_{ch} indicates the average chemical exchange rate; k_{obs} indicates the observed exchange rate (Hvidt and Nielsen, 1966). The lower limit of ΔG for the unfolding reaction was estimated according to $\Delta G = -RT \ln(K_{unf}) = -RT \ln(k_{obs}/k_{ch})$ setting for the non-exchanging amide hydrogens the lowest exchange rates (0.0001 s^{-1}) detectable in our experiment.

Data analysis of pulsed HX labelling experiments (HtpG)

For the kinetic analysis of the transition of I- to T-state in HX experiments, full length protein mass spectra of 10 time points of three independent measurements were deconvoluted using MagTran software (Zhang and Smith, 1993) and the abundance of the two deuterated mass species was calculated by fitting two Gaussian peaks into the deconvoluted spectra using the following equation:

$$y = \frac{A_1}{\sigma\sqrt{2\pi}} e^{-\frac{1}{2}\left(\frac{x-\bar{x}_1}{\sigma}\right)^2} + \frac{A_2}{\sigma\sqrt{2\pi}} e^{-\frac{1}{2}\left(\frac{x-\bar{x}_2}{\sigma}\right)^2}$$

with A_1, A_2, x_1 and x_2 being area and mean of the first and second peak and σ the standard deviation of the Gaussian peaks. The ration of A_1 to the sum of A_1 and A_2 represented the relative amount of the T state. The increasing amount of the T-state in dependence of time was fitted using a first order rate equation.

For the analysis of the transition kinetics in deuterated peptides, peptide MS spectra of three independent experiments (8 time points) were extracted, smoothed, normalized to the highest peak of the isotope cluster and the intensity of two peaks determined: the peak, which is highest at 10 s preincubation with ATP (I state), and the peak, which is highest at 300 s preincubation with ATP (T state). We plotted the T state peak intensity divided by the sum of

the intensities of the two peaks versus time (T/(T+I)). This ratio followed first order rate kinetics.

5 References

Aebersold, R., and Mann, M. (2003). Mass spectrometry-based proteomics. Nature *422*, 198-207.

Ali, J. A., Jackson, A. P., Howells, A. J., and Maxwell, A. (1993). The 43-kilodalton N-terminal fragment of the DNA gyrase B protein hydrolyzes ATP and binds coumarin drugs. Biochemistry *32*, 2717-2724.

Ali, M. M., Roe, S. M., Vaughan, C. K., Meyer, P., Panaretou, B., Piper, P. W., Prodromou, C., and Pearl, L. H. (2006). Crystal structure of an Hsp90-nucleotide-p23/Sba1 closed chaperone complex. Nature *440*, 1013-1017.

Andreasson, C., Fiaux, J., Rampelt, H., Mayer, M. P., and Bukau, B. (2008). Hsp110 Is a Nucleotide-activated Exchange Factor for Hsp70. J Biol Chem *283*, 8877-8884.

Arndt, V., Rogon, C., and Hohfeld, J. (2007). To be, or not to be--molecular chaperones in protein degradation. Cell Mol Life Sci *64*, 2525-2541.

Bai, Y. (2006). Protein folding pathways studied by pulsed- and native-state hydrogen exchange. Chem Rev *106*, 1757-1768.

Bai, Y., Milne, J. S., Mayne, L., and Englander, S. W. (1993). Primary structure effects on peptide group hydrogen exchange. Proteins *17*, 75-86.

Barth, A. (2000). The infrared absorption of amino acid side chains. Prog Biophys Mol Biol *74*, 141-173.

Barthel, T. K., Zhang, J., and Walker, G. C. (2001). ATPase-Defective Derivatives of Escherichia coli DnaK That Behave Differently with Respect to ATP-Induced Conformational Change and Peptide Release. J Bacteriol *183*, 5482-5490.

Beausoleil, S. A., Villen, J., Gerber, S. A., Rush, J., and Gygi, S. P. (2006). A probability-based approach for high-throughput protein phosphorylation analysis and site localization. Nat Biotechnol *24*, 1285-1292.

Bertelsen, E. B., Zhou, H., Lowry, D. F., Flynn, G. C., and Dahlquist, F. W. (1999). Topology and dynamics of the 10 kDa C-terminal domain of DnaK in solution. Protein Sci *8*, 343-354.

Biemann, K. (1992). Mass spectrometry of peptides and proteins. Annu Rev Biochem *61*, 977-1010.

Bimston, D., Song, J., Winchester, D., Takayama, S., Reed, J. C., and Morimoto, R. I. (1998). BAG-1, a negative regulator of Hsp70 chaperone activity, uncouples nucleotide hydrolysis from substrate release. Embo J *17*, 6871-6878.

Bougault, C., Feng, L., Glushka, J., Kupce, E., and Prestegard, J. H. (2004). Quantitation of rapid proton-deuteron amide exchange using hadamard spectroscopy. J Biomol NMR *28*, 385-390.

Bradford, M. M. (1976). A rapid and sensitive method for the quantitation of microgram quantities of protein utilizing the principle of protein-dye binding. Anal Biochem *72*, 248-254.

Brehmer, D., Gassler, C., Rist, W., Mayer, M. P., and Bukau, B. (2004). Influence of GrpE on DnaK-substrate interactions. J Biol Chem *279*, 27957-27964.

Brinker, A., Scheufler, C., Von Der Mulbe, F., Fleckenstein, B., Herrmann, C., Jung, G., Moarefi, I., and Hartl, F. U. (2002). Ligand discrimination by TPR domains. Relevance and selectivity of EEVD-recognition in Hsp70 x Hop x Hsp90 complexes. J Biol Chem *277*, 19265-19275.

Brooks, C., Karplus, M., and Pettitt, B. (1990). Proteins: A Theoretical Perspective of Dynamics, Structure, and Thermodynamics.

Buchberger, A., Theyssen, H., Schroder, H., McCarty, J. S., Virgallita, G., Milkereit, P., Reinstein, J., and Bukau, B. (1995). Nucleotide-induced conformational changes in the ATPase and substrate binding domains of the DnaK chaperone provide evidence for interdomain communication. J Biol Chem *270*, 16903-16910.

Buchberger, A., Valencia, A., McMacken, R., Sander, C., and Bukau, B. (1994). The chaperone function of DnaK requires the coupling of ATPase activity with substrate binding through residue E171. Embo J *13*, 1687-1695.

Bukau, B., and Horwich, A. L. (1998). The Hsp70 and Hsp60 chaperone machines. Cell *92*, 351-366.

Chappell, T. G., Konforti, B. B., Schmid, S. L., and Rothman, J. E. (1987). The ATPase core of a clathrin uncoating protein. J Biol Chem *262*, 746-751.

Cheung, K. M., Matthews, T. P., James, K., Rowlands, M. G., Boxall, K. J., Sharp, S. Y., Maloney, A., Roe, S. M., Prodromou, C., Pearl, L. H.*, et al.* (2005). The identification, synthesis, protein crystal structure and in vitro biochemical evaluation of a new 3,4-diarylpyrazole class of Hsp90 inhibitors. Bioorg Med Chem Lett *15*, 3338-3343.

Chiosis, G., Huezo, H., Rosen, N., Mimnaugh, E., Whitesell, L., and Neckers, L. (2003a). 17AAG: low target binding affinity and potent cell activity--finding an explanation. Mol Cancer Ther *2*, 123-129.

Chiosis, G., Lucas, B., Huezo, H., Solit, D., Basso, A., and Rosen, N. (2003b). Development of purine-scaffold small molecule inhibitors of Hsp90. Curr Cancer Drug Targets *3*, 371-376.

Chiti, F., and Dobson, C. M. (2006). Protein misfolding, functional amyloid, and human disease. Annu Rev Biochem *75*, 333-366.

Cliff, M. J., Harris, R., Barford, D., Ladbury, J. E., and Williams, M. A. (2006). Conformational diversity in the TPR domain-mediated interaction of protein phosphatase 5 with Hsp90. Structure *14*, 415-426.

Cliff, M. J., Williams, M. A., Brooke-Smith, J., Barford, D., and Ladbury, J. E. (2005). Molecular recognition via coupled folding and binding in a TPR domain. J Mol Biol *346*, 717-732.

Cortajarena, A. L., and Regan, L. (2006). Ligand binding by TPR domains. Protein Sci *15*, 1193-1198.

Cravatt, B. F., Simon, G. M., and Yates, J. R., 3rd (2007). The biological impact of mass-spectrometry-based proteomics. Nature *450*, 991-1000.

D'Andrea, L. D., and Regan, L. (2003). TPR proteins: the versatile helix. Trends Biochem Sci *28*, 655-662.

Daniel, S., Bradley, G., Longshaw, V. M., Soti, C., Csermely, P., and Blatch, G. L. (2008). Nuclear translocation of the phosphoprotein Hop (Hsp70/Hsp90 organizing protein) occurs under heat shock, and its proposed nuclear localization signal is involved in Hsp90 binding. Biochim Biophys Acta.

Das, A. K., Cohen, P. W., and Barford, D. (1998). The structure of the tetratricopeptide repeats of protein phosphatase 5: implications for TPR-mediated protein-protein interactions. Embo J *17*, 1192-1199.

Dehner, A., Furrer, J., Richter, K., Schuster, I., Buchner, J., and Kessler, H. (2003). NMR chemical shift perturbation study of the N-terminal domain of Hsp90 upon binding of ADP, AMP-PNP, geldanamycin, and radicicol. Chembiochem *4*, 870-877.

Dekker, P. J., and Pfanner, N. (1997). Role of mitochondrial GrpE and phosphate in the ATPase cycle of matrix Hsp70. J Mol Biol *270*, 321-327.

Demand, J., Alberti, S., Patterson, C., and Hohfeld, J. (2001). Cooperation of a ubiquitin domain protein and an E3 ubiquitin ligase during chaperone/proteasome coupling. Curr Biol *11*, 1569-1577.

Dempsey, C. E. (2001). Hydrogen exchange in peptides and proteins using NMR-spectroscopy. Progress In Nuclear Magnetic Resonance Spectroscopy *39*, 135-170.

Deng, Y., Zhang, Z., and Smith, D. L. (1999). Comparison of continuous and pulsed labeling amide hydrogen exchange/mass spectrometry for studies of protein dynamics. J Am Soc Mass Spectrom *10*, 675-684.

Deuerling, E., Schulze-Specking, A., Tomoyasu, T., Mogk, A., and Bukau, B. (1999). Trigger factor and DnaK cooperate in folding of newly synthesized proteins. Nature *400*, 693-696.

Dinner, A. R., Sali, A., Smith, L. J., Dobson, C. M., and Karplus, M. (2000). Understanding protein folding via free-energy surfaces from theory and experiment. Trends Biochem Sci *25*, 331-339.

Dole, M., Mack, L. L., Hines, R. L., Mobley, R. C., Ferguson, L. D., and Alice, M. B. (1968). Molecular beams of macroions. Journal of Chemical Physics *49*, 2240-2249.

Dollins, D. E., Warren, J. J., Immormino, R. M., and Gewirth, D. T. (2007). Structures of GRP94-Nucleotide Complexes Reveal Mechanistic Differences between the hsp90 Chaperones. Mol Cell *28*, 41-56.

Domon, B., and Aebersold, R. (2006). Mass spectrometry and protein analysis. Science *312*, 212-217.

Dutta, R., and Inouye, M. (2000). GHKL, an emergent ATPase/kinase superfamily. Trends Biochem Sci *25*, 24-28.

Dymock, B. W., Barril, X., Brough, P. A., Cansfield, J. E., Massey, A., McDonald, E., Hubbard, R. E., Surgenor, A., Roughley, S. D., Webb, P.*, et al.* (2005). Novel, potent small-molecule inhibitors of the molecular chaperone Hsp90 discovered through structure-based design. J Med Chem *48*, 4212-4215.

Dyson, H. J., and Wright, P. E. (2004). Unfolded proteins and protein folding studied by NMR. Chem Rev *104*, 3607-3622.

Dyson, H. J., and Wright, P. E. (2005). Intrinsically unstructured proteins and their functions. Nat Rev Mol Cell Biol *6*, 197-208.

Ellis, J. (1987). Proteins as molecular chaperones. Nature *328*, 378-379.

Eng, J. K., McCormack, A. L., and Yates, J. R., III (1994). An approach to correlate tandem mass spectral data of peptides with amino acid sequences in a protein database. Journal of the American Society for Mass Spectrometry *5*, 976-989.

Englander, S. W., and Kallenbach, N. R. (1983). Hydrogen exchange and structural dynamics of proteins and nucleic acids. Q Rev Biophys *16*, 521-655.

Feng, L., Orlando, R., and Prestegard, J. H. (2006). Amide proton back-exchange in deuterated peptides: applications to MS and NMR analyses. Anal Chem *78*, 6885-6892.

Flaherty, K. M., DeLuca-Flaherty, C., and McKay, D. B. (1990). Three-dimensional structure of the ATPase fragment of a 70K heat-shock cognate protein. Nature *346*, 623-628.

Flaherty, K. M., Wilbanks, S. M., DeLuca-Flaherty, C., and McKay, D. B. (1994). Structural basis of the 70-kilodalton heat shock cognate protein ATP hydrolytic activity. II. Structure of the active site with ADP or ATP bound to wild type and mutant ATPase fragment. J Biol Chem *269*, 12899-12907.

Flynn, G. C., Chappell, T. G., and Rothman, J. E. (1989). Peptide binding and release by proteins implicated as catalysts of protein assembly. Science *245*, 385-390.

Frey, S., Leskovar, A., Reinstein, J., and Buchner, J. (2007). The ATP-ase cycle of the endoplasmic chaperone GRP94. J Biol Chem.

Gamer, J., Multhaup, G., Tomoyasu, T., McCarty, J. S., Rudiger, S., Schonfeld, H. J., Schirra, C., Bujard, H., and Bukau, B. (1996). A cycle of binding and release of the DnaK, DnaJ and GrpE chaperones regulates activity of the Escherichia coli heat shock transcription factor sigma32. Embo J *15*, 607-617.

Gao, B., Emoto, Y., Greene, L., and Eisenberg, E. (1993). Nucleotide binding properties of bovine brain uncoating ATPase. J Biol Chem *268*, 8507-8513.

Garnier, C., Lafitte, D., Tsvetkov, P. O., Barbier, P., Leclerc-Devin, J., Millot, J. M., Briand, C., Makarov, A. A., Catelli, M. G., and Peyrot, V. (2002). Binding of ATP to heat shock protein 90: evidence for an ATP-binding site in the C-terminal domain. J Biol Chem *277*, 12208-12214.

Gassler, C. S., Wiederkehr, T., Brehmer, D., Bukau, B., and Mayer, M. P. (2001). Bag-1M accelerates nucleotide release for human Hsc70 and Hsp70 and can act concentration-dependent as positive and negative cofactor. J Biol Chem *276*, 32538-32544.

Geller, R., Vignuzzi, M., Andino, R., and Frydman, J. (2007). Evolutionary constraints on chaperone-mediated folding provide an antiviral approach refractory to development of drug resistance. Genes Dev *21*, 195-205.

Gill, S. C., and von Hippel, P. H. (1989). Calculation of protein extinction coefficients from amino acid sequence data. Anal Biochem *182*, 319-326.

Glover, J. R., and Lindquist, S. (1998). Hsp104, Hsp70, and Hsp40: a novel chaperone system that rescues previously aggregated proteins. Cell *94*, 73-82.

Goloubinoff, P., Mogk, A., Zvi, A. P., Tomoyasu, T., and Bukau, B. (1999). Sequential mechanism of solubilization and refolding of stable protein aggregates by a bichaperone network. Proc Natl Acad Sci U S A *96*, 13732-13737.

Gooljarsingh, L. T., Fernandes, C., Yan, K., Zhang, H., Grooms, M., Johanson, K., Sinnamon, R. H., Kirkpatrick, R. B., Kerrigan, J., Lewis, T.*, et al.* (2006). A biochemical rationale for the anticancer effects of Hsp90 inhibitors: slow, tight binding inhibition by geldanamycin and its analogues. Proc Natl Acad Sci U S A *103*, 7625-7630.

Guex, N., and Peitsch, M. C. (1997). SWISS-MODEL and the Swiss-PdbViewer: an environment for comparative protein modeling. Electrophoresis *18*, 2714-2723.

Ha, J. H., and McKay, D. B. (1994). ATPase kinetics of recombinant bovine 70 kDa heat shock cognate protein and its amino-terminal ATPase domain. Biochemistry *33*, 14625-14635.

Harris, S. F., Shiau, A. K., and Agard, D. A. (2004). The crystal structure of the carboxy-terminal dimerization domain of htpG, the Escherichia coli Hsp90, reveals a potential substrate binding site. Structure *12*, 1087-1097.

Harrison, C. J., Hayer-Hartl, M., Liberto, M. D., Hartl, F. U., and Kuriyan, J. (1997). Crystal Structure of the Nucleotide Exchange Factor GrpE Bound to the ATPase Domain of the Molecular Chaperone DnaK. Science *276*, 431-435.

Hartl, F. U., and Hayer-Hartl, M. (2002). Molecular Chaperones in the Cytosol: from Nascent Chain to Folded Protein. Science *295*, 1852-1858.

He, H., Zatorska, D., Kim, J., Aguirre, J., Llauger, L., She, Y., Wu, N., Immormino, R. M., Gewirth, D. T., and Chiosis, G. (2006). Identification of potent water soluble purine-scaffold inhibitors of the heat shock protein 90. J Med Chem *49*, 381-390.

Heitzer, A., Mason, C. A., Snozzi, M., and Hamer, G. (1990). Some effects of growth conditions on steady state and heat shock induced htpG gene expression in continuous cultures of Escherichia coli. Arch Microbiol *155*, 7-12.

Henzel, W. J., Watanabe, C., and Stults, J. T. (2003). Protein identification: the origins of peptide mass fingerprinting. J Am Soc Mass Spectrom *14*, 931-942.

Henzler-Wildman, K., and Kern, D. (2007). Dynamic personalities of proteins. Nature *450*, 964-972.

Hernandez, H., and Robinson, C. V. (2007). Determining the stoichiometry and interactions of macromolecular assemblies from mass spectrometry. Nat Protoc *2*, 715-726.

Hernandez, M. P., Chadli, A., and Toft, D. O. (2002). HSP40 binding is the first step in the HSP90 chaperoning pathway for the progesterone receptor. J Biol Chem *277*, 11873-11881.

Hoofnagle, A. N., Resing, K. A., and Ahn, N. G. (2003). Protein analysis by hydrogen exchange mass spectrometry. Annu Rev Biophys Biomol Struct *32*, 1-25.

Hossain, M. M., and Nakamoto, H. (2003). Role for the cyanobacterial HtpG in protection from oxidative stress. Curr Microbiol *46*, 70-76.

Huai, Q., Wang, H., Liu, Y., Kim, H. Y., Toft, D., and Ke, H. (2005). Structures of the N-terminal and middle domains of E. coli Hsp90 and conformation changes upon ADP binding. Structure *13*, 579-590.

Hvidt, A., and Nielsen, S. O. (1966). Hydrogen exchange in proteins. Adv Protein Chem *21*, 287-386.

Imami, K., Sugiyama, N., Kyono, Y., Tomita, M., and Ishihama, Y. (2008). Automated Phosphoproteome Analysis for Cultured Cancer Cells by Two-Dimensional NanoLC-MS Using a Calcined Titania/C18 Biphasic Column. Anal Sci *24*, 161-166.

Iribarne, J. V., and Thomson, B. A. (1976). On the evaporation of small ions from charged droplets. Journal of Chemical Physics *64*, 2287-2294.

Jackson, A. P., and Maxwell, A. (1993). Identifying the catalytic residue of the ATPase reaction of DNA gyrase. Proc Natl Acad Sci U S A *90*, 11232-11236.

Jakob, U., Lilie, H., Meyer, I., and Buchner, J. (1995). Transient interaction of Hsp90 with early unfolding intermediates of citrate synthase. Implications for heat shock in vivo. J Biol Chem *270*, 7288-7294.

Jares-Erijman, E. A., and Jovin, T. M. (2003). FRET imaging. Nat Biotechnol *21*, 1387-1395.

Jentsch, S., Seufert, W., Sommer, T., and Reins, H. A. (1990). Ubiquitin-conjugating enzymes: novel regulators of eukaryotic cells. Trends Biochem Sci *15*, 195-198.

Jiang, J., Ballinger, C. A., Wu, Y., Dai, Q., Cyr, D. M., Hohfeld, J., and Patterson, C. (2001). CHIP is a U-box-dependent E3 ubiquitin ligase: identification of Hsc70 as a target for ubiquitylation. J Biol Chem *276*, 42938-42944.

Jiang, J., Maes, E. G., Taylor, A. B., Wang, L., Hinck, A. P., Lafer, E. M., and Sousa, R. (2007). Structural basis of J cochaperone binding and regulation of Hsp70. Mol Cell *28*, 422-433.

Jiang, J., Prasad, K., Lafer, E. M., and Sousa, R. (2005). Structural basis of interdomain communication in the Hsc70 chaperone. Mol Cell *20*, 513-524.

Jordan, R., and McMacken, R. (1995). Modulation of the ATPase activity of the molecular chaperone DnaK by peptides and the DnaJ and GrpE heat shock proteins. J Biol Chem *270*, 4563-4569.

Kabani, M., Beckerich, J. M., and Brodsky, J. L. (2002a). Nucleotide exchange factor for the yeast Hsp70 molecular chaperone Ssa1p. Mol Cell Biol *22*, 4677-4689.

Kabani, M., McLellan, C., Raynes, D. A., Guerriero, V., and Brodsky, J. L. (2002b). HspBP1, a homologue of the yeast Fes1 and Sls1 proteins, is an Hsc70 nucleotide exchange factor. FEBS Lett *531*, 339-342.

Kaltashov, I. A., and Eyles, S. J. (2002). Studies of biomolecular conformations and conformational dynamics by mass spectrometry. Mass Spectrometry Reviews *21*, 37-71.

Kamal, A., Thao, L., Sensintaffar, J., Zhang, L., Boehm, M. F., Fritz, L. C., and Burrows, F. J. (2003). A high-affinity conformation of Hsp90 confers tumour selectivity on Hsp90 inhibitors. Nature *425*, 407-410.

Karas, M., and Kruger, R. (2003). Ion formation in MALDI: the cluster ionization mechanism. Chemical Reviews *103*, 427-440.

Karzai, A. W., and McMacken, R. (1996). A Bipartite Signaling Mechanism Involved in DnaJ-mediated Activation of the Escherichia coli DnaK Protein. J Biol Chem *271*, 11236-11246.

Kasibhatla, S. R., Hong, K., Biamonte, M. A., Busch, D. J., Karjian, P. L., Sensintaffar, J. L., Kamal, A., Lough, R. E., Brekken, J., Lundgren, K.*, et al.* (2007). Rationally designed high-affinity 2-amino-6-halopurine heat shock protein 90 inhibitors that exhibit potent antitumor activity. J Med Chem *50*, 2767-2778.

Kelley, W. L. (1998). The J-domain family and the recruitment of chaperone power. Trends Biochem Sci *23*, 222-227.

Kim, S. C., Sprung, R., Chen, Y., Xu, Y., Ball, H., Pei, J., Cheng, T., Kho, Y., Xiao, H., Xiao, L.*, et al.* (2006). Substrate and functional diversity of lysine acetylation revealed by a proteomics survey. Mol Cell *23*, 607-618.

Koch, M. H., Vachette, P., and Svergun, D. I. (2003). Small-angle scattering: a view on the properties, structures and structural changes of biological macromolecules in solution. Q Rev Biophys *36*, 147-227.

Konermann, L., and Simmons, D. A. (2003). Protein-folding kinetics and mechanisms studied by pulse-labeling and mass spectrometry. Mass Spectrom Rev *22*, 1-26.

Koshland, D. E. (1958). Application of a Theory of Enzyme Specificity to Protein Synthesis. Proc Natl Acad Sci U S A *44*, 98-104.

Koshland, D. E., Jr. (1998). Conformational changes: how small is big enough? Nat Med *4*, 1112-1114.

Kunkel, T. A., Roberts, J. D., and Zakour, R. A. (1987). Rapid and efficient site-specific mutagenesis without phenotypic selection. Methods in Enzymology *154*, 367-382.

Kussmann, M., and Roepstorff, P. (2000). Sample preparation techniques for peptides and proteins analyzed by MALDI-MS. Methods Mol Biol *146*, 405-424.

Laemmli, U. K. (1970). Cleavage of structural proteins during the assembly of the head of bacteriophage T4. Nature *227*, 680-685.

Laufen, T., Mayer, M. P., Beisel, C., Klostermeier, D., Mogk, A., Reinstein, J., and Bukau, B. (1999). Mechanism of regulation of Hsp70 chaperones by DnaJ cochaperones. PNAS *96*, 5452-5457.

Leskovar, A., Wegele, H., Werbeck, N. D., Buchner, J., and Reinstein, J. (2008). The ATPase cycle of the mitochondrial Hsp90 analog Trap1. J Biol Chem.

Levinthal, C. (1968). Are there pathways to protein folding? J Chim Phys *65*, 44-45.

Liberek, K., Marszalek, J., Ang, D., Georgopoulos, C., and Zylicz, M. (1991a). Escherichia coli DnaJ and GrpE Heat Shock Proteins Jointly Stimulate ATPase Activity of DnaK. PNAS *88*, 2874-2878.

Liberek, K., Skowyra, D., Zylicz, M., Johnson, C., and Georgopoulos, C. (1991b). The Escherichia coli DnaK chaperone, the 70-kDa heat shock protein eukaryotic equivalent, changes conformation upon ATP hydrolysis, thus triggering its dissociation from a bound target protein. J Biol Chem *266*, 14491-14496.

Linderstrøm-Lang, K. (1956). Exchange reactions between D2O and proteins. Acta Chemica Scandinavica *10*, 149.

Liu, Q., and Hendrickson, W. A. (2007). Insights into hsp70 chaperone activity from a crystal structure of the yeast Hsp110 Sse1. Cell *131*, 106-120.

Longshaw, V. M., Chapple, J. P., Balda, M. S., Cheetham, M. E., and Blatch, G. L. (2004). Nuclear translocation of the Hsp70/Hsp90 organizing protein mSTI1 is regulated by cell cycle kinases. J Cell Sci *117*, 701-710.

Lutz, R., and Bujard, H. (1997). Independent and tight regulation of transcriptional units in *Escherichia coli* via the LacR/O, the TetR/O and AraC/I_1-I_2 regulatory elements. Nucleic Acids Research *25*, 1203-1210.

Lyman, S. K., and Schekman, R. (1997). Binding of secretory precursor polypeptides to a translocon subcomplex is regulated by BiP. Cell *88*, 85-96.

Main, E. R., Xiong, Y., Cocco, M. J., D'Andrea, L., and Regan, L. (2003). Design of stable alpha-helical arrays from an idealized TPR motif. Structure *11*, 497-508.

Malakhov, M. P., Mattern, M. R., Malakhova, O. A., Drinker, M., Weeks, S. D., and Butt, T. R. (2004). SUMO fusions and SUMO-specific protease for efficient expression and purification of proteins. J Struct Funct Genomics *5*, 75-86.

Mamyrin, B. A., Karataev, V. I., Shmikk, D. V., and Zagulin, V. A. (1973). Mass reflectron. New nonmagnetic time-of-flight high-resolution mass spectrometer. Zhurnal Eksperimental'noi i Teoreticheskoi Fiziki *64*, 82-89.

Maniatis, T., Sambrook, J., and Fritsch, E. F. (1989). Molecular cloning: a laboratory manual: Cold spring harbour laboratory press).

Mann, M., and Wilm, M. (1994). Error-tolerant identification of peptides in sequence databases by peptide sequence tags. Analytical Chemistry *66*, 4390-4399.

Marcu, M. G., Chadli, A., Bouhouche, I., Catelli, M., and Neckers, L. M. (2000). The heat shock protein 90 antagonist novobiocin interacts with a previously unrecognized ATP-binding domain in the carboxyl terminus of the chaperone. J Biol Chem *275*, 37181-37186.

Maroney, A. C., Marugan, J. J., Mezzasalma, T. M., Barnakov, A. N., Garrabrant, T. A., Weaner, L. E., Jones, W. J., Barnakova, L. A., Koblish, H. K., Todd, M. J.*, et al.* (2006). Dihydroquinone ansamycins: toward resolving the conflict between low in vitro affinity and high cellular potency of geldanamycin derivatives. Biochemistry *45*, 5678-5685.

Matlack, K. E., Misselwitz, B., Plath, K., and Rapoport, T. A. (1999). BiP acts as a molecular ratchet during posttranslational transport of prepro-alpha factor across the ER membrane. Cell *97*, 553-564.

Matsuoka, S., Ballif, B. A., Smogorzewska, A., McDonald, E. R., 3rd, Hurov, K. E., Luo, J., Bakalarski, C. E., Zhao, Z., Solimini, N., Lerenthal, Y.*, et al.* (2007). ATM and ATR substrate analysis reveals extensive protein networks responsive to DNA damage. Science *316*, 1160-1166.

Mayer, M. P., Brehmer, D., Gassler, C. S., and Bukau, B. (2001). Hsp70 chaperone machines. Adv Protein Chem *59*, 1-44.

Mayer, M. P., and Bukau, B. (1998). Hsp70 chaperone systems: diversity of cellular functions and mechanism of action. Biol Chem *379*, 261-268.

Mayer, M. P., and Bukau, B. (2005). Hsp70 chaperones: cellular functions and molecular mechanism. Cell Mol Life Sci *62*, 670-684.

Mayer, M. P., Nikolay, R., and Bukau, B. (2002). Aha, another regulator for hsp90 chaperones. Mol Cell *10*, 1255-1256.

Mayer, M. P., Rudiger, S., and Bukau, B. (2000). Molecular basis for interactions of the DnaK chaperone with substrates. Biol Chem *381*, 877-885.

McCarty, J. S., Buchberger, A., Reinstein, J., and Bukau, B. (1995). The role of ATP in the functional cycle of the DnaK chaperone system. J Mol Biol *249*, 126-137.

McCarty, J. S., Rudiger, S., Schonfeld, H. J., Schneider-Mergener, J., Nakahigashi, K., Yura, T., and Bukau, B. (1996). Regulatory region C of the E. coli heat shock transcription factor, sigma32, constitutes a DnaK binding site and is conserved among eubacteria. J Mol Biol *256*, 829-837.

McClellan, A. J., Xia, Y., Deutschbauer, A. M., Davis, R. W., Gerstein, M., and Frydman, J. (2007). Diverse cellular functions of the Hsp90 molecular chaperone uncovered using systems approaches. Cell *131*, 121-135.

McLaughlin, S. H., Smith, H. W., and Jackson, S. E. (2002). Stimulation of the weak ATPase activity of human hsp90 by a client protein. J Mol Biol *315*, 787-798.

McLaughlin, S. H., Sobott, F., Yao, Z. P., Zhang, W., Nielsen, P. R., Grossmann, J. G., Laue, E. D., Robinson, C. V., and Jackson, S. E. (2006). The co-chaperone p23 arrests the Hsp90 ATPase cycle to trap client proteins. J Mol Biol *356*, 746-758.

McLaughlin, S. H., Ventouras, L. A., Lobbezoo, B., and Jackson, S. E. (2004). Independent ATPase activity of Hsp90 subunits creates a flexible assembly platform. J Mol Biol *344*, 813-826.

Meyer, P., Prodromou, C., Hu, B., Vaughan, C., Roe, S. M., Panaretou, B., Piper, P. W., and Pearl, L. H. (2003). Structural and functional analysis of the middle segment of hsp90: implications for ATP hydrolysis and client protein and cochaperone interactions. Mol Cell *11*, 647-658.

Meyer, P., Prodromou, C., Liao, C., Hu, B., Mark Roe, S., Vaughan, C. K., Vlasic, I., Panaretou, B., Piper, P. W., and Pearl, L. H. (2004). Structural basis for recruitment of the ATPase activator Aha1 to the Hsp90 chaperone machinery. Embo J *23*, 511-519.

Miao, B., Davis, J. E., and Craig, E. A. (1997). Mge1 functions as a nucleotide release factor for Ssc1, a mitochondrial Hsp70 of Saccharomyces cerevisiae. J Mol Biol *265*, 541-552.

Minami, Y., Kimura, Y., Kawasaki, H., Suzuki, K., and Yahara, I. (1994). The carboxy-terminal region of mammalian HSP90 is required for its dimerization and function in vivo. Mol Cell Biol *14*, 1459-1464.

Moffat, K. (2001). Time-resolved biochemical crystallography: a mechanistic perspective. Chem Rev *101*, 1569-1581.

Mogk, A., Tomoyasu, T., Goloubinoff, P., Rudiger, S., Roder, D., Langen, H., and Bukau, B. (1999). Identification of thermolabile Escherichia coli proteins: prevention and reversion of aggregation by DnaK and ClpB. Embo J *18*, 6934-6949.

Montgomery, D. L., Morimoto, R. I., and Gierasch, L. M. (1999). Mutations in the substrate binding domain of the Escherichia coli 70 kDa molecular chaperone, DnaK, which alter substrate affinity or interdomain coupling. J Mol Biol *286*, 915-932.

Morishima, Y., Kanelakis, K. C., Murphy, P. J., Lowe, E. R., Jenkins, G. J., Osawa, Y., Sunahara, R. K., and Pratt, W. B. (2003). The hsp90 cochaperone p23 is the limiting component of the multiprotein hsp90/hsp70-based chaperone system in vivo where it acts to stabilize the client protein: hsp90 complex. J Biol Chem *278*, 48754-48763.

Morshauser, R. C., Hu, W., Wang, H., Pang, Y., Flynn, G. C., and Zuiderweg, E. R. (1999). High-resolution solution structure of the 18 kDa substrate-binding domain of the mammalian chaperone protein Hsc70. J Mol Biol *289*, 1387-1403.

Murata, S., Minami, Y., Minami, M., Chiba, T., and Tanaka, K. (2001). CHIP is a chaperone-dependent E3 ligase that ubiquitylates unfolded protein. EMBO Rep *2*, 1133-1138.

Nazabal, A., Laguerre, M., Schmitter, J. M., Vaillier, J., Chaignepain, S., and Velours, J. (2003). Hydrogen/deuterium exchange on yeast ATPase supramolecular protein complex

analyzed at high sensitivity by MALDI mass spectrometry. J Am Soc Mass Spectrom *14*, 471-481.

Neckers, L. (2007). Heat shock protein 90: the cancer chaperone. J Biosci *32*, 517-530.

Nikolay, R., Wiederkehr, T., Rist, W., Kramer, G., Mayer, M. P., and Bukau, B. (2004). Dimerization of the human E3 ligase CHIP via a coiled-coil domain is essential for its activity. J Biol Chem *279*, 2673-2678.

Nishimura, A., Morita, M., Nishimura, Y., and Sugino, Y. (1990). A rapid and highly efficient method for preparation of competent Escherichia coli cells. Nucleic Acids Res *18*, 6169.

O'Brien, M. C., Flaherty, K. M., and McKay, D. B. (1996). Lysine 71of the Chaperone Protein Hsc70 Is Essential for ATP Hydrolysis. J Biol Chem *271*, 15874-15878.

Obermann, W. M., Sondermann, H., Russo, A. A., Pavletich, N. P., and Hartl, F. U. (1998). In vivo function of Hsp90 is dependent on ATP binding and ATP hydrolysis. J Cell Biol *143*, 901-910.

Odunuga, O. O., Hornby, J. A., Bies, C., Zimmermann, R., Pugh, D. J., and Blatch, G. L. (2003). Tetratricopeptide repeat motif-mediated Hsc70-mSTI1 interaction. Molecular characterization of the critical contacts for successful binding and specificity. J Biol Chem *278*, 6896-6904.

Okamoto, T., Nishimura, Y., Ichimura, T., Suzuki, K., Miyamura, T., Suzuki, T., Moriishi, K., and Matsuura, Y. (2006). Hepatitis C virus RNA replication is regulated by FKBP8 and Hsp90. Embo J *25*, 5015-5025.

Olsen, J. V., Blagoev, B., Gnad, F., Macek, B., Kumar, C., Mortensen, P., and Mann, M. (2006). Global, in vivo, and site-specific phosphorylation dynamics in signaling networks. Cell *127*, 635-648.

Onuchic, J. N., Nymeyer, H., Garcia, A. E., Chahine, J., and Socci, N. D. (2000). The energy landscape theory of protein folding: insights into folding mechanisms and scenarios. Adv Protein Chem *53*, 87-152.

Packschies, L., Theyssen, H., Buchberger, A., Bukau, B., Goody, R. S., and Reinstein, J. (1997). GrpE accelerates nucleotide exchange of the molecular chaperone DnaK with an associative displacement mechanism. Biochemistry *36*, 3417-3422.

Palaiomylitou, M., Tartas, A., Vlachakis, D., Tzamarias, D., and Vlassi, M. (2008). Investigating the structural stability of the Tup1-interaction domain of Ssn6: evidence for a conformational change on the complex. Proteins *70*, 72-82.

Panaretou, B., Prodromou, C., Roe, S. M., O'Brien, R., Ladbury, J. E., Piper, P. W., and Pearl, L. H. (1998). ATP binding and hydrolysis are essential to the function of the Hsp90 molecular chaperone in vivo. Embo J *17*, 4829-4836.

Panaretou, B., Siligardi, G., Meyer, P., Maloney, A., Sullivan, J. K., Singh, S., Millson, S. H., Clarke, P. A., Naaby-Hansen, S., Stein, R.*, et al.* (2002). Activation of the ATPase activity of hsp90 by the stress-regulated cochaperone aha1. Mol Cell *10*, 1307-1318.

Pearl, L. H., and Prodromou, C. (2001). Structure, function, and mechanism of the Hsp90 molecular chaperone. Adv Protein Chem *59*, 157-186.

Pearl, L. H., and Prodromou, C. (2006). Structure and mechanism of the Hsp90 molecular chaperone machinery. Annu Rev Biochem *75*, 271-294.

Pearl, L. H., Prodromou, C., and Workman, P. (2008). The Hsp90 molecular chaperone: an open and shut case for treatment. Biochem J *410*, 439-453.

Peitsch, M. C. (1996). ProMod and Swiss-Model: Internet-based tools for automated comparative protein modelling. Biochem Soc Trans *24*, 274-279.

Pellecchia, M., Montgomery, D. L., Stevens, S. Y., Vander Kooi, C. W., Feng, H. P., Gierasch, L. M., and Zuiderweg, E. R. (2000). Structural insights into substrate binding by the molecular chaperone DnaK. Nat Struct Biol *7*, 298-303.

Pelton, J. T., and McLean, L. R. (2000). Spectroscopic methods for analysis of protein secondary structure. Anal Biochem *277*, 167-176.

Perkins, D. N., Pappin, D. J., Creasy, D. M., and Cottrell, J. S. (1999). Probability-based protein identification by searching sequence databases using mass spectrometry data. Electrophoresis *20*, 3551-3567.

Perutz, M. F. (1972). Nature of haem-haem interaction. Nature *237*, 495-499.

Perutz, M. F., Wilkinson, A. J., Paoli, M., and Dodson, G. G. (1998). The stereochemical mechanism of the cooperative effects in hemoglobin revisited. Annu Rev Biophys Biomol Struct *27*, 1-34.

Phillips, J. J., Yao, Z. P., Zhang, W., McLaughlin, S., Laue, E. D., Robinson, C. V., and Jackson, S. E. (2007). Conformational Dynamics of the Molecular Chaperone Hsp90 in Complexes with a Co-chaperone and Anticancer Drugs. J Mol Biol *372*, 1189-1203.

Picard, D. (2006). Chaperoning steroid hormone action. Trends Endocrinol Metab *17*, 229-235.

Pickart, C. M. (2001). Mechanisms underlying ubiquitination. Annu Rev Biochem *70*, 503-533.

Pratt, W. B., and Toft, D. O. (1997). Steroid receptor interactions with heat shock protein and immunophilin chaperones. Endocr Rev *18*, 306-360.

Pratt, W. B., and Toft, D. O. (2003). Regulation of signaling protein function and trafficking by the hsp90/hsp70-based chaperone machinery. Exp Biol Med (Maywood) *228*, 111-133.

Prodromou, C., Panaretou, B., Chohan, S., Siligardi, G., O'Brien, R., Ladbury, J. E., Roe, S. M., Piper, P. W., and Pearl, L. H. (2000). The ATPase cycle of Hsp90 drives a molecular 'clamp' via transient dimerization of the N-terminal domains. Embo J *19*, 4383-4392.

Prodromou, C., Roe, S. M., O'Brien, R., Ladbury, J. E., Piper, P. W., and Pearl, L. H. (1997a). Identification and structural characterization of the ATP/ADP-binding site in the Hsp90 molecular chaperone. Cell *90*, 65-75.

Prodromou, C., Roe, S. M., Piper, P. W., and Pearl, L. H. (1997b). A molecular clamp in the crystal structure of the N-terminal domain of the yeast Hsp90 chaperone. Nat Struct Biol *4*, 477-482.

Prodromou, C., Siligardi, G., O'Brien, R., Woolfson, D. N., Regan, L., Panaretou, B., Ladbury, J. E., Piper, P. W., and Pearl, L. H. (1999). Regulation of Hsp90 ATPase activity by tetratricopeptide repeat (TPR)-domain co-chaperones. Embo J *18*, 754-762.

Queitsch, C., Sangster, T. A., and Lindquist, S. (2002). Hsp90 as a capacitor of phenotypic variation. Nature *417*, 618-624.

Raviol, H., Sadlish, H., Rodriguez, F., Mayer, M. P., and Bukau, B. (2006). Chaperone network in the yeast cytosol: Hsp110 is revealed as an Hsp70 nucleotide exchange factor. Embo J *25*, 2510-2518.

Revington, M., Zhang, Y., Yip, G. N., Kurochkin, A. V., and Zuiderweg, E. R. (2005). NMR investigations of allosteric processes in a two-domain Thermus thermophilus Hsp70 molecular chaperone. J Mol Biol *349*, 163-183.

Richter, K., Moser, S., Hagn, F., Friedrich, R., Hainzl, O., Heller, M., Schlee, S., Kessler, H., Reinstein, J., and Buchner, J. (2006). Intrinsic inhibition of the Hsp90 ATPase activity. J Biol Chem *281*, 11301-11311.

Richter, K., Muschler, P., Hainzl, O., and Buchner, J. (2001). Coordinated ATP hydrolysis by the Hsp90 dimer. J Biol Chem *276*, 33689-33696.

Richter, K., Muschler, P., Hainzl, O., Reinstein, J., and Buchner, J. (2003). Sti1 is a non-competitive inhibitor of the Hsp90 ATPase. Binding prevents the N-terminal dimerization reaction during the atpase cycle. J Biol Chem *278*, 10328-10333.

Richter, K., Soroka, J., Skalniak, L., Leskovar, A., Hessling, M., Reinstein, J., and Buchner, J. (2008). Conserved conformational changes in the ATPase cycle of human Hsp90. J Biol Chem.

Richter, K., Walter, S., and Buchner, J. (2004). The Co-chaperone Sba1 connects the ATPase reaction of Hsp90 to the progression of the chaperone cycle. J Mol Biol *342*, 1403-1413.

Rist, W., Graf, C., Bukau, B., and Mayer, M. P. (2006). Amide hydrogen exchange reveals conformational changes in hsp70 chaperones important for allosteric regulation. J Biol Chem *281*, 16493-16501.

Rist, W., Jorgensen, T. J. D., Roepstorff, P., Bukau, B., and Mayer, M. P. (2003). Mapping Temperature-induced Conformational Changes in the Escherichia coli Heat Shock Transcription Factor {sigma}32 by Amide Hydrogen Exchange. J Biol Chem *278*, 51415-51421.

Rist, W., Mayer, M. P., Andersen, J. S., Roepstorff, P., and Jorgensen, T. J. (2005a). Rapid desalting of protein samples for on-line microflow electrospray ionization mass spectrometry. Anal Biochem *342*, 160-162.

Rist, W., Rodriguez, F., Jorgensen, T. J., and Mayer, M. P. (2005b). Analysis of subsecond protein dynamics by amide hydrogen exchange and mass spectrometry using a quenched-flow setup. Protein Sci *14*, 626-632.

Roe, S. M., Ali, M. M., Meyer, P., Vaughan, C. K., Panaretou, B., Piper, P. W., Prodromou, C., and Pearl, L. H. (2004). The Mechanism of Hsp90 regulation by the protein kinase-specific cochaperone p50(cdc37). Cell *116*, 87-98.

Roe, S. M., Prodromou, C., O'Brien, R., Ladbury, J. E., Piper, P. W., and Pearl, L. H. (1999). Structural basis for inhibition of the Hsp90 molecular chaperone by the antitumor antibiotics radicicol and geldanamycin. J Med Chem *42*, 260-266.

Roepstorff, P., and Fohlman, J. (1984). Proposal for a common nomenclature for sequence ions in mass spectra of peptides. Biomedical Mass Spectrometry *11*, 601.

Rosser, M. F., Washburn, E., Muchowski, P. J., Patterson, C., and Cyr, D. M. (2007). Chaperone functions of the E3 ubiquitin ligase CHIP. J Biol Chem *282*, 22267-22277.

Rudiger, S., Buchberger, A., and Bukau, B. (1997a). Interaction of Hsp70 chaperones with substrates. Nat Struct Biol *4*, 342-349.

Rudiger, S., Germeroth, L., Schneider-Mergener, J., and Bukau, B. (1997b). Substrate specificity of the DnaK chaperone determined by screening cellulose-bound peptide libraries. Embo J *16*, 1501-1507.

Sangster, T. A., Lindquist, S., and Queitsch, C. (2004). Under cover: causes, effects and implications of Hsp90-mediated genetic capacitance. Bioessays *26*, 348-362.

Sato, S., Fujita, N., and Tsuruo, T. (2000). Modulation of Akt kinase activity by binding to Hsp90. Proc Natl Acad Sci U S A *97*, 10832-10837.

Scheufler, C., Brinker, A., Bourenkov, G., Pegoraro, S., Moroder, L., Bartunik, H., Hartl, F. U., and Moarefi, I. (2000). Structure of TPR domain-peptide complexes: critical elements in the assembly of the Hsp70-Hsp90 multichaperone machine. Cell *101*, 199-210.

Schlichting, I., Berendzen, J., Chu, K., Stock, A. M., Maves, S. A., Benson, D. E., Sweet, R. M., Ringe, D., Petsko, G. A., and Sligar, S. G. (2000). The catalytic pathway of cytochrome p450cam at atomic resolution. Science *287*, 1615-1622.

Schmelzeisen-Redeker, G., Buetfering, L., and Roellgen, F. W. (1989). Desolvation of ions and molecules in thermospray mass spectrometry. International Journal of Mass Spectrometry and Ion Processes *90*, 139-150.

Schulte, T. W., Akinaga, S., Soga, S., Sullivan, W., Stensgard, B., Toft, D., and Neckers, L. M. (1998). Antibiotic radicicol binds to the N-terminal domain of Hsp90 and shares important biologic activities with geldanamycin. Cell Stress Chaperones *3*, 100-108.

Scroggins, B. T., Robzyk, K., Wang, D., Marcu, M. G., Tsutsumi, S., Beebe, K., Cotter, R. J., Felts, S., Toft, D., Karnitz, L.*, et al.* (2007). An acetylation site in the middle domain of Hsp90 regulates chaperone function. Mol Cell *25*, 151-159.

Sharon, M., and Robinson, C. V. (2007). The role of mass spectrometry in structure elucidation of dynamic protein complexes. Annu Rev Biochem *76*, 167-193.

Shi, L., Kataoka, M., and Fink, A. L. (1996). Conformational characterization of DnaK and its complexes by small-angle X-ray scattering. Biochemistry *35*, 3297-3308.

Shiau, A. K., Harris, S. F., Southworth, D. R., and Agard, D. A. (2006). Structural Analysis of E. coli hsp90 reveals dramatic nucleotide-dependent conformational rearrangements. Cell *127*, 329-340.

Siligardi, G., Panaretou, B., Meyer, P., Singh, S., Woolfson, D. N., Piper, P. W., Pearl, L. H., and Prodromou, C. (2002). Regulation of Hsp90 ATPase activity by the co-chaperone Cdc37p/p50cdc37. J Biol Chem *277*, 20151-20159.

Slepenkov, S. V., and Witt, S. N. (1998). Peptide-induced conformational changes in the molecular chaperone DnaK. Biochemistry *37*, 16749-16756.

Smith, D. F. (2000). Chaperones in progesterone receptor complexes. Semin Cell Dev Biol *11*, 45-52.

Smith, D. F. (2004). Tetratricopeptide repeat cochaperones in steroid receptor complexes. Cell Stress Chaperones *9*, 109-121.

Smith, D. F., and Toft, D. O. (1993). Steroid receptors and their associated proteins. Mol Endocrinol *7*, 4-11.

Solit, D. B., and Chiosis, G. (2008). Development and application of Hsp90 inhibitors. Drug Discov Today *13*, 38-43.

Sondermann, H., Scheufler, C., Schneider, C., Hohfeld, J., Hartl, F. U., and Moarefi, I. (2001). Structure of a Bag/Hsc70 Complex: Convergent Functional Evolution of Hsp70 Nucleotide Exchange Factors. Science *291*, 1553-1557.

Soti, C., Racz, A., and Csermely, P. (2002). A Nucleotide-dependent molecular switch controls ATP binding at the C-terminal domain of Hsp90. N-terminal nucleotide binding unmasks a C-terminal binding pocket. J Biol Chem *277*, 7066-7075.

Stebbins, C. E., Russo, A. A., Schneider, C., Rosen, N., Hartl, F. U., and Pavletich, N. P. (1997). Crystal structure of an Hsp90-geldanamycin complex: targeting of a protein chaperone by an antitumor agent. Cell *89*, 239-250.

Steen, H., and Mann, M. (2004). The ABC's (and XYZ's) of peptide sequencing. Nat Rev Mol Cell Biol *5*, 699-711.

Stevens, S. Y., Cai, S., Pellecchia, M., and Zuiderweg, E. R. (2003). The solution structure of the bacterial HSP70 chaperone protein domain DnaK(393-507) in complex with the peptide NRLLLTG. Protein Sci *12*, 2588-2596.

Stryer, L. (1978). Fluorescence energy transfer as a spectroscopic ruler. Annu Rev Biochem *47*, 819-846.

Swain, J. F., Dinler, G., Sivendran, R., Montgomery, D. L., Stotz, M., and Gierasch, L. M. (2007). Hsp70 chaperone ligands control domain association via an allosteric mechanism mediated by the interdomain linker. Mol Cell *26*, 27-39.

Tanaka, N., and Nakamoto, H. (1999). HtpG is essential for the thermal stress management in cyanobacteria. FEBS Lett *458*, 117-123.

Teter, S. A., Houry, W. A., Ang, D., Tradler, T., Rockabrand, D., Fischer, G., Blum, P., Georgopoulos, C., and Hartl, F. U. (1999). Polypeptide flux through bacterial Hsp70: DnaK cooperates with trigger factor in chaperoning nascent chains. Cell *97*, 755-765.

Theyssen, H., Schuster, H. P., Packschies, L., Bukau, B., and Reinstein, J. (1996). The second step of ATP binding to DnaK induces peptide release. J Mol Biol *263*, 657-670.

Thomson, B. A., and Iribarne, J. V. (1979). Field-induced ion evaporation from liquid surfaces at atmospheric pressure. Journal of Chemical Physics *71*, 4451-4463.

Thomson, J. J. (1913). Rays of Positive Electricity and their Application to Chemical Analysis (London: Longmans, Green and Co. Ltd.).

Ungewickell, E. (1985). The 70-kd mammalian heat shock proteins are structurally and functionally related to the uncoating protein that releases clathrin triskelia from coated vesicles. Embo J *4*, 3385-3391.

Vasilescu, J., and Figeys, D. (2006). Mapping protein-protein interactions by mass spectrometry. Curr Opin Biotechnol *17*, 394-399.

Vaughan, C. K., Gohlke, U., Sobott, F., Good, V. M., Ali, M. M., Prodromou, C., Robinson, C. V., Saibil, H. R., and Pearl, L. H. (2006). Structure of an Hsp90-Cdc37-Cdk4 complex. Mol Cell *23*, 697-707.

Vogel, M., Bukau, B., and Mayer, M. P. (2006a). Allosteric regulation of Hsp70 chaperones by a proline switch. Mol Cell *21*, 359-367.

Vogel, M., Mayer, M. P., and Bukau, B. (2006b). Allosteric regulation of Hsp70 chaperones involves a conserved interdomain linker. J Biol Chem *281*, 38705-38711.

Voisine, C., Craig, E. A., Zufall, N., von Ahsen, O., Pfanner, N., and Voos, W. (1999). The protein import motor of mitochondria: unfolding and trapping of preproteins are distinct and separable functions of matrix Hsp70. Cell *97*, 565-574.

Wales, T. E., and Engen, J. R. (2006). Hydrogen exchange mass spectrometry for the analysis of protein dynamics. Mass Spectrom Rev *25*, 158-170.

Wang, D., Xu, W., McGrath, S. C., Patterson, C., Neckers, L., and Cotter, R. J. (2005). Direct identification of ubiquitination sites on ubiquitin-conjugated CHIP using MALDI mass spectrometry. J Proteome Res *4*, 1554-1560.

Wang, H., Kurochkin, A. V., Pang, Y., Hu, W., Flynn, G. C., and Zuiderweg, E. R. (1998). NMR solution structure of the 21 kDa chaperone protein DnaK substrate binding domain: a preview of chaperone-protein interaction. Biochemistry *37*, 7929-7940.

Wang, L., Pan, H., and Smith, D. L. (2002). Hydrogen exchange-mass spectrometry: optimization of digestion conditions. Mol Cell Proteomics *1*, 132-138.

Wegele, H., Haslbeck, M., Reinstein, J., and Buchner, J. (2003). Sti1 is a novel activator of the Ssa proteins. J Biol Chem *278*, 25970-25976.

Wegele, H., Wandinger, S. K., Schmid, A. B., Reinstein, J., and Buchner, J. (2006). Substrate transfer from the chaperone Hsp70 to Hsp90. J Mol Biol *356*, 802-811.

Weikl, T., Muschler, P., Richter, K., Veit, T., Reinstein, J., and Buchner, J. (2000). C-terminal regions of Hsp90 are important for trapping the nucleotide during the ATPase cycle. J Mol Biol *303*, 583-592.

Whitesell, L., and Lindquist, S. L. (2005). HSP90 and the chaperoning of cancer. Nat Rev Cancer *5*, 761-772.

Whitesell, L., Mimnaugh, E. G., De Costa, B., Myers, C. E., and Neckers, L. M. (1994). Inhibition of heat shock protein HSP90-pp60v-src heteroprotein complex formation by benzoquinone ansamycins: essential role for stress proteins in oncogenic transformation. Proc Natl Acad Sci U S A *91*, 8324-8328.

Wilbanks, S. M., Chen, L., Tsuruta, H., Hodgson, K. O., and McKay, D. B. (1995). Solution small-angle X-ray scattering study of the molecular chaperone Hsc70 and its subfragments. Biochemistry *34*, 12095-12106.

Wilm, M., and Mann, M. (1996). Analytical properties of the nanoelectrospray ion source. Analytical Chemistry *68*, 1-8.

Windheim, M., Peggie, M., and Cohen, P. (2008). Two different classes of E2 ubiquitin-conjugating enzymes are required for the mono-ubiquitination of proteins and elongation by polyubiquitin chains with a specific topology. Biochem J *409*, 723-729.

Worrall, L. J., and Walkinshaw, M. D. (2007). Crystal structure of the C-terminal three-helix bundle subdomain of C. elegans Hsp70. Biochem Biophys Res Commun *357*, 105-110.

Wright, L., Barril, X., Dymock, B., Sheridan, L., Surgenor, A., Beswick, M., Drysdale, M., Collier, A., Massey, A., Davies, N.*, et al.* (2004). Structure-activity relationships in purine-based inhibitor binding to HSP90 isoforms. Chem Biol *11*, 775-785.

Xu, Z., Devlin, K. I., Ford, M. G., Nix, J. C., Qin, J., and Misra, S. (2006). Structure and interactions of the helical and U-box domains of CHIP, the C terminus of HSP70 interacting protein. Biochemistry *45*, 4749-4759.

Young, J. C., Agashe, V. R., Siegers, K., and Hartl, F. U. (2004). Pathways of chaperone-mediated protein folding in the cytosol. Nat Rev Mol Cell Biol *5*, 781-791.

Young, J. C., and Hartl, F. U. (2000). Polypeptide release by Hsp90 involves ATP hydrolysis and is enhanced by the co-chaperone p23. Embo J *19*, 5930-5940.

Zenobi, R., and Knochenmuss, R. (1999). Ion formation in MALDI mass spectrometry. Mass Spectrometry Reviews *17*, 337-366.

Zhang, L., Fan, J., Vu, K., Hong, K., Le Brazidec, J. Y., Shi, J., Biamonte, M., Busch, D. J., Lough, R. E., Grecko, R.*, et al.* (2006). 7'-substituted benzothiazolothio- and pyridinothiazolothio-purines as potent heat shock protein 90 inhibitors. J Med Chem *49*, 5352-5362.

Zhang, M., Windheim, M., Roe, S. M., Peggie, M., Cohen, P., Prodromou, C., and Pearl, L. H. (2005). Chaperoned ubiquitylation--crystal structures of the CHIP U box E3 ubiquitin ligase and a CHIP-Ubc13-Uev1a complex. Mol Cell *20*, 525-538.

Zhang, W., Hirshberg, M., McLaughlin, S. H., Lazar, G. A., Grossmann, J. G., Nielsen, P. R., Sobott, F., Robinson, C. V., Jackson, S. E., and Laue, E. D. (2004). Biochemical and structural studies of the interaction of Cdc37 with Hsp90. J Mol Biol *340*, 891-907.

Zhang, Y., and Zuiderweg, E. R. P. (2004). The 70-kDa heat shock protein chaperone nucleotide-binding domain in solution unveiled as a molecular machine that can reorient its functional subdomains. PNAS *101*, 10272-10277.

Zhang, Z., and Marshall, A. G. (1998). A universal algorithm for fast and automated charge state deconvolution of electrospray mass-to-charge ratio spectra. J Am Soc Mass Spectrom *9*, 225-233.

Zhang, Z., and Smith, D. L. (1993). Determination of amide hydrogen exchange by mass spectrometry: a new tool for protein structure elucidation. Protein Science *2*, 522-531.

Zhu, X., Zhao, X., Burkholder, W. F., Gragerov, A., Ogata, C. M., Gottesman, M. E., and Hendrickson, W. A. (1996). Structural Analysis of Substrate Binding by the Molecular Chaperone DnaK. Science *272*, 1606-1614.

6 Abbreviations

σ^{32}	Sigma32, heat shock transcription factor in *E. coli*
µM	micromolar
17-AAG	17-allylaminogeldanamycin
17-DMAG	17-dimethylaminoethylamino-demethoxygeldanamycin
Å	Ångström
aa	amino acids
ADP	adenosine diphosphate
AMPPNP	adenylyl imido diphosphate
apo	ligand free state
APS	ammonium persulfate
ATP	adenosine triphosphate
BMH	bis(maleimido)hexane
BMOE	bis(maleimido)ethane
bp	base pairs
BSA	bovine serum albumine
CD	circular dichroism
CFTR	cystic fibrosis transmembrane regulator
CHIP	C-terminus of Hsc70 interacting protein
CID	collision induced dissociation
D = ^{2}H	deuterium
Da	Dalton (atomic mass unit)
DC	direct current
DD	dimerization domain
DEAE	diethylaminoethyl
DMF	dimethylformamide
DMSO	dimethylsulfoxide
DNA	desoxyribonucleic acid
DnaJ	Hsp40 co-chaperone in *E. coli*
DnaK	Hsp70 chaperone in *E. coli*
DTT	1,4-dithiothreitol
E. coli	*Escherichia coli*
E2	ubiquitin-conjugating enzyme
E3	ubiquitin-ligase
EDTA	ethylenediamine-N,N,N',N'-tetraacetic acid
ESI	electrospray ionization
FA	formic acid
FRET	fluorescence resonance energy transfer
GA	geldanamycin
GHKL	GyraseB/Hsp90/Histidine Kinase/MutL ATPase superfamily
GroEL	Hsp60 chaperone in *E. coli*
GroES	Hsp10 chaperone in *E. coli*
GrpE	nucleotide exchange factor for DnaK
HCCA	4-hydroxy-α-cyanocinnamic acid
HECT	homologous to E6-AP carboxy terminus
HEPES	4-(2-hydroxyethyl)piperazine-1-ethanesulfonic acid
Hop	Hsp70-Hsp90-organizing protein
HPLC	high-performance liquid chromatography

Hsc	constitutively expressed heat shock protein (cognate)
Hsp	heat shock protein
Hsp90β	constitutively expressed isoform of Hsp90
HtpG	high temperature protein G in *E. coli*
HX	amide hydrogen exchange
ID	inner diameter
IPTG	isopropyl-β-D-thiogalactopyranoside
J	Joule
JDP	J-domain protein
kDa	kilodalton
LC	liquid chromatography
m/z	mass-to-charge ratio
MALDI	matrix assisted laser desorption/ionization
MD	middle domain
MeOH	methanol
mRNA	messenger ribonucleic acid
MS	mass spectrometry
MS/MS	tandem mass spectrometry
NBD	nucleotide binding domain
NEF	nucleotide exchange factor
nM	nanomolar
NMR	nuclear magnetic resonance
OD	optical density
PAGE	polyacrylamide gel electrophoresis
PCR	polymerase chain reaction
PDB	protein data bank
P_i	inorganic phosphate
PMSF	phenylmethanesulfonyl fluoride
PP5	protein phosphatase 5
ppm	parts per million
PU-H71	purine scaffold inhibitor H71
RF	radio frequency
RING	really interesting new gene
RNA	ribonucleic acid
RP	reversed-phase
SAXS	small angle X-ray scattering
SBD	substrate binding domain
SDS	sodium dodecyl sulphate
SHR	steroid hormone receptor
TCEP	tris(2-carboxyethyl) phosphine
TEMED	N,N,N',N'-tetramethylethylendiamine
TFA	trifluoroacetic acid
TOF	time-of-flight
TPR	tetratricopeptide repeat
Tris	2-amino-2-(hydroxymethyl)-1,3-propanediol
wt	wildtype
z	number of charges on an ion

The 1-letter code or the 3-letter code for amino acids was used

7 Appendix

Peptic peptide identification lists

DnaK

first residue	last residue	mass (theo.)	m/z (theo.)	charge	sequence
2	9	827.5117	414.7637	2	GKIIGIDL
2	15	1390.7126	696.3641	2	GKIIGIDLGTTNSC
16	41	2726.3909	909.8048	3	VAIMDGTTPRVLENAEGDRTTPSIIA
17	41	2627.3225	876.7820	3	AIMDGTTPRVLENAEGDRTTPSIIA
17	49	3534.7148	1179.2461	3	AIMDGTTPRVLENAEGDRTTPSIIAYTQDGETL
18	41	2556.2854	853.1029	3	IMDGTTPRVLENAEGDRTTPSIIA
18	49	3463.6777	1155.5670	3	IMDGTTPRVLENAEGDRTTPSIIAYTQDGETL
41	49	996.4400	499.2278	2	AYTQDGETL
42	49	925.4029	463.7093	2	YTQDGETL
42	66	2728.378	910.4671	3	IAYTQDGETLVGQPAKRQAVTNPQNTLFA
50	66	1820.9857	608.0030	3	VGQPAKRQAVTNPQNTL
50	66	1820.9857	911.5007	2	VGQPAKRQAVTNPQNTL
50	67	1968.0541	657.0258	3	VGQPAKRQAVTNPQNTLF
67	80	1747.9846	583.6693	3	FAIKRLIGRRFQDE
67	81	1877.0272	470.2646	4	FAIKRLIGRRFQDEE
67	81	1877.0272	626.6835	3	FAIKRLIGRRFQDEE
67	85	2375.2822	594.8284	4	FAIKRLIGRRFQDEEVQRD
82	101	2159.1045	720.7093	3	VQRDVSIMPFKIIAADNGDA
82	101	2159.1045	1080.5601	2	VQRDVSIMPFKIIAADNGDA
86	97	1303.7210	652.8683	2	VSIMPFKIIAAD
86	101	1660.8494	831.4325	2	VSIMPFKIIAADNGDA
102	117	1767.9342	590.3192	3	WVEVKGQKMAPPQISA
102	117	1767.9342	884.9749	2	WVEVKGQKMAPPQISA
102	118	1896.9768	633.3334	3	WVEVKGQKMAPPQISAE
102	118	1896.9768	949.4962	2	WVEVKGQKMAPPQISAE
103	118	1710.8975	571.3070	3	VEVKGQKMAPPQISAE
119	129	1289.7377	645.8767	2	VLKKMKKTAED
119	137	2178.1606	727.0613	3	VLKKMKKTAEDYLGEPVTE
119	137	2178.1606	1090.0881	2	VLKKMKKTAEDYLGEPVTE
119	138	2249.1977	750.7404	3	VLKKMKKTAEDYLGEPVTEA
119	139	2384.2873	795.7702	3	VLKKMKKTAEDYLGEPVTEAV
138	163	2745.4562	687.3719	4	AVITVPAYFNDAQRQATKDAGRIAGL
138	163	2745.4562	916.1599	3	AVITVPAYFNDAQRQATKDAGRIAGL
146	163	1930.9973	644.6736	3	FNDAQRQATKDAGRIAGL
147	163	1783.9289	595.6508	3	NDAQRQATKDAGRIAGL
164	174	1268.7088	635.3622	2	EVKRIINEPTA
164	176	1410.7831	706.3994	2	EVKRIINEPTAAA
164	177	1523.8671	508.9635	3	EVKRIINEPTAAAL
164	177	1523.8671	762.9414	2	EVKRIINEPTAAAL
166	177	1295.7561	648.8859	2	KRIINEPTAAAL
173	191	1862.985	622.0028	3	TAAALAYGLDKGTGNRTIA
177	192	1647.8944	550.3059	3	LAYGLDKGTGNRTIAV
177	192	1647.8944	824.9550	2	LAYGLDKGTGNRTIAV
178	192	1534.8104	512.6113	3	AYGLDKGTGNRTIAV
178	192	1534.8104	512.6113	3	AYGLDKGTGNRTIAV
178	192	1534.8104	768.4130	2	AYGLDKGTGNRTIAV
188	203	1683.8468	562.2901	3	RTIAVYDLGGGTFDIS
205	217	1522.7039	762.3598	2	IEIDEVDGEKTFE
207	216	1151.5346	576.7751	2	IDEVDGEKTF
207	219	1492.7297	747.3727	2	IDEVDGEKTFEVL
218	231	1397.6423	699.8290	2	VLATNGDTHLGGED
220	231	1185.4898	593.7527	2	ATNGDTHLGGED
220	232	1332.5582	667.2869	2	ATNGDTHLGGEDF
220	236	1803.8024	602.2753	3	ATNGDTHLGGEDFDSRL
220	236	1803.8024	902.9090	2	ATNGDTHLGGEDFDSRL
231	252	2656.3384	886.4539	3	DFDSRLINYLVEEFKKDQGIDL
244	259	1859.9564	620.9933	3	FKKDQGIDLRNDPLAM
244	273	3467.8922	694.5862	5	FKKDQGIDLRNDPLAMQRLKEAAEKAKIEL
260	273	1625.9465	542.9900	3	QRLKEAAEKAKIEL
260	283	2669.4348	890.8194	3	QRLKEAAEKAKIELSSAQQTDVNL

274	283	1061.4989	531.7573	2	SSAQQTDVNL
281	289	1004.5179	503.2668	2	VNLPYITAD
284	305	2424.3311	607.0906	4	PYITADATGPKHMNIKVTRAKL
284	305	2424.3311	809.1182	3	PYITADATGPKHMNIKVTRAKL
289	305	1879.0462	470.7694	4	DATGPKHMNIKVTRAKL
289	305	1879.0462	627.3565	3	DATGPKHMNIKVTRAKL
289	308	2208.2049	553.0590	4	DATGPKHMNIKVTRAKLESL
309	329	2278.2533	760.4256	3	VEDLVNRSIEPLKVALQDAGL
309	329	2278.2533	1140.1345	2	VEDLVNRSIEPLKVALQDAGL
311	329	2050.1422	684.3885	3	DLVNRSIEPLKVALQDAGL
311	329	2050.1422	1026.0789	2	DLVNRSIEPLKVALQDAGL
312	329	1935.1153	646.0462	3	LVNRSIEPLKVALQDAGL
312	329	1935.1153	968.5655	2	LVNRSIEPLKVALQDAGL
313	329	1822.0312	608.3515	3	VNRSIEPLKVALQDAGL
337	356	2230.2330	558.5661	4	VILVGGQTRMPMVQKKVAEF
337	356	2230.2330	744.4188	3	VILVGGQTRMPMVQKKVAEF
340	356	1904.9965	477.2569	4	VGGQTRMPMVQKKVAEF
340	356	1904.9965	636.0066	3	VGGQTRMPMVQKKVAEF
340	356	1904.9965	953.5061	2	VGGQTRMPMVQKKVAEF
357	369	1529.7474	510.9236	3	FGKEPRKDVNPDE
357	369	1529.7474	765.8815	2	FGKEPRKDVNPDE
357	370	1600.7845	534.6026	3	FGKEPRKDVNPDEA
357	370	1600.7845	801.4001	2	FGKEPRKDVNPDEA
357	370	1600.7845	801.4001	2	FGKEPRKDVNPDEA
357	372	1770.8901	591.3045	3	FGKEPRKDVNPDEAVA
370	391	2065.1783	689.4006	3	AVAIGAAVQGGVLTGDVKDVLL
370	391	2065.1783	1033.5970	2	AVAIGAAVQGGVLTGDVKDVLL
371	382	1053.6182	527.8169	2	VAIGAAVQGGVL
371	391	1994.1412	665.7215	3	VAIGAAVQGGVLTGDVKDVLL
371	391	1994.1412	998.0784	2	VAIGAAVQGGVLTGDVKDVLL
371	392	2107.2252	703.4162	3	VAIGAAVQGGVLTGDVKDVLLL
383	391	958.5335	480.2746	2	TGDVKDVLL
389	392	456.3312	457.3390	1	VLLL
392	399	856.4906	429.2531	2	LLDVTPLSL
392	399	856.4906	857.4984	1	LLDVTPLSL
400	408	893.3987	447.7072	2	GIETMGGVM
400	408	893.3987	894.4065	1	GIETMGGVM
412	425	1536.8624	513.2953	3	IAKNTTIPTKHSQV
412	430	2072.0902	691.7045	3	IAKNTTIPTKHSQVFSTAE
412	435	2587.2878	863.4371	3	IAKNTTIPTKHSQVFSTAEDNQSA
412	437	2787.4039	930.1424	3	IAKNTTIPTKHSQVFSTAEDNQSAVT
436	457	2466.3455	617.5942	4	VTIHVLQGERKRAADNKSLGQF
438	457	2266.2294	567.5652	4	IHVLQGERKRAADNKSLGQF
438	457	2266.2294	756.4176	3	IHVLQGERKRAADNKSLGQF
438	457	2266.2294	1134.1225	2	IHVLQGERKRAADNKSLGQF
458	473	1720.8567	861.4362	2	NLDGINPAPRGMPQIE
472	484	1419.7176	710.8666	2	IEVTFDIDADGIL
512	532	2462.2224	821.7486	3	IQKMVRDAEANAEADRKFEEL
531	564	3798.925	950.7391	4	ELVQTRNQGDHLLHSTRKQVEEAGDKLPADDKTA
541	552	1475.7845	738.9001	2	HLLHSTRKQVEE
553	568	1600.7944	534.6059	3	AGDKLPADDKTAIESA
591	600	1145.6114	573.8135	2	LAQVSQKLME
601	625	2595.1546	866.0593	3	IAQQQHAQQQTAGADASANNAKDDD
601	628	2908.3183	970.4472	3	IAQQQHAQQQTAGADASANNAKDDDVVD
601	630	3108.3980	1037.1405	3	IAQQQHAQQQTAGADASANNAKDDDVVDAE

HtpG

first residue	last residue	mass (theo)	m/z (theo)	charge	sequence
1	19	2228.1735	743.7323	3	MKGQETRGFQSEVKQLLHL
20	31	1480.7384	494.5873	3	MIHSLYSNKEIF
32	48	1918.0272	640.3502	3	LRELISNASDAADKLRF
35	56	2386.2600	796.4278	3	LISNASDAADKLRFRALSNPDL
64	88	2865.4900	717.3803	4	RVRVSFDKDKRTLTISDNGVGMTRD
70	88	2121.0484	708.0239	3	DKDKRTLTISDNGVGMTRD
78	88	1163.5240	582.7698	2	ISDNGVGMTRD
86	106	2287.2171	763.4135	3	TRDEVIDHLGTIAKSGTKSFL
89	98	1066.5658	534.2907	2	EVIDHLGTIA
89	106	1915.0414	639.3549	3	EVIDHLGTIAKSGTKSFL
99	106	866.4900	434.2528	2	KSGTKSFL
107	119	1376.6419	689.3288	2	ESLGSDQAKDSQL
120	127	823.4228	824.4306	1	IGQFGVGF
132	153	2356.2862	786.4365	3	IVADKVTVRTRAAGEKPENGVF
154	165	1297.5462	649.7809	2	WESAGEGEYTVA
162	175	1596.7631	533.2622	3	YTVADITKEDRGTE
179	187	1130.4992	566.2574	2	HLREGEDEF
191	202	1508.8099	503.9444	3	WRVRSIISKYSD
191	206	1943.1045	648.7093	3	WRVRSIISKYSDHIAL
200	206	817.3970	409.7063	2	YSDHIAL
207	219	1557.7682	520.2639	3	PVEIEKREEKDGE
220	233	1599.8984	534.3073	3	TVISWEKINKAQAL
234	244	1377.6500	460.2245	3	WTRNKSEITDE
246	277	3951.8969	988.9820	4	EEYKEFYKHIAHDFNDPLTWSHNRVEGKQEYTSLLY
278	299	2704.3696	902.4643	3	SLLYIPSQAPWDMWNRDHKHGLKLYV
300	305	810.4388	406.2272	2	YVQRVF
300	308	1169.5903	585.8030	2	YVQRVFIMD
309	317	1113.3637	557.6897	2	DAEQFMPNY
318	334	1913.0492	638.6909	3	LRFVRGLIDSSDLPLNV
319	334	1799.9894	601.0043	3	RFVRGLIDSSDLPLNV
335	359	2941.6243	981.5492	3	NVSREILQDSTVTRNLRNALTKRVLQMLE
361	374	1684.8308	562.6181	3	EKLAKDDAEKYQTF
375	382	989.5334	495.7745	2	WQQFGLVL
383	393	1204.5360	603.2758	2	KEGPAEDFANQ
400	416	1819.9064	607.6433	3	LRFASTHTDSSAQTVSL
417	435	2322.1201	775.0478	3	EDYVSRMKEGQEKIYYITA
438	449	1285.6666	429.5633	3	YAAAKSSPHLEL
450	458	1054.6862	528.3509	2	LRKKGIEVL
459	466	959.4924	480.7540	2	LLSDRIDE
472	490	2125.0570	709.3601	3	LTEFDGKPFQSVSKVDESL
475	490	1781.8835	594.9690	3	FDGKPFQSVSKVDESL
500	521	2385.3267	796.1167	3	SAKEAEKALTPFIDRVKALLGE
522	541	2277.2917	760.1050	3	RVKDVRLTHRLTDTPAIVST
526	545	2209.1339	737.3858	3	VRLTHRLTDTPAIVSTDADE
554	566	1406.7557	469.9264	3	FAAAGQKVPEVKY
567	576	1195.6237	598.8197	2	IFELNPDHVL
570	585	1791.9115	598.3116	3	LNPDHVLVKRAADTED
585	599	1820.8800	911.4478	2	DEAKFSEWVELLLDQ
602	613	1326.6779	664.3468	2	LAERGTLEDPNL
615	621	929.5229	465.7693	2	IRRMNQL

hHsp90β

first residue	last residue	mass (theo)	m/z (theo)	charge	sequence	modification
1	10	1192.48	597.24	2	MPEEVHHGEE	
2	14	1519.64	507.55	3	PEEVHHGEEEVET	
15	20	712.32	713.32	1	FAFQAE	
15	24	1136.59	569.30	2	FAFQAEIAQL	
28	39	1487.77	744.89	2	IINTFYSNKEIF	
32	39	1046.51	524.26	2	FYSNKEIF	
40	51	1300.7	651.35	2	LRELISNASDAL	
41	51	1187.61	594.81	2	RELISNASDAL	
52	65	1663.88	555.63	3	DKIRYESLTDPSKL	
57	65	988.51	495.26	2	ESLTDPSKL	
57	70	1504.73	502.58	3	ESLTDPSKLDSGKE	
66	81	1794.94	599.31	3	DSGKELKIDIIPNPQE	
66	83	2052.09	685.03	3	DSGKELKIDIIPNPQERT	
71	81	1278.72	640.36	2	LKIDIIPNPQE	
71	83	1535.87	512.96	3	LKIDIIPNPQERT	
71	86	1863.08	622.03	3	LKIDIIPNPQERTLTL	
87	98	1219.61	610.81	2	VDTGIGMTKADL	
87	98	1235.61	618.81	2	VDTGIGMTKADL	Oxidation (M)
99	114	1664.89	555.96	3	INNLGTIAKSGTKAFM	
99	114	1680.89	561.30	3	INNLGTIAKSGTKAFM	Oxidation (M)
105	114	1052.57	527.29	2	IAKSGTKAFM	
105	114	1068.56	535.28	2	IAKSGTKAFM	Oxidation (M)
113	126	1495.71	748.85	2	FMEALQAGADISMI	
126	133	823.42	824.42	1	IGQFGVGF	
139	154	1822.94	608.65	3	VAEKVVVITKHNDDEQ	
141	154	1652.84	551.95	3	EKVVVITKHNDDEQ	
142	154	1523.79	508.93	3	KVVVITKHNDDEQ	
155	165	1160.48	581.24	2	YAWESSAGGSF	
166	183	1918.07	640.36	3	TVRADHGEPIGRGTKVIL	
184	192	1161.53	581.77	2	HLKEDQTEY	
194	208	1898.05	633.68	3	EERRVKEVVKKHSQF	
196	208	1639.96	547.65	3	RRVKEVVKKHSQF	
209	214	775.45	776.45	1	IGYPITL	
216	229	1781.83	594.94	3	YLEKEREKEISDDE	
216	231	1981.91	661.64	3	YLEKEREKEISDDEAE	
216	256	4869.18	974.84	5	YLEKEREK……..DEEKPKIEDVGSD	
257	282	3151.66	788.92	4	EEDDSGKDKKKKTKKIKEKYIDQEEL	
283	300	2184.08	729.03	3	NKTKPIWTRNPDDITQEE	
290	300	1316.58	659.29	2	TRNPDDITQEE	
301	304	515.21	516.21	1	YGEF	
305	316	1519.69	507.56	3	YKSLTNDWEDHL	
317	324	915.48	458.74	2	AVKHFSVE	
317	327	1213.65	607.83	2	AVKHFSVEGQL	
317	328	1342.69	672.35	2	AVKHFSVEGQLE	
317	329	1489.76	745.88	2	AVKHFSVEGQLEF	
333	342	1230.69	616.35	2	LFIPRRAPFD	
344	355	1502.89	501.96	3	FENKKKKNNIKL	
356	363	1082.61	542.31	2	YVRRVFIM	
367	376	1251.60	626.80	2	DELIPEYLNF	
368	376	1136.58	569.29	2	ELIPEYLNF	
377	390	1538.83	770.42	2	IRGVVDSEDLPLNI	
383	390	899.46	450.73	2	SEDLPLNI	
384	393	1184.6	593.30	2	EDLPLNISRE	
386	393	940.53	471.27	2	LPLNISRE	
394	403	1202.71	401.90	3	MLQQSKILKV	Oxidation (M)
394	415	2624.60	875.87	3	REMLQQSKILKVIRKNIVKKCLELFS	
416	419	495.25	496.25	1	FSEL	
420	429	1270.62	424.54	3	AEDKENYKKF	
433	443	1284.72	429.24	3	FSKNLKLGIHE	
437	443	808.48	405.24	2	LKLGIHE	
437	454	2136.18	713.06	3	LKLGIHEDSTNRRRLSEL	
455	465	1291.58	646.79	2	LRYHTSQSGDE	
455	466	1438.61	480.54	3	LRYHTSQSGDEM	Oxidation (M)
470	484	1863.90	622.30	3	SEYVSRMKETQKSIY	Oxidation (M)
472	484	1647.83	550.28	3	YVSRMKETQKSIY	Oxidation (M)
473	484	1484.77	495.92	3	VSRMKETQKSIY	Oxidation (M)
485	498	1495.72	748.86	2	YITGESKEQVANSA	
485	499	1642.78	822.39	2	YITGESKEQVANSAF	

500	512	1635.92	546.31	3	VERVRKRGFEVVY	
526	535	1108.58	555.29	2	KEFDGKSLVS	
536	547	1357.66	679.83	2	VTKEGLELPEDE	
567	584	2159.23	720.74	3	MKEILDKKVEKVTISNRL	Oxidation (M)
572	584	1528.89	510.63	3	DKKVEKVTISNRL	
591	602	1342.62	672.31	2	IVTSTYGWTANM	
596	602	841.34	421.67	2	YGWTANM	
603	611	1058.59	530.30	2	ERIMKAQAL	
603	613	1329.72	444.24	3	ERIMKAQALRD	
603	613	1345.71	449.57	3	ERIMKAQALRD	Oxidation (M)
603	617	1794.87	599.29	3	ERIMKAQALRDNSTM	2 Oxidation (M)
621	636	1885.97	629.66	3	MAKKHLEINPDHPIVE	Oxidation (M)
621	638	2100.10	701.03	3	MAKKHLEINPDHPIVETL	Oxidation (M)
622	636	1738.94	580.65	3	AKKHLEINPDHPIVE	
637	653	1929.03	644.01	3	TLRQKAEADKNDKAVKD	
637	654	2042.11	681.70	3	TLRQKAEADKNDKAVKDL	
638	653	1827.98	610.33	3	LRQKAEADKNDKAVKD	
638	654	1941.06	648.02	3	LRQKAEADKNDKAVKDL	
639	654	1827.98	610.33	3	RQKAEADKNDKAVKDL	
655	658	443.32	444.32	1	VVLL	
659	663	579.29	580.29	1	FETAL	
664	683	2337.12	780.04	3	LSSGFSLEDPQTHSNRIYRM	
668	680	1542.74	515.25	3	FSLEDPQTHSNRI	
669	680	1395.67	466.22	3	SLEDPQTHSNRI	
669	683	1845.88	616.29	3	SLEDPQTHSNRIYRM	
684	692	956.55	479.28	2	IKLGLGIDE	
684	693	1071.58	536.79	2	IKLGLGIDED	
684	694	1200.62	601.31	2	IKLGLGIDEDE	
697	713	1746.83	874.42	2	AEEPNAAVPDEIPPLEG	
697	715	1990.90	664.63	3	AEEPNAAVPDEIPPLEGDE	
697	716	2105.93	702.98	3	AEEPNAAVPDEIPPLEGDED	
697	717	2176.96	726.65	3	AEEPNAAVPDEIPPLEGDEDA	
697	720	2551.14	851.38	3	AEEPNAAVPDEIPPLEGDEDASRM	

Hsc82

1st residue	last residue	mass (theo)	m/z (theo)	charge	sequence	modification
1	7	783.31	784.31	1	MAGETFE	
6	15	1224.6	613.30	2	FEFQAEITQL	
8	15	948.49	475.25	2	FQAEITQL	
19	30	1439.77	720.89	2	IINTVYSNKEIF	
31	42	1300.7	651.35	2	LRELISNASDAL	
31	47	1976.07	659.69	3	LRELISNASDALDKIRY	
34	47	1577.84	526.95	3	LISNASDALDKIRY	
34	49	1776.94	593.31	3	LISNASDALDKIRYQA	
34	55	2445.29	816.10	3	LISNASDALDKIRYQALSDPKQ	
43	55	1560.83	521.28	3	DKIRYQALSDPKQ	
43	62	2358.21	787.07	3	DKIRYQALSDPKQLETEPDL	
48	63	1829.9	915.95	2	QALSDPKQLETEPDLF	
50	62	1483.74	742.87	2	LSDPKQLETEPDL	
50	63	1630.81	816.41	2	LSDPKQLETEPDLF	
53	62	1168.6	585.30	2	PKQLETEPDL	
63	75	1568.93	523.98	3	FIRITPKPEEKVL	
63	76	1697.97	566.99	3	FIRITPKPEEKVLE	
64	76	1550.9	517.97	3	IRITPKPEEKVLE	
73	89	1859.02	620.67	3	KVLEIRDSGIGMTKAEL	
75	89	1631.86	544.95	3	LEIRDSGIGMTKAEL	
76	89	1518.77	507.26	3	EIRDSGIGMTKAEL	
77	89	1389.73	695.87	2	IRDSGIGMTKAEL	
77	89	1405.72	469.57	3	IRDSGIGMTKAEL	Oxidation (M)
90	105	1664.89	555.96	3	INNLGTIAKSGTKAFM	
90	105	1680.89	561.30	3	INNLGTIAKSGTKAFM	Oxidation (M)
90	107	1864.97	622.66	3	INNLGTIAKSGTKAFMEA	
114	124	1140.56	571.28	2	VSMIGQFGVGF	
117	124	823.42	412.71	2	IGQFGVGF	
129	145	1955.99	653.00	3	LVADRVQVISKNNEDEQ	

132	145	1672.8	558.60	3	DRVQVISKNNEDEQ	
132	146	1835.86	612.95	3	DRVQVISKNNEDEQY	
133	145	1557.77	520.26	3	RVQVISKNNEDEQ	
133	146	1720.84	574.61	3	RVQVISKNNEDEQY	
146	156	1229.54	615.77	2	YIWESNAGGSF	
157	175	2140.2	714.40	3	TVTLDEVNERIGRGTVLRL	
183	200	2332.25	778.42	3	EYLEEKRIKEVIKRHSEF	
184	200	2203.21	735.40	3	YLEEKRIKEVIKRHSEF	
185	200	2040.15	681.05	3	LEEKRIKEVIKRHSEF	
186	200	1927.06	643.35	3	EEKRIKEVIKRHSEF	
188	200	1668.98	557.33	3	KRIKEVIKRHSEF	
201	207	802.46	402.23	2	VAYPIQL	
201	208	915.54	458.77	2	VAYPIQLL	
245	263	2327.26	776.75	3	EEEEKKPKTKKVKEEVQEL	
263	279	2040.06	681.02	3	LEELNKTKPLWTRNPSD	
263	282	2382.25	795.08	3	LEELNKTKPLWTRNPSDITQ	
264	279	1926.98	643.33	3	EELNKTKPLWTRNPSD	
289	300	1465.67	733.84	2	YKSISNDWEDPL	
301	311	1305.67	653.84	2	YVKHFSVEGQL	
301	312	1434.71	718.36	2	YVKHFSVEGQLE	
301	313	1581.78	791.89	2	YVKHFSVEGQLEF	
314	327	1655.99	553.00	3	RAILFIPKRAPFDL	
318	328	1349.75	675.88	2	FIPKRAPFDLF	
328	339	1475.88	492.96	3	FESKKKKNNIKL	
340	349	1296.68	649.34	2	YVRRVFITDE	
349	357	1100.5	551.25	2	EAEDLIPEW	
349	359	1300.62	651.31	2	EAEDLIPEWLS	
350	357	971.46	486.73	2	AEDLIPEW	
350	358	1084.54	543.27	2	AEDLIPEWL	
350	359	1171.58	586.79	2	AEDLIPEWLS	
359	374	1730.91	866.46	2	SFVKGVVDSEDLPLNL	
360	374	1643.88	822.94	2	FVKGVVDSEDLPLNL	
361	374	1496.81	749.41	2	VKGVVDSEDLPLNL	
364	374	1212.62	607.31	2	VVDSEDLPLNL	
367	374	899.46	450.73	2	SEDLPLNL	
382	399	2137.35	713.45	3	NKIMKVIRKNIVKKLIEA	
388	400	1570.99	524.66	3	IRKNIVKKLIEAF	
417	427	1254.71	419.24	3	FAKNIKLGVHE	
417	435	2124.14	709.05	3	FAKNIKLGVHEDTQNRAAL	
418	435	1977.08	660.03	3	AKNIKLGVHEDTQNRAAL	
421	431	1252.64	627.32	2	IKLGVHEDTQN	
421	435	1663.9	555.63	3	IKLGVHEDTQNRAAL	
424	435	1309.64	655.82	2	GVHEDTQNRAAL	
439	450	1423.73	712.87	2	LRYNSTKSVDEL	
456	468	1677.83	560.28	3	YVTRMPEHQKNIY	
456	468	1693.82	565.61	3	YVTRMPEHQKNIY	Oxidation (M)
456	469	1840.89	614.63	3	YVTRMPEHQKNIYY	
457	468	1514.77	505.92	3	VTRMPEHQKNIY	
476	492	1905.07	636.02	3	KAVEKSPFLDALKAKNF	
478	484	818.45	410.23	2	VEKSPFL	
504	519	1887.96	630.32	3	YAFTQLKEFEGKTLVD	
506	519	1653.86	552.29	3	FTQLKEFEGKTLVD	
507	519	1506.79	503.26	3	TQLKEFEGKTLVD	
510	519	1164.6	583.30	2	KEFEGKTLVD	
527	542	1990.93	664.64	3	EETDEEKAEREKEIKE	
540	554	1773.03	592.01	3	IKEYEPLTKALKDIL	
540	556	1945.08	649.36	3	IKEYEPLTKALKDILGD	
540	557	2073.14	692.05	3	IKEYEPLTKALKDILGDQ	
543	556	1574.86	525.95	3	YEPLTKALKDILGD	
543	556	1574.86	525.95	3	YEPLTKALKDILGD	
543	559	1931.03	966.52	2	YEPLTKALKDILGDQVE	
560	567	934.59	468.30	2	KVVVSYKL	
560	573	1472.86	737.43	2	KVVVSYKLLDAPAA	
574	584	1235.6	618.80	2	IRTGQFGWSAN	
574	585	1366.65	684.33	2	IRTGQFGWSANM	
574	585	1382.64	692.32	2	IRTGQFGWSANM	Oxidation (M)
586	599	1634.82	545.94	3	ERIMKAQALRDSSM	
586	601	1808.89	603.96	3	ERIMKAQALRDSSMSS	
602	620	2212.18	738.39	3	YMSSKKTFEISPKSPIIKE	
603	620	2049.12	684.04	3	MSSKKTFEISPKSPIIKE	
604	620	1918.08	640.36	3	SSKKTFEISPKSPIIKE	
621	641	2327.28	776.76	3	LKKRVDEGGAQDKTVKDLTNL	

621	642	2440.36	814.45	3	LKKRVDEGGAQDKTVKDLTNLL	
648	652	523.26	524.26	1	LTSGF	
648	660	1413.67	707.84	2	LTSGFSLEEPTSF	
652	660	1055.48	528.74	2	FSLEEPTSF	
668	672	501.62	502.62	1	ISLGL	
677	701	2676.11	893.04	3	DEETETAPEASTEAPVEEVPADTEM	

CHIP wt

first residue	last residue	mass (theo)	m/z (theo)	charge	sequence
1	28	2771.35	924.78	3	MKGKEEKEGGARLGAGGGSPEKSPSAQE
1	36	3709.88	928.47	4	MKGKEEKEGGARLGAGGGSPEKSPSAQELKEQGNRL
37	45	1065.56	533.78	2	FVGRKYPEA
37	48	1310.64	656.32	2	FVGRKYPEAAAC
49	60	1329.75	444.25	3	YGRAITRNPLVA
49	60	1329.75	665.88	2	YGRAITRNPLVA
49	61	1428.82	477.27	3	YGRAITRNPLVAV
49	62	1591.88	531.63	3	YGRAITRNPLVAVY
53	60	882.53	442.27	2	ITRNPLVA
53	61	981.6	491.80	2	ITRNPLVAV
53	62	1144.66	573.33	2	ITRNPLVAVY
61	68	998.52	500.26	2	VYYTNRAL
61	69	1101.53	551.77	2	VYYTNRALC
61	70	1264.59	633.30	2	VYYTNRALCY
62	69	1002.46	502.23	2	YYTNRALC
62	70	1165.52	583.76	2	YYTNRALCY
63	70	1002.46	502.23	2	YTNRALCY
70	82	1573.76	787.88	2	YLKMQQHEQALAD
70	83	1676.77	559.92	3	YLKMQQHEQALADC
71	80	1224.63	613.32	2	LKMQQHEQAL
71	82	1410.69	706.35	2	LKMQQHEQALAD
71	83	1513.7	505.57	3	LKMQQHEQALADC
84	98	1725.93	576.31	3	RRALELDGQSVKAHF
89	98	1100.56	551.28	2	LDGQSVKAHF
90	98	987.48	494.74	2	DGQSVKAHF
90	105	1776.86	593.29	3	DGQSVKAHFFLGQCQL
99	105	807.39	404.70	2	FLGQCQL
99	106	936.44	469.22	2	FLGQCQLE
107	117	1254.54	628.27	2	MESYDEAIANL
118	131	1722.92	575.31	3	QRAYSLAKEQRLNF
118	139	2491.28	831.43	3	QRAYSLAKEQRLNFGDDIPSAL
121	131	1367.72	456.91	3	YSLAKEQRLNF
121	138	2023	675.33	3	YSLAKEQRLNFGDDIPSA
121	139	2136.09	713.03	3	YSLAKEQRLNFGDDIPSAL
124	131	1004.54	503.27	2	AKEQRLNF
124	139	1772.91	591.97	3	AKEQRLNFGDDIPSAL
125	139	1701.87	568.29	3	KEQRLNFGDDIPSAL
127	138	1331.65	666.83	2	QRLNFGDDIPSA
130	138	934.4	468.20	2	NFGDDIPSA
139	151	1640.98	547.99	3	LRIAKKKRWNSIE
140	151	1527.90	510.30	3	RIAKKKRWNSIE
152	161	1295.66	648.83	2	ERRIHQESEL
162	168	874.47	438.24	2	HSYLSRL
169	179	1343.67	672.83	2	IAAERERELEE
169	198	3519.58	880.89	4	IAAERERELEECQRNHEGDEDDSHVRAQQA
180	197	2122.88	708.63	3	CQRNHEGDEDDSHVRAQQ
180	198	2193.92	732.31	3	CQRNHEGDEDDSHVRAQQA
199	211	1553.67	518.89	3	CIEAKHDKYMADM
200	210	1319.62	440.87	3	IEAKHDKYMAD
202	211	1208.53	605.27	2	AKHDKYMADM
215	233	2296.16	766.39	3	FSQVDEKRKKRDIPDYLCG
215	238	2900.49	967.83	3	FSQVDEKRKKRDIPDYLCGKISFE
238	246	1090.52	546.26	2	ELMREPCIT
238	252	1708.82	855.41	2	ELMREPCITPSGITY
238	259	2594.24	865.75	3	ELMREPCITPSGITYDRKDIEE
239	246	961.47	481.74	2	LMREPCIT

239	249	1202.58	602.29	2	LMREPCITPSG
239	252	1579.77	790.89	2	LMREPCITPSGITY
240	246	848.39	425.20	2	MREPCIT
240	252	1466.69	734.35	2	MREPCITPSGITY
240	259	2352.11	785.04	3	MREPCITPSGITYDRKDIEE
243	252	1050.51	526.26	2	PCITPSGITY
243	259	1935.92	646.31	3	PCITPSGITYDRKDIEE
247	259	1521.73	508.24	3	PSGITYDRKDIEE
253	261	1153.57	577.79	2	DRKDIEEHL
260	277	2087.1	696.70	3	HLQRVGHFDPVTRSPLTQ
260	278	2216.15	739.72	3	HLQRVGHFDPVTRSPLTQE
260	284	2894.55	724.64	4	HLQRVGHFDPVTRSPLTQEQLIPNL
262	277	1836.96	613.32	3	QRVGHFDPVTRSPLTQ
262	278	1966	656.33	3	QRVGHFDPVTRSPLTQE
262	284	2644.41	662.10	4	QRVGHFDPVTRSPLTQEQLIPNL
279	286	898.49	450.25	2	QLIPNLAM
285	293	1022.51	512.26	2	AMKEVIDAF
287	293	820.43	411.22	2	KEVIDAF
294	303	1210.52	606.26	2	ISENGWVEDY

8 Danksagung

Die vorliegende Arbeit wurde in den Arbeitsgruppen Bukau und Mayer am Zentrum für Molekulare Biologie der Universität Heidelberg (ZMBH) unter der Leitung von PD Dr. Matthias P. Mayer durchgeführt.

Prof. Bernd Bukau danke ich für die freundliche Aufnahme in die Arbeitsgruppe und für die die ausgezeichneten Arbeitsbedingungen.

PD Dr. Matthias Mayer möchte ich herzlich für die Betreuung dieser Arbeit in seiner Forschungsgruppe und für die zuverlässige Unterstützung danken. Sein Engagement, seine ständige Diskussionsbereitschaft sowie seine fachliche und technische Expertise waren die Voraussetzung für das Gelingen der Arbeit.

Prof. Irmi Sinning danke ich für die Übernahme des Zweitgutachtens.

Ich bedanke mich außerdem bei Prof. Rüdiger Hell und Dr. Viktor Sourjik für ihre Bereitschaft, als Prüfer in meiner Doktorprüfung zu fungieren.

Ein Dank geht an alle Mitstreiter im HX-MS-Feld für Diskussionen und die kooperative Arbeitsatmosphäre. Dies sind insbesondere Dr. Wolfgang Rist für die Einarbeitung in die HPLC und Massenspektrometrie sowie Dr. Fernanda Rodriguez, Dr. Jocelyne Fiaux und Chung-Tien Lee.

Desweiteren danke ich Dr. Thomas Ruppert und seinem Team in der ZMBH-Massenspektrometrie-Abteilung für die Zusammenarbeit und technische Hilfe.

Dr. Günter Kramer danke ich für die Bereitstellung der HtpG–Proteine und für sein beständiges Interesse an den Hsp90-Projekten.

Marta Stankiewicz möchte ich für die Bereitstellung von Plasmiden, Proteinen und für die Durchführung der ATPase-Assays danken.

Bei allen Kollegen der AG Mayer sowie der AG Bukau möchte ich mich für die gute Zusammenarbeit, Diskussionen und die angenehme Arbeitsatmosphäre bedanken. Insbesondere sind dies Rainer Schlecht, Marta Stankiewicz, Chung-Tien Lee, Andrea Döhner, Elsbeth Pirkl und die aktuellen und ehemaligen Mitglieder der „Hsp70-Gruppe“, Heike Rampelt, Dr. Claes Andreasson, Dr. Jocelyne Fiaux, Dr. Fernanda Rodriguez, Dr. Heather Sadlish, Dr. Rainer Nikolay, Dr. Holger Raviol und Dr. Markus Vogel.

Dr. Matthias Mayer, Rainer Schlecht und Dr. Damon Huber danke ich für das schnelle Korrekturlesen der Arbeit.

Mein größter Dank geht schließlich an meine Familie, die mich während meines Studiums und während der Promotion immer tatkräftig und liebevoll unterstützt hat.